Thèse d'Habilitation à Diriger des Recherches
Spécialité : Neurosciences

Alexandre Charlet

Chargé de recherche CNRS
Institut des Neurosciences Cellulaires et Intégratives – INCI
CNRS UPR3212

INCI
UPR 3212

Neuropeptidergic Modulation of Emotions

Membres du Jury :

Dr. Stéphane Oliet	Rapporteur
Dr. Luis Villanueva	Rapporteur
Dr. Jean-Christophe Cassel	Rapporteur
Dr. Isabelle Décosterd	Examinatrice
Dr. Pierrick Poisbeau	Garant d'habilitation

Table of Contents

Curriculum Vitae

Personal Statements

Alexandre Charlet
34 years old (born in 1982/11/24, Mulhouse, France)
Married, 2 children
+33(0)607082506
acharlet@unistra.fr

I have a broad background in system neuroscience. I completed my PhD work at University of Strasbourg working on the emotional and physiological expression of pain using radiotelemetry monitoring of autonomous nervous system. Later at University of Lausanne during my post-doctoral years I focused on the modulation by neuropeptides of amygdala microcircuits both *in vitro* and *in vivo* as related to anxious and bravery behavior. Recruited as junior scientist by the CNRS in 2013/10 and thanks to the financial support awarded by several agencies and foundations, I am supervising one of the 2 research axis of the team using state-of-the-art optogenetic tools to decipher the emotional modulation by oxytocin, a neuropeptide released by hypothalamus and well known to impact on a wide range of complex behaviors, such as fear, pain, social interaction and sexual behavior. This work is carried out by two PhD students and one postdoc, directly placed under my supervision. My projects associate several and renowned researchers working in the field (from France, Germany, Italy, Switzerland, USA) and was already recently highlighted by the publication of a high-profile peer-reviewed article. My ongoing projects examine *i)* the involvement of astrocytes to neuron communication in the anxiolytic effect of oxytocin within the central amygdala, and *ii)* the neuronal circuits behind the oxytocinergic engrams sustaining the regulation of emotions of different valences.

Education

2016   **Accreditation to perform surgeries on small animals**

2010   **PhD in Neurosciences**
              University of Strasbourg, UMR 7519 Department Nociception and Pain
              Title: Exploration fonctionnelle de la douleur et de sa modulation spinale chez le rongeur
              Supervisor: Prof. Pierrick Poisbeau

2009   **Accreditation to perform animal experimentation** (lvl1; conceptor)

2006   **Master in Neurosciences**
              University of Strasbourg

2004   **Bachelor in Physiology and Cellular Biology**
              University of Strasbourg

Positions and Honors

Current Position

Chargé de recherche de 2ème classe CNRS
2013- Institute for Cellular and Integrative Neurosciences, Strasbourg, France
2014-2017 University of Strasbourg Institute for Advanced Study, Strasbourg, France

Professional Memberships and Responsibilities

2015- Member, Animation Committee, Neuropôle de Strasbourg
2015- Member, Treasurer, Regional Committee of Ethics in Animal Experimentation
2011- Member, International Association for the Study of Pain
2010- Member, Society for Neuroscience
2006- Member, Société Française des Neurosciences

Awards

2016-2019 CNRS, Doctoral Supervision and Research Award
2016 National Academy of Pharmacy, Maurice Girard Award
2013 National Academy of Medicine, Albert Sézary Award
2012 Swiss Society of Biological Psychiatry, Young Investigator Award
2010 AFSTAL, Chantal Autissier PhD Award
2007 Alsace Region, PhD Fellowship
2006 Neurex, Best Communication Award

Students Supervision

Postdoctoral Students

2016- Mai Iwasaki
Role of Oxytocinergic Control of the PAG Activity and Emotions

PhD Students Supervision

2015-2018 Stéphanie Goyon
Emotions-Related Circuits of Oxytocin
2013-2017 Jérôme Wahis
Involvement of Astrocyte-Neuron Interactions in the Endogenous Oxytocin
Modification of Amygdala Microcircuits

Master 2 Students Supervision

2015 Benjamin Bellanger
Oxytocin-Induced Modifications of Astrocyte Membrane Potential
2011-2012 Jérôme Wahis
In vivo Study of the Oxytocin Effect in the Central Amygdala
2010-2011 Marios Abatis
In vitro Study of the Oxytocin Effect in the Central Amygdala

Research Grants

ANR-DFG Collaborative Research Grant   2017-2020
NARSAD Young Investigator Grant   2017-2018

  Title: **Deciphering the Brain Circuits behind Oxytocinergic Modulation of Emotions**
  Goal: To study how the oxytocinergic system is able to modulate the emotional valence.
  Role: PI (NARSAD); Co-PI together with Valery Grinevich (ANR-DFG)
  Amount: 70.000 USD + 410.000/2 €

Initiative of Excellence Interdisciplinarity Grant   2015-2016

  Title: **Oxytocin and Emotions: from Receptor to Behavior**
  Goal: To develop new specific non peptidergic agonists for the oxytocin receptor and to
  validate their use *in vitro* and *in vivo*.
  Role: Co-PI together with Marcel Hibert
  Amount: 50.000/2 €

Hubert Curien Partnership PROCOPE   2015-2016

  Title: **Oxytocinergic Connections between PVN and SON**
  Goal: To study the intrahyothalamic oxytocinergic connections.
  Role: Co-PI together with Valery Grinevich
  Amount: 14.000/2 €

Fyssen Foundation Research Grant   2015-2016
University of Strasbourg Institute for Advanced Study Fellowship   2014-2017

  Title: **Deciphering the Oxytocinergic Neuronal Population Involved in the Pain Matrix**
  Goal: To study the oxytocinergic circuits at the basis of the regulation of pain.
  Role: PI
  Amount: 35.000 € + 240.000 €

Initiative of Excellence Attractivity Grant   2013-2015
FP7 Career Integration Grant (n°334455)   2013-2017
International Association for the Study of Pain Early Career Research Grant   2012

  Title: **Involvement of Astrocyte-Neuron Interactions in the Endogenous Oxytocin
  Modification of Amygdala Microcircuits and the Emotional Aspects of Pain**
  Goal: To study the relevance of astrocytes-neurons interaction to oxytocin-mediated
  network modifications and behavioral effects.
  Role: PI
  Amount: 130.000 € + 100.000 € + 20.000 USD

Publications List

Publications in Peer Reviewed Journals

Online track record
PubMed - Google Scholar

Legend

Corresponding and Co-senior authors
* Co-first authors
Names of the students I have driven for the study are underligned

1. Eliava M*, Melchior M*, Knobloch-Bollmann HS*, Wahis J*, da Silva Gouveia M, Tang Y, Ciobanu AC, Triana del Rio R, Roth LC, Althammer F, Chavant V, Goumon Y, Gruber T, Petit-Demoulière N, Busnelli M, Chini B, Tan L, Mitre M, Froemke RC, Chao MV, Giese G, Sprengel R, Kuner R, Poisbeau P, Seeburg PH, Stoop R, **Charlet A**#, Grinevich V#.
A new population of parvocellular oxytocin neurons controlling magnocellular neuron activity and acute pain processing.
Neuron, 89: 1291-1304. 2016.
Press release: CNRS Press 16/03/03; DNA 16/03/03; Agence France Presse 16/03/03; L'Alsace 16/03/04; Science et Avenir 16/03/03; Le Monde 16/03/07; Pour la Science 16/04; National Geographic France 16/03/04 …

2. Zeitler A*, Kamoun N*, Goyon S, Wahis J, **Charlet A**, Poisbeau P, Darbon P.
Favoring inhibitory synaptic drive mediated by GABAA receptors in the basolateral nucleus of the amygdala efficiently reduces pain symptoms in neuropathic mice.
European Journal of Neuroscience, 43(8):1082-8. 2016.

3. Juif PE*, Breton JD*, Rajalu M, **Charlet A**, Goumon Y, Poisbeau P.
Long-lasting spinal oxytocin analgesia is ensured by the stimulation of allopregnanolone-like neurosteroid synthesis which potentiates GABAA receptor-mediated synaptic inhibition.
Journal of Neurosciences, 33(42):16617-16626. 2013.
Press release: CNRS Press 13/10/16

4. Knobloch HS*, **Charlet A***, Hoffmann LC, Eliava M, Khrulev S, Cetin AH, Osten P, Schwarz MK, Seeburg PH, Stoop R#, Grinevich V#.
Evoked axonal oxytocin release in the central amygdala attenuates fear response.
Neuron, 73(3):553-566. 2012.
Press release: Neuron Preview 12/02/09; Nat Reviews Neuroscience Highlight 12/02/29; Le Temps 2012/02/09; Lausanne University Press 12/02/09; CHUV Press 12/02/10; Impatience 12/02/10; Süddeutsche Zeitung 12/03/03; …

5. Yalcin I, **Charlet A**, Cordero-Erausquin M, Tessier L-H, Picciotto M, Schlichter R, Poisbeau P, Freund Mercier M-J, Barrot M.
Nociceptive thresholds are controlled through spinal β2-subunit-containing nicotinic acetylcholine receptors.
Pain, 152(9):2131-7. 2011.

6. **Charlet A**, Rodeau JL, Poisbeau P.
Poincaré plot descriptors of heart rate variability as markers of persistent pain expression in freely moving rats.
Physiology & Behavior, 104(5):694-701. 2011.

7. Viviani D, **Charlet A**, Robinet C, van den Burg E, Hurni N, Abatis M, Magara F, Stoop R.
Oxytocin selectively gates fear responses through distinct outputs from central amygdala.
Science, 333(6038):104-7. 2011.

Press release: Le Temps 11/07/01; Lausanne University Press 11/07/03; CHUV Press 11/07/03

8. **Charlet A***, Muller A*, Laux A, Schweitzer A, Delalande F, Aunis D, Andrieux A, Poisbeau P*, Goumon Y*.
Abnormal nociception and opiate sensitivity of stable tubule only peptide (STOP) null mice exhibiting elevated levels of the endogenous alkaloid morphine.
Molecular Pain, 6:96. 2011.

9. **Charlet A**, Rodeau JL, Poisbeau P.
Radiotelemetric and symptomatic evaluation of postoperative pain in the rat: long-term anti-hyperalgesic effect of perioperative ropivacaine.
The Journal of Pain, 12(2):246-56. 2011.

10. Aouad M, **Charlet A**, Rodeau JL, Poisbeau P.
Reduction and prevention of vincristine-induced neuropathic pain symptoms by the nonbenzodiazepine anxiolytic etifoxine are mediated by 3α-reduced neurosteroids.
Pain, 147(1-3):54-9. 2009.

11. Yalcin I*, **Charlet A***, Freund-Mercier MJ, Barrot M, Poisbeau P.
Differentiating thermal allodynia and hyperalgesia using dynamic hot and cold plate in rodents.
The Journal of Pain, 10(7):767-73. 2009.

12. **Charlet A**, Lasbennes F, Darbon P, Poisbeau P.
Fast non-genomic effects of progesterone-derived neurosteroids on nociceptive thresholds and pain symptoms.
Pain, 139(3):603-9. 2008.

Publications as Book Chapters

1. Tang Y*, Wahis J*, Melchior M*, Grinevich V[#], **Charlet A**[#].
Optogenetics for Neurohormones and Neuropeptides: Focus on Oxytocin.
OPTOGENETICS: From Neuronal Function to Mapping & Disease Biology, Cambridge University Press of England *(in press)*.

2. Knobloch S*, **Charlet A***, Stoop R, Grinevich V.
Viral Vectors for Optogenetics of Hypothalamic Neuropeptides.
Neuromethods 82, pp 311-329, Humana Press. 2014.

Invited Conferences

1. Ocytocine : un nouvel analgésique ?
   16e congrès de la Société d'Etude & de Traitement de la Douleur
   Paris, France, 25/11/2016.

2. Astrocytes, a new cellular target for oxytocin signaling.
   Society for Neurosciences
   San Diego, USA, 16/11/2016.

3. Oxytocin Neuron Cross Talk Attenuates Nociception.
   12e Symposium du Réseau National Douleur
   Nice, France, 17/03/2016.

4. Oxytocin Neuron Cross Talk Attenuates Nociception.
   Neuropole Conference
   Strasbourg, France, 20/02/2015.

5. Oxytocin Enhance Inhibition in the Central Lateral Amygdala.
   Neurex Annual Meeting
   Basel, Switzerland, 10/06/2013.

6. Improvement of Postoperative Pain by Ropivacaine.
   Measuring Behavior Annual Meeting
   Maastricht, Netherlands, 27/08/2008.

7. Importance of Post-Operative Pain Management.
   Groupe Francophone de Réflexion sur la Télémétrie
   Paris, France, 17/06/2008.

Diffusion of Science

1. « Bibliothèque Médicis: le cerveau dans tous ses états », presented by J. P. Elkabbach
   Bibliothèque Médicis
   Paris, France, 18/11/2016

2. « Les Emotions » discussion around the movie « Inside Out »
   Nef des Sciences
   Mulhouse, France, 29/03/2016.

3. **Charlet A**.
   [Evaluation objective de la douleur spontanée chez l'animal libre de ses mouvements par analyse de la variabilité du rythme cardiaque] (Article in French).
   STAL, 38:25-40. 2012

Past Scientific Work

Introduction

My scientific focus is to better understand how brain networks shape the cognitive processing and emotional status governing our daily life, and how this regulates the dynamics of adaptation driving the suitable reaction of the living organism in its complex environment.

As a first step towards achieving this goal, I joined the lab of Prof. P. Poisbeau (Strasbourg, France) as a PhD student (2006-2009). I developed radiotelemetry monitoring of physiological functions to decipher what are the reactions of the autonomic nervous system to an external threat in a complex emotional experience involving reactions from the entire body: pain. Our main goal was to understand the physiological alterations of autonomic nervous system activity induced by a spontaneous pain. Notably, we found that specific heart rate variability indexes are strongly related to nociceptive inputs, especially if the mean heart rate remains unchanged. This provides strong arguments supporting the adaptability of the autonomic nervous system to a physiological condition, hypothetically as core actor of the classically described "fight or flight" reaction to an identified danger (Charlet et al., *The Journal of Pain*, 2011a; Charlet et al., *Physioly & Behavior*, 2011b; see Past Scientific Work I).

Because brain reactions to the living organism environment are mediated by complex circuits and network interactions, I decided to acquire mandatory electrophysiological and optogenetic skills which nicely complete my radiotelemetry and behavior expertise. Thus, I moved as a postdoctoral fellow in the lab of Prof. R. Stoop (Lausanne, Switzerland) from 2010 to 2013. Here, my goal was to understand and decipher the *ex vivo* and behavioral effects of oxytocin within the amygdala, a core structure in the integration and reaction to stressful events such as fear and pain. We were able to demonstrate that hypothalamic magnocellular oxytocinergic neurons send functional axonal projections to the central amygdala (Knobloch*, Charlet* et al., *Neuron*, 2012), where oxytocin activates a subset of GABA interneurons inhibiting the neurons projecting to the periaqueducal grey - but not to the dorsal vagal complex (Viviani et al., *Science*, 2011). Thus, endogenous oxytocin release decreases the anxious behavior without interfering with heart rate increase, hence eliciting a hypothesized "reaction of courage" when facing a fearful danger (see Past Scientific Work II).

This expertise allowed me to develop in the course of the last years (2013 - *now*) a fully independent research team that expands on the hypothesis that oxytocin is a critical factor modulating our emotional status and cognitive processing. I indeed recently joined the Institute for Cellular and Integrative Neuroscience (INCI, CNRS, Strasbourg, France) as a tenured associate researcher. Supported by strong international collaborations, I created a unique research space using *ex vivo* and *in vivo* electrophysiology, *ex vivo* spinning disk calcium imaging, opto- and pharmaco-genetics. I now wish to develop *in vivo* freely moving calcium imaging and two-photon laser scanning microscopy to tackle our hypothesis with the best accuracy. It offers a unique environment in Strasbourg that will help us to unravel the intermingle between cortical processing and emotions.

In this frame, I am currently responsible of two PhD students (Jérôme Wahis 2013-2017 and Stéphanie Goyon 2015-2018), occasionally supervise a third one (Meggane Melchior 2014-2017) and plan to recruit up to two more PhD students in 2017 (Damien Kerspern, granted by ANR-DFG; Joana Duarte, potentially granted by local doctoral school competition). A

postdoctoral researcher join the lab in 2015 and is responsible for the *in vivo* electrophysiology recordings (Mai Iwasaki 2015-2017). Our research interests are in line with my past experiment, focusing on the neuropeptidergic modulation of emotions with a strong emphasis on oxytocin and neuro-glia interactions.

As a first outcome of my scientific activity as CNRS researcher, we identified a small population of only thirty parvocellular oxytocinergic neurons of particular interest in the control of pain (see Past Scientific Work III-1). Two of PhD students that I supervised are co-firsts authors while I share the co-seniors and corresponding author position on this high-profile publication which has received a particular attention from media with a Metrics score of 207 and already cited by peers (Eliava*, Melchior*, Knobloch*, Wahis* et al., *Neuron*, 2016; see Past Scientific Work III-1). Eventually, we recently submitted the results from Jerome's PhD thesis in a high-profile journal for evaluation and, hopefully, publication in 2017 (see Past Scientific Work III-2).

In addition to my regular scientific responsibilities, I am now expert and treasurer of the local ethical committee (CREMEAS). While time consuming, there is strong interests in such activity: first to address the general public questions regarding animal experimentation and second to ensure good practices and responsibilities of scientists towards their employers (EPST) and funders (public associations and international agencies). Finally, because the communication within the scientific community is necessary to the diffusion of science, I participate to the organization of monthly scientific seminars granted by the Neuropole of Strasbourg – with best wishes for the neurosciences community in our region being wise and intelligent enough to build up a strong and visible unique research institute in the coming years… I believe these two "side" activities are essential to the general interest of scientific activities, particularly in the current difficult context.

The next pages of this manuscript provide a detailed description of the most significant scientific results emerging from my scientific activities, collaborations and supervisions. Finally, the two emerging projects from my lab are briefly described – one is granted, the second is under evaluation and maturation.

I - Functional Exploration of Pain and its Spinal Modulation in Rodents

From 2006 to 2010, I did my PhD research thesis at University of Strasbourg. My work was mainly dedicated to the development of new tools and methods able to objectively quantify the spontaneous expression of pain in rodents.

Pain is defined by the International Association for the Study of Pain as "an unpleasant sensory and emotional experience associated with actual or potential tissue damage or described in terms of such damage". This definition highlights the complexity and the subjective character of such a sensation. Because pain verbalization is not always possible and/or reliable in human patients, the development of new methods in order to quantify objectively pain expression is still of actuality (Hummel et al., 2006). Evaluation of pain in animal experimentation is also a major ethical issue in our modern society and represents a challenge for research in the field.

Radiotelemetry probes are intraperitoneal implantable biosensor allowing the monitoring of up to four physiological parameters (electrocardiogram, blood pressure, temperature, locomotor activity) in freely-moving and unstressed animals (Kramer and Kinter, 2003; Figure 1). This is an optimal technique to monitor the activation of the autonomic nervous system and thus allowed us:

1) To monitor the postoperative pain following probe implantation and to demonstrate the efficacy of local anaesthetics during the perioperative period (Charlet et al., *The Journal of Pain*, 2011a);

2) To characterize the autonomic nervous system activity modifications in response to a spontaneous painful episode (Charlet et al., *Physiology and Behavior*, 2011b). This was the basis for my PhD "Chantal Autissier" Award, from AFSTAL, and the publication dedicated to non-scientific readers in the STAL journal (Charlet, *STAL*, 2012).
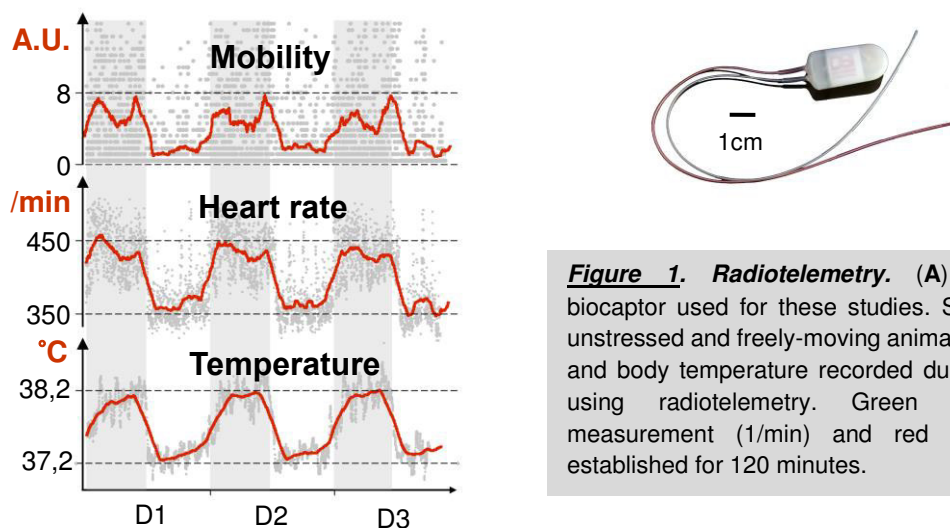

Figure 1. Radiotelemetry. (**A**) The intra-peritoneal biocaptor used for these studies. Signal is recorded form unstressed and freely-moving animal. (**B**) Activity, heart rate and body temperature recorded during 3 continuous days using radiotelemetry. Green dots are individual measurement (1/min) and red line a mean-average established for 120 minutes.

1 - Radiotelemetric and Symptomatic Evaluation of Pain in the Rat after Laparotomy

Postoperative pain is a form of acute pain directly resulting from the surgical trauma. It produces a severe inflammatory reaction and initiates an afferent neuronal barrage leading to several unpleasant sensory/emotional experiences associated with abnormal autonomic, endocrine–metabolic, physiological and behavioral responses (Janig, 1995; Le Bars et al., 2001). At the site of injury, local hyperexcitability is responsible for major peripheral and central plastic changes affecting the processing of nociceptive messages (Scholtz and Woolf, 2002). The risk of transition from acute pain into a chronic pain state is a challenge for future research, as well as the potential of effective acute pain treatment (possibly pre-emptive) to reduce the risk of chronic pain. There is a vast and controversial literature regarding the clinical efficacy of perioperative analgesia care aimed at improving recovery from surgery, while it is strongly recommended and frequently used in clinic (Wilder-Smith and Arendt-Nielsen, 2006). The reason is that it is theoretically expected that a reduction in the excitability of freshly-cut peripheral sensory nerves will prevent an excessive peripheral/central sensitization and, therefore, will presumably reduce pain expression as well as recovery time from surgery (Moiniche et al., 2002).

To extend our general knowledge on postoperative pain and its possible means of improvement, we analyzed simultaneously behavioural and physiological/autonomic alterations associated with the presence of pain symptoms and focus on two objectives:

a) **To identify and quantify spontaneous pain expressio**n after major abdominal surgery using a radiotelemetric monitoring of several physiological parameters in freely-moving animals. These physiological changes were further considered as being spontaneous signs of pain if they were timely correlated with the presence of a skin hyperalgesia around the scar and sensitive to the alkaloid morphine, the non-steroidal anti-inflammatory drug ketoprofen and the local anesthetic ropivacaine;

b) **To assess the efficacy of a perioperative pain care** using the local anesthetic ropivacaine, a compound that has not been characterized with a combined symptomatic and physiological approach in a major surgery involving skin, muscles, and peritoneum incisions. We also chose ropivacaine because it exerts a preferred action on tetrodotoxin-resistant voltage-gated sodium channel subtypes that are expressed by small unmyelinated C-fibres in physiological conditions and are submitted to major plastic changes in pathological pain situations. Moreover, ropivacaine displays limited motor block, has no effect on basal cardiovascular parameter and, when used acutely, shows little central nervous system and cardiac toxicity.

Finally, we succeed to provide strong experimental evidence that perioperative analgesia using the long acting local anesthetic ropivacaine is efficient to prevent postoperative pain following a controlled abdominal surgery in the rat. During the postoperative period we have been able to measure the time course of mechanical hyperalgesia and the timely-correlated signs of pain seen as long-lasting alteration of the animal mobility, elevated heart rate and variability. Hyperalgesia and pain-associated physiological alterations persisted for up to ten days in our experimental conditions and were fully precluded by a single preventive ropivacaine treatment during the perioperative period but not at later stages.

Radiotelemetric and Symptomatic Evaluation of Pain in the Rat After Laparotomy: Long-Term Benefits of Perioperative Ropivacaine Care

Alexandre Charlet,* Jean-Luc Rodeau,* and Pierrick Poisbeau*,†

*Centre National de la Recherche Scientifique, Institut des Neurosciences Cellulaires et Intégratives, Unité Propre de Recherche 3212, Nociception and Pain Department, Strasbourg, France.
†Université de Strasbourg, Strasbourg, France.

Abstract: Effective relief of acute and long-term postoperative pain is of utmost importance to patients undergoing surgery. Here, we worked on a controlled procedure of abdominal surgery in the rat inducing persistent postoperative pain symptoms for up to 10 days and tested the efficacy of perioperative care with the local anesthetic ropivacaine. Laparotomy was likewise used to implant radiotelemetric probes by which electrocardiogram, body temperature, and locomotor activity were recorded in freely moving animals. We showed that postoperative pain symptoms (mechanical allodynia) measured in periphery of the scar were associated over time with persistent tachycardia, elevated heart rate variability, and loss of mobility. Furthermore, a single subcutaneous infiltration of the local anesthetic ropivacaine in the periphery of the abdominal incision was sufficient to prevent the appearance of allodynia and the associated cardiac and motor signs of pain, monitored by radio-telemetry. These beneficial effects were observed when the infiltration was performed in the perioperative period, but not later. This study on freely moving animals exhibiting long-lasting postoperative pain symptoms and altered autonomic/motor function illustrates well the importance of the timing of preemptive analgesia care with long-acting local anesthetics. Moreover, it emphasizes the utility of monitoring heart rate variability to quantify spontaneous expression of long-lasting postoperative pain.

Perspective: *Speeding the recovery time after surgery using perioperative ropivacaine care is of significant clinical relevance because it might limit the risk of chronic pain and postoperative complications. In humans, chronobiological analysis of heart rate variability could also help quantify spontaneous pain expression with minimal emotional bias.*

© 2011 by the American Pain Society
Key words: Incisional pain, autonomic nervous system, local anesthetics.

Postoperative pain is a form of acute pain directly resulting from surgical trauma. It produces a severe inflammatory reaction and initiates an afferent neuronal barrage leading to several unpleasant sensory/emotional experiences associated with abnormal autonomic, endocrine-metabolic, physiological, and behavioral responses. At the site of injury, local hyperexcitability is responsible for major peripheral and central plastic changes affecting the processing of nociceptive messages.[38,47] If most of the short-term pathogenic mechanisms of incisional pain are now fairly well understood, the long-term consequences of postoperative pain still require investigation. In particular, the risk of transition from acute pain into a chronic pain state is a challenge for future research, as well as the potential of effective acute pain treatment (possibly pre-emptive) to reduce the risk of chronic pain.

To extend our general knowledge on postoperative pain and its possible means of improvement, new approaches must be developed to quantify the intensity and duration of spontaneous pain expression in animal experimentation. For instance, behavioral[20,23] and physiological/autonomic[18] alterations associated with the presence of pain symptoms need to be analyzed

simultaneously in pertinent animal models of postoperative pain.[20] Interesting tools are presently available to detect and possibly measure physiological expression of nociception in freely-moving animals using implanted miniaturized radiotelemetric probes.[22] These probes are capable of monitoring simultaneously 3 to 4 physiological parameters, with a high resolution and for long periods of time. Because they are generally implanted in the abdominal space, they also offer a unique opportunity to study postoperative pain signs in rodents submitted to a precisely defined surgery procedure. Though some data are presently available regarding the alteration of physiological parameters following probe implantation,[1,4,13,39] there are none which directly describe the time-course correlation between pain-related changes in physiological parameters, behaviors, and sensory-motor threshold sensitivity (allodynia and/or hyperalgesia) around the scar. Apart from monitoring pain-associated alteration of locomotion, skin conductance, or body temperature, pain expression has been successfully related to excessive heart rate variability in anesthetized humans[19,24] and infants.[27] It is, therefore, particularly important to focus on cardiovascular parameters while using animal models of acute and persistent pain. In most pain models, no changes in the mean heart rate can be detected and, based on human studies, the heart rate variability (eg, variability between RR waves of the ECG) is postulated to be an interesting alternative pain marker.[19,24,35] Until now, there are little data available regarding its possible use to monitor postoperative recovery from surgery in relation with the progressive disappearance of pain symptoms and the efficacy of perioperative analgesia care.[1]

There is a vast and controversial literature regarding the clinical efficacy of perioperative analgesia care aimed at improving recovery from surgery.[26] At the same time, perioperative analgesia is strongly recommended and frequently, if not systematically, prescribed at the hospital. The reason is that it is theoretically expected that a reduction in the excitability of freshly-cut peripheral sensory nerves will prevent an excessive peripheral/central sensitization[7,38,46] and, therefore, will presumably reduce pain expression as well as recovery time from surgery. In contrast to many animal studies, data from human trials do not fully support this hypothesis[26] and point out the importance of timing for the analgesia care. Among the numerous drugs that are used during the perioperative period in humans, local anaesthetics are efficient to block the peripheral afferent neuronal barrage of nociceptive messages resulting from surgery. In many instances, they have been used with success[44] to prevent episodes of pain seen immediately after awakening (ie, 24 hours after surgery) and more rarely at later time points.[11,15,41,42,44] In animal models, beneficial effects of perioperative analgesia care were found following injections of local anaesthetics in studies of the tonic inflammatory nociceptive responses to intraplantar formalin,[9,48] of the autotomy frequency rates following sciatic nerve transection,[14] or of the failed back-surgery syndrome.[36]

The first objective of the present study was to identify and quantify spontaneous pain expression after major abdominal surgery using a radiotelemetric monitoring of several physiological parameters in freely-moving animals. These physiological changes were further considered as being spontaneous signs of pain if they were correlated over time with the presence of a skin hyperalgesia around the scar and sensitive to the alkaloid morphine, the nonsteroidal anti-inflammatory drug ketoprofen, and the local anesthetic ropivacaine. In a second step, we also sought to test the efficacy of a perioperative pain care using the local anesthetic ropivacaine, a compound that has not been characterized with a combined symptomatic and physiological approach in a major surgery involving skin, muscles, and peritoneum incisions. We chose ropivacaine because it exerts a preferred action on tetrodotoxin-resistant voltage-gated sodium channel subtypes[28] that are expressed by small unmyelinated C-fibres (and neurons) in physiological conditions and are submitted to major plastic changes in pathological pain situations.[43] Moreover, ropivacaine displays limited motor block,[40] has no effect on cardiovascular parameters,[29] and, when used acutely, shows little central nervous system and cardiac toxicity.

Methods

Ethical Approval

All experiments were conducted in conformity with the recommendations of the European Committee Council Direction of November 24, 1986 (86/609/EEC), with an authorization for animal experimentation from the French Department of Agriculture (License 67-116 to P.P.) and with the agreement of the regional ethical committee (authorization number AL/10/13/03/07).

Animals

Male Sprague-Dawley rats (Janvier, Le Genest-Saint-Isle, France) weighing ~350 g at the beginning of experiments were used for this study. Animals were housed individually under standard conditions (room temperature 22°C; 12 hour light/dark cycle; lights on at 0700) with ad libitum access to food and water. Before the onset of the experiment, all animals were subject to at least 1 week habituation to the experimental room, to handling, and to behavioral testing. Behavioral tests were done during the light period (between 1000 and 1600 hours).

Surgical Implantation of the Radiotelemetric Probe

Implantation of the radiotelemetric transmitter (model TA11CTA-F40; Data Sciences International, St Paul, MN) was performed under sterile conditions while animals were deeply anesthetized with a cocktail of ketamine (87 mg/kg; Imalgène 1000; Merial, Lyon, France) and xylazine (13 mg/kg; Sigma, St Louis, MO). The surgery field was shaved and carefully cleaned with povidone iodine dermal solution (Betadine Scrub 4%; Viatris, Mérignac, France). A first incision of about

2 cm was made medially through the skin, the abdominal muscle and the peritoneum to implant the transmitter. Inside the peritoneal space, the transmitter was tightly stitched to the abdominal muscles with 3 points using a nonresorbing suture (Silcam 4/0, Braun, France). The 2 electrodes used to record the electrocardiogram (ECG) were placed under the skin and firmly sutured to the muscles at the level of the last left rib and under the right axilla. Two cutaneous incisions allowing placement of the ECG electrodes were sutured and cleaned with betadine. A precise 50-minute surgery time was respected, and incised muscles were retracted during this whole period. Transmitters were activated immediately after surgery in order to monitor mobility, heart rate, and abdominal temperature from the freely-moving animals during the postoperative recovery period.

Radiotelemetry Analysis

Mobility, heart rate, and abdominal temperature were recorded using DSI Data Exchange Matrices (Data Sciences International). Data were transmitted on-line using radio frequency waves at 455 kHz and stored on a remote-controlled computer. Animal locomotor activity (in arbitrary unit, AU), heart rate (beats per minute, bpm) and abdominal temperature (°C) were calculated every minute during a recording waveform of 20 seconds at an acquisition rate of 1 kHz for each animal, using DataQuest ART 4.0 (Data Sciences International). After acquisition, data were exported as Excel and text files for further analysis.

Noninvasive baseline measurements of mobility were also made with the ActiV-Meter (Bioseb, Chaville, France) actimetry measurement system. Stable mobility values for telemetry-implanted rats, 15 to 20 days after surgery, were similar to the baseline values for naïve rats (data not shown).

Rhythmograms were constructed by double-plotting successive 24-hour periods (horizontal scale) over days after surgery (vertical scale). Mobility was displayed on standard actograms with scale cutoff at 20 AU. Pseudo-color scales were used for heart rate and temperature. Mean graphs were built by calculating the average of each parameter over the 12 hours of each day (7–19 hours, light period) or night (19–7 hours, dark period) period.

For heart rate variability (HRV) analysis, RR intervals and heart rate were calculated for successive segments of 20-second electrocardiogram recording (ie, giving more than 100 PQRST complexes given the heart rate of rats), over a period of 20 minutes. R waves were automatically detected and individual errors were manually checked using Clampfit 10.2 software (Molecular Devices, MDS Analytical Technologies, Toronto, Canada) before extracting RR intervals. Time domain analysis of heart rate variability (HRV) allowed to obtain SD1, 1 descriptor of the Poincaré plot for RR intervals,[5,31] describing the short-term HRV. SD1 was calculated as $SD1 = SDSD/\sqrt{2}$, where SDSD is the standard deviation of the successive differences of the RR intervals, $\Delta RRn = RRn-RRn+1$.[5] SD1 was calculated for each 20-second segment. The mean and the standard deviation of the values obtained for all segments provided a global SD1 for each animal, as well as an estimation of its variability, SD(SD1). Part of this variability was found to arise from occasional large alterations of the RR interval which were clearly not artifactual. We therefore counted, for each 20-second segment, the number of ΔRRn values larger than ~10% of the mean value. They are referred in the text as pNN18, expressed in ‰, and correspond to an arbitrary threshold change in the RR interval of 18 ms.

Evaluation of Postoperative Pain Symptoms

Before the beginning of experiment, animals were habituated to handling and testing for about 1 week. Touch test von Frey filaments with logarithmic incremental stiffness (4, 6, 8, 10, 15, 26, 60 g; Bioseb, Chaville, France) were used to determine the nociceptive mechanical threshold at the periphery of the abdominal scar. Animals were placed in clear Plexiglas (Arkema Inc, Philadelphia, PA) enclosures (24 × 14 × 30 cm) on an elevated metallic mesh. After 15 minutes habituation to the testing box, filaments with increasing stiffness were successively applied at a time interval of at least 30 seconds and after full return of the animal to its resting behavior. Each filament was applied 5 times during 2 seconds with a test-free interval of 5 seconds at the periphery of the abdominal scar. The nociceptive pressure threshold was reached when the animal exhibited a minimum of 3 aversive behavioral responses for 5 consecutive stimuli (based on Chapman et al[8]). Licking of the scar, abdominal withdrawal, or escape behavior were all counted as aversive responses. The 26-g filament was the stiffest tested (ie, maximum measured value), because the 60-g filament was too stiff to bend when applied on rat abdomen. The von Frey tests were conducted blind with respect to the treatments received by animals.

Drugs

Postoperative pain symptoms sensitivity to some analgesics was characterized after a unique intradermal injection (300 μl) around the scar of ketoprofen (Centravet, Taden, France; 10 mg/kg), morphine hydrochloride (Sigma Aldrich, St Louis, MO; 5 mg/kg) or ropivacaine (Naropeine; AstraZeneca, France; 2 mg/ml). Mechanical von Frey thresholds were measured 1 hour after the injection. Perioperative ropivacaine care was evaluated with single systemic administration or subcutaneous injection around the scar (300 μl; 2 mg/mL), before awakening of the animal, before, or after surgery. For all injections done in hyperalgesic animals, we used short-term and rapidly reversible anesthesia with 3% halothane (Belamont, Paris, France) to limit stress. Animals were tested for mechanical nociception 30 minutes later.

Statistical Analysis

Data in text are expressed as mean ± standard deviation. Mean values of the mobility, heart rate, temperature or mechanical hypersensitivity were compared at different times and between treatment groups. Repeated-measures 2-way or 3-way ANOVA, with factors treatment (between), time and day/night (within), were

performed with Statistica 5.1 (Statsoft, Tulsa, OK). When the ANOVA test was significant, the Tukey test was used for post hoc multiple comparisons between individual groups. The ordinal data from von Frey experiments were analyzed with nonparametric statistics on ranks using KyPlot 2.15 (KyensLab, Tokyo, Japan). Friedman test for the effect of time within a given treatment group and Wilcoxon-Mann-Whitney or Kruskal-Wallis test for between-groups comparison at a given time were used, followed by Steel test for multiple comparisons. Differences were considered significant for $P < .05$.

Results

Time-Course of Postoperative Abdominal Hyperalgesia and Sensitivity to Analgesics

The long-lasting procedure of laparotomy used in this study to implant radiotelemetric probes is obviously expected to induce a significant abdominal incisional pain. In a first set of experiments, we measured the evolution of mechanical nociceptive thresholds with von Frey's filaments applied around the scar (see Methods) during the postoperative period (Fig 1A). At day 1 after surgery, the mean pressure threshold to induce a nociceptive response was of 8.0 ± 1.6 g (Fig 1A; n = 4), a value corresponding to severe hyperalgesia when compared to values found in the same animals after shaving before surgery (20.5 ± 6.4 g, n = 4). Rats remained hyperalgesic for about 9 days and normal mechanical threshold values of the skin to nociceptive pressure stimulus were recovered after 10 days (Fig 1A).

We next tested the sensitivity of postoperative pain symptoms to various analgesics (Fig 1B). This was done at postoperative day 3, where von Frey threshold mean value was 8.3 ± 1.3 g (n = 8), indicating that the animals were still hyperalgesic. One hour after a single intradermal infiltration around the scar of the long-lasting local anesthetic ropivacaine (2 mg/kg), mean von Frey threshold reached its maximum cut-off value of 26.0 g (n = 8). This full antihyperalgesic effect of ropivacaine, however, was transient, returning back to a hyperalgesic value of 10.0 ± 3.3 g after 24 hours (Fig 1B; day 4; n = 8). Similarly to ropivacaine action, the intradermal infiltration of morphine around the scar (5 mg/kg) induced a strong anti-hyperalgesic effect: The von Frey threshold reached the maximal cut-off value of 26.0 g (Fig 1B; n = 6) 30 minutes after infiltration, whereas this threshold was 7.8 ± 3.6 g just before infiltration (Day 3; n = 6) and 8.5 ± 3.6 g at day 4. Eventually, intradermal infiltration of the nonsteroidal anti-inflammatory drug (NSAID) ketoprofen at 10 mg/kg induced a significant but smaller increase of von Frey threshold (Fig 1B), from 7.7 ± 2.0 g before injection (Day 3) to 14.0 ± 6.5 g after 30 minutes, and back to 8.5 ± 3.6 g after 24 hours (Day 4; n = 6).

Physiological Consequences of the Radiotelemetric Probe Implantation

One of the major interests of radiotelemetry is the continuous and parallel monitoring of several physiological
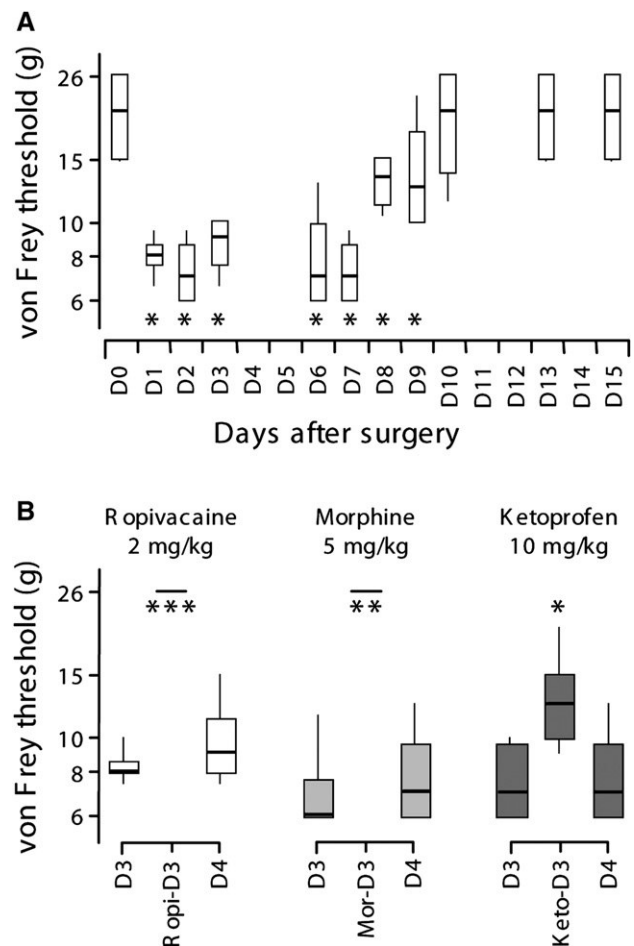

Figure 1. Postoperative pain development and sensitivity to some analgesics. **(A)** Time course of mechanical hyperalgesia measured with the Von Frey's filaments before (Day 0) and after abdominal surgery (D1–15) of rats (n = 4). Results are expressed as median with first and third quartiles (boxes), and 10th and 90th percentiles (whiskers). After surgery, a mechanical hypersensitivity around the scar developed with time (Friedman test, $\chi^2_{10} = 33.7$, $P = .0002$) and was no longer detectable after day 10. **(B)** Effects of intradermal infiltrations of ropivacaine (2 mg/kg; n = 8), morphine (5 mg/kg; n = 6), and ketoprofen (10 mg/kg; n = 6) in hyperalgesic rats, 3 days after surgery. Thresholds were measured 1 hour after the injection. Results are expressed as median with first and third quartiles (boxes), and 10th and 90th percentiles (whiskers). With all 3 substances, a statistically significant transient analgesia was observed 30 minutes after injection (Test) that disappeared at 24 hours (D4). Ketoprofen had a lesser effect than morphine and ropivacaine. Significance code: *$P < .05$; **$P < .01$; ***$P < .001$. (D3 versus Test; Friedman test followed by Steel test).

parameters in nonhandled freely-moving animals. We used this interesting feature to characterize the physiological consequences of our major surgical procedure (Fig 2).

Rats are nocturnal animals, normally active at night and resting during day. They thus display more elevated values of heart rate and body temperature during night than during their diurnal resting period (Fig 2). As shown in Fig 2A, the normal circadian rhythm of alternating high and low values of physiological parameters was strongly altered after surgery. In this representative example (but also seen for all animals monitored), we noted an impaired mobility during night time, reduced
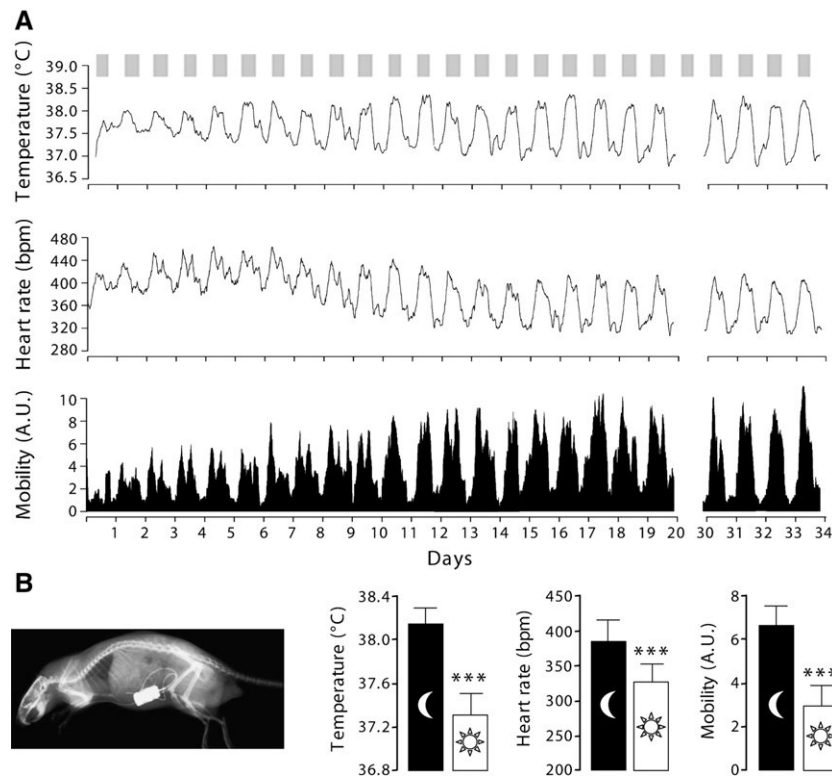
Figure 2. Radiotelemetric monitoring of some physiological parameters during the postoperative period. **(A)** Values of abdominal temperature (in °C; top graph), heart rate (in beat per minute; middle graph), and mobility (in arbitrary unit; lower graph) continuously monitored in a rat just after abdominal surgery (day 0) and for about a month. Each black line or bar (lower graph) corresponds to a moving average over a 120-minute time window and clearly illustrates the circadian fluctuations between day and night time (gray bars: 12 hours from 1900 to 0700). **(B)** Radiography of an implanted rat (courtesy of Data Science International) showing the intraperitoneal implantation of the core of the transmitter, as well as the subcutaneous electrodes for ECG recording. Graphs on the right giving mean values (±SD) over 12 hours of night (moon symbol) and day (sun symbol) were averaged for 16 healthy rats at postoperative day 15. Significance code: ***$P < .001$ (Student t-test).

abdominal temperature changes between night and day time, and long-lasting tachycardia, for about 10 days after surgery. It should be noted that we did not show pretest (eg, before surgery) for radiotelemetric studies because transmitters cannot record parameters before being implanted. To overcome this difficulty, we used day 15 as a control, because, from day 15 and for up to 2 months, mean heart rate, mobility, and abdominal temperature remained stable and were not significantly different (Fig 2B, see also Fig 3). It should be noted that postoperative stabilized values were previously shown to be similar to baseline values, at least for heart rate, in mice.[1]

Long-Lasting Mechanical Hyperalgesia Following Surgery is Prevented by Local but Not Systemic Perioperative Ropivacaine Care

In an attempt to reduce recovery time from surgery and to limit pain symptoms of the implanted rats, we decided to use ropivacaine during the perioperative period. In a first group of animals (n = 4), a single subcutaneous infiltration of ropivacaine was performed around the scapula (eg, far from the incision) in order to reveal a possible systemic effect. Under these conditions, we failed to reveal any systemic effect on pain symptoms

because mechanical hyperalgesia (Fig 4A) followed the same time course as saline controls (not shown but see Fig 1A). We next performed a single intradermal infiltration of ropivacaine just after surgery and before awakening of animals (Fig 4B). Surprisingly, this single infiltration fully prevented the appearance of mechanical hyperalgesia (Fig 4B) after surgery. The initial mean nociceptive threshold (20.5 ± 6.4 g at day 1; n = 4) was similar to that observed for naïve animals and for untreated rats having fully recovered from surgery (Fig 1). As seen in Fig 4B, ropivacaine infiltration fully prevented the appearance of hyperalgesia during the 10 days following surgery, although ropivacaine should have been fully cleared after a much shorter time (Fig 1B). When ropivacaine was administered immediately before laparotomy, a similar result was observed (Fig 4C). Measured with von Frey filaments around the scar, nociceptive mean threshold value of this group was 22.0 ± 8.0 g at day 1 (n = 4). It remained stable and not significantly different during the following days (Fig 4C).

The spectacular effect of perioperative ropivacaine care on pain symptoms was extremely intriguing because there is little, if any, consensus regarding the use of local anesthetics for improving recovery from surgery in human and very little evidence in animal experimentation. For all these reasons, we took advantage of our highly resolutive radiotelemetric monitoring of heart rate,
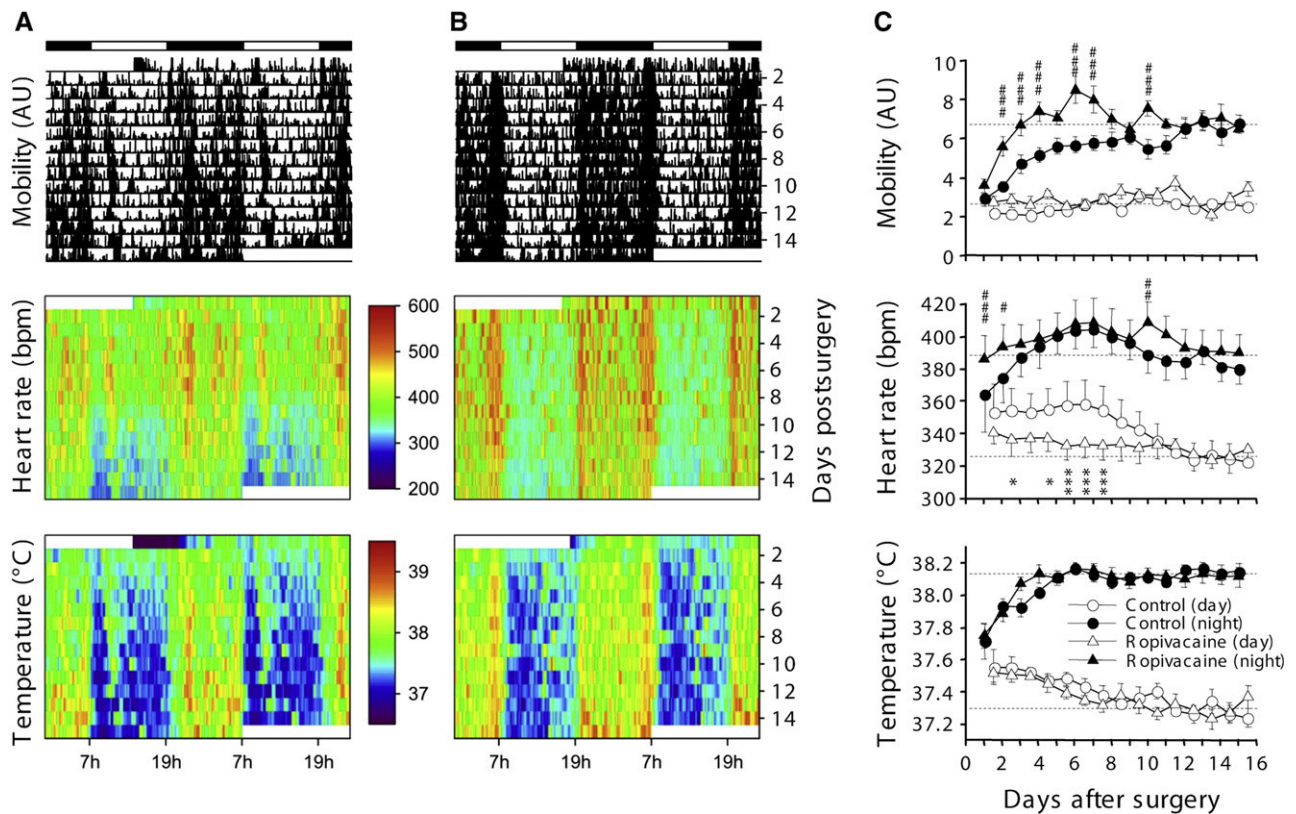
Figure 3. Consequences of perioperative ropivacaine care on the recovery of mobility heart rate and abdominal temperature. **(A, B)** Representative rhythmograms of mobility (top), heart rate (middle), and temperature (bottom) in a control (saline-injected: **A**) and ropivacaine-treated animal **(B)**. In the ropivacaine-treated animal, a regular day/night pattern was established from the first day for each mobility and heart rate while this rhythm was strongly altered in control animals. The pattern of temperature changes was similar in both animals. **(C)** Average values of recorded parameters over 12 hours for 15 postoperative days. The values are given during the resting period (7–19 hours, light; white symbols) or the active period (19–7 hours, dark; black symbols) in control (n = 8) and ropivacaine-treated rats (n = 8). Three-way ANOVA, with between factor treatment (control versus ropivacaine) and within factors bio-rhythm (night versus day) and days after treatment, showed a significant effect of the interaction of the 3 factors in the case of mobility ($F_{14, 196}$ = 3.72, $P <$ .001) and of heart rate ($F_{14, 196}$ = 3.39, $P <$ .001), and, in the case of temperature, no effect of treatment, but an effect of the interaction of the 2 within factors ($F_{14, 196}$ = 30.00, $P <$ .001). Statistically significant differences between the control group (n = 8) and the ropivacaine-treated group (n = 8) are marked by # for night and * for day values. Dashed horizontal lines show stabilized values (average at day 15).

mobility, and abdominal temperature to objectively characterize postoperative recovery in nonhandled freely-moving animals.

Perioperative Care With Ropivacaine Improves Recovery From Surgery

Implanted rats received a perioperative intradermal infiltration of either ropivacaine or saline (.9% NaCl) at the end of the surgery. As previously seen (Fig 2; noninjected rats), the normal circadian rhythm of alternating high and low values of physiological parameters was strongly altered after laparotomy in the control group (saline-injected). This is particularly well illustrated in Fig 3A in the form of rhythmograms for a single animal. The diurnal and nocturnal average value of each parameter over 12 hours was also calculated for each animal and displayed in Fig 3C as group means.

During the first nights following surgery, all animals had a reduced mobility. They were mainly active at the beginning and at the end of the night, with recurrent

periods of immobility in the interval (Fig 3A, upper panel). This resting period was progressively reduced as the animals recovered. The mobility index for the active period had a low initial mean value of 2.9 ± 1.0 AU (arbitrary units, n = 8) during the night after surgery, and progressively increased to a stable value of 6.8 ± 1.1 AU at day 15 (Fig 3C, upper panel, black circles). Night mobility values significantly differed from the value at day 15 during the first 4 days after surgery. Consistent with reduced mobility, nocturnal values of heart rate and abdominal temperature were initially lower (respectively 364 ± 64 bpm and 37.71 ± .30°C at day 1, n = 8) than after full recovery (380 ± 26 bpm and 38.15 ± .07°C at day 15; Fig 3C, middle and lower panels, black circles). During the diurnal resting period, mobility remained minimal, with an overall average value of 2.7 ± .3 AU (Fig 3C, upper panel, open circles). It was never significantly different from the diurnal value at day 15. However, heart rate was elevated immediately after surgery (Figs 3A and C, middle panels), reaching 358 ± 42 bpm at day 6, before decreasing to a stable control value of 322 ± 26 bpm at day 15 (Fig 3C,
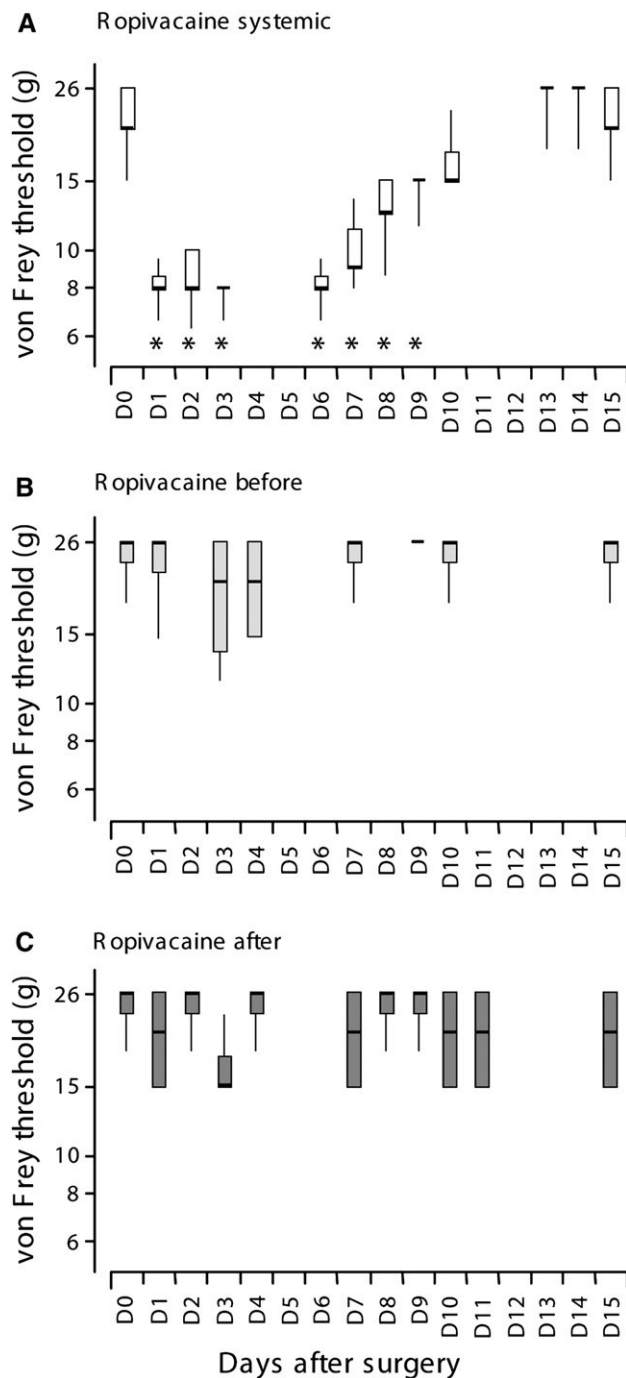
Figure 4. Development and recovery of postoperative pain symptoms in ropivacaine treated animals. Results are expressed as median with first and third quartiles (boxes), and 10th and 90th percentiles (whiskers). Rats injected with ropivacaine before (**B**; n = 4) and after surgery (**C**; n = 4) are compared with those having received a systemic ropivacaine injection (**A**, n = 4). After surgery, a mechanical hypersensitivity developed with time in animals with a scapular (systemic) injection of ropivacaine (Friedman test χ^2_{12} = 40.4; *P < .0001) whereas no significant change with time was observed in animals injected with ropivacaine next to the incision, either before (χ^2_7 = 7, P = .43; panel **B**) or after surgery (χ^2_{10} = 4.39, P = .93; panel **C**). A significant difference (Wilcoxon test, P < .05) was observed between animals receiving a local (panels **B** and **C**) or a systemic injection of ropivacaine (panel **A**) from day 1 to day 7.

middle panel, open circles). Diurnal heart rate values were significantly different from that at day 15 during the first 8 days after surgery. The initial recorded values of body temperature were about 33°C, due to the partial loss of homeothermic regulation while animals were still recovering from general anesthesia in their home cage. Although this is not obvious on the temperature rhythmograms (Fig 3A, lower panel), during the first week following surgery the animals displayed a slight diurnal hyperthermia, which was better seen on average values (37.55 ± .31°C at day 2; Fig 3C, lower panel, open circles). This hyperthermia progressively disappeared and abdominal temperature stabilized at 37.24 ± .15°C. Diurnal average temperature was significantly different from the value at day 15 during the first 5 days after surgery, whereas night values were no longer different from the final stabilized value after the 3 first days.

Altogether, full recovery of physiological parameters was achieved after about 8 days in control rats (saline-injected; n = 8; Fig 3) similarly to noninjected animals (n = 4; see Fig 2). As animals recovered their basal day/night rhythm, the difference between the diurnal and the nocturnal values of physiological parameters progressively increased.

In good agreement with the absence of pain symptoms following surgery, with respect to control animals (saline-injected), ropivacaine-treated animals showed less disturbed circadian rhythms for mobility, heart rate, and abdominal temperature, immediately after surgery and during the following days (Fig 3B). Moreover, they did not show reduced nocturnal mobility or diurnal tachycardia, as did control animals. As soon as day 2, these animals exhibited stable values of diurnal heart rate (336 ± 30 bpm; n = 8) and nocturnal mobility (5.6 ± 1.4 AU), similar to those obtained at day 15 for the corresponding parameters (330 ± 20 bpm, and 6.5 ± .6 AU respectively) (Fig 3C, upper and middle panels). It should be noted, however, that the initial diurnal hyperthermia, probably resulting from the scarring process, resisted ropivacaine treatment, because both vehicle- and ropivacaine-treated animals displayed the same temperature time course (Fig 3C, lower panel). It should also be noted that we failed to reveal any effect of systemic perioperative ropivacaine (n = 8; not shown) or intradermal ropivacaine at postoperative day 3 (not shown; n = 8) on the recorded physiological parameters.

Taken together, these results show that an immediate postoperative ropivacaine infiltration is able to suppress the durable postoperative hyperalgesia and the associated motor and autonomic manifestations of pain, such as the elevation of diurnal heart rate. We also performed a single infiltration of ropivacaine 10 minutes before starting the surgery. Similarly to what was found in animals treated with ropivacaine after surgery, animals rapidly showed normal circadian rhythms, stable values for nocturnal mobility and diurnal heart rate (not shown, n = 4). In good agreement with the lack of pain signs using radiotelemetry, the mechanical thresholds were not significantly different from naïve animals or from implanted animals having received ropivacaine at the end of the surgery before awakening.

Heart Rate Variability Analysis is a Good Quantitative Indicator of Pain Expression and Confirms the Interest of Perioperative Ropivacaine Care

To reinforce our conclusions, we performed a heart rate variability (HRV) analysis using the high-resolution ECG recorded from our implanted animals (see Methods). HRV changes are indeed widely used to monitor levels of consciousness during anesthesia and elevated HRV are sometimes claimed to be associated with the presence of chronic pain.

We first characterized mean HRV parameters (SD1, SD [SD1], and pNN18) at postoperative day 3 (eg, on hyperalgesic animals), before and after intradermal infiltration of ropivacaine (Fig 5). This treatment was previously shown to transiently suppress abdominal hyperalgesia resulting from the implantatory surgery (Fig 1B). Hyperalgesic rats treated or not with ropivacaine did not show any significant differences in their mean heart rate which remained around 300 bpm (not shown). This was not the case for HRV parameters (Figs 5A–C), which were clearly different between hyperalgesic (Day 3 before injection; Day 4, 24 hours after injection) and nonhyperalgesic rats (Day 3, just after injection; Day 15, control, long after recovery from hyperalgesia). After intradermal infiltration of ropivacaine (Figs 5A–C; black bars) SD1 and SD (SD1) mean value were of 1.78 ± .15 seconds and of .68 ± .16 seconds and statistically smaller than their respective control measured before infiltration (SD1: 3.96 ± .72 seconds ; SD(SD1): 2.86 ± .43 seconds ; n = 4). RR event intervals differing by more than 18 ms were fre-

quently observed in hyperalgesic animals (Day 3: 6.59 ± 1.15‰; Day 4: 7.38 ± 2.05‰; n = 4) whereas they were extremely rare after ropivacaine treatment (Day 3 after ropivacaine: 1.09 ± .85‰; n = 4) or after full recovery from surgery (Day 15: .49 ± .34‰; n = 4).

To understand further the effects of ropivacaine in perioperative care, we performed a similar HRV analysis on animals recovering from surgery and having received an intradermal infiltration of ropivacaine (Figs 5D–F, black bars) or saline (Figs 5D–F, white bars) at the end of surgery and before awakening. Saline-treated animals at day 3 exhibited high values for SD1 (3.72 ± 1.07 seconds; n = 8), SD(SD1) (2.76 ± 1.32 seconds; n = 8), and pNN18 (5.39 ± 2.33‰; n = 8). These values were significantly reduced ropivacaine-injected rats (Figs 5D–F, black bars; SD1: 1.65 ± .17 seconds; SD(SD1): .48 ± .12 seconds; pNN18: .35 ± .23‰; n = 8) and similar to those found in nonhyperalgesic rats, eg, having fully recovered from hyperalgesia at day 15.

Altogether, these results strongly suggest that HRV analysis and in particular the quantification of SD1, SD (SD1), and pNN18 are precious quantitative indexes of pain expression. Moreover, they are likely to be useful in order to monitor spontaneous pain expression, at least in this model of abdominal hyperalgesia following surgery.

Discussion

The findings indicate that perioperative analgesia using the long-acting local anesthetic ropivacaine is efficient to prevent postoperative pain following a controlled
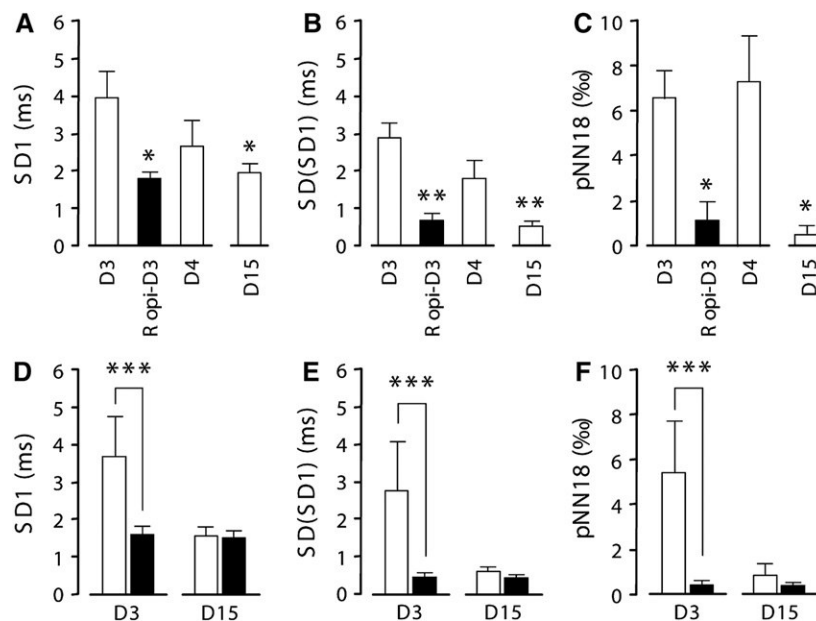

Figure 5. Heart rate variability analysis of hyperalgesic animals, treated or not with ropivacaine. **(A–C)** Effect of ropivacaine infiltration (black bars) on some HRV parameters of hyperalgesic rats (n = 4). Infiltration was performed at day 3 (D3), and HRV changes were analyzed 1 hour after ropivacaine infiltration (Ropi-D3), after a 24-hour washout (D4) and compared to values found at day 15 (D15). SD1, SD(SD1), and pNN18 mean values were all transiently reduced 24 hours after ropivacaine injection and were similar to those found in asymptomatic animals, having fully recovered from surgery (D15). **(D–F)** Effect of a perioperative ropivacaine care on the rat HRV parameters (n = 8). In comparison to saline-injected controls (white bars), ropivacaine-treated rats (black bars) exhibit very low values for SD1, SD(SD1), and pNN18 at postoperative day 3. These values were comparable to those found after full recovery (D15). Significance code: *$P < .05$; **$P < .01$; ***$P < .001$ (D3 versus Test; Friedman test followed by Steel test).

abdominal surgery aimed at implanting a miniaturized radiotelemetric probe in the rat. During the postoperative period we were able to measure the time course of mechanical hyperalgesia and the timely-correlated signs of pain seen as long-lasting alteration of the animal mobility, elevated heart rate, and variability. Hyperalgesia and pain-associated physiological alterations persisted for up to 10 days in our experimental conditions and were fully precluded by a single preventive ropivacaine treatment during the perioperative period (before animal awakening) but not at later stages.

Postoperative pain is a major issue for clinicians,[30,45] but its basic mechanisms as well as any attempt for its prevention in the long term still need to be clarified. The most widely used model is the incisional paw pain model,[6] but postoperative pain has also been studied after abdominal surgery[25] and skin/muscle incision and retraction,[12] mostly illustrating short-term alterations in the behavior and pain hypersensitivity with variable pharmacological sensitivity to analgesics. Our surgical procedure produced an important mechanical hyperalgesia during the postoperative period, which could be reduced by an acute treatment with ropivacaine, morphine, or ketoprofen in awake animals (Fig 5). This analgesic effect was, however, transient because hyperalgesia was detected 24 hours after the injection of all drugs. Focusing on the properties of local anesthetic action, this time-course is consistent with the half-life of ropivacaine which is of about 2 hours, as characterized in human studies but never in rodents.[16] A similar finding was observed in other models with local anesthetics or other analgesics.[6,12,25,32] During night and daytime, radiotelemetry allowed us to monitor autonomic parameters (electrocardiogram and body temperature) as well as locomotor activity in freely moving animals. This high time resolution monitoring gave us precious complementary information on the postsurgical recovery of the implanted rats. In particular, elevated autonomic parameters, a well-known response to a nociceptive stimulus,[17,18] were timely correlated with the presence of mechanical hyperalgesia in implanted rats. The mobility impairment also followed the same time course and was accompanied by parallel physiological changes in temperature.

One of the most interesting observations of this work was the effect of a single perioperative injection of ropivacaine, ie, an injection made while the animals were yet under anesthesia, either before the incision or after being sutured. We found that ropivacaine was efficient in removing mechanical hyperalgesia around the scar not only after the immediate awakening of the animal, an expected result,[16,28,32] but also during the following days of recovery. The reasons for the long-lasting effect of the local anesthetic ropivacaine are not yet clear. Indeed, pre- and post-incisional hindpaw injection with the local anesthetic bupivacaine was previously shown to be unable to reduce or prevent the development of persistent mechanical hyperalgesia resulting from superficial skin incision.[10,32] Our work further suggests that ropivaine perioperative care is efficient in more traumatic surgery involving skin, muscle, and peritoneum incision. At the same time, bupivacaine efficiently reduced dorsal horn

neuronal hyperexcitability associated with pain symptoms in awake animals for about 2 hours after incision or at latter stages. Here, the long-term efficacy of ropivacaine preventive analgesia is also supported by the monitoring of heart rate and locomotor activity which, in the case of ropivacaine-treated animals, were not significantly different from animals having fully recovered from surgery (>15 days). Interestingly, there is increasing evidence in the human literature for a beneficial long-term effect of ropivacaine treatment, which has been shown sometimes to accelerate postoperative recovery[3] and to limit the use of opioid.[2]

The results obtained in the current study and in the human studies cited above suggest that ropivacaine perioperative analgesia represents an interesting procedure to limit or block the peripheral afferent barrage of nociceptive messages which occurs after anesthesia and gives rise to persistent mechanical hyperalgesia. By preventing this hyperexcitability resulting from the surgical incisions and trauma, ropivacaine might be effective to fully block the establishment of peripheral and central pain sensitization, 2 mechanisms that are known to trigger pathological plastic changes in the nociceptive system.[38,47] This hypothesis may explain the absence of hyperalgesic phenotypes in implanted rats recovering from surgery (from day 0 to day 15) after perioperative ropivacaine treatment. At the molecular level, central sensitization is thought to be mediated by the establishment of long-term potentiation of glutamatergic sensori-spinal synapses,[34,37] the duration of which is determined by the intensity of the afferent stimulation. In good agreement, our surgical procedure involves large incisions of skin, abdominal muscles, and peritoneum, performed in a standard time of 50 minutes. This long surgery time was indeed associated to a prolonged postoperative pain period (about 10 days) that was significantly shortened (3 days, not shown) if the same surgery was achieved within 15 minutes. Interestingly, sensori-spinal LTP is mediated, for a large part, by the recruitment of NMDA type glutamate receptors, a mechanism which may be critical for the expression of postoperative hyperalgesia in the incisional paw model.[33] In our model, we used the NMDA antagonist ketamine to anesthetize the animal during probe implantation. It is thus tempting to speculate that perioperative ropivacaine prevents NMDA-mediated LTP during the progressive clearance of ketamine. This point requires further investigation. In any case, it seems that persistent hyperalgesia following incisional surgery needs to be accompanied by a sustained nociceptive stimulation,[32] and this might be the result of a maintained peripheral/central hyperexcitability (not tested here, but see Pogatzki et al[32]) or the uncomfortable mechanical stimulation of the newly implanted radiotelemetric probe.

In conclusion, we show here that ropivacaine preventive analgesia is efficient not only to control immediate postoperative pain, but also to prevent long-lasting alteration of motor and autonomic function. The efficacy of such a preventive analgesia is time dependent and needs to be performed before awakening of the animal because ropivacaine analgesia was only transient at

day 3 and could not improve the long-term expression of pain symptoms, autonomic sensitization, and mobility impairment. This procedure for successful surgery and fast-track rehabilitation[21] is crucial not only in the case of human studies, which are still controversial, but also in animal experimentation to be in optimal conditions regarding ethical issues. This study provides novel and original findings to support this point.

References

1. Arras M, Rettich A, Cinelli P, Kasermann HP, Burki K: Assessment of post-laparotomy pain in laboratory mice by telemetric recording of heart rate and heart rate variability. BMC Vet Res 3:16, 2007

2. Bamigboye AA, Justus HG: Ropivacaine abdominal wound infiltration and peritoneal spraying at cesarean delivery for preemptive analgesia. Int J Gynaecol Obstet 102:160-164, 2008

3. Beaussier M, El'Ayoubi H, Schiffer E, Rollin M, Parc Y, Mazoit JX, Azizi L, Gervaz P, Rohr S, Biermann C, Lienhart A, Eledjam JJ: Continuous preperitoneal infusion of ropivacaine provides effective analgesia and accelerates recovery after colorectal surgery: A randomized, double-blind, placebo-controlled study. Anesthesiology 107:461-468, 2007

4. Blaha MD, Leon LR: Effects of indomethacin and buprenorphine analgesia on the postoperative recovery of mice. J Am Assoc Lab Anim Sci 47:8-19, 2008

5. Brennan M, Palaniswami M, Kamen P: Do existing measures of Poincare plot geometry reflect nonlinear features of heart rate variability? IEEE Trans Biomed Eng 48:1342-1347, 2001

6. Brennan TJ, Vandermeulen EP, Gebhart GF: Characterization of a rat model of incisional pain. Pain 64:493-501, 1996

7. Brennan TJ, Zahn PK, Pogatzki-Zahn EM: Mechanisms of incisional pain. Anesthesiol Clin North America 23:1-20, 2005

8. Chaplan SR, Bach FW, Pogrel JW, Chung JM, Yaksh TL: Quantitative assessment of tactile allodynia in the rat paw. J Neurosci Methods 53:55-63, 1994

9. Coderre TJ, Vaccarino AL, Melzack R: Central nervous system plasticity in the tonic pain response to subcutaneous formalin injection. Brain Res 535:155-158, 1990

10. Duarte AM, Pospisilova E, Reilly E, Mujenda F, Hamaya Y, Strichartz GR: Reduction of postincisional allodynia by subcutaneous bupivacaine: Findings with a new model in the hairy skin of the rat. Anesthesiology 103:113-125, 2005

11. Ejlersen E, Andersen HB, Eliasen K, Mogensen T: A comparison between preincisional and postincisional lidocaine infiltration and postoperative pain. Anesth Analg 74:495-498, 1992

12. Flatters SJ: Characterization of a model of persistent postoperative pain evoked by skin/muscle incision and retraction (SMIR). Pain 135:119-130, 2008

13. Goecke JC, Awad H, Lawson JC, Boivin GP: Evaluating postoperative analgesics in mice using telemetry. Comp Med 55:37-44, 2005

14. Gonzalez-Darder JM, Barbera J, Abellan MJ: Effects of prior anaesthesia on autotomy following sciatic transection in rats. Pain 24:87-91, 1986

15. Gordon SM, Dionne RA, Brahim J, Jabir F, Dubner R: Blockade of peripheral neuronal barrage reduces postoperative pain. Pain 70:209-215, 1997

16. Hansen TG: Ropivacaine: A pharmacological review. Expert Rev Neurother 4:781-791, 2004

17. Janig W: Systemic and specific autonomic reactions in pain: Efferent, afferent and endocrine components. Eur J Anaesthesiol 2:319-346, 1985

18. Janig W: The sympathetic nervous system in pain. Eur J Anaesthesiol Suppl 10:53-60, 1995

19. Jeanne M, Logier R, De Jonckheere J, Tavernier B: Validation of a graphic measurement of heart rate variability to assess analgesia/nociception balance during general anesthesia. Conf Proc IEEE Eng Med Biol Soc 1:1840-1843, 2009

20. Jourdan D, Ardid D, Eschalier A: Automated behavioural analysis in animal pain studies. Pharmacol Res 43:103-110, 2001

21. Kehlet H, Dahl JB: Anaesthesia, surgery, and challenges in postoperative recovery. Lancet 362:1921-1928, 2003

22. Kramer K, Kinter LB: Evaluation and applications of radiotelemetry in small laboratory animals. Physiol Genomics 13:197-205, 2003

23. Le Bars D, Gozariu M, Cadden SW: Animal models of nociception. Pharmacol Rev 53:597-652, 2001

24. Logier R, Jeanne M, Tavernier B, De Jonckheere J: Pain/analgesia evaluation using heart rate variability analysis. Conf Proc IEEE Eng Med Biol Soc 1:4303-4306, 2006

25. Martin TJ, Buechler NL, Kahn W, Crews JC, Eisenach JC: Effects of laparotomy on spontaneous exploratory activity and conditioned operant responding in the rat: A model for postoperative pain. Anesthesiology 101:191-203, 2004

26. Moiniche S, Kehlet H, Dahl JB: A qualitative and quantitative systematic review of preemptive analgesia for postoperative pain relief: The role of timing of analgesia. Anesthesiology 96:725-741, 2002

27. Oberlander T, Saul JP: Methodological considerations for the use of heart rate variability as a measure of pain reactivity in vulnerable infants. Clin Perinatol 29:427-443, 2002

28. Oda A, Ohashi H, Komori S, Iida H, Dohi S: Characteristics of ropivacaine block of Na+ channels in rat dorsal root ganglion neurons. Anesth Analg 91:1213-1220, 2000

29. Oliveira NE, Lima Filho NS, Lima EG, Vasquez EC: Effects of regional anesthesia with ropivacaine on arterial pressure and heart rate in healthy subjects. Eur J Oral Sci 114:27-32, 2006

30. Perkins FM, Kehlet H: Chronic pain as an outcome of surgery. A review of predictive factors. Anesthesiology 93:1123-1133, 2000

31. Piskorski J, Guzik P: Geometry of the Poincare plot of RR intervals and its asymmetry in healthy adults. Physiol Meas 28:287-300, 2007

32. Pogatzki EM, Vandermeulen EP, Brennan TJ: Effect of plantar local anesthetic injection on dorsal horn neuron activity and pain behaviors caused by incision. Pain 97:151-161, 2002

33. Pogatzki EM, Zahn PK, Brennan TJ: Effect of pretreatment with intrathecal excitatory amino acid receptor antagonists on the development of pain behavior caused by plantar incision. Anesthesiology 93:489-496, 2000

34. Randic M: Plasticity of excitatory synaptic transmission in the spinal cord dorsal horn. Prog Brain Res 113:463-506, 1996

35. Rietmann TR, Stauffacher M, Bernasconi P, Auer JA, Weishaupt MA: The association between heart rate, heart rate variability, endocrine and behavioural pain measures in horses suffering from laminitis. J Vet Med A Physiol Pathol Clin Med 51:218-225, 2004

36. Rooney BA, Crown ED, Hulsebosch CE, McAdoo DJ: Preemptive analgesia with lidocaine prevents Failed Back Surgery Syndrome. Exp Neurol 204:589-596, 2007

37. Sandkuhler J, Liu X: Induction of long-term potentiation at spinal synapses by noxious stimulation or nerve injury. Eur J Neurosci 10:2476-2480, 1998

38. Scholz J, Woolf CJ: Can we conquer pain? Nat Neurosci 2002;(5 Suppl):1062-1067, 2002

39. Sharp J, Zammit T, Azar T, Lawson D: Recovery of male rats from major abdominal surgery after treatment with various analgesics. Contemp Top Lab Anim Sci 42:22-27, 2003

40. Simpson D, Curran MP, Oldfield V, Keating GM: Ropivacaine: A review of its use in regional anaesthesia and acute pain management. Drugs 65:2675-2717, 2005

41. Sisk AL, Dionne RA, Wirdzek PR: Evaluation of etidocaine hydrochloride for local anesthesia and postoperative pain control in oral surgery. J Oral Maxillofac Surg 42: 84-88, 1984

42. Tverskoy M, Cozacov C, Ayache M, Bradley EL Jr., Kissin I: Postoperative pain after inguinal herniorrhaphy with different types of anesthesia. Anesth Analg 70:29-35, 1990

43. Waxman SG, Dib-Hajj S, Cummins TR, Black JA: Sodium channels and pain. Proc Natl Acad Sci U S A 96:7635-7639, 1999

44. White PF: The changing role of non-opioid analgesic techniques in the management of postoperative pain. Anesth Analg 101:S5-22, 2005

45. Wilder-Smith OH, Arendt-Nielsen L: Postoperative hyperalgesia: Its clinical importance and relevance. Anesthesiology 104:601-607, 2006

46. Woolf CJ: Evidence for a central component of postinjury pain hypersensitivity. Nature 306:686-688, 1983

47. Woolf CJ, Salter MW: Neuronal plasticity: Increasing the gain in pain. Science 288:1765-1769, 2000

48. Yashpal K, Katz J, Coderre TJ: Effects of preemptive or postinjury intrathecal local anesthesia on persistent nociceptive responses in rats. Confounding influences of peripheral inflammation and the general anesthetic regimen. Anesthesiology 84:1119-1128, 1996

2 - Poincaré Plot Descriptors of Heart Rate Variability as Markers of Persistent Pain.

Pain in animals is currently evaluated either by the identification of spontaneous behavioral signs of suffering or by the hypersensitivity of sensorimotor reflexes in response to an acute electric, chemical, mechanical or thermal stimulation (Le Bars et al., 2001). To measure abnormal pain expression in response to a non-noxious stimulus (*i.e.* allodynia) and pain hypersensitivity to a noxious stimulus (i.e. hyperalgesia), it is however necessary to induce pain and to handle the animal. This can profoundly alter its state of awareness and its emotional status; two parameters which are well known to modify the expression of pain (Tracey and Mantyh, 2007)). The expression of pain is not only seen as sensory hypersensitivity but is associated with many other physiological changes such as locomotor impairment or sympathetic nervous system activation (Janig, 1995). These changes, although not always nociceptive-specific, might be of interest in order to detect and quantify spontaneous pain-related symptoms. Indeed, autonomic activation in response to pain results from complex anatomo-functional interactions with the nociceptive processing pathways, at every level of the neuraxis, and involves superior structures of the central system, such as amygdala, hypothalamus and periaqueductal gray (Willis, 1991). Analysis of the heart rate variability (HRV) has recently been pointed to identify and quantify pain, with the vast majority of studies implemented a frequency domain analysis and identified alterations in parasympathetic control in painful patients (Tousignant-Laflamme et al., 2005). However, there are very few HRV data available obtained from animal models of persistent pain.

Here, **we aimed at describing potential physiological markers of spontaneous pain**.

To do so, we analyzed the changes in HRV parameters in rats suffering from acute and inflammatory pain sensitization. Possible emotional bias related to animal handling was minimized by using remote-controlled nociceptive testing in freely-moving rats. In parallel to the frequency domain method, we also performed a time domain method to extract simple Poincaré plot descriptors in order to identify possible markers of spontaneous pain expression. To validate our procedure, rats were first submitted to acute thermal hot and cold painful stimulation and, in a second step, to a persistent inflammatory pain sensitization resulting from intraplantar injection of formalin or carrageenan. The radiotelemetric monitoring of physiological functions was combined to classical nociceptive tests in order to quantify the intensity of pain symptoms.

We found that heart rate variability indexes SD(SD1) and pNN18 are strongly related to nociceptive stimulations, especially if the mean heart rate remains unchanged. This provides strong arguments to support the adaptability of the autonomic nervous system in a physiological condition, potentially as core actor of the classically described fight or flight reaction. However, the question by which mechanisms increases in HRV is produced by pain and if these indexes can be used for other persistent pain states is still open.

Poincaré plot descriptors of heart rate variability as markers of persistent pain expression in freely moving rats

Alexandre Charlet, Jean-Luc Rodeau, Pierrick Poisbeau *

Institut des Neurosciences Cellulaires et Intégratives, Centre National de la Recherche Scientifique et Université de Strasbourg, Département Nociception et Douleur, Strasbourg, France

ABSTRACT

Evaluation of pain is a critical issue in human pathologies but also in animal experimentation. In human studies there is growing evidence that cardiovascular outputs such as heart rate variability (HRV) might be of interest to detect and measure pain expression. Indeed, systems controlling cardiovascular function are closely coupled to the perception of pain. To demonstrate the interest of HRV, we have combined radiotelemetry and remote-controlled nociceptive tests in rats submitted to various situations of acute and persistent inflammatory pain. We found the Poincaré plot descriptor SD1 and pNN18 to represent robust indicators of pain, especially in the case of persistent inflammatory states. Further studies will be performed in order to understand by which mechanisms pain-related increases in HRV are produced and if these descriptors can be used for other persistent pain states.

© 2011 Elsevier Inc. All rights reserved.

1. Introduction

Pain is defined by the *International Association for the Study of Pain* as "an unpleasant sensory and emotional experience associated with actual or potential tissue damage or described in terms of such damage" [1]. This definition highlights the complexity and the subjective character of such a sensation. Because pain verbalization is not always possible and/or reliable in human patients [2], there is still an urgent need to develop new methods in order to quantify objectively pain expression. Evaluation of pain in animal experimentation is also a major ethical issue in our modern society and represents a challenge for research in the field [3–5]. Indeed, many animal models are used to identify mechanisms leading to chronic pain states and to test novel strategies to obtain analgesia.

Animal pain is currently evaluated either by the identification of spontaneous behavioral signs of suffering or by the hypersensitivity of sensorimotor reflexes in response to an acute electric, chemical, mechanical or thermal stimulation [4]. Abnormal pain expression in response to a non noxious stimulus (*i.e.* allodynia) and pain hypersensitivity to a noxious stimulus (i.e. hyperalgesia) corresponds

here to symptoms that are also observed in humans [1]. To measure these symptoms, it is however necessary to induce pain and to handle the animal. This can profoundly alter its state of awareness and its emotional status, two parameters which are well known to modify the expression of pain [6–9]. The expression of pain is not only seen as sensory hypersensitivity but is associated with many other physiological changes such as locomotor impairment or sympathetic nervous system activation [10]. These changes, although not always nociceptive-specific [4], might be of interest in order to detect and quantify spontaneous pain-related symptoms. For example, autonomic activation in response to pain results from complex anatomo–functional interactions with the nociceptive processing pathways, at every level of the neuraxis, and involves superior structures of the central system, such as amygdala, hypothalamus and periaqueductal gray matter [11,12]. This autonomic stimulation enables the organism to manage any dangerous situation and has a preparatory and protective role under normal conditions [13]. So, when facing pain, stereotyped behaviors occur, such as fight and flight, both characterized, among other signs, by hypertension, tachycardia and decreased blood flow [14].

To limit emotional distress in anticipation of pain while handling the animal and gain access to spontaneous signs of pain, chronically implanted radiotelemetric probes represent an interesting and complementary approach since it allows to monitor simultaneously several physiological parameters (including autonomic activation) in freely-moving animals at a high time resolution (1 kHz) and for long periods of time [15]. There is still a limited number of reports describing its utility

* Corresponding author at: CNRS UPR-3212, Département Nociception et Douleur, 21 rue René Descartes, 67084 Strasbourg, France. Tel.: +33 3 68 85 14 76; fax: +33 3 88 61 33 47.
E-mail address: poisbeau@inci-cnrs.unistra.fr (P. Poisbeau).

for pain detection and evaluation in transient and persistent pathological states [16–22]. The main reason is that it is crucial to demonstrate that the observed physiological signs of pain are related to a real painful state and are sensitive to analgesic treatments. Moreover, this demonstration is further complicated because parameters recorded from acute pain states may often be slightly different from those obtained in persistent pathological pain situations. This is the case while measuring the cardiac parameters. In most cases, an acute nociceptive stimulation induces an expected increase in mean heart rate. Using radiotelemetry probes, it has been shown for example that an acute duodenal or colorectal distension [16,23] induces an increase in heart rate which lasts the duration of the stimulation. Longer-lasting abdominal pain resulting from the implantatory surgery of the radiotelemetric probe was also reported to increase mean heart rate during the postoperative period [17,19]. This increase was, however, transient and returned rapidly to normal control values although animals were still hyperalgesic [19]. A persistent increase in heart rate has already been seen in horses suffering from laminitis [24] and in the rat model of chronic constriction injury (CCI) of the sciatic nerve [21]. In the latter example, the increase of the heart rate was accompanied by an increase in blood pressure, which returns to basal level two weeks after the injury but before the full recovery of the pain symptoms (hyperalgesia, allodynia). Analysis of the heart rate variability (HRV) has also recently been used to identify and quantify pain in human [25]. The vast majority of studies implemented a frequency domain analysis and identified alterations in parasympathetic control in painful patients [26–28].

There is very few HRV data available obtained from animal models of persistent pain and collected by means of implanted radiotelemetric probes [19,21]. In this study, we decided to analyze changes in HRV parameters in rats suffering from acute and inflammatory pain sensitization. Possible emotional bias related to animal handling was minimized by using remote-controlled nociceptive testing in freely-moving rats. In parallel to the frequency domain method, we also performed a time domain method to extract simple Poincaré plot descriptors (see Methods) in order to identify possible markers of spontaneous pain expression. To validate our procedure, rats were first submitted to acute thermal hot and cold painful stimulation and, in a second step, to a persistent inflammatory pain sensitization resulting from intraplantar injection of formalin or carrageenan. The radiotelemetric monitoring of physiological functions was combined to classical nociceptive tests in order to quantify the intensity of pain symptoms.

2. Materials and methods

2.1. Animals

Male Sprague–Dawley rats (Janvier, Le Genest-Saint-Isle, France) weighing ~350 g at the beginning of experiments were used for this study. Animals were housed individually under standard conditions (room temperature 22 °C; 12 h/12 h light/dark cycle; lights on at 7:00 AM) with *ad libitum* access to food and water. Before the onset of the experiment, all animals were submitted to at least 1 week habituation to the experimental room, to handling and to behavioral testing. Behavioral tests were done during the light period (between 10:00 AM and 4:00 PM). All experiments were conducted in conformity with the recommendations of the European Committee Council Direction of September 22, 2010 (2010/63/EU), with an authorization for animal experimentation from the French Department of Agriculture (License 67–116 to PP) and with the agreement of the regional ethical committee (authorization numbers AL/10/13/03/07, AL/11/14/03/07 and AL/12/15/03/07). The health status of the colony from which were issued the animals used in this study is specific pathogen free, according to the standard set by the Federation of European Laboratory Animal Science Associations (FELASA) [29].

2.2. Inflammatory and tonic pain models

Short-term inflammatory pain sensitization was obtained after a single intraplantar injection of 150 μl λ-carrageenan (3% prepared in 0.9% NaCl). Tonic pain was induced by a single unilateral intraplantar injection of 50 μl formalin (5% prepared in 0.9% NaCl). Both compounds were purchased from Sigma (St Louis, MO, USA) and the intraplantar injections were performed under rapidly reversible halothane anesthesia (3%). Baseline values were obtained in both groups of rats the day before injection of either λ-carrageenan or formalin.

2.3. Nociceptive stimulation and pain threshold measures

Mechanical hyperalgesia was tested using the calibrated forceps (Bioseb, Chaville, France) previously developed in our laboratory [30]. The habituated rat was loosely restrained with a towel masking the eyes in order to limit environmental stress. The tips of the forceps were placed at each side of the paw and graduate force was applied. The pressure producing a withdrawal of the paw corresponded to the nociceptive threshold value. This manipulation was performed 3 times for each hindpaw and the values were averaged.

Thermal heat hyperalgesia was evaluated with the Plantar test (Ugo Basile, Comerio, Italy) following Hargreaves' method [31]. Briefly, rats were placed in a clear Plexiglas box (22 × 19 × 14 cm) on a glass surface, and testing began after exploration and grooming behaviors ended (~15 min). An infrared beam was then applied to the plantar surface of each hindpaw in order to determine the paw withdrawal latency (in seconds). Measures of the paw withdrawal latency were repeated 3 times for each hindpaw and the values were averaged.

Thermal cold allodynia was characterized by scoring the aversive behaviors of rats using the acetone test [32]. Rats were placed on a wire mesh delimited by a Plexiglas box (20 × 25 × 40 cm) and allowed to accommodate for at least 15 min. A drop of acetone was then placed on the dorsal side of the hindpaw and the behavioral response was scored as follows during the 20 s following acetone application: 0: no response of the animal; 1: quick withdrawal, flicking or stamping of the paw; 2: prolonged withdrawal or repeated flicking of the paw; 3: licking of the paw. The manipulation was performed 3 times for each paw and the values were added (maximal score: 18).

2.3.1. Dynamic hot/cold plate testing

A computer-controlled hot and cold plate protocol (Bioseb, Vitroles, France), recently validated in our laboratory [33], allowed to perform a nociceptive stimulation in freely-moving animals. To do so, animals were placed on the plate for a habituation period of at least 30 min. The basal temperature of the plate was set at 20 °C or 30 °C when the testing was planned for cold or hot nociceptive temperature, respectively. Using a remote control and under video monitoring, the plate temperature was then quickly increased from 30 °C to 45 °C (hot stimulation) or decreased from 20 °C to 4 °C (cold stimulation) at a rate of 10 °C/min. A 2 min period of ECG recording was started when the nociceptive temperature was reached, 45 °C for hot and 4 °C for cold stimulation respectively, unless the animal displayed unbearable nociceptive behavior.

2.4. Radiotelemetry

2.4.1. Surgical implantation of the probes

Implantation of the radiotelemetric transmitter (model TA11CTA-F40; Data Sciences International, St. Paul, MN, USA) was performed under sterile conditions while animals were deeply anesthetized with a cocktail of ketamine (87 mg/kg; Imalgène 1000, Merial, Lyon, France) and xylazine (13 mg/kg; Sigma, St Louis, USA). The surgery field was shaved and carefully cleaned with povidone iodine dermal solution (Betadine® Scrub 4%, Viatris, Mérignac, France). A first

incision of about 2 cm was made medially through the skin, the abdominal muscle and the peritoneum to implant the transmitter. Inside the peritoneal space, the transmitter was tightly stitched to the abdominal muscles with 3 points using a non resorbing suture (Silcam 4/0, Braun, France). The two electrodes used to record the electrocardiogram (ECG) were placed under the skin and firmly sutured to the muscles at the level of the last left rib and under the right axilla. Two cutaneous incisions allowing placement of the ECG electrodes were sutured and cleaned with betadine. The complete procedure required about 20 min. Before the surgery, all animals received a preventive analgesia treatment consisting in a subcutaneous injection of 2 mg/kg ropivacaine (Naropeine®, AstraZeneca, France) which was shown to accelerate postoperative recovery [19]. Although perioperative ropivacaine analgesia shortened recovery of normal physiological parameters and nociceptive thresholds [19], we nevertheless started the radiotelemetry recordings only after 3 weeks and confirmed that physiological parameters were stable. Inflammatory pain models were started after an additional 1–2 week period of baseline measurement to extract basal nociceptive thresholds.

2.4.2. Analysis procedures

Mobility, heart rate, and abdominal temperature were recorded in series of 4 rats, using DSI Data Exchange Matrices (Data Sciences International, St. Paul, MN, USA). Data were transmitted on-line using radio frequency waves at 455 kHz and stored on a remote-controlled computer. Animal locomotor activity (in arbitrary unit, AU, based on changes in the amplitude and slope of the signal), heart rate (beats per minute, bpm) and abdominal temperature (°C) were calculated every minute during a recording waveform of 20 s at an acquisition rate of 1 kHz for each animal, using DataQuest ART 4.0 (Data Sciences International, St. Paul, MN, USA). After acquisition, data were exported as Excel and text files for further analysis. In standard routine conditions, average values for each parameter were calculated over time periods of 1 h for the carrageenan experiment, 20 min for

the formalin experiment and 2 min for the hot and cold nociceptive stimulation experiments,

RR intervals and heart rate were calculated for successive 20 s segments of ECG (Fig. 1A). Each 20 s segment normally provided more than 100 PQRST complexes given the heart rate of rats. ECG was continuously recorded over 2 min periods in dynamic cold/hot nociceptive stimulations or with one 20 s segment every minute during 20 min in other experiments. R waves were automatically detected and individual errors were manually checked using Clampfit 10.2 software (Molecular Devices, MDS Analytical Technologies, Toronto, Canada) before extracting RR intervals (RRi). Time domain analysis of heart rate variability (HRV) allowed to obtain SD1 and SD2, two descriptors of the Poincaré plot of RR intervals [34,35] (Fig. 1B). On the Poincaré plot it describes the variability along the perpendicular to the identity line and is associated with short-term HRV. The dispersion along the identity line is measured by SD2 and is thought to indicate the level of long-term variability. SD2 was calculated from $SD2^2 = 2 \cdot SDRR^2 - SD1^2$, where SDRR is the standard deviation of the ΔRR intervals. SD1 and SD2 were calculated as $SD1 = SDSD/\sqrt{2}$, where SDSD is the standard deviation of the successive differences of the RR intervals, $\Delta RR_n = RR_n - RR_{n+1}$. SD1 was calculated for each 20 s segment. The mean and the standard deviation of the values obtained for all segments provided a global SD1 for each animal, as well as an estimation of its variability, SD(SD1) (Fig. 1C). Both SD1 and SD(SD1), but not SD2 (see Fig. 1 for example), displayed a variability that was time-correlated with pain states. We therefore kept SD1 and SD(SD1) as indexes of pain signs. Part of this variability was found to arise from occasional large alterations of the RR interval which were clearly not artifactual. By analogy with the commonly used pNN50 parameter (the percentage of consecutive RR intervals in humans differing by more than 50 ms), we therefore defined pNN18 (in ‰) as the number, for each 20 s segment, of ΔRR_n values differing by more than 18 ms (*i.e.* ~10%) from the mean value. In the case of carrageenan experiments, a frequency domain analysis of HRV was
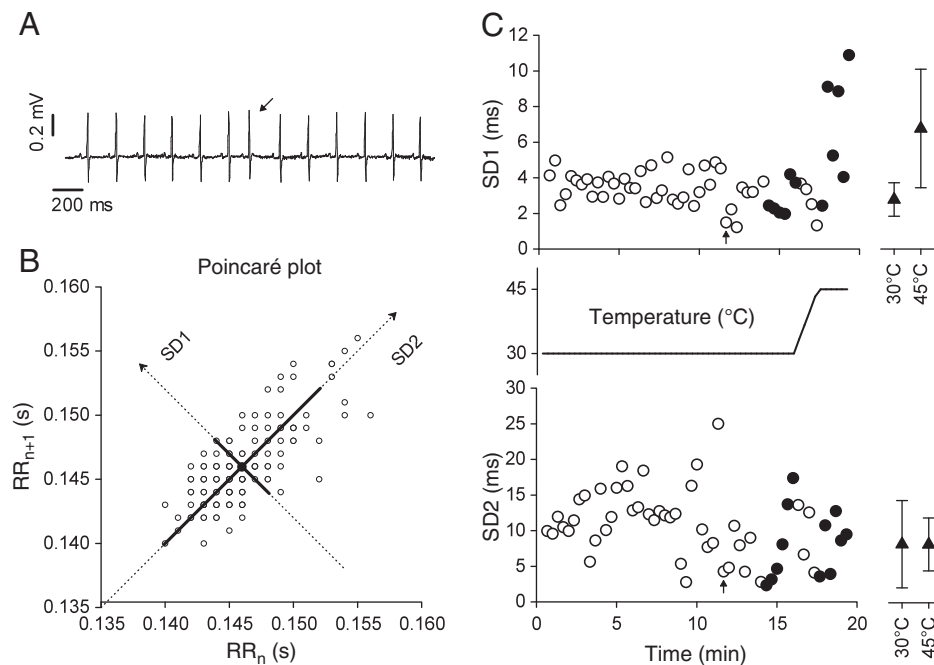

Fig. 1. Heart rate variability methodology. A. Short fragment of an ECG recording. The arrow points to an RR interval presenting a large deviation from the average value. Such occasional alterations were counted in the pNN18 index. B. Poincaré plot for a 20 s ECG segment recorded during a dynamic hot plate test. The length of each RR interval is plotted as a function of the length of the preceding interval. The dispersion of the cloud of points along the line of identity is characterized by SD2 and that across this line by SD1. Thick lines correspond to ±2 SD. C. In a dynamic hot plate test, where the plate temperature was raised from 30 °C to 45 °C, the values of SD1 and SD2 were calculated for each 20 s segment of the ECG record (circles). SD1 increases when temperature is too hot, as well as its variability characterized by the standard deviation SD(SD1). Black circles correspond to the two 2 min sections at 30 °C and at 45 °C for which mean values of SD1 and SD2, as well as the corresponding standard deviations, were calculated for this animal (black triangles at right). The arrow points at the 20 s segment used for the Poincaré plot in B.

also performed with the HRV Analysis 1.1 software (Niskanen et al, 2004), using the following parameters: detrending of RR intervals with smoothness priors method (alpha = 1000); interpolation rate, 20 Hz; low-frequency range (LF), 0.2–0.6 Hz; high-frequency range (HF), 1.0–2.5 Hz [36]. Frequency spectra presented no significant alterations correlated with pain symptoms and are therefore not further described here.

2.5. Statistical analysis

Data in text are expressed as mean ± standard deviation. Mean values of the mobility, heart rate, temperature or mechanical hypersensitivity were compared at different times and between treatment groups. Repeated-measures two-way ANOVA, with factors *treatment* (between), *time* (within), were performed in most experiments. The ordinal data from the acetone test were analyzed with the non parametric Friedman's test. When the global test was significant, the Tukey or Dunnett tests (parametric) or the Steel test (non parametric) were used for post-hoc multiple comparisons between individual groups. The Student *t*-test for paired data was used for experiments with hot and cold nociceptive stimulations. Statistical analysis was performed with Statistica v8.0 (Statsoft, Tulsa, Oklahoma, USA). Differences were considered significant for p < 0.05.

3. Results

3.1. Evaluation of acute pain in response to thermal nociceptive stimulus

It can be particularly difficult to use cardiovascular parameters as possible indexes of pain expression because they are strongly modified by animal handling, environmental stress and many other factors. In an attempt to prove their possible utility for pain exploration, we first combined radiotelemetry with a remote-controlled dynamic nociceptive test in freely-moving rats (see Methods). After a period of habituation on the plate (see Methods), the animals were submitted to an acute cold or hot nociceptive stimulation.

Using this procedure and after analysis of the ECG, we observed an increase of SD1 in both cold (from 2.0 ± 0.2 s to 4.2 ± 0.5 s; n = 6, p = 0.0031) and hot nociceptive conditions (from 2.3 ± 0.4 s to 5.6 ± 0.7 s; n = 7, p = 0.0001; Fig. 2B). This was accompanied by an increase of SD(SD1) value, limited in cold stimulation from 1.0 ± 0.2 s to 2.2 ± 0.4 s (p = 0.0255) and fairly more marked in hot stimulation from 0.7 ± 0.2 s to 3.5 ± 0.5 s (p = 0.0028; Fig. 2C). In the case of cold stimulation, the mean heart rate was decreased (20 °C: 456 ± 14 bpm; 4 °C: 392 ± 29 bpm; p = 0.0139; Fig. 2A), whereas it was increased in the case of a hot nociceptive stimulation (30 °C: 402 ± 15 bpm; 52 °C: 459 ± 15 bpm; p = 0.0247; Fig. 2A). To go one step further, we decided to express our HRV result as pNN18 (see Methods) which quantifies extreme changes in RR intervals (over 18 ms) often seen during acute pain (Fig. 1A). Indeed, we observed an increase in the number of such events after cold stimulation from 3.6 ± 1.4‰ to 16.0 ± 3.7‰ (p = 0.0075; Fig. 2D). Interestingly, a dramatic enhancement of this value was also noted in the case of a hot nociceptive stimulation where pNN18 reached an extreme value of 33.2 ± 9.0‰ (p = 0.0104).

3.2. Tonic pain evaluation following intraplantar formalin injection

In order to verify that the selected HRV parameters were able to indicate the presence of a tonic pain, we used the classical formalin test. The immediate behavioral pattern of pain expression following the intraplantar injection of formalin is well described in rodents. We concentrated on changes occurring during the tonic phase of pain, i.e. 20–40 min after formalin injection [37]. During this period of tonic pain and in comparison to saline-injected animals (n = 7), we noted that formalin injected rats (n = 7) exhibited a significantly elevated locomotor activity (8.4 ± 0.7 AU *vs.* 1.1 ± 0.3 AU for saline; p = 0.00014) and heart rate (Fig. 3A; 402 ± 28 bpm *vs.* 329 ± 16 bpm for saline, p = 0.0075). Locomotor activity and heart rate were back to normal 80–100 min after formalin injection, (0.8 ± 0.5 AU and 294 ± 10 bpm,
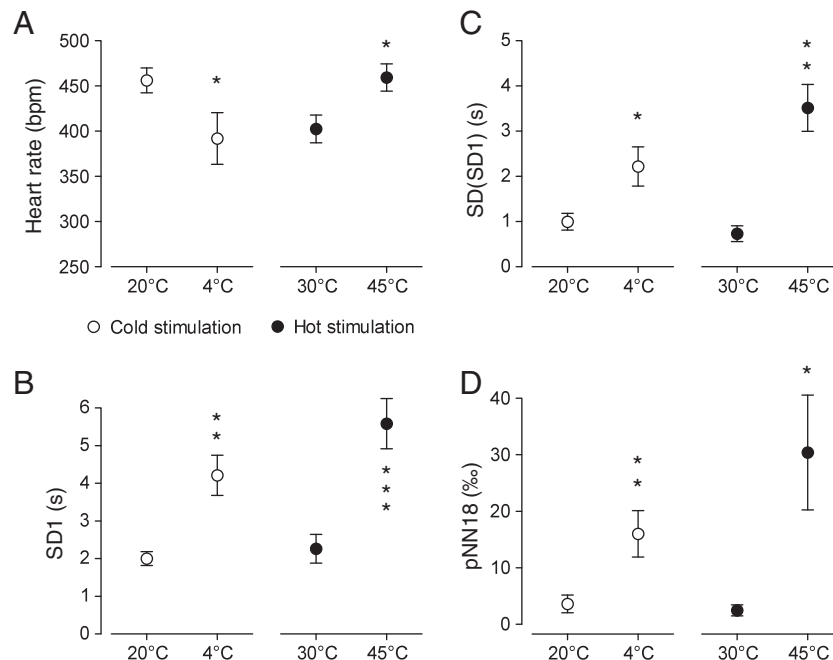

Fig. 2. Heart rate variability analyses during acute thermal nociceptive stimulations. Experiments were conducted during either a cold or heat nociceptive stimulus, with analyses performed over a 2 min stimulation period. For the cold stimulation (white circles; n = 6), analyses were completed before (at 20 °C) and during (at 4 °C) the nociceptive stimulus. Similarly, for heat experiments (black circles; n = 7), measurements were made before (at 30 °C) and during (at 45 °C) the nociceptive stimulus. (A) Heart rate evolution after thermal nociceptive stimulation. (B and C) Changes in the values of SD1 (B) and its standard deviation SD(SD1) (C) after cold or heat stimuli. (D) Changes in the number of ΔRR_n values deviating by more than 10% from the 18 ms mean value after a thermal nociceptive stimulus. Note that the increase observed, from control to nociceptive values, is relatively larger than in previous panels. Significance code for *p*-values of comparisons between reference and nociceptive temperature points: 0 < *** < 0.001 < ** < 0.01 < * < 0.05.

respectively, n = 7), and undistinguishable from saline-injected animals (0.8 ± 0.3 AU and 296 ± 10 bpm).

We next performed an HRV analysis using radiotelemetric recording of saline and formalin-injected rats (Fig. 3). During the tonic phase of pain, significantly higher values were observed in formalin than in saline-injected animals, both for SD1 (3.8 ± 0.5 s vs. 2.5 ± 0.2 s, p = 0.0133, Fig. 3B) and for SD(SD1) (2.6 ± 0.2 s vs. 0.8 ± 0.2 s, p = 0.00014, Fig. 3C). Interestingly here, SD1 and SD(SD1) values in formalin-injected animals were not different from the saline group after 80 min. As previously illustrated, pNN18 events were rare in control (i.e. before injection; 1.4 ± 0.7‰, n = 14) and, at any time point, in the saline-injected group (Fig. 3D). This value was significantly elevated 20–30 min after formalin (11.1 ± 2.4‰, p = 0.00015) but returned to basal levels after 80 min (1.2 ± 0.5‰). Altogether, there was a good correlation in this model between the behavioral expression of pain and its radiotelemetric signs (mean heart rate, locomotor hyperreactivity and HRV indexes).

3.3. Carrageenan-induced inflammatory pain symptoms and associated radiotelemetric alterations

In order to evaluate the potential interest of specific HRV parameters, namely SD1, SD(SD1) and pNN18, in the evaluation of peripheral inflammatory pain, we used the carrageenan model. Carrageenan-λ is a sulfated polysaccharide producing a short-term inflammatory pain sensitization after a single unilateral intraplantar injection in the rat hindpaw. In line with previous experiments, we decided to use this well-studied model in order to correlate paw nociceptive thresholds with possible spontaneous signs of pain monitored by radiotelemetry. As illustrated in Fig. 4A, a significant mechanical hyperalgesia developed

Fig. 3. Heart rate variability analyses during the tonic phase of the formalin test. Analyses were performed in formalin- (black circles; n = 7) and saline-treated animals (white circles; n = 7) before injection (Control) and at significant time points after injection: 20–40 min (maximal pain symptoms) and 80–100 min (i.e. when pain symptoms are classically no longer detected). Heart rate (A), SD1 (B), SD(SD1) (C) and pNN18 (D) all present a significant increase after 20 min and full recovery after 80 min. Significance code for p-values of comparisons between formalin and saline groups at a given time point: 0 < *** < 0.001 < ** < 0.01 < * < 0.05.

rapidly after carrageenan intraplantar injection and persisted for about a week. From a basal pre-test value of 335.0 ± 2.4 g (Day 0; Fig. 4A; n = 18 rats per group), the mechanical thresholds rapidly dropped to 21.0 ± 1.6 g at 7 h following carrageenan injection and progressively returned to normal values around day 6. Saline-treated animals always displayed stable values which were not significantly different from the pre-test (334.0 ± 2.5 g at day 0). Thermal heat hyperalgesia was also observed in carrageenan-injected animals (Fig. 4B) and was seen as a significant decrease in paw withdrawal latency value from 6.2 ± 0.3 s (day 0 before injection) to 3.0 ± 0.3 s at 7 h (n = 18 per group, p < 0.001). From day 3, thermal heat hyperalgesia was no longer detected and paw withdrawal latency values were similar to that of saline-injected animals.

We then used two other groups of animals (saline: n = 4; carrageenan: n = 8), implanted with the radiotelemetric probe for more than 15 days. At this stage, animals had fully recovered from the implantatory surgery and expressed stable values for locomotor activity, heart rate and abdominal temperature. As shown in Fig. 4, in saline-injected animals (white symbols) these physiological parameters did not change with time: their values were not significantly different from pre-test values obtained before injection (Fig. 4, day 0). In sharp contrast, carrageenan-injected animals showed impaired locomotor activity (Fig. 4C), intense tachycardia (Fig. 4D) and hyperthermia (Fig. 2E) which were maximal 7 h after the injection (Activity: 6.2 ± 1.6 AU vs. 1.5 ± 0.4 AU; heart rate: 304.0 ± 8.3 bpm vs. 365.7 ± 9.7 bpm, p = 0.0027; temperature: 37.01 ± 0.1 °C vs. 38.9 ± 0.3 °C; p = 0.00017). Although the time course of the physiological alterations followed the onset of hyperalgesia during the first 7 h, these radiotelemetric changes did not persist during the following days. We therefore decided to explore the possibility of a persistent alteration in heart rate variability (HRV, see Methods) using high-resolution recording of the ECG at 7, 24, 48 and 96 h following the induction of inflammation (n = 6 animals per group).

As shown previously (Fig. 4D but see also Fig. 5A), a significant increase in the mean heart rate was only seen within the 12 h following carrageenan injection and not the days after (black symbols). Interestingly, no alterations of the HRV could be seen during this early episode of tachycardia (Fig. 5B–C). In comparison to saline-injected animals (white symbols), significant increases in SD1 and SD(SD1) were detected 24 h and 48 h after the start of the inflammatory pain sensitization. SD1 values (Fig. 5B) in carrageenan-injected animals (black symbols), as compared to saline-treated animals (white symbols), were 3.4 ± 0.6 s vs. 1.7 ± 0.1 s at 24 h (n = 6, p = 0.00017) and 3.3 ± 0.5 s vs. 1.8 ± 0.2 s at 48 h (p = 0.00021). The same increase was observed for SD(SD1) values (Fig. 5C) of carrageenan animals with respect to saline controls: 1.7 ± 0.5 s vs. 0.4 ± 0.0 s at 24 h (p = 0.00027) and 2.7 ± 0.3 s vs. 0.4 ± 0.1 s at 48 h (p = 0.00016). Moreover, as shown in Fig. 3D, pNN18 events are significantly more frequent 24 h (7.3 ± 2.3‰) and 48 h (8.2 ± 2.1‰) after carrageenan. They were rare, if present, for saline-injected animals at all time points and for carrageenan-injected animals, at 7 h (2.9 ± 1.5‰) and 96 h (0.5 ± 0.3‰).

4. Discussion

The objective of the present work was to implement a systematic correlation between inflammatory pain symptoms and possible spontaneous signs of pain, measured by means of radiotelemetry, and corresponding to physiological changes in locomotor activity, abdominal temperature or heart rate. We focused our attention on mean heart rate and on some heart rate variability parameters (HRV parameters: SD1, SD(SD1) and pNN18) because these values were strongly increased after an acute (thermal) and tonic (e.g. formalin) nociceptive stimulation. All values returned to basal levels (pain free situation) after these acute episodes of pain. In the carrageenan model of long-term inflammatory sensitization, mean heart rate was only increased shortly after carrageenan injection (e.g. at 7 h). Interestingly, elevated HRV
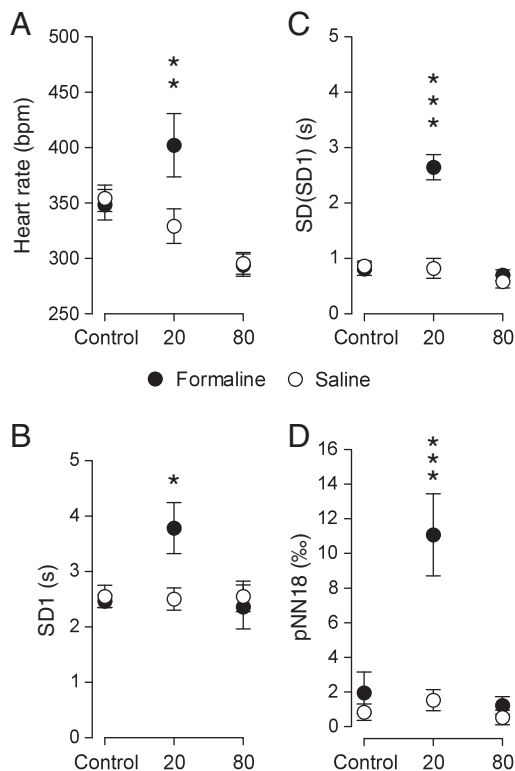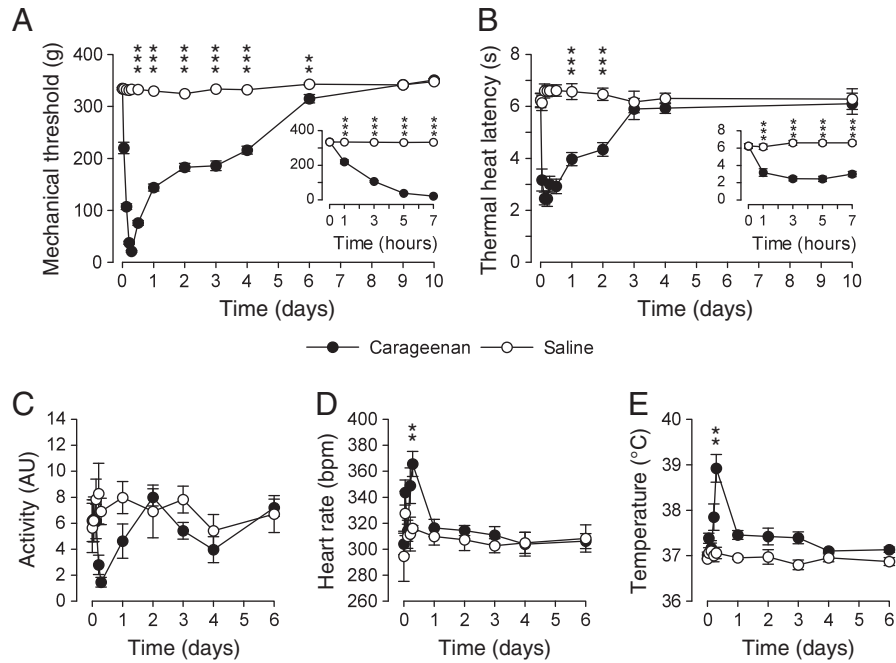
Fig. 4. Time course of carrageenan inflammatory pain associated symptoms. (A and B) Time course of (A) mechanical threshold and (B) thermal heat latency after unilateral intraplantar injection of either carrageenan (black circles; n = 18) or saline solution (white circles; n = 18). The insets show the evolution of the corresponding sensitivity during the 7 first hours. (C, D, and E) Monitoring of (C) activity, (D) heart rate and (E) abdominal temperature for carrageenan (black circles; n = 8) and saline (white circles; n = 4) treated animals. Note that nociceptive hypersensitivity and physiological alterations are both maximal at 7 h after carrageenan injection, and that majority of symptoms disappear after 48 h. Significance code for p-values of comparisons between formalin and saline groups at a given time point: $0 < *** < 0.001 < ** < 0.01 < * < 0.05$.

values, but normal mean heart rate, were observed in carrageenan-injected animals during the period where they exhibited thermal heat hyperalgesia. This result suggests that heart rate variability values such as SD(SD1) and pNN18 might be good indicators of spontaneous persistent pain expression in rats, especially if the mean heart rate remains unchanged.

The RR interval variations (e.g. heart rate variability) observed during resting conditions represent a fine tuning of the beat-to-beat control mechanisms and are claimed to be a good indicator of pain in human suffering from neuropathic [26,38], postsurgical [39], low back pain [27] and irritable bowel syndrome [40,41]. Most of these studies were conducted using a frequency domain analysis in order to obtain
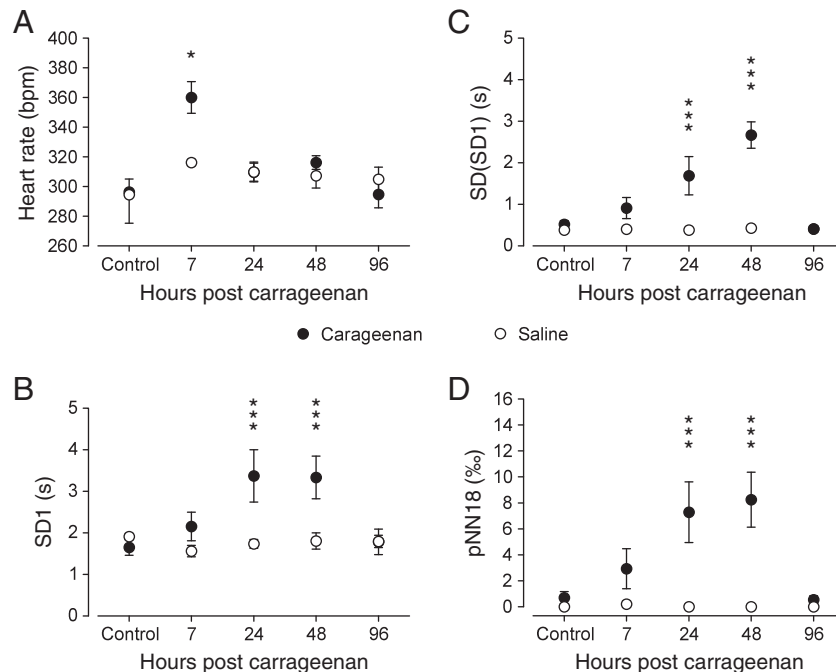

Fig. 5. Heart rate variability analyses of carrageenan inflammatory pain model. Analyses were performed in carrageenan- (black circles; n = 6) and saline-treated animals (white circles; n = 6) before injection (Control) and at 7, 24, 48 and 96 h after injection. Whereas mean heart rate (A) showed a significant increase at 7 h, indexes of heart rate variability, SD1 (B), SD(SD1) (C) and pNN18 (D), were not changed from control at this time point, but all presented a later significant increase at 24 h and 48 h, followed by full recovery at 96 h. Significance code for p-values of comparisons between carrageenan and saline groups at a given time point (Tukey post hoc test, after significant interaction term in two-way ANOVA): $0 < *** < 0.001 < ** < 0.01 < * < 0.05$.

information on sympathetic and parasympathetic contributions to heart rate. Indeed, variability in the heart rate is first controlled (i) by a balance between the vagal cholinergic inhibitory tone which prevails at rest and by sympathetic excitatory (nor)epinephrinergic influences that dominate in adaptative situations. This balance is also affected by central oscillators (vasomotor and respiratory centers), humoral factors and by the sinus node itself [42].

Using a classical frequency domain analysis, the typical spectral pattern of HRV includes two main spectral peaks: a low frequency region (LF; see Methods), affected by both sympathetic and parasympathetic activity, and a high frequency (HF) peak centered at the respiratory frequency, which is associated with parasympathetic activity [42]. Most studies focused on the HF component, believed to be generated by central coupling of the respiratory oscillator with autonomic centers in the brainstem, which primarily reflects respiration-driven vagal modulation of sinus arrhythmia. In the human literature, there is growing evidence that high pain scores [25,26,39,40,43–46] and anxiety [47] are correlated with a decrease in the HF power, thus reflecting a drop in the vagal tone. In good agreement, HRV biofeedback aimed at restoring vagal tone was recently shown to improve abdominal pain in infants [48]. Some studies have also shown the exact opposite result regarding HF parasympathetic tone, in human painful states [49–51] and animal models [19,52]. Surprisingly, we failed to reveal any changes in HF and LF in our different animal models of acute pain and inflammatory pain. Of course, many hypotheses and speculations could be raised to explain this result but we decided to go one step further and to illustrate possible HRV changes using simple descriptors extracted from the time domain analysis.

Combining a remote-controlled dynamic hot/cold plate procedure and radiotelemetric monitoring in freely-moving rats, we have been able to demonstrate that heart rate variability descriptors SD1, SD(SD1) and pNN18 were increased at nociceptive temperatures in a well established hot and cold range of nociceptive stimulation [33]. These changes were timely associated to unambiguous aversive behaviors during the test and were no longer detected after the disappearance of pain stimuli. It is interesting to note that mean heart rate values were significantly different at 20 °C and 30 °C (Student's t-test: p = 0.026). Under these basal conditions, we failed to observe any aversive behaviors and HRV parameters remained low. To explain this difference, we can only speculate that heart rate changes could reflect possible discomfort of the animals. Alternatively, because animals were randomly tested for both cold and hot ramps but only once a week, an intrinsic environmental variability could have biased this basal measure. When applying cold temperature ramps and below 4 °C (nociceptive threshold), we have been surprised to observe a significant decrease in the mean heart rate associated with elevated HRV measures (Fig. 2) and aversive behaviors. It is known that rare pain-induced bradycardia can be observed in human studies but we never had such a response using acute or persistent nociceptive stimulus (other than cold). Alternatively, decreased heart rate might be related to an overall decrease in blood temperature, thus reducing the excitability of pacemaker cardiac cells. In good agreement, radiotelemetric probes indicated a reduced temperature (1–2°) at the end of the cold ramp (at 0 °C). This might reflect the influence of the cold plate on the abdominal probe itself and/or the difficulty of the animal to maintain homeothermia. In any case, these conditions were optimal to show that elevated HRV parameters could be used as markers of pain expression since animals showed clear pain-related behaviors.

In good agreement with this result, we also observed similar phenomenon during the tonic pain phase following intraplantar formalin (20–30 min after injection). Although very few examples are available in the literature, this result was also observed in painful patients during early postoperative recovery [42] and in postoperative complications like myocardial ischemia [53]. Interestingly, time domain

descriptors are generally well correlated with parasympathetic activity and this could suggest that high SD1, SD(SD1) and pNN18 reflect the recruitment of a vagal tone aimed at limiting hypernociception.

Carrageenan intraplantar injection is a well-described model of inflammatory pain sensitization leading to mechanical and thermal hot hyperalgesia which last, in our hand, 9 days and 2 days, respectively. When the intensity of pain is maximal (e.g. 7 h after the injection) there is a clear concomitant decrease in locomotor activity, elevation of mean heart rate and abdominal temperature. Interestingly, no change in indexes of heart rate variability could be detected during this period. This is in sharp contrast with the previously discussed results but likely indicates a reduction in the fluctuations between parasympathetic and sympathetic controls on the sinusal node of the heart. Interestingly, frequency domain analysis show a parallel increase in HF and LF values (no change in HF/LF ratio). With this preliminary experiment, we can only speculate that this phenomenon might be the result of a loss of contrast in the extrinsic heart rate control balance due to a predominance of sympathetic and parasympathetic activity [42]. After 24 h, the mean values for heart rate, locomotor activity and abdominal temperature were back to normal values (e.g. undistinguishable from control group of rats) but we found an increased RR variability and pNN18 events, nicely corresponding to the persistence of pain symptoms.

In conclusion, we give strong argument here to support the use of radiotelemetry as a complementary tool to evaluate pain expression in freely-moving animals. In particular, we propose heart rate variability indexes, such as SD1, SD(SD1) and pNN18, to be of significant interest in order to detect, quantify and monitor spontaneous pain expression and recovery. Further studies will, however, be required in order to understand by which mechanisms increases in HRV are produced by pain and if these indexes can be used for other persistent pain states.

Acknowledgements

References

[1] Loeser JD, Treede RD. The Kyoto protocol of IASP Basic Pain Terminology. Pain 2008;137:473–7.
[2] Hummel P, van Dijk M. Pain assessment: current status and challenges. Semin Fetal Neonatal Med 2006;11:237–45.
[3] Mogil JS, Graham AC, Ritchie J, Hughes SF, Austin JS, Schorscher-Petcu A, Langford DJ, Bennett GJ. Hypolocomotion, asymmetrically directed behaviors (licking, lifting, flinching, and shaking) and dynamic weight bearing (gait) changes are not measures of neuropathic pain in mice. Mol Pain 2010;6:34.
[4] Le Bars D, Gozariu M, Cadden SW. Animal models of nociception. Pharmacol Rev 2001;53:597–652.
[5] Langford DJ, Bailey AL, Chanda ML, Clarke SE, Drummond TE, Echols S, Glick S, Ingrao J, Klassen-Ross T, Lacroix-Fralish ML, Matsumiya L, Sorge RE, Sotocinal SG, Tabaka JM, Wong D, van den Maagdenberg AM, Ferrari MD, Craig KD, Mogil JS. Coding of facial expressions of pain in the laboratory mouse. Nat Methods 2010;7:447–9.
[6] Craig AD. A new view of pain as a homeostatic emotion. Trends Neurosci 2003;26:303–7.
[7] Melzack R. From the gate to the neuromatrix. Pain 1999(Suppl 6):S121–6.
[8] Rainville P. Brain mechanisms of pain affect and pain modulation. Curr Opin Neurobiol 2002;12:195–204.
[9] Tracey I, Mantyh PW. The cerebral signature for pain perception and its modulation. Neuron 2007;55:377–91.
[10] Janig W. The sympathetic nervous system in pain. Eur J Anaesthesiol Suppl 1995;10:53–60.
[11] Guirimand F, Le Bars D. Physiology of nociception. Ann Fr Anesth Reanim 1996;15:1048–79.
[12] Willis Jr WD. Role of the forebrain in nociception. Prog Brain Res 1991;87:1–12.
[13] Bandler R, Shipley MT. Columnar organization in the midbrain periaqueductal gray: modules for emotional expression? Trends Neurosci 1994;17:379–89.

[14] Janig W, Habler HJ. Sympathetic nervous system: contribution to chronic pain. Prog Brain Res 2000;129:451–68.

[15] Kramer K, Kinter LB. Evaluation and applications of radiotelemetry in small laboratory animals. Physiol Genomics 2003;13:197–205.

[16] Nijsen MJ, Ongenae NG, Coulie B, Meulemans AL. Telemetric animal model to evaluate visceral pain in the freely moving rat. Pain 2003;105:115–23.

[17] Arras M, Rettich A, Cinelli P, Kasermann HP, Burki K. Assessment of post-laparotomy pain in laboratory mice by telemetric recording of heart rate and heart rate variability. BMC Vet Res 2007;3:16.

[18] Blaha MD, Leon LR. Effects of indomethacin and buprenorphine analgesia on the postoperative recovery of mice. J Am Assoc Lab Anim Sci 2008;47:8–19.

[19] Charlet A, Rodeau JL, Poisbeau P. Radiotelemetric and symptomatic evaluation of pain in the rat after laparotomy: long-term benefits of perioperative ropivacaine care. J Pain 2011;12:246–56.

[20] Goecke JC, Awad H, Lawson JC, Boivin GP. Evaluating postoperative analgesics in mice using telemetry. Comp Med 2005;55:37–44.

[21] Jin Y, Sato J, Yamazaki M, Omura S, Funakubo M, Senoo S, Aoyama M, Mizumura K. Changes in cardiovascular parameters and plasma norepinephrine level in rats after chronic constriction injury on the sciatic nerve. Pain 2008;135:221–31.

[22] Leon LR, Walker LD, DuBose DA, Stephenson LA. Biotelemetry transmitter implantation in rodents: impact on growth and circadian rhythms. Am J Physiol Regul Integr Comp Physiol 2004;286:R967–74.

[23] Brusberg M, Ravnefjord A, Lindgreen M, Larsson H, Lindstrom E, Martinez V. Oral clonidine inhibits visceral pain-related viscerosomatic and cardiovascular responses to colorectal distension in rats. Eur J Pharmacol 2008;591:243–51.

[24] Rietmann TR, Stauffacher M, Bernasconi P, Auer JA, Weishaupt MA. The association between heart rate, heart rate variability, endocrine and behavioural pain measures in horses suffering from laminitis. J Vet Med A Physiol Pathol Clin Med 2004;51:218–25.

[25] Logier R, Jeanne M, Tavernier B, De Jonckheere J. Pain/analgesia evaluation using heart rate variability analysis. Conf Proc IEEE Eng Med Biol Soc 2006;1:4303–6.

[26] Gandhi RA, Marques JL, Selvarajah D, Emery CJ, Tesfaye S. Painful diabetic neuropathy is associated with greater autonomic dysfunction than painless diabetic neuropathy. Diabetes Care 2010;33:1585–90.

[27] Roy RA, Boucher JP, Comtois AS. Heart rate variability modulation after manipulation in pain-free patients vs patients in pain. J Manipulative Physiol Ther 2009;32:277–86.

[28] Tousignant-Laflamme Y, Rainville P, Marchand S. Establishing a link between heart rate and pain in healthy subjects: a gender effect. J Pain 2005;6:341–7.

[29] Nicklas W, Baneux P, Boot R, Decelle T, Deeny AA, Fumanelli M, Illgen-Wilcke B. Recommendations for the health monitoring of rodent and rabbit colonies in breeding and experimental units. Lab Anim 2002;36:20–42.

[30] Luis-Delgado OE, Barrot M, Rodeau JL, Schott G, Benbouzid M, Poisbeau P, Freund-Mercier MJ, Lasbennes F. Calibrated forceps: a sensitive and reliable tool for pain and analgesia studies. J Pain 2006;7:32–9.

[31] Hargreaves K, Dubner R, Brown F, Flores C, Joris J. A new and sensitive method for measuring thermal nociception in cutaneous hyperalgesia. Pain 1988;32:77–88.

[32] Flatters SJ, Bennett GJ. Ethosuximide reverses paclitaxel- and vincristine-induced painful peripheral neuropathy. Pain 2004;109:150–61.

[33] Yalcin I, Charlet A, Freund-Mercier MJ, Barrot M, Poisbeau P. Differentiating thermal allodynia and hyperalgesia using dynamic hot and cold plate in rodents. J Pain 2009;10:767–73.

[34] Brennan M, Palaniswami M, Kamen P. Do existing measures of Poincare plot geometry reflect nonlinear features of heart rate variability? IEEE Trans Biomed Eng 2001;48:1342–7.

[35] Piskorski J, Guzik P. Geometry of the Poincare plot of RR intervals and its asymmetry in healthy adults. Physiol Meas 2007;28:287–300.

[36] Cosson E, Herisse M, Laude D, Thomas F, Valensi P, Attali JR, Safar ME, Dabire H. Aortic stiffness and pulse pressure amplification in Wistar–Kyoto and spontaneously hypertensive rats. Am J Physiol Heart Circ Physiol 2007;292:H2506–12.

[37] Capone F, Aloisi AM. Refinement of pain evaluation techniques. The formalin test. Ann Ist Super Sanita 2004;40:223–9.

[38] Pereira EA, Lu G, Wang S, Schweder PM, Hyam JA, Stein JF, Paterson DJ, Aziz TZ, Green AL. Ventral periaqueductal grey stimulation alters heart rate variability in humans with chronic pain. Exp Neurol 2010;223:574–81.

[39] Faye PM, De Jonckheere J, Logier R, Kuissi E, Jeanne M, Rakza T, Storme L. Newborn infant pain assessment using heart rate variability analysis. Clin J Pain 2010;26:777–82.

[40] Cain KC, Jarrett ME, Burr RL, Hertig VL, Heitkemper MM. Heart rate variability is related to pain severity and predominant bowel pattern in women with irritable bowel syndrome. Neurogastroenterol Motil 2007;19:110–8.

[41] Tousignant-Laflamme Y, Goffaux P, Bourgault P, Marchand S. Different autonomic responses to experimental pain in IBS patients and healthy controls. J Clin Gastroenterol 2006;40:814–20.

[42] Laitio T, Jalonen J, Kuusela T, Scheinin H. The role of heart rate variability in risk stratification for adverse postoperative cardiac events. Anesth Analg 2007;105:1548–60.

[43] Appelhans BM, Luecken LJ. Heart rate variability and pain: associations of two interrelated homeostatic processes. Biol Psychol 2008;77:174–82.

[44] Jeanne M, Logier R, De Jonckheere J, Tavernier B. Heart rate variability during total intravenous anesthesia: effects of nociception and analgesia. Auton Neurosci 2009;147:91–6.

[45] Oberlander TF, Grunau RE, Pitfield S, Whitfield MF, Saul JP. The developmental character of cardiac autonomic responses to an acute noxious event in 4- and 8-month-old healthy infants. Pediatr Res 1999;45:519–25.

[46] Oberlander TF, Grunau RE, Whitfield MF, Fitzgerald C, Pitfield S, Saul JP. Biobehavioral pain responses in former extremely low birth weight infants at four months' corrected age. Pediatrics 2000;105:e6.

[47] Miu AC, Heilman RM, Miclea M. Reduced heart rate variability and vagal tone in anxiety: trait versus state, and the effects of autogenic training. Auton Neurosci 2009;145:99–103.

[48] Sowder E, Gevirtz R, Shapiro W, Ebert C. Restoration of vagal tone: a possible mechanism for functional abdominal pain. Appl Psychophysiol Biofeedback 2010;35:199–206.

[49] Adeyemi EO, Desai KD, Towsey M, Ghista D. Characterization of autonomic dysfunction in patients with irritable bowel syndrome by means of heart rate variability studies. Am J Gastroenterol 1999;94:816–23.

[50] Jorgensen LS, Christiansen P, Raundahl U, Ostgaard S, Christensen NJ, Fenger M, Flachs H. Autonomic nervous system function in patients with functional abdominal pain. An experimental study. Scand J Gastroenterol 1993;28:63–8.

[51] Punyabati O, Deepak KK, Sharma MP, Dwivedi SN. Autonomic nervous system reactivity in irritable bowel syndrome. Indian J Gastroenterol 2000;19:122–5.

[52] Stewart M, Verkerk GA, Stafford KJ, Schaefer AL, Webster JR. Noninvasive assessment of autonomic activity for evaluation of pain in calves, using surgical castration as a model. J Dairy Sci 2010;93:3602–9.

[53] Laitio TT, Makikallio TH, Huikuri HV, Kentala ES, Uotila P, Jalonen JR, Helenius H, Hartiala J, Yli-Mayry S, Scheinin H. Relation of heart rate dynamics to the occurrence of myocardial ischemia after coronary artery bypass grafting. Am J Cardiol 2002;89:1176–81.

II - Oxytocinergic Modulation of Anxiety through Intra-Amygdala Circuits

From 2010 to 2013, I was a postdoctoral fellow Lausanne. My scientific project was to understand and decipher the effects on fear and anxiety of oxytocin within the central amygdala, from *in vitro* in slice to *in vivo* in freely moving animals.

Fear and anxiety are normal reactions to danger and may drive important aspects of our behavior. Under normal circumstances, fear can lead to "fear-conditioned learning", a process during which a relation is established between a harmful stimulus (unconditioned stimulus) and a neutral stimulus (conditioned stimulus). Recently, it has become clear that "fear-conditioned learning" can be directly related to synaptic plasticity in the amygdala. The amygdala encompasses a lateral (LA) and basolateral nucleus (BLA) to form the basolateral complex, which receives sensory information directly from the hippocampus, thalamus and the medial prefrontal and sensory association cortex. The basolateral complex projects to the central amygdala (CeA), which mediates the emotional expression of the learned association (Killcross et al., 1997). The CeA is the relay with the autonomic systems that trigger the physiological aspects of the fear response. The central medial part of the CeA (CeM), represents the main output of the CeA (Hopkins & Holstege, 1978) and is under an inhibitory control by GABAergic projections from the lateral part of the CeA (CeL, Petrovich & Swanson, 1997).

Oxytocin (OT) is a nonapeptide synthesized in the hypothalamus (Swanson and Sawchenko, 1983). OT has become over the last several years a centre of attention for the regulation of functions in emotional behavior, among which anxiety and fear (De Dreu et al., 2010). Previous work revealed that OT can activate a subpopulation of GABAergic interneurons in the lateral part (CeL) of the central amygdala (CeA) that projects to the medial part of the

Figure 2: *Central amygdala circuits.* **(A)** Histoautoradiographs showing the binding-site areas for OT (red) and vasopressin (green) in the CeA. **(B)** Model of local circuitry in the CeA showing processing of different excitatory inputs (+) and GABAergic connections (−) between OT and vasopressin receptor–expressing regions (CeL/C and CeM). *Adapted from Huber et al, 2005.*

CeA (CeM). Their excitation leads to the inhibition of CeM neurons that can in turn be directly activated by vasopressin receptors (Figure 2). The OT excited neurons thus form a major inhibitory projection from the CeL onto the CeM nucleus (Huber et al., 2005). However, two major questions remained and I focused to the following:
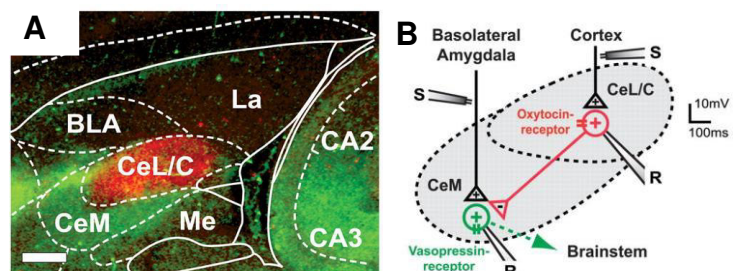
1) To address how oxytocin gates the fear response, by deciphering the selectivity of its action to different amygdala outputs (Viviani et al., *Science*, 2011).

2) To demonstrate that endogenous oxytocin reach and have physiological action within the CeA via long-range projection axons, at this time a minority hypothesis versus the established dentritic release assumption (Knobloch, Charlet et al., *Neuron*, 2012). These drove the awards I received from SSBP in 2012 and French Academy of Medicine in 2013.

1 - Oxytocin Selectively Gates Fear Response through Distinct Outputs from the CeA

Previous work from Ron Stoop lab (Huber et al., 2005), have shown the effects of vasopressin and oxytocin on the neuronal activity of the rat central amygdala. It led to a first model for the modulation of information processing in the central amygdala by neuropeptides, in which the opposing behavioral effects of vasopressin and oxytocin are caused by the selective activation of two distinct populations of neurons in the GABAergic network of the central amygdala (Figure 2).

Directly following this findings, we have investigated how projections from the CeA to the brainstem are organized and how neuropeptides such as oxytocin (OT) and bombesin (BB) can modulate these.

To do so, **considering the large number of projections emanating from the CeA to different brain stem nuclei and the large number of different neuropeptide receptors in this nucleus we hypothesized that neuropeptides specificity may constitute a basis for selective gating of fear responses**. To test this hypothesis, we used fluorescent latex microbeads to retrogradely trace projections from the CeA to the periaqueductal grey (involved in freezing behavior) or to the dorsal vagal complex (controlling heart rhythm) and then recorded the response of the labeled cell to OT and BB applications.

We found that projection to either of these nuclei originated from different subpopulations of neurons in the CeA. Interestingly, it appeared that the indirect inhibitory effects of OT were only able to gate neurons with projections to the PAG, leaving those with projections to the dorsal vagal complex unaffected, while BB was able to modulate all projecting neurons. *In vivo,* these effects were paralleled with injections of oxytocin in the CeA inhibiting fear-conditioned evoked freezing behavior, but leaving fear-evoked changes in heart rate unaffected, while bombesin CeA injection led to a decrease in both the freezing and heart rate response.

In conclusion, we found that OT only affects distinct aspects of the fear response and thus, that fear is not a simple standard behavioral program, but can be modulated specifically at the level of the CeA. The CeA is thus able to finetune its output through neuropeptidergic modulations.

Oxytocin Selectively Gates Fear Responses Through Distinct Outputs from the Central Amygdala

Daniele Viviani, *et al.*

References and Notes

1. R. E. Ley, P. J. Turnbaugh, S. Klein, J. I. Gordon, *Nature* **444**, 1022 (2006).
2. T. A. Clayton, D. Baker, J. C. Lindon, J. R. Everett, J. K. Nicholson, *Proc. Natl. Acad. Sci. U.S.A.* **106**, 14728 (2009).
3. R. J. Xavier, D. K. Podolsky, *Nature* **448**, 427 (2007).
4. J. Qin *et al.*, *Nature* **464**, 59 (2010).
5. P. J. Turnbaugh *et al.*, *Proc. Natl. Acad. Sci. U.S.A.* **107**, 7503 (2010).
6. P. J. Turnbaugh *et al.*, *Sci. Transl. Med.* **1**, 6ra14 (2009).
7. B. D. Muegge *et al.*, *Science* **332**, 970 (2011).
8. J. Handelsman, *DNA Cell Biol.* **27**, 219 (2008).
9. J. J. Faith *et al.*, *ISME J.* **4**, 1094 (2010).
10. F. E. Rey *et al.*, *J. Biol. Chem.* **285**, 22082 (2010).
11. M. A. Mahowald *et al.*, *Proc. Natl. Acad. Sci. U.S.A.* **106**, 5859 (2009).
12. A. L. Goodman *et al.*, *Cell Host Microbe* **6**, 279 (2009).
13. Materials and methods are available as supporting material on *Science* Online.
14. A. Mortazavi, B. A. Williams, K. McCue, L. Schaeffer, B. Wold, *Nat. Methods* **5**, 621 (2008).
15. X. Fu *et al.*, *BMC Genomics* **10**, 161 (2009).
16. J. M. Chase, M. A. Leibold, *Ecological Niches: Linking Classical and Contemporary Approaches (Interspecific interactions)* (University of Chicago Press, Chicago, 2003).

Acknowledgments: We are indebted to D. O'Donnell, M. Karlsson, and S. Wagoner for their help with various aspects of gnotobiotic mouse husbandry and to B. Mickelson, I. Mogno, A. Goodman, N. Griffin, H. Seedorf, G. Simon, J. Chase, and B. Cohen for their many helpful suggestions during the course of this work. This work was supported by grants from NIH (DK30292 and DK70977) and the Crohn's and Colitis Foundation of America. COPRO-seq and microbial RNA-seq data are available in the Gene Expression Omnibus (accession GSE26687). Processed data can be obtained at http://gordonlab.wustl.edu/modeling_microbiota/.

Oxytocin Selectively Gates Fear Responses Through Distinct Outputs from the Central Amygdala

Daniele Viviani,[1] Alexandre Charlet,[1] Erwin van den Burg,[1]* Camille Robinet,[1]* Nicolas Hurni,[1] Marios Abatis,[1] Fulvio Magara,[1] Ron Stoop[1,2]†

Central amygdala (CeA) projections to hypothalamic and brain stem nuclei regulate the behavioral and physiological expression of fear, but it is unknown whether these different aspects of the fear response can be separately regulated by the CeA. We combined fluorescent retrograde tracing of CeA projections to nuclei that modulate fear-related freezing or cardiovascular responses with in vitro electrophysiological recordings and with in vivo monitoring of related behavioral and physiological parameters. CeA projections emerged from separate neuronal populations with different electrophysiological characteristics and different response properties to oxytocin. In vivo, oxytocin decreased freezing responses in fear-conditioned rats without affecting the cardiovascular response. Thus, neuropeptidergic signaling can modulate the CeA outputs through separate neuronal circuits and thereby individually steer the various aspects of the fear response.

Fear can be severely immobilizing but can also be a major driving force for some of humans' most heroic acts. In both cases, the internal emotional experience may be similar, although it may lead to substantially different behavioral outcomes (*1–3*). Studies on human emotions often use autonomic nervous system parameters to assess arousal, because of the role of our internal organs in the emotional state (*4, 5*). Projections from the central nucleus of the amygdala (CeA) to the hypothalamus and different brain stem nuclei coordinate behavioral and physiological fear expression (*6*). It has been postulated that different fear responses, characterized by more active or passive behavioral coping strategies, can be triggered by a neuronal switch within the CeA (*7*). The question thus arises whether fear responses only vary in intensity, or whether different qualities of fear responses exist, reflected in different associations between behavioral and physiological components. We investigated whether a neurophysiological basis for such a distinct regulation could be found in the CeA.

[1]Centre for Psychiatric Neuroscience, Department of Psychiatry, Lausanne University Hospital Center, University of Lausanne, CH-1015 Lausanne, Switzerland. [2]Department of Physiology, University of Lausanne, CH-1015 Lausanne, Switzerland.

*These authors contributed equally to this work.
†To whom correspondence should be addressed. E-mail: rstoop@unil.ch

Fig. 1. Distinct neuronal populations of the CeM project to PAG and DVC. (**A** and **B**) Coronal views of injection sites (A) in PAG of fluorescent green and (B) in DVC of red microspheres (left), corresponding CeM labeling (right). Scale bars: left, 1 mm; right, 500 μm. lPAG, lateral PAG; vlPAG, ventrolateral PAG; sp5, spinal trigeminal tract. (**C**) Separately labeled CeM neurons after coinjections of green and red microspheres in respective PAG and DVC (left) versus colabeled neurons after injections of both microspheres in DVC (right, scale bar, 50 μm). (**D**) Quantification of colabeled (coloc) CeM neurons (see also table S2). (**E**) Electrophysiological characteristics of CeM→PAGs, "PAG" and CeM→DVCs "DVC." (*$P < 0.05$; **$P < 0.01$, $n = 22$ to 43 neurons) Error bars indicate SEM.

n=7	PAG	DVC	Coloc
Total	313	327	40
% cells	46.0	48.1	5.9
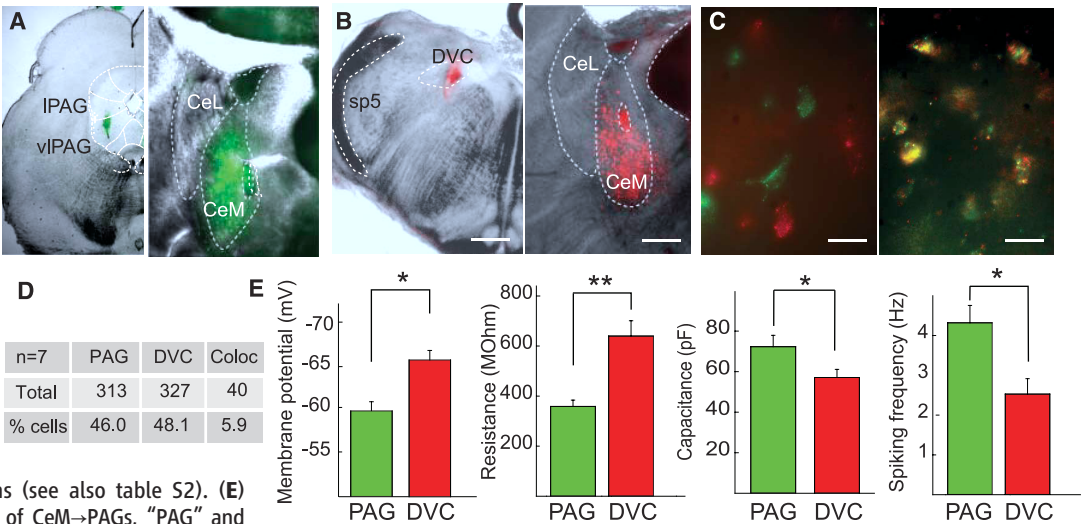
Most projections from the CeA to the hypothalamus and brain stem nuclei originate from the medial part of the CeA (CeM) (6). Oxytocin can inhibit neurons in the CeM through its excitatory effects on γ-aminobutyric acid (GABA) inhibitory (GABAergic) projections that originate from the lateral and capsular part of the CeA (8) (henceforth referred to as CeL). The CeL contains distinct neuronal populations (7–10) whose individual activation may differentially regulate active versus passive fear responses (7). Can a similar distinction of neuronal popula-

tions be found in the CeM (10)? Do projections from the CeM to selective targets in the hypothalamus and brain stem arise from distinct neuronal populations and, if so, are these under a specific inhibitory control from the CeL? Such specificity might provide a neurophysiological basis within the CeA to selectively regulate behavioral and physiological components of the fear response.

We first evaluated the target specificity of CeM projections by double fluorescent retrograde tracing of the ventrolateral column of the peri-

aqueductal gray (PAG), which is implicated in the freezing response (6), and the dorsal vagal complex (DVC), which modulates cardiovascular responses (11). We injected green and red fluorescent latex microspheres, respectively, into the PAG and DVC of 3- to 4-week-old Sprague-Dawley rats (12, 13). After allowing 48 hours of retrograde transport, we killed the animals, verified the injection sites (Fig. 1, A and B), and assessed retrograde label in horizontal brain slices of the CeM. Both green and red microspheres were present throughout the CeM (Fig. 1, A and B), yet in separate neurons that were intermingled without any obvious clusters (Fig. 1C and fig. S1). Confocal quantification revealed 5.9% colabeling ($n = 680$ neurons, Fig. 1D, fig. S1, and table S1). Injecting a mixture of green and red microspheres in the DVC resulted in their copresence in all labeled CeM neurons (Fig. 1C), confirming sensitivity to detect colabeling.

We next compared electrophysiological properties by whole-cell recordings from fluorescently labeled PAG- and DVC-projecting neurons (henceforth called CeM→PAGs and CeM→DVCs, respectively). CeM→PAGs ($n = 42$) were, on average, significantly more depolarized (-59.6 ± 1.6 versus -65.4 ± 1.2 mV) and had lower membrane resistance (358 ± 25 versus 640 ± 61 MΩ) and higher membrane capacitance (72.3 ± 5.6 versus 58.5 ± 4.0 pF) than CeM→DVCs ($n = 43$, Fig. 1E). In cell-attached configuration, average basic spiking frequencies of CeM→PAGs ($n = 22$) were significantly higher than CeM→DVCs (4.1 ± 0.5 versus 2.5 ± 0.4 Hz, $n = 28$).

Prompted by these anatomical and electrophysiological differences, we also tested their pharmacological characteristics. Although both projection neurons were similarly excited or inhibited by a range of neuropeptides (table S2), oxytocin—known to increase spontaneous inhib-

Fig. 2. Distinct effects of TGOT on CeM→DVC and CeM→PAG neurons. (**A** and **B**) Representative traces of sIPSCs (top) and their average frequencies (bottom) recorded before (control) and after (TGOT) application of (A) CeM→PAGs and (B) CeM→DVCs. (**C** and **D**) The same for spontaneous spiking activity (*$F_{2,36} = 8.4$, $P < 0.005$; **$F_{2,122} = 17.8$, $P < 0.0001$, $n = 20$ to 34 neurons) Error bars indicate SEM.
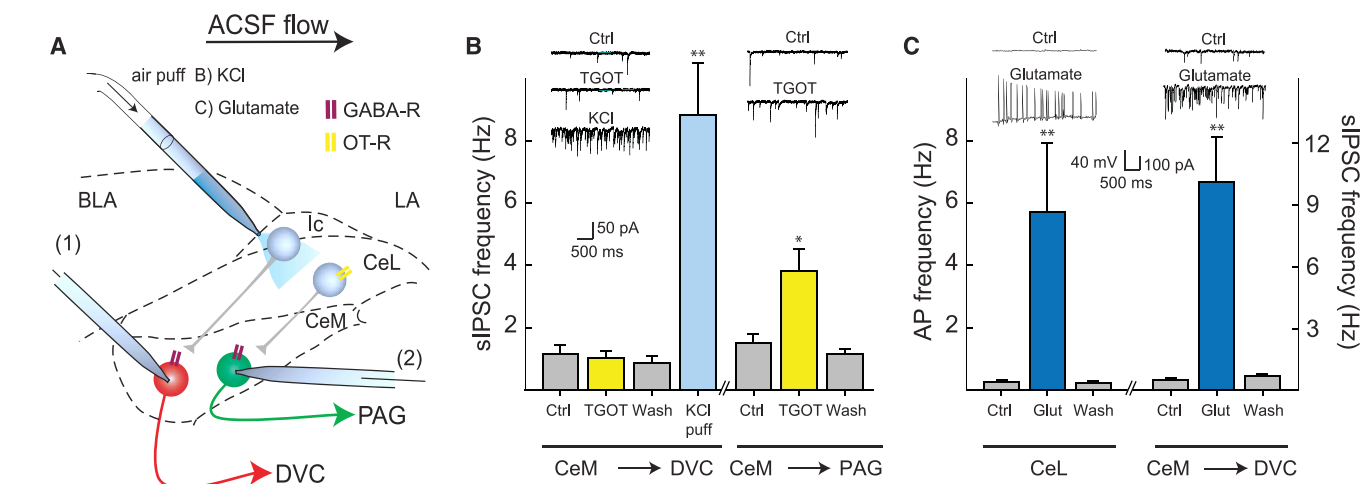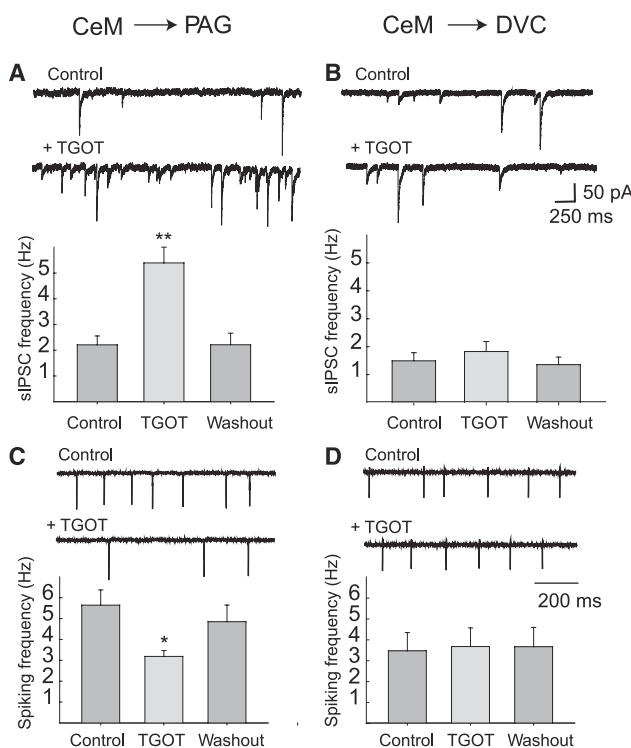

Fig. 3. Local stimulation reveals inhibitory projections on TGOT-insensitive CeM→DVCs. (**A**) Local perfusion of neurons that project to CeM→DVCs (red) and CeM→PAGs (green) in a horizontal brain slice of the CeA with ACSF flow away from CeM. GABA-R, GABA$_A$ receptor; OT-R, oxytocin receptor; BLA, basolateral amygdala; LA, lateral amygdala; Ic, Intercalated neurons. (**B**) Average sIPSC frequencies in CeM→DVCs recorded with patch pipette "(1)" after bath-perfused TGOT followed by locally puffed KCl ($n = 6$), subsequently, in the same slice, in CeM→PAGs recorded with pipette "(2)" after bath-perfused TGOT ($n = 6$). (**C**) Action potential and sIPSC frequencies in respective CeL ($n = 5$) and CeM→DVC neurons ($n = 5$) after local perfusion with glutamate. (*$P < 0.05$, **$P < 0.005$) Error bars indicate SEM.

itory postsynaptic current (sIPSC) frequencies of CeM neurons (8) (fig. S2A)—only affected CeM→PAGs. Thus, bath perfusion of the oxytocin agonist [Thr^4,Gly^7]-oxytocin (TGOT) specifically and reversibly increased sIPSC frequencies in CeM→PAGs (from 2.2 ± 0.3 to 5.6 ± 0.7 Hz, n =

34) (Fig. 2A) but not in CeM→DVCs (from 1.5 ± 0.3 to 1.7 ± 0.2 Hz, n = 32) (Fig. 2B) (see also fig. S3). In cell-attached recordings, this translated into a selective inhibition of spontaneous spiking frequencies of CeM→PAGs (from 5.6 ± 0.7 to 3.1 ± 0.2 Hz, n = 10) (Fig. 2C) versus

CeM→DVCs (from 3.5 ± 1.0 to 3.7 ± 0.9 Hz, n = 10) (Fig. 2D) (8).

To verify whether the failure of TGOT to inhibit CeM→DVCs was caused by the absence of inhibitory projections, we locally depolarized by puffing KCl (35 mM) from a patch pipette (13)
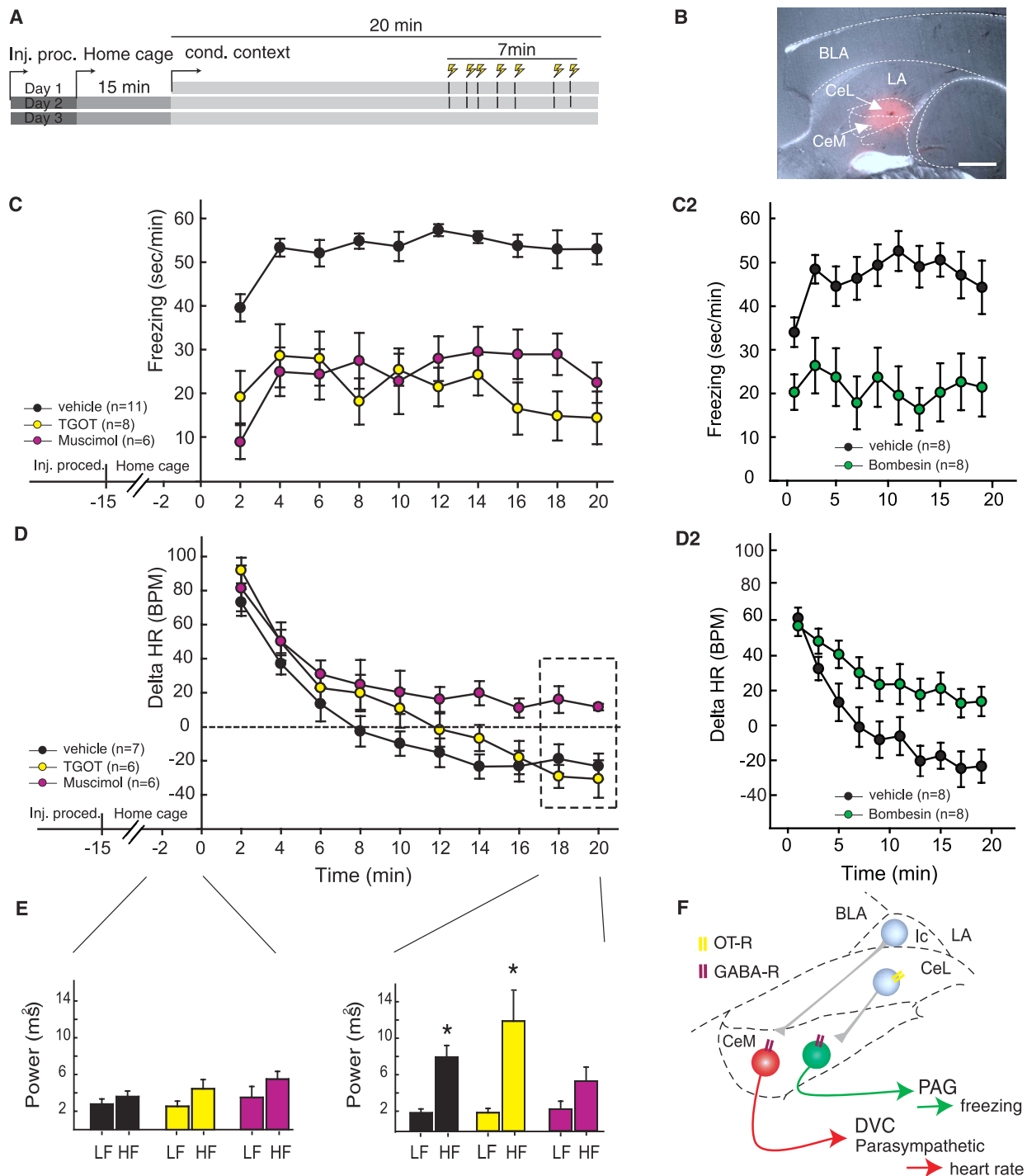

Fig. 4. Differential effects of drugs injected in the CeA on freezing and heart rate during a conditioned fear response. (**A**) Three-day fear-conditioning protocol: Inj. proc, sham injection procedure; yellow lightings, electric shocks. (**B**) Postmortem analysis showing fluorescent muscimol Bodipy diffusion inside the CeA. Scale bar, 1 mm. (**C**) Freezing responses measured on day 3 in the context alone. (**D**) The same for heart rate responses [D

(left): $F_{2,16}$ = 3.8, $P < 0.05$; D2: $F_{1,14}$ = 5.3, $P < 0.05$]. (**E**) Power spectrum histograms of HRV −2 to 0 min before and 18 to 20 min after placing rats in conditioning context. LF, low-frequency component; HF, high-frequency component. Error bars indicate SEM (*$P < 0.05$). (**F**) Final model illustrating specific TGOT-inhibited freezing through selective inhibition of CeM→PAGs. Abbreviations as in (Fig. 3A).

(Fig. 3A) and simultaneously recorded sIPSCs from CeM→DVCs. Although bath-perfused TGOT did not affect sIPSC frequencies (from 1.2 ± 0.3 to 1.0 ± 0.2 Hz, $n = 6$), rapid increases occurred with KCl puffs at distinct locations in the CeL (from 0.9 ± 0.2 to 8.4 ± 1.6 Hz, $n = 6$) (Fig. 3B). In the same slice, TGOT remained capable of increasing sIPSC frequencies in CeM→PAGs (from 1.5 ± 0.3 to 3.8 ± 0.7 Hz, $n = 6$) (Fig. 3C). Puffing glutamate (Fig. 3C) or bombesin (fig. S4), for which receptors are expressed in the CeL and adjacent intercalated inhibitory neurons, gave similar results, which suggested an activation of inhibitory projections arising from either of these regions [discussed further in (13)].

To investigate how these specific in vitro effects of oxytocin translated in vivo into fear-induced freezing behavior (mediated by the PAG) (6, 14) and cardiovascular changes (modulated by the DVC) (11, 15), we equipped rats with bilateral cannulae for local drug administration into the CeA and implanted radiotelemetric devices to monitor heart rate. To activate the amygdala, we applied a 2-day contextual fear-conditioning protocol (13) that resulted in >90% freezing after conditioning and >80% freezing responses upon reexposure to the context in all vehicle-injected animals (Fig. 4, A and C, and fig. S2B). Bilateral injection of TGOT or GABA$_A$ receptor agonist muscimol decreased these freezing responses to <50%) (Fig. 4C). In rats where TGOT had not decreased freezing, the injection sites, identified with fluorescent muscimol (Fig. 4B), were outside the CeA (fig. S5), which confirmed the CeA role in these contextual freezing responses [further discussed in (13)]. Although baseline heart rate before reexposure and the initial elevation in heart rate upon reexposure to the context were similar for all groups [baseline: artificial cerebrospinal fluid (ACSF) 400 ± 10; TGOT 394 ± 10; muscimol 394 ± 12 beats per min (bpm)] (Fig. 4D), the typical decrease that followed in the second 10-min period was inhibited by muscimol but not by TGOT. Bombesin reduced freezing and prevented the decrease in heart rate (Fig. 4C2 and 4D2) consistent with its inhibition of both CeM→PAGs and CeM→DVCs. Together, these data not only support the selective action of oxytocin on freezing behavior via CeM→PAGs, but also suggest a critical role of CeM→DVC neurons in the control of cardiovascular changes to fearful stimuli. Finally, heart rate variability (HRV) analysis (13) revealed an absence of increase in the high frequency band in the muscimol-treated rats (Fig. 4E), which indicated an inhibition of the parasympathetic activation (13) (table S3 and fig. S7). The failure of TGOT to affect this parasympathetic cardiovascular response is consistent with the absence of TGOT effects on CeM→DVCs (11, 15).

The present findings provide evidence that specific behavioral and physiological components of the fear response are controlled by distinct neuronal populations in the CeM (Fig. 4F). These project to the PAG and the DVC; exhibit

unique electrophysiological characteristics; and despite being spatially intermingled, are selectively modulated by oxytocin through inhibitory projections from the CeL. The functionality of this selectivity was further revealed at the behavioral and physiological level by oxytocin's inhibition of freezing responses without affecting cardiovascular changes. Previous studies have distinguished neuronal populations in the CeL on the basis of expression of CRF or opioids (16) or on mutually inhibitory connections (10). These may play a specific role in the inhibition of CeM→PAGs, and, in combination with the distinct electrophysiological characteristics of CeM neurons, affect further local information processing [see e.g., (17)].

A specific regulation by the CeL of CeM neurons with different projections could have important implications for the mechanisms underlying the expression of fear. Distinct neuronal populations in the CeL are activated or inhibited during the expression of fear (9, 10) and this might represent a switch between active versus passive fear and associated coping strategies (7). Our present findings imply that the CeM differentially controls expressions of the fear response through separate projections to the brain stem. Our findings, instead of supporting a rigid association between behavioral and physiological expressions of fear (1, 2), suggest that these expressions may be specifically controlled by the CeL. This underlines, first, the importance of considering multiple parameters in the correct assessment of fear responses in animals, but it also opens the potential for new therapeutic applications (fig S8). In humans, panic disorder can manifest itself at the visceral level predominantly by increases in heart rate, respiratory rhythm, or gastrointestinal motility (18). While its onset appears to be triggered in the lateral and basal amygdala (19), its specific expression may result from a differential gating within the CeA. Although panic and other anxiety disorders are typically treated with benzodiazepines, future neuropeptide-based therapies might offer a more precise inhibition of their expression.

The amygdala orchestrates behavioral responses to both negative (fearful) and positive (rewarding) salient stimuli (20, 21), although the precise underlying circuits are still unclear. Distinct, intercalated CeL and CeM populations, targeted by projections from the basolateral amygdala (22) and brain stem (11), could play a role in regulating behavioral and physiological expressions associated with different emotions (3–5). Furthermore, the CeA expresses a multitude of neuropeptide receptors that can specifically affect local activity (8, 23–25). Levels of oxytocin and its receptors can vary between individual rats according to genetic background (26), early life experience (27), internal state (28), or environment (24, 29) and have been associated with different degrees of anxiety and fear (27). As we found that oxytocin decreases freezing responses, yet leaves cardiovascular responses unaffected,

this specific regulation could preserve the internal, visceral expression of fear, but alleviate the behavioral inhibition that leads to freezing. Such individual regulation may provide the most adequate reaction in circumstances when a proactive behavioral response is required, while preserving an internal, visceral adaptive response to fear.

References and Notes
1. J. LeDoux, *Cell. Mol. Neurobiol.* **23**, 727 (2003).
2. M. Davis, in *The Amygdala*, J.P. Aggleton, Ed. (Wiley-Liss, NY, 1992), pp. 255–306.
3. S. W. Porges, *Ann. N.Y. Acad. Sci.* **1008**, 31 (2003).
4. E. P. Vianna, D. Tranel, *Int. J. Psychophysiol.* **61**, 70 (2006).
5. P. Rainville, A. Bechara, N. Naqvi, A. R. Damasio, *Int. J. Psychophysiol.* **61**, 5 (2006).
6. J. E. LeDoux, J. Iwata, P. Cicchetti, D. J. Reis, *J. Neurosci.* **8**, 2517 (1988).
7. A. Gozzi et al., *Neuron* **67**, 656 (2010).
8. D. Huber, P. Veinante, R. Stoop, *Science* **308**, 245 (2005).
9. S. Ciocchi et al., *Nature* **468**, 277 (2010).
10. W. Haubensak et al., *Nature* **468**, 270 (2010).
11. A. D. Loewy, in *Central Regulation of Autonomic Functions*, A. D. Loewy and K. M. Spyer Eds. (Oxford Univ. Press, New York, 1990), pp. 88–103.
12. L. C. Katz, A. Burkhalter, W. J. Dreyer, *Nature* **310**, 498 (1984).
13. Further information including materials and methods is available as supporting material on *Science* Online.
14. T. M. da Costa Gomez, M. M. Behbehani, *Brain Res.* **689**, 21 (1995).
15. J. S. Schwaber, B. S. Kapp, G. A. Higgins, P. R. Rapp, *J. Neurosci.* **2**, 1424 (1982).
16. H. E. Day, E. J. Curran, S. J. Watson Jr., H. Akil, *J. Comp. Neurol.* **413**, 113 (1999).
17. E. C. Dumont, M. Martina, R. D. Samson, G. Drolet, D. Paré, *Eur. J. Neurosci.* **15**, 545 (2002).
18. R. A. Sansone, L. A. Sansone, *Psychiatry* **6**, 33 (2009).
19. A. E. Ziemann et al., *Cell* **139**, 1012 (2009).
20. J. J. Paton, M. A. Belova, S. E. Morrison, C. D. Salzman, *Nature* **439**, 865 (2006).
21. K. M. Tye, G. D. Stuber, B. de Ridder, A. Bonci, P. H. Janak, *Nature* **453**, 1253 (2008).
22. K. M. Tye et al., *Nature* **471**, 358 (2011).
23. B. C. Chieng, M. J. Christie, P. B. Osborne, *J. Comp. Neurol.* **497**, 910 (2006).
24. T. J. Sajdyk, A. Shekhar, D. R. Gehlert, *Neuropeptides* **38**, 225 (2004).
25. A. Bisetti et al., *Neuroscience* **142**, 999 (2006).
26. O. J. Bosch, S. L. Meddle, D. I. Beiderbeck, A. J. Douglas, I. D. Neumann, *J. Neurosci.* **25**, 6807 (2005).
27. F. A. Champagne, M. J. Meaney, *Biol. Psychiatry* **59**, 1227 (2006).
28. M. M. McCarthy, C. H. McDonald, P. J. Brooks, D. Goldman, *Physiol. Behav.* **60**, 1209 (1996).
29. M. Waldherr, I. D. Neumann, *Proc. Natl. Acad. Sci. U.S.A.* **104**, 16681 (2007).

2 - Evoked Axonal Oxytocin Release in the CeA Attenuates Fear Response

Oxytocin is synthetized in the paraventricular (PVN), supraoptic (SON), and accessory magnocellular (AN) nuclei of the hypothalamus but the way by which oxytocin reaches the CeA to affect fear has remained unclear (Neumann, 2008). Neuropeptides can be secreted over the entire cell membrane into the extracellular space and ultimately reach receptors by way of diffusion. Alternatively, they can be coreleased at synapses together with classical neurotransmitters such as GABA or glutamate. Depending on the amount released and because of relatively long half-lives due to slow degradation in the extracellular space, neuropeptides often spill over from synapses to bind extrasynaptic receptors. Passive diffusion along concentration gradients following dendritic release or synaptic spillover presents a mechanism through which neuropeptides, such as OT or vasopressin, without using direct cell-to-cell connections, can modulate the activity of their target cells (Ludwig and Leng, 2006). However, because these diffusion processes are both slow and undirected, this comes at cost of temporal as well as spatial specificity of neuropetidergic signaling.

In this study, **we investigated how OT reaches the CeA and to characterize the mechanism by which OT modulates neuronal circuits within the CeA to reduce fear**.

To do so, we used state-of-the adeno-associated virus to introduce a protein of interest under control of OT promoter for both anatomical tracing and optogenetical manipulation of OT projections.

We found that OT neurons send long-range projecting axons. Surprisingly, the magnocellular OT neurons are the main source of OT in the CeA innervations, while they were mainly known to project to the pituitary in order to release OT in the blood. Moreover, the main source of OT projections to the CeA appears to be the AN with, in a lesser extent, the PVN. Interestingly, these (rare) axonal projections are able to increase GABAergic local network activity in one third of the recorded cell (Figure 3). This was mainly mediated by axonal OT release with small glutamatergic contribution. Finally, the evoked release of endogenous OT within the CeA lead to a strong, but reversible, decrease of the conditioned fear response.

**Figure 3**: Curbing fear by axonal oxytocin release in the CeA. Hypothalamic nuclei send projections of varying strength (indicated by red line thickness) to the CeA. Light activation of ChR2-expressing OT axon terminals in the CeL results in local release of OT (dark blue circles), causing enhanced activity of inhibitory CeL cells (light blue) that project to the CeM. Increased inhibition of CeM output cells (green) leads to attenuation of fear. _From Tovote and Lüthi comment in Neuron, 2012._

Taken together, these results demonstrate for the first time the OT axonal projections to distant nuclei and suggest the existence of small and segregated oxytocinergic neuronal populations sending rare but strong projections to their distant targets.
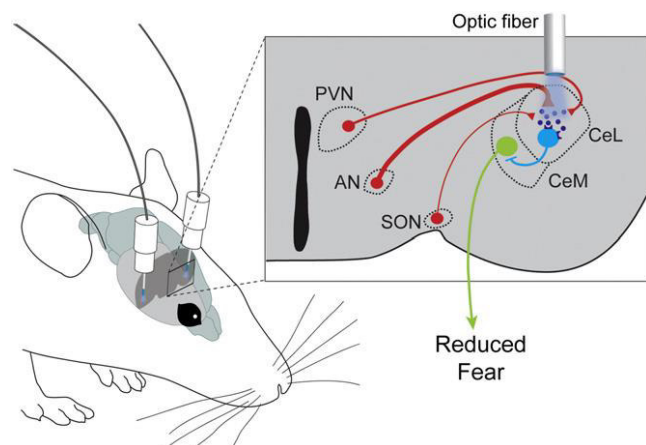
Evoked Axonal Oxytocin Release
in the Central Amygdala
Attenuates Fear Response

H. Sophie Knobloch,[1,4] Alexandre Charlet,[2,4] Lena C. Hoffmann,[1] Marina Eliava,[1,3] Sergey Khrulev,[1,5] Ali H. Cetin,[1,6]
Pavel Osten,[1,7] Martin K. Schwarz,[1] Peter H. Seeburg,[1] Ron Stoop,[2,*] and Valery Grinevich[1,*]
[1]Department of Molecular Neurobiology, Max Planck Institute for Medical Research, Heidelberg 69120, Germany
[2]Centre for Psychiatric Neuroscience, Department of Psychiatry, University Hospital Center Lausanne, Prilly-Lausanne CH-1008, Switzerland
[3]Department of Clinical Neurobiology, German Cancer Research Institute, Heidelberg 69120, Germany
[4]These authors contributed equally to this work
[5]Present address: Leibniz Institute for Molecular Pharmacology, Berlin 10117, Germany
[6]Present address: Systems Neurobiology Laboratory, The Salk Institute for Biological Studies, La Jolla, CA 92037, USA
[7]Present address: Cold Spring Harbor Laboratory, Cold Spring Harbor, NY 11724, USA
*Correspondence: rstoop@unil.ch (R.S.), valery.grinevich@mpimf-heidelberg.mpg.de (V.G.)
DOI 10.1016/j.neuron.2011.11.030

SUMMARY

The hypothalamic neuropeptide oxytocin (OT), which controls childbirth and lactation, receives increasing attention for its effects on social behaviors, but how it reaches central brain regions is still unclear. Here we gained by recombinant viruses selective genetic access to hypothalamic OT neurons to study their connectivity and control their activity by optogenetic means. We found axons of hypothalamic OT neurons in the majority of forebrain regions, including the central amygdala (CeA), a structure critically involved in OT-mediated fear suppression. In vitro, exposure to blue light of channelrhodopsin-2-expressing OT axons activated a local GABAergic circuit that inhibited neurons in the output region of the CeA. Remarkably, in vivo, local blue-light-induced endogenous OT release robustly decreased freezing responses in fear-conditioned rats. Our results thus show widespread central projections of hypothalamic OT neurons and demonstrate that OT release from local axonal endings can specifically control region-associated behaviors.

INTRODUCTION

Oxytocin (OT) is an evolutionarily ancient neuropeptide found in species ranging from invertebrates to mammals (Donaldson and Young, 2008). In mammals, the major sources of OT are the hypothalamic paraventricular (PVN), supraoptic (SON), and accessory magnocellular nuclei (AN) (Sofroniew, 1983; Swanson and Sawchenko, 1983). Axons of the vast majority of OT neurons and vasopressin (VP) neurons terminate in the posterior lobe of the pituitary, forming the classic hypothalamic-neurohypophyseal system (Brownstein et al., 1980). From the posterior pitui-

tary, OT reaches the general blood circulation and acts on target organs, exerting uterine contraction and milk ejection from the mammary glands.

Besides these well-known neuroendocrine effects, OT attracts increasing interest for its effects in the forebrain, affecting fear, trust, and other social behaviors (Lee et al., 2009). OT exerts powerful anxiolytic effects (Neumann, 2008) in the central nucleus of amygdala (CeA), the core brain structure underlying fear responses (Hitchcock and Davis, 1991; Kapp et al., 1979; Wilensky et al., 2006). In the lateral CeA (CeL), local application of OT activates a subpopulation of GABAergic interneurons that inhibits neurons in the medial CeA (CeM), the main output of the CeA to the brainstem (Huber et al., 2005), thereby attenuating behavioral fear responses (Viviani et al., 2011).

Although these behavioral effects of OT are well documented, the pathway through which OT reaches the amygdala and other forebrain regions and its precise cellular origins still remain unknown. Systemic OT cannot pass the blood-brain barrier (McEwen, 2004), and hence, there must be central OT release. The prevailing hypothesis over the last 20 years has been that central OT function is mediated by dendritic OT release in the hypothalamus, followed by passive diffusion to various brain structures (Landgraf and Neumann, 2004; Ludwig and Leng, 2006; Veenema and Neumann, 2008). However, OT receptors (OT-R; Gimpl and Fahrenholz, 2001) occur throughout the brain at various distances from the hypothalamus, and hence, passive diffusion would put severe limitations on the time course and specificity of OT signaling. Such limitations could be overcome by long-range axonal projections of hypothalamic OT neurons (Ross and Young, 2009).

To resolve this important outstanding issue in the field, we sought evidence for axonal OT-containing processes of hypothalamic origin that demonstrate functional OT release. To visualize OT axons, we selectively expressed fluorescent marker proteins from an OT gene promoter by infecting hypothalamic neurons with a recombinant adeno-associated virus (rAAV). Expression and activation of rAAV-directed channelrhodopsin-2 (ChR2; Nagel et al., 2003) in OT neurons revealed that blue light
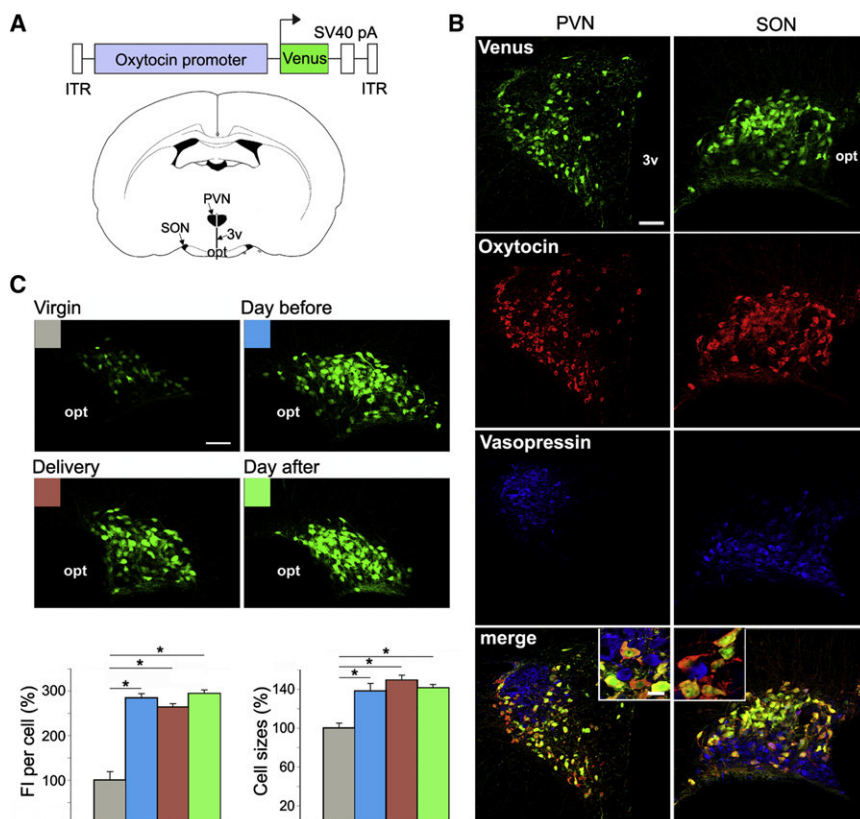
Figure 1. Cell-Type Specificity of Virally Infected OT Neurons

(A) An rAAV-expressing Venus under the control of a 2.6 kb mouse OT promoter was injected into PVN and SON of adult female rats.

(B) Viral infection resulted in Venus expression in OT, but not VP, neurons.

(C) Increased intrinsic Venus fluorescence intensity (FI) and sizes of cell bodies in the SON on the day before delivery (blue), day of delivery (orange) and day after delivery (green) compared to virgin rats (gray), as presented in graphs below. *p < 0.01. Scale bars represent 50 μm in (B) and (C) and 10 μm in insets in (B). 3v, third ventricle; opt, optic tract.

studies (Theodosis, 2002). Despite these differences in size and Venus expression, we found no significant changes in the absolute numbers of identified OT neurons (Table 1).

Efferent Projections from Hypothalamic OT Neurons to Forebrain Structures

In view of these important differences in OT expression, we used lactating rats to reveal the fine, thin projections of OT axonal arbors in the forebrain (see Figure S1 available online). OT neurons of the PVN and SON projected to a wide range of OT-R-expressing forebrain structures (Figures 2 and S2; Gimpl and Fahrenholz, 2001), though PVN neurons provided many more prominent projections to more numerous structures (29 of 34 regions analyzed; Figure 2) than SON neurons (five regions; see Figure S2 for quantification). Previous studies reported high OT-R expression and OT-R-mediated effects in the CeA, a structure critically involved in the expression of conditioned fear (Huber et al., 2005; Bosch et al., 2005). We found Venus-positive processes from the PVN to engulf and enter the CeA but only marginally observed single Venus-positive processes from the SON, mostly at the ventrolateral CeA (Figures 3 and S2). In animals targeted in all OT nuclei, including AN, we observed significantly more Venus-positive fibers in the CeA, preferentially located in the CeL (Figures 3A and S3). These contained OT-positive puncta (Figure 3B), confirming their exclusive origin from OT neurons (see Figure S3 for quantification).

Cytochemical Markers in CeA Projections from Hypothalamic OT Neurons

At the light microscopic level, the small-diameter, branching, and en passant varicosities of Venus-positive processes suggested that the above-observed fibers were axons. To corroborate their axonal nature, we expressed in OT neurons the axonal marker Tau tagged by enhanced green fluorescent protein (EGFP). We observed an EGFP signal in all fibers within the CeA and in axonal terminals in the posterior pituitary (Figure 3C).

triggered, in vitro, an OT-receptor-mediated increase in neuronal activity in the CeL, enhanced the frequency of inhibitory postsynaptic currents (IPSCs) in the CeM, and decreased, in vivo, context-evoked freezing responses in fear-conditioned rats. Our findings provide direct evidence for local, endogenous OT signaling in the suppression of CeA-mediated fear (Roozendaal et al., 1992a, 1992b; Viviani et al., 2011).

RESULTS

Specificity of Virus-Directed Gene Expression in Neurons of the Rat Hypothalamus

We constructed an rAAV-expressing Venus from a 2.6 kb region upstream of OT exon 1 (Figure 1A) and conserved in mammalian species (see Experimental Procedures). The injection of this rAAV into the PVN or SON of rats (Figure 1A) resulted in the selective expression of Venus in OT, but not VP, neurons (Figure 1B). Quantitative analysis in the SON, PVN, and AN of virgin and lactating rats showed more than 97% colocalization of OT and Venus expression and only 1.70% ± 0.36% of Venus-positive neurons expressing VP, revealing a very efficient and highly specific virus expression (Table 1).

The virally introduced OT promoter appears to be regulated during late pregnancy (Zingg and Lefebvre, 1988) and lactation (Burbach et al., 2001), like its chromosomal counterpart. We indeed found a 3-fold increase in fluorescent intensity, as well as larger sized green fluorescent OT cells around delivery compared to virgin rats (Figure 1C), in accordance with earlier

Table 1. Quantification of OT-Promoter Specificity in OT-ergic Nuclei in the Hypothalamus of Virgin and Lactating Rats. Results are Presented as Percentage ± SEM.

Animals	Comparison	SON	PVN	rSON	CN	DLN
Virgin Rats	OT versus Venus	99.57% ± 0.66%	99.8% ± 0.49%	99.07% ± 2.27%	98.48% ± 3.71%	98.47% ± 2.59%
		n = 1,091	n = 936	n = 115	n = 69	n = 210
	Venus versus OT	98.01% ± 3.09%	97.34% ± 2.03%	98.13% ± 2.97%	97.57% ± 3.82%	97.66% ± 2.15%
		n = 1,091	n = 936	n = 115	n = 69	n = 210
Lactating Rats	OT versus Venus	100%	99.57% ± 0.85%	100%	100%	99.56% ± 1.07%
		n = 987	n = 969	n = 116	n = 74	n = 207
	Venus versus OT	99.06% ± 1.48%	99.06% ± 2.3%	100%	100%	99.55% ± 1.10%
		n = 987	n = 969	n = 116	n = 74	n = 207

n, absolute number of identified neurons per structure and condition; CN, circular nucleus; DLN, dorsolateral nucleus; rSON, retrochiasmatic part of the SON.

Similarly, expression of a synaptophysin-EGFP fusion protein revealed synaptic terminals in both structures (Figure 3D). Costaining of synaptophysin-EGFP puncta with antibodies against OT

Figure 2. Distributions of Venus-Labeled OT Fibers from the PVN in Extrahypothalamic Forebrain Regions of Lactating Rats
(A and B) OT/GFP fiber pattern in subcortical (A) and cortical (B) areas. The infected PVN in one hemisphere is colored in green. The density of fibers is depicted in the following colors: yellow, orange, red, and violet. The detailed information on forebrain projections from ipsi- and contralateral PVN and SON, as well as examples of stained GFP fibers, are presented in Figure S2. For abbreviations of structures, see Figure S2.

and vesicular glutamate transporter 2 (VGluT2), the mRNA of which was detected in OT neurons (Kawasaki et al., 2005), demonstrated overlap of EGFP, VGluT2, and OT signals (Figure 3E), confirming previous reports on magnocellular neurons enriched by microvesicles that associate with synaptophysin (Navone et al., 1989) and contain glutamate (Meeker et al., 1991). Higher-resolution electron microscopic analysis revealed the presence of synaptic contacts between immunoreactive axon terminals and local dendrites in the CeL (Figure 3F), most likely dendrites of GABAergic interneurons, of which the CeL is predominantly composed (Davis, 2000; Huber et al., 2005). In the three cases analyzed, we encountered synaptic appositions bearing the features of asymmetric (Gray's type 2) synapses, proposed to be of excitatory nature (Figure 3F). Importantly, we were unable to find synaptic contacts within the CeM (M.E., unpublished data), where fibers are traversing the region without branching and forming varicosities, as was the case in the CeL (Figure S3A). Our collective findings strongly suggest a presence in the CeL of axonal terminals that originate from OT neurons and form glutamatergic synapses.
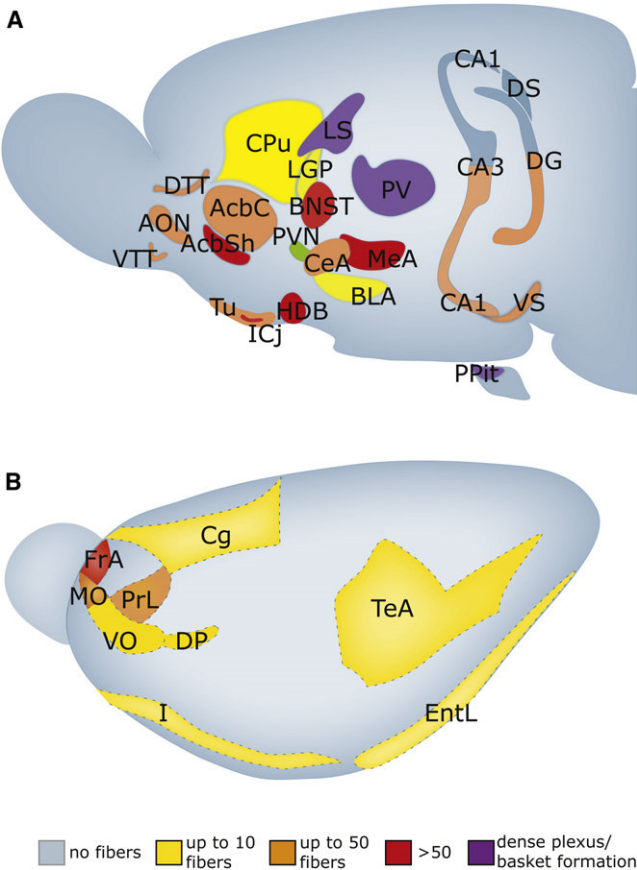
Blue-Light Activation of ChR2-Expressing Axons In Vitro Induces Local OT Release

Based on the anatomical evidence for OT-containing axonal fibers of hypothalamic origin in the CeA, we selectively expressed the blue-light (BL)-sensitive ChR2 protein (Nagel et al., 2003) fused to mCherry (Figure 4A) in all hypothalamic OT neurons via an rAAV. Whole-cell voltage-patch-clamp recordings in vitro in coronal slices of mCherry fluorescent cells (Figures 4A and 4B, top) revealed functional ChR2 expression in PVN, SON, and AN neurons, as evident from the presence of BL induced currents with a characteristic rapidly inactivating peak followed by a stable tail (Boyden et al., 2005; Figures 4C and S4). Because high frequencies of action potentials are thought to be necessary to trigger release of neuropeptides, in contrast to release of classical neurotransmitters (Hökfelt, 1991), we quantified the effect of different BL stimulations on AP frequencies of PVN and SON neurons. Current-clamp recordings from these neurons showed that AP frequencies up to 20 Hz could be reliably induced by stimulation frequencies with short BL pulses of 10 ms applied at 30 Hz, as well as by continuous BL exposure (Figures 4C and S4A).
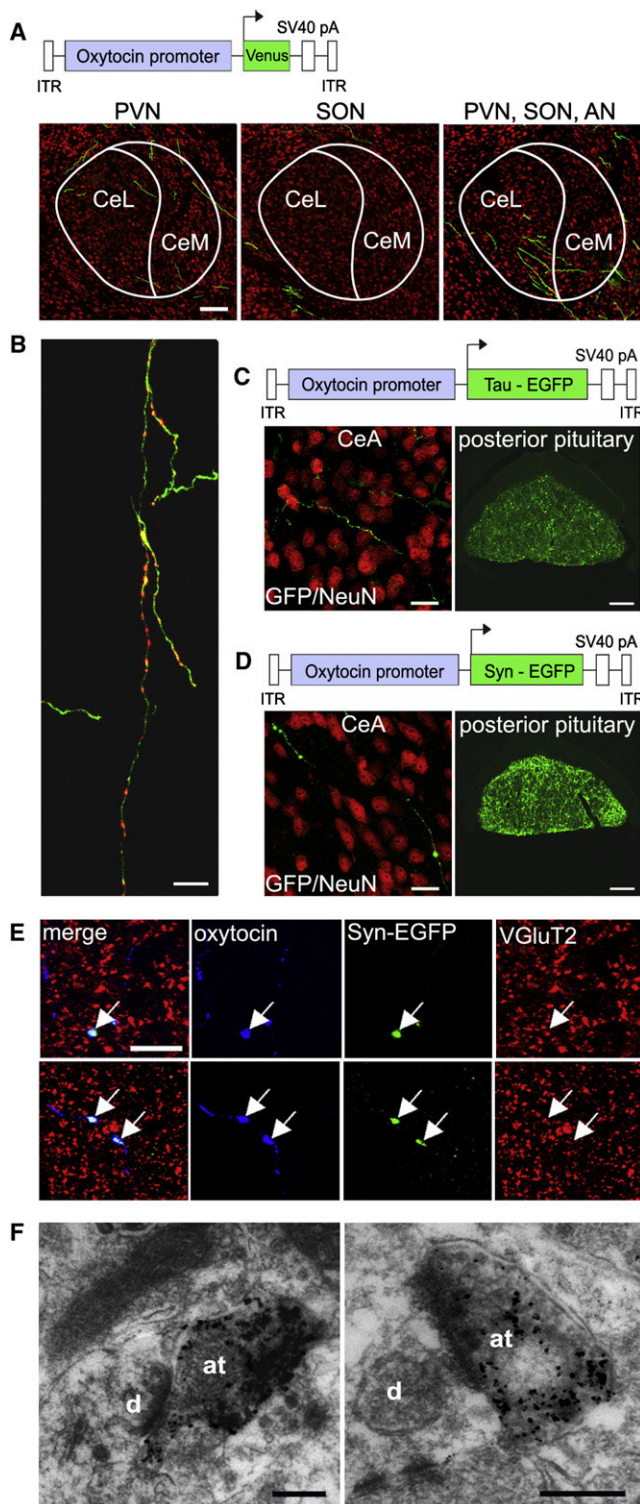
Figure 3. Venus-Positive Fibers from OT Neurons within the CeA Exhibit Axonal Features and Form Synapses

(A) Venus-positive fibers in the CeA originate from the PVN, SON, and AN and are infected with rAAV-expressing Venus from the OT promoter. The confocal images of the right CeAs were taken from coronal sections of the nucleus at Bregma, −2.7 mm. The external borders and the approximate borders

Having shown functional ChR2 expression in the OT cell bodies, we tested whether BL could also release endogenous OT from axonal projections in horizontal slices of the CeA (Figure 4B, bottom). Exposure of the CeL to BL (20 s) evoked clear, reversible increases in AP frequencies in one-third (11/33) of CeL neurons in cell-attached recordings (from 0.24 ± 0.02 to 0.85 ± 0.24 Hz; Student's t test, p < 0.01; Figures 4D1 and 4D2). Preincubation with the OT-receptor antagonist (OTA), though not affecting basic AP frequencies, significantly and reversibly blocked these increases (>70% remaining response 0.46 ± 0.09 Hz, n = 5; one-way analysis of variance [ANOVA], p < 0.05; Figures 4D1 and 4D2). The GABA(A) blocker picrotoxin (PTX) caused, on average, a significant increase in baseline AP frequencies (from 0.27 ± 0.09 to 0.61 ± 0.26 Hz, n = 5; one-way ANOVA, p < 0.05), possibly as a result of inhibition of local inhibitory circuits in the CeL (Ciocchi et al., 2010; Haubensak et al., 2010). In summary, endogenous release of OT from hypo-thalamic fibers leads to an efficient, OT-R-mediated activation of CeL neurons.

Because CeL neurons project to and release GABA in the CeM (Huber et al., 2005), we also tested for rapid transient increases in IPSC frequencies in the CeM. CeL exposure to BL (20 s) evoked abrupt increases in IPSC frequencies in 36 out of 107 tested CeM neurons (Figure 4B, bottom trace and Figure 4E1), on average from 0.5 ± 0.1 Hz to 3.7 ± 0.8 Hz (Figure 4E2, first panel; Student's t test, p < 0.01), without affecting average IPSC ampli-tudes (Figure S4B). These increases depended on the precise area exposed to BL. Thus, BL applied outside the CeL, e.g., focused on the CeM (Figure 4E2, fifth panel, n = 6), never modi-fied IPSC frequencies in CeM neurons that responded with increases in IPSCs after BL exposure of the CeL. Similar to the AP increases in the CeL (Figure 4D2), these increases in IPSC frequencies in CeM were significantly and reversibly blocked by OTA (>70%, 1.3 ± 0.2 Hz, n = 9; one-way ANOVA, p < 0.05; Figure 4E2, third panel). Subsequent PTX application blocked spontaneous IPSCs as well as any further BL effects (n = 5, Fig-ure 4E2, fourth panel), confirming the GABAergic nature of the observed responses.

Although OTA significantly inhibited BL-induced increases of AP frequencies in the CeL and IPSC frequencies in the CeM, in both cases small but significant responses remained. In both CeA subdivisions, these responses could be entirely abolished by adding the AMPA-receptor antagonist NBQX to the OTA incu-bations (Figure 4D2, left panel, 0.25 ± 0.01 Hz for APs, n = 5; and Figure 4E2, third panel, 0.6 ± 0.1Hz for IPSCs, n = 4). This

between CeL (comprising two parts, the central central and central lateral) and the CeM are outlined.

(B) OT-immunoreactive puncta along Venus-positive fibers.

(C and D) Tau-EGFP (C) and Synaptophysin-EGFP (D) signals detected in OT fibers within the CeA and posterior pituitary. In (A)–(D), the brain sections were costained with antibody against the neuronal marker NeuN and were visual-ized in red by CY-3 conjugated antibodies.

(E) Synaptophysin-EGFP puncta overlap with OT and VGlut2.

(F) Asymmetric synapses in the CeL, formed by GFP-positive axonal terminals (at) of OT neurons on dendrites (d) of amygdala neurons. Scale bars represent 100 μm in (A), 5 μm in (B) and (E), 10 μm in left panels in (C) and (D), 100 μm in right panels in (C) and (D), and 250 nm and 500 nm for left and right electro-nograms, respectively, in (F).
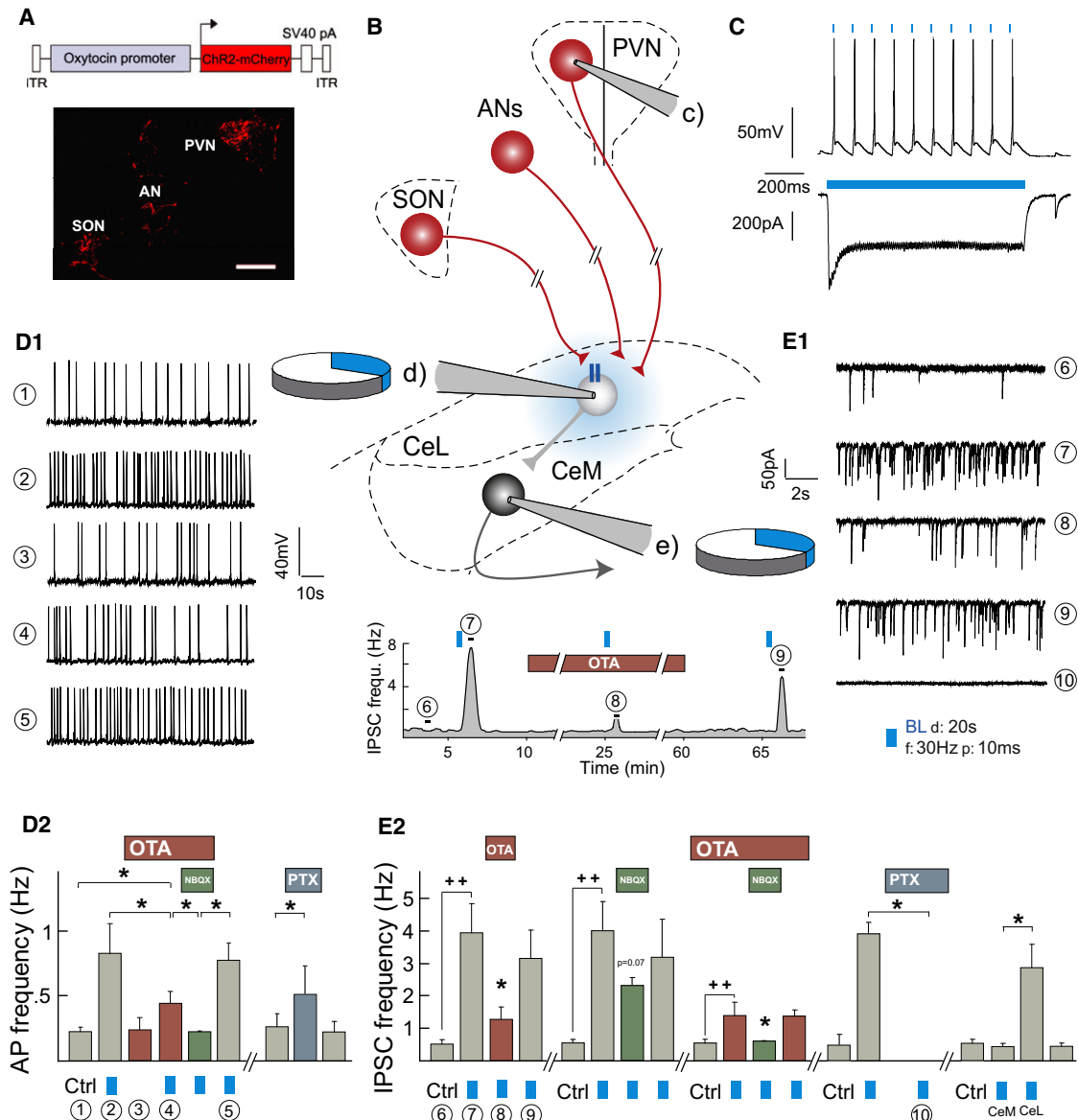
Figure 4. ChR2-Evoked Oxytocin Release from Fibers in the CeA

(A) The PVN, SON, and AN (coronal section) display mCherry expression after infection with OT promoter-ChR2-mCherry rAAV.

(B) Scheme of experimental set up showing (in coronal plane) the three hypothalamic nuclei and (in horizontal plane) the electrophysiological slice preparation (see Experimental Procedures). Labels c, d, and e refer to pipettes used for recordings in (C), (D1) and (D2), and (E1) and (E2), respectively, with pie charts indicating proportions of cells responding to BL.

(C) Action potentials evoked by 10 ms, 10 Hz, and currents induced by 1 s continuous BL stimulations in a fluorescent PVN cell.

(D1 and D2) Effects of 20 s BL (30 Hz, 10ms pulses) on CeL AP frequencies, both in CeL.

(D1) Example traces of APs recorded (1) without BL, (2) after BL, (3) with OTA alone, (4) with OTA + BL, and (5) BL after OTA washout.

(D2) Left: average AP frequencies of CeL neurons (1) without BL, (2) after BL, (3) with OTA alone, (4) OTA + BL, or (5) together with NBQX (n = 5) and after washout. Right: in presence of PTX without BL (n = 5).

(E1 and E2) Effects of BL in CeL (except where indicated) on IPSCs recorded in CeM neurons.

(E1) Example traces of IPSCs recorded (6) without BL, (7) after BL, (8) OTA + BL, (9) BL after OTA washout, and (10) BL in presence of PTX. (Example trace, below [B].) Rate-meter trace of IPSC frequencies recorded from a CeM neuron in response to (7) BL, (8) presence of OTA + BL, and (9) OTA washout + BL.

(E2) Average IPSC frequencies after BL in presence of OTA (first panel) (n = 9), NBQX only (second panel) (n = 5), both OTA and NBQX (third panel) (n = 4), PTX (fourth panel) (n = 4), and BL focused either on CeM or CeL (fifth panel) (n = 6). Statistical significances: Student's t test, ++ $p < 0.01$; one-way ANOVA, *$p < 0.05$. Blue squares represent BL stimulation.
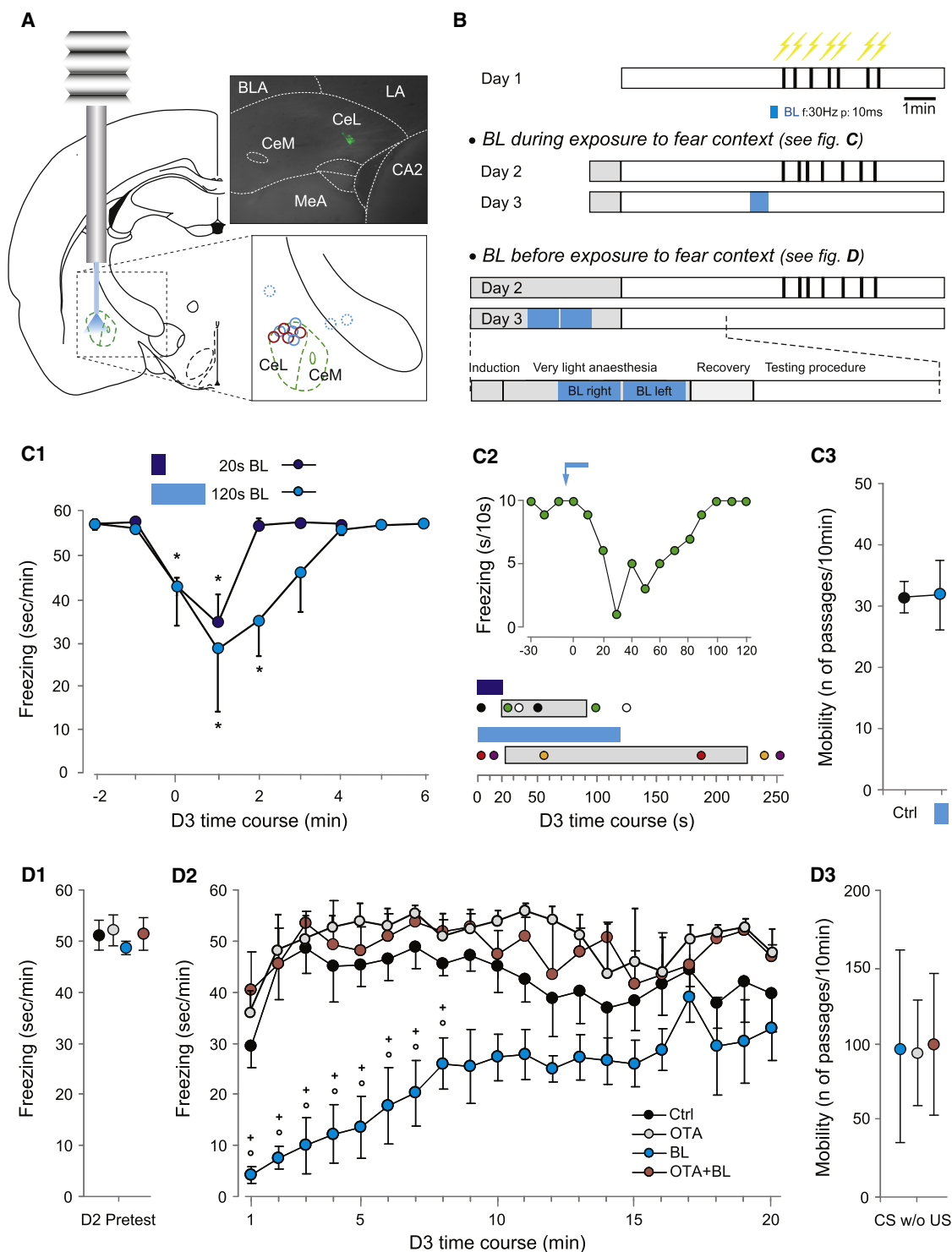
Figure 5. Evoked Release of Endogenous Oxytocin Attenuates Freezing Behavior

(A) Left: scheme of the placement of guide cannulae and optic fibers for BL application in CeL. Right: detail of the tip of the glass fiber position obtained after microinjection of fluorescent beads (see Experimental Procedures). Top right: example picture of fluorescent beads injected in CeL. Bottom right: example of eight correctly targeted CeLs in the left hemisphere (four of BL group, in blue; four of OTA + BL group, in red) and the three outliers (dotted blue circles).

(B) Three-day experimental contextual fear-conditioning protocol. Vertical black bars show the timing of foot shock during conditioning. Grey segments, pre-conditioning procedure including light anesthesia of the animal; blue segments, BL application.

(C1–C3) Effects of BL application during exposure to fear context.

suggests that the BL-evoked release of OT in the CeA is accompanied by the release of another factor, which requires AMPA-receptor activation. Indeed, we found that NBQX alone also decreased BL-induced IPSC responses in the CeM (Figure 4E2, second panel).

Blue-Light-Induced Activation of ChR2-Expressing OT Axons in the CeA Suppresses Contextual Freezing in Fear-Conditioned Rats

To determine whether BL-evoked release in vivo of endogenous OT in the CeA affects behavior, we expressed the ChR2-mCherry fusion protein in all hypothalamic OT structures of virgin female rats (see above). These rats were implanted bilaterally with guide cannulae to target blue-laser-coupled optical fibers above the CeA. Correct placement of the cannulae and fibers was verified by injections of fluorescent beads and post hoc analysis. Based on incorrect positioning, three rats (in which BL, as a consequence, did not decrease freezing responses) were excluded from further analysis. (Figure 5A, see also Experimental Procedures). To ensure basic activation of the amygdala during the behavioral experiments, we trained all rats in a 2-day contextual fear-conditioning protocol (see Figure 5B and Experimental Procedures) that resulted in similar freezing in the majority of animals (n = 25) after 2 days of conditioning (Figures 5C1 and 5D1). One animal was excluded from the experiment due to unusually low freezing levels. Hormonal cycle did not appear to affect these freezing levels (Figure S5).

To assess acute effects of BL on freezing behavior, we placed rats on day 3 in the fear-conditioning box after optic fibers had been inserted through the guide cannulae to target the CeL. All rats exhibited maximal freezing upon and throughout exposure to the context (Figure 5C1). After 10 min, 10 ms, 30 Hz BL pulses were given for either 20 or 120 s. As expected from the central role of the CeM in freezing behavior (Ciocchi et al., 2010; Haubensak et al., 2010) and the inhibitory effects of BL on the CeM in vitro (Figure 4), BL efficiently decreased freezing (from 57.5 ± 0.9 to 32.1 ± 5.6 s/min, n = 6; one-way ANOVA, p < 0.05; Figure 5C1). The onset of this decrease (Figure 5C2; see also Movie S1) started in two rats as fast as 2 s after BL onset and on average with a delay time of 21.5 ± 9.7 s across all animals (n = 6). Freezing returned after 70 ± 21 s upon termination of the 20 s BL stimulation and 108 ± 20 s after the 120 s BL exposure (n = 3 per group). The inhibiting effects of BL appeared specific to the fear-induced freezing response, because BL exposure in the same animals in a non-fear-conditioning context did not affect basic locomotor activity (Figure 5C3).

To confirm involvement of endogenous OT release in these BL responses, we injected OTA on day 3 through the same guide cannulae through which the optic fibers were subsequently inserted and applied BL immediately for 120 s before the rats were re-exposed (after removal of the optic fibers) to the fear-conditioning context. We thus measured the remaining block on the effects of BL by OTA, while at the same time providing more freedom of movement to the rats (now unobstructed by any attached optic fibers). We compared freezing behavior between four groups of rats, namely "Ctrl" (no BL, but optic fibers inserted prior to testing), "OTA" (OTA injected + optic fibers without BL), "BL" (BL application prior to exposure to context) and "OTA + BL" (injection of OTA followed by BL application prior to exposure to context). Ctrl or OTA-injected rats exhibited high freezing levels (Figure 5D2) comparable to those measured previously (Figure 5C1). On the other hand, BL-exposed rats immediately exhibited lower freezing levels upon exposure to the context. This reduced freezing persisted in these more freely moving rats over the first half of the testing period (Figure 5D2).

Of interest and importance, the BL inhibition of freezing was completely abolished in rats injected with OTA, which now exhibited similar freezing levels as rats that had not been exposed to BL (Figure 5D2). Because all rats demonstrated similar levels of freezing responses after 2 days of fear conditioning (Figure 5D1), and their mobility (tested by placing the animal in a different context) was not affected by BL exposure (Figure 5D3), these effects seem specific to the pharmacological and optogenetic exposures of the CeL. In conclusion, our in vivo findings, in addition to our in vitro findings, reveal that the activation of local OT fibers of hypothalamic origin triggers specific, OT-R-mediated reduction of fear responses, thereby further demonstrating the functional and physiological role of these OT projections.

Synaptic Contacts by Hypothalamic OT Projections as Revealed by Retrograde Tracing with Deletion-Mutant Pseudotyped Rabies Virus

The above findings suggest a specific targeting of OT from the hypothalamus to the CeA through local release from axonal endings. To retrogradely trace their precise cellular origins, we employed the deletion-mutant pseudotyped rabies virus SADΔG-EGFP (EnvA) (henceforth termed PS-Rab-EGFP, see Figure S6A for expression efficiency). We delivered into several hypothalamic projection sites, including the CeA, of 10-day pregnant rats (Figure 6A) two rAAVs expressing from the chicken β-actin-enhanced CMV promoter the avian sarcoma and leucosis virus receptor (TVA, coupled by IRES to tdTomato) and the rabies glycoprotein (RG). Expression of TVA is essential for PS-Rab entry into neurons, whereas expression of RG allows

---

(C1) Mean effects upon BL for 20 s (dark blue, n = 3) or 120 s (light blue, n = 3).

(C2) Top: example of BL effects on one animal. Each point represents the time of freezing during 10 s. Bottom: offset and return of total freezing for individual animals (color coded by dots) after 20 s (dark blue bar) or 120 s (light blue bar), with averages of dot values represented by gray bars.

(C3) Effect of BL on mobility, measured for the same animals, at day 4 in a different contextual box.

(D1–D3) Effects of BL application prior to exposure to the context.

(D1) Pretest quantification of freezing behavior obtained at the end of conditioning day 2.

(D2) Time course of freezing behavior for control (Ctrl, n = 4), 120 s BL (BL, 30Hz, 10ms pulses, n = 4), after OTA + BL (OTA + BL, n = 4), and after OTA alone (OTA, n = 4).

(D3) Mobility of different groups of animals (OTA, BL, and OTA + BL) at day 3 in the context without exposure to US during day 1 and 2 (n = 3 per group). Statistical significance: one-way ANOVA,*p < 0.05 in (C1)–(C3); two-ways ANOVA, + p < 0.05 BL versus Ctrl; p < 0.05 BL versus OTA + BL in (D1)–(D3).
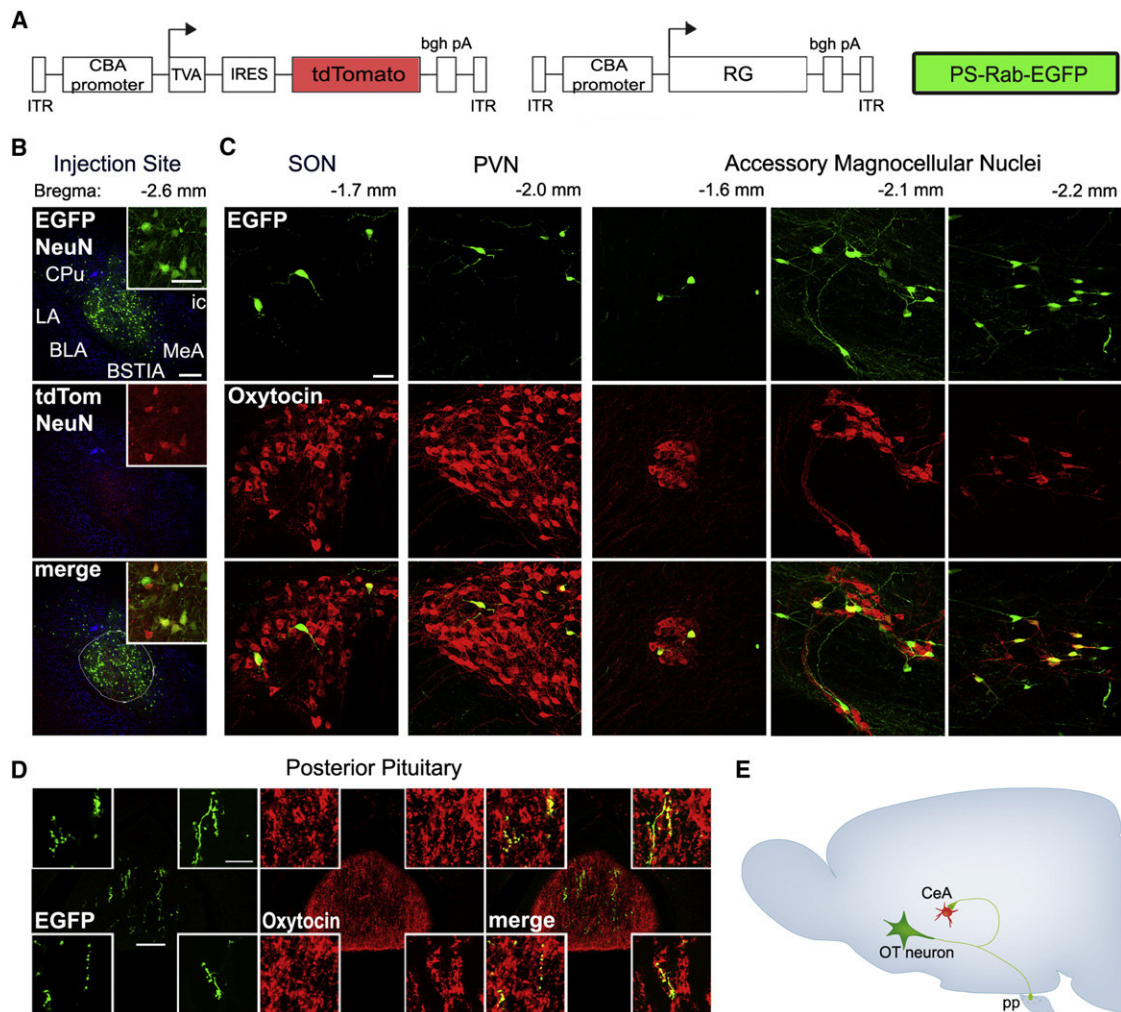
Figure 6. PS-Rab-Based Retrograde Labeling of Hypothalamic OT Neurons Monosynaptically Projecting to the CeA

(A) Pregnant rats were injected into the CeA with rAAVs expressing TVA-IRES-tdTomato and RG, followed by PS-Rab-EGFP.

(B) Primary infected neurons in the CeA show colocalization of tdTomato and EGFP (insets).

(C) Retrogradely labeled OT-positive neurons found in the SON, PVN, and especially in AN.

(D) EGFP-positive axonal endings in the posterior pituitary are also positive for OT (insets), indicating that magnocellular OT neurons project axons to the posterior pituitary and CeA.

(E) Schematic drawing of results in (C) and (D). Green cell denotes OT neurons, which project green collaterals simultaneously to the central sites (CeA, red cell) and to the posterior pituitary, from where OT reaches general circulation. Scale bars represent 100 μm in (B) and (D), 20 μm in the inset of (B), 50 μm in (C), and 20 μm in the insets of (D). BLA, basolateral amygdala; BSTIA, bed nucleus of stria terminalis (intraamygdaloid division); CPu, caudate putamen; ic, internal capsule; LA and MeA, lateral and medial amygdala; pp, posterior pituitary.

monosynaptically restricted retrograde transsynaptic transmission of PS-Rab (Wickersham et al., 2007). Subsequent injection of PS-Rab-EGFP into the same sites (CeA; Figure 6A) permitted analysis of retrogradely connected neurons on day 7 of lactation. Whereas primarily infected neurons in the injected sites should emit both red (tdTomato) and green (EGFP) fluorescence, retrogradely labeled neurons should emit green fluorescence only (Figure 6B). After infection of the CeA, we found EGFP-positive neurons mostly in the areas surrounding the PVN and SON, with a small number of neurons containing both OT and EGFP immunoreactivity (Figure 6C). As expected from the anterograde-labeling study (see Figure 3A), the highest number of

double-positive neurons was observed within the AN (Figure 6C), identifying the AN as the major source for the OT innervation of the CeA. Neurons expressing only green fluorescence were also observed in various extrahypothalamic sources of CeA innervation (Figure S6B; Swanson and Petrovich, 1998), and injections of both rAAVs in two other hypothalamic targets (the nucleus accumbens, Acb, and nucleus of solitary tract, NTS) also resulted in EGFP-positive neurons in the hypothalamus (Figure S6C), attesting to the efficient retrograde monotranssynaptic labeling with this method. Thus, these findings confirm the presence of functional monosynaptic hypothalamic projections in the CeA.

Magnocellular OT Neurons Control CeA-Dependent Fear Responses

Hypothalamic nuclei contain magno- and parvocellular OT neurons, which are nonsegregated within the PVN (Swanson and Sawchenko, 1983), and both were indeed labeled by our OT-specific rAAVs (see Figure 1B; Figure S1A). Because magnocellular neurons, in contrast to parvocellular neurons, also send collateral branches to the posterior pituitary in addition to the extrahypothalamic forebrain, retrograde labeling of magnocellular brain projections may anterogradely label posterior pituitary endings. We used pseudotyped rabies virus to identify the magno- versus parvocellular origin of forebrain projections. Infection of CeA and Acb by PS-Rab-EGFP resulted in a fluorescent label in the pituitary in both cases (Figures 6D and S6C, top), but not following infection of the NTS (Figure S6C, bottom panel). Injection of the unpseudotyped rabies virus (UPS-Rab) in the pituitary (which can infect intact or damaged axons without the presence of TVA receptor) did not lead to labeling in the hypothalamus (Figure S6D), thereby confirming the specific transsynaptic labeling by PS-Rab. In summary, although these findings do not exclude a contribution by the parvocellular OT neuron population to innervation of all three nuclei, they provide clear evidence for the magnocellular origin and axon collateral nature of OT fibers in the CeA and Acb.

DISCUSSION

A longstanding unresolved question in the field of OT signaling in the brain concerns the precise sites of OT release and the pathways and mechanism through which OT reaches its target structures. The prevailing hypothesis in the field has been in favor of a dendritic release of OT in the hypothalamus, followed by OT diffusion to target areas. Through a combination of anatomical, electrophysiological, optical, and behavioral approaches, we provide in the present study morphological and functional evidence for the presence of axonal endings through which OT, produced in the hypothalamus, can reach the CeA and be locally delivered to exert direct effects both at the cellular and behavioral level.

Magnocellular OT Neurons Project Axonal Collaterals to Diverse Brain Regions

Application of cell-type-specific rAAV results in infection of the vast majority of OT neurons in both virgin and lactating rats. However, taking advantage of the higher transcriptional activity of virally introduced OT promoter in lactating rats and, hence, higher levels of expression of Venus (at least 3-fold; Figures 1C and S1) we visualized and semiquantified OT projections in 34 forebrain regions. The distribution of Venus-positive fibers in the forebrain agreed with anatomical studies from the 1980s (Sofroniew, 1983; Buijs, 1983), which showed OT-immunoreactive fibers in a limited number of forebrain structures, such as the tenia tecta, Acb, lateral septum, amygdala, and hippocampus. However, due to our highly sensitive method for detecting soluble marker proteins (Grinevich et al., 2005) and higher levels of Venus expression in lactating rats, we found many more fine Venus-positive axons in all major forebrain regions than by direct staining for OT. Moreover, classical immunohisto-

chemistry does not reveal the sources of these fibers, which may originate from the PVN, SON, or AN. According to our results, the PVN and AN neurons project extensively to forebrain structures, whereas the SON contributes less to forebrain innervation. But even from the SON, which features only magnocellular neurons, a moderate number of fibers were observed in five forebrain regions (the horizontal limb of the diagonal band of Broca, Acb, CeA, lateral septum, and CA1 of the ventral hippocampus).

Additional evidence that magnocellular neurons project to higher brain regions was obtained with PS-Rab delivered into the CeA or the Acb. After injection of EGFP-expressing PS-Rab into these structures, we observed EGFP-positive back-labeled OT neurons residing in magnocellular nuclei, as well as their axonal terminals in the posterior pituitary. Importantly, only magnocellular hypothalamic neurons, but no other neuronal cell types, project to the posterior pituitary lobe (Brownstein et al., 1980; Sofroniew, 1983; Swanson and Sawchenko, 1983; Burbach et al., 2001).

In support of our observations, injection of the retrograde marker fluorogold into the Acb of voles led to the appearance of back-labeled OT neurons in the PVN and SON, with fluorogold-containing terminals in the posterior pituitary (Ross et al., 2009). In contrast, injection of PS-Rab into the NTS (Figure S6B) resulted in back-labeling of PVN parvocellular OT neurons, which do not project to the posterior pituitary (Sawchenko and Swanson, 1983; Swanson and Sawchenko, 1983). Collectively, the PS-Rab data in conjunction with light and, in particular, electron microscopic results provide compelling evidence that the fibers in the CeA and Acb are axonal collaterals of magnocellular OT neurons.

Our finding that magnocellular OT neurons simultaneously project to forebrain structures and the posterior pituitary is consistent with results demonstrating that the induced central and peripheral OT releases can be associated, for instance, in a situation of stress (Neumann, 2007). More specifically, it was previously demonstrated that an ethologically relevant stressor (such as forced swim in rats) induces an increase in OT plasma levels (Wotjak et al., 1998), as well as OT release within the CeA.

Inhibitory Effects of Endogenous OT Release in the Central Amygdala

Our anatomical results provide the basis for OT action within the CeA in both virgin and lactating rats. Although the density of OT fibers is lower in virgin than in lactating animals, the profile of axonal innervation of the CeA was similar in animals of both groups. In the CeM, we detected smooth nonbranching fibers which exceed the axons in the CeL in length. This type of fiber appears to represent transitory axons, traversing the CeM with no synaptic contacts. The appearance of axons in the CeL was strictly different: they exhibited single small branches, often possessing varicosities (as a substrate for presynaptic terminals; see Figures 3F, S3A, and 6), which may also represent sites for axonal OT release.

In accordance with this proposition, we found that release of endogenous OT from axonal endings, triggered by blue-light exposure of the CeL (but not the CeM), significantly modified the CeA signaling by increased activity of GABAergic interneurons in the CeL through an OT-R-dependent process. The

activation of these CeL neurons caused an increase of postsynaptic currents in CeM neurons, which were completely abolished by GABA(A) receptor antagonists, thus identifying their inhibitory nature. Accordingly, this increase of endogenous OT, by inhibiting neurons in the CeM, the main output center of the CeA, caused an attenuation of the freezing response (see below). It therefore appears that even relatively sparse innervation by OT-releasing axons in the CeL is sufficient to trigger significant inhibition through activation of GABAergic neurons projecting from the CeL to the CeM.

Our light and electron microscopic results demonstrate that OT neurons form synapses in the CeL analogous to OT-containing synapses within the SON (Theodosis, 1985), NTS (Peters et al., 2008), and at the lateral border of the hypothalamic ventromedial nucleus (Griffin et al., 2010). Furthermore, the asymmetric nature of these synapses and the occurrence of VGluT2 in the OT axons raise the question whether glutamate may be coreleased with OT. Both our recordings in the CeL and CeM indeed revealed, in the presence of the OT-R antagonist OTA, a remaining blue-light-evoked response that could be efficiently blocked by AMPA-receptor blockade, consistent with presynaptic glutamate release. Only application of NBQX revealed that AMPA-receptor activation is not required for OT release, which would preclude an involvement of presynaptic AMPA receptors on OT fibers. However, other ionotropic and possibly metabotropic glutamate receptors may facilitate OT release by contributing to axonal depolarization upon presynaptic glutamate release. In view of the recent discovery of distinct, mutually inhibitory neuronal populations in the CeL (Ciocchi et al., 2010; Haubensak et al., 2010), it will be of interest to determine how individual neuronal activity in this nucleus may be differentially affected by endogenous OT and/or glutamate release.

Behavioral Effects of Endogenous OT Release in Amygdala

A considerable and long-standing body of evidence indicates that OT can exert important effects on anxiety and fear responses by its effects in the CeA, following initial studies by Roozendaal and coauthors (Roozendaal et al., 1992a, 1992b, 1993). Further, in vivo experiments indicated that enhanced hypothalamic OT expression (Caldwell et al., 1987) and dendritic release (Neumann, 2007) might underlie the alterations in behavioral patterns seen during lactation, such as anxiety and aggression (Ferris et al., 1992; Lubin et al., 2003). Notably, in a rat strain with high anxiety-related behavior, the CeA level of OT was prominently increased in parallel with more intense maternal care, maternal offensive, and stress-coping behaviors, and these effects were reversed by local OTA infusion (Bosch et al., 2005). Very recent work also reports an effect on fear behavior by exogenous OT infusion into the CeA (Viviani et al., 2011). In this context, our study demonstrates that the blue-light-stimulated release of endogenous OT in the CeA drastically suppresses freezing behavior of fear-conditioned rats, with the effect abolished by infusion of OTA. The rapid onset and the time course of the reversibility of these effects provide further evidence in favor of a local release of OT from these fibers in the central amygdala, as opposed to slow diffusion from distant hypothalamic nuclei.

Our retrograde transsynaptic tracing with PS-Rab further assigned a magnocellular origin for OT in the hypothalamus. Indeed, Krause et al. (2011) reported recently how an osmotic challenge (dehydration) specifically activated OT-producing magnocellular neurons in the PVN, which in turn evoked profound anxiolytic effects. Taken together, these findings place the magnocellular neurons at a crucial intersection of transmitting environmental stimuli to the amygdala and provide a pathway through which these stimuli can lead to rapid OT-mediated regulation of anxiety and fear responses.

In conclusion, we employed an efficient and specific OT promoter, which allowed us to genetically manipulate OT neurons via insertion or deletion of genes of interest. Although we demonstrated the cell-type-specific targeting of OT neurons in rats and mice (unpublished data), the same OT promoter should work in other species because it is highly conserved among mammals. Furthermore, our evidence for functional OT axons in the CeA provides proof of principle for the local, targeted release of a modulatory neuropeptide by long-range axon collaterals in other forebrain regions, which can be used to specifically control region-associated behaviors. Our physiological and anatomical findings now open the technical prospect for studying the effects of endogenous OT release in various brain regions with respect to distinct forms of social behavior (Landgraf and Neumann, 2004; Ludwig and Leng, 2006; Donaldson and Young, 2008; Lee et al., 2009; Ross and Young, 2009). Because the role of OT in human psychopathology has become subject of many translational studies (De Dreu et al., 2010; Simeon et al., 2011; Skrundz et al., 2011), the experimental alteration in endogenous OT release may open the way to dissect OT-related pathogenic mechanisms underlying emotional and psychiatric disorders in human patients.

EXPERIMENTAL PROCEDURES

Cloning of rAAV Vectors

For generating rAAVs with specific expression in OT cells, we used the software BLAT from University of California, Santa Cruz (http://genome.ucsc.edu/cgi-bin/hgBlat) and selected a conserved 2.6 kb promoter directly upstream of the OT gene exon 1. This DNA was amplified from an EcoRI-linearized BAC clone RP24-388N9 (RPCI-24 Mouse, BACPAC Resources) using a 5′ primer containing a NotI-restriction site (5′-ATTAGCGGCCGCAGATGAGCTGGTGAGCATGTGAAGACATGC-3′) and a 3′ primer with a SalI-restriction site (5′-ATTAGTCGACGGCGATGGTGCTCAGTCTGAGATCCGCTGT-3′), subcloned into pBlueScript SK and further cloned into the rAAV2 backbone, pAAV-αCaMKII-htTA, thereby substituting the αCaMKII-promoter. The resulting rAAV expression vector was used for exchange of the htTA-gene for the following genes of interest: Venus, Channelrhodopsin-2 -mCherry, Tau-EGFP, and Synaptophysin-EGFP.

We also designed rAAV vectors equipped with the cytomegalovirus enhancer/chicken-β-actin promoter, expressing the rabies glycoprotein (RG) and the avian sarcoma and leucosis virus (TVA) receptor linked via an internal ribosomal entry site (IRES) to the fluorescent marker tdTomato.

Production of rAAVs

Production and purification of rAAVs (Serotype 1/2) were as described (Pilpel et al., 2009). rAAV genomic titers were determined with QuickTiter AAV Quantitation Kit (Cell Biolabs) and RT-PCR using the ABI 7700 cycler (Applied Biosystems). rAAVs titers were ∼10^{10} genomic copies per μl.

Rabies Viruses

Propagation of PS-Rab was performed as reported previously (Wickersham et al., 2010; Rancz et al., 2011). Briefly, after infection of BHK-B19G cells by SADΔG-GFP or SADΔG-mCherry, the supernatant containing unpseudotyped deletion-mutant rabies virus (UPS-Rab) was filtered and stored at −80°C (Figures S6A and S6D). Rabies virus pseudotyping (Wickersham et al., 2010; Rancz et al., 2011) and purification were as with lentivirus (Dittgen et al., 2004).

Animals

For anatomical studies, adult female Wistar rats were separated into 11 groups, according to the purposes of the study (Table S1). For stereotactic coordinates (Paxinos and Watson, 1998) and volumes of virus-containing solution, see Table S2. Stereotactic injections were performed as described (Cetin et al., 2006).

Histology

Double Fluorescence Immunohistochemistry

Vibratome sections of brains (50 μm) perfused with 4% paraformaldehyde (PFA) were stained with chicken anti-GFP (Abcam; 1:10,000) and combined with various antibodies against the following: OT and VP (1:300; provided by Harold Gainer; Ben-Barak et al., 1985); NeuN (Chemicon; 1:1,000); VGluT2 (Synaptic Systems; 1:1,000); and tdTomato (1:1,000; Clonthech). Whereas Venus and EGFP signals were enhanced by FITC-conjugated IgGs, other proteins and markers were visualized by CY3-conjugated or CY5-conjugated antibodies (1:300; Jackson Immuno-Research Laboratories). All images were acquired on a confocal Leica TCS NT and Zeiss LSM5 microscopes; digitized images were analyzed using Adobe Photoshop (Adobe).

Cell-Type Specificity and Inducibility of Venus Expression in OT Neurons

To analyze the specificity of OT promoter-Venus rAAV in neurons of the PVN and SON, we counted all Venus- and OT-immunoreactive neurons (80–150 neurons/section dependent on the anterior-posterior Bregma level) in three sections per animal at three different rostro-caudal Bregma levels (PVN: −1.5, −1.8, and −2.0 mm; SON: −1.1, −1.4, and −1.7 mm). Sections were taken from three virgin rats and three lactating rats, the latter killed on day 14 after parturition. For the analysis of the AN of three virgin and three lactating rats, we counted all Venus- and OT-immunoreactive neurons in two sections per animal (due to the shorter anterior-posterior extent of the AN compared to the SON and PVN) at two different Bregma levels (rSON: −2.0 and −2.1 mm; CN: −1.4 and −1.5 mm; DLN: −2.1 and −2.2 mm) and on average per section 12 neurons for the CN, 35 neurons for the DLN, and 19 neurons for the rSON. The number of identified and counted cells in both groups of animals was 4,774 neurons in total (more details on cell numbers are in Table 1). The comparison between the numbers of identified neurons per each rat and structure between groups of virgin and lactating rats was evaluated statistically (see below). The duration of infection was similar in all animals (25 days; see Table S1).

To exclude the possibility that our viral vector also infects VP neurons, the same analysis was performed on SON sections of three rats (see above). The sections were costained with antibodies against OT (visualized by CY3-conjugated secondary antibodies) and VP (visualized with CY5-conjugated antibodies) for subsequent counting of all cells visible in the SON positive for Venus, OT, and VP at three different Bregma levels (−1.1, −1.4, and −1.7 mm).

To analyze the inducibility of our viral vector, we analyzed the SONs of pregnant rats and virgin rats 1 day before delivery, on the day of delivery, and the day after delivery with Fiji (National Institute of Mental Health) to manually measure direct fluorescence intensity and cell sizes (25 cells/section; 3–4 sections per rat, 3 rats in each group, 12 animals in total). The selection of cells in the SON was done randomly at similar Bregma levels of the rostro-caudal extend of the nucleus (Bregmas: −0.92, −1.3, −1.4, and −1.6 mm). The total number of cells counted in each group was 180 (virgins), 180 (day before delivery), 240 (day of delivery), and 180 (day after delivery).

Statistical significance was determined by Student's t test for colocalization experiments and by one-way ANOVA for the inducibility of virally introduced OT-promoter fragment during peripartum period. Statistical analysis was performed with use of Prism 5 for Mac OS X. Results are presented as mean ± SEM. p < 0.05 were considered statistically significant.

Electron Microscopy

Rats were perfused transcardially with 4% PFA in phosphate buffer containing 0.05% glutaraldehyde at pH 7. The 50 μm coronal brain sections containing the CeA were incubated with rabbit polyclonal anti-GFP antibodies (Molecular Probes; 1:5,000). The GFP signals were visualized using the standard avidin-biotin complex protocol and DAB chromogen, intensified by silver-gold (Liposits et al., 1986) and processed (Eliava et al., 2003).

Electrophysiological In Vitro Experiments

Slice Preparation. Four-to-eight weeks after injection of ChR2-mCherry rAAV into the SON, PVN, and AN of adult virgin female rats, brains were removed, cut into 400 μm horizontal slices (described in Huber et al., 2005), and kept in artificial cerebrospinal fluid in the dark to avoid ChR2 activation.

Electrophysiological Recordings. Whole-cell patch-clamp recordings were visually guided by infrared videomicroscopy (DM-LFS; Leica), using 4–9 MOhm borosilicate pipettes filled with 140 mM KCl, 10 mM HEPES, 2 mM MgCl₂, 0.1 mM CaCl₂, 0.1 mM BAPTA, 2 mM ATP Na salt, 0.3 mM GTP Na salt (pH 7.3), 300 mOsm, and amplified with an Axopatch 200B (Axon Instruments). For cell-attached recordings, KCl was replaced with KMeSO4. ChR2-mCherry expression was identified by fluorescent microscopy and post hoc immunohistochemistry.

Blue-Light Stimulation. For in vitro experiments, optical stimulation was done via a mercury lamp (Short Arc 103W/2, Osram; ∼5 mW/mm²) in combination with a shutter (VS25S22M1R1, Uniblitz) or a TTL-pulsed LED source (LXHL-LB3C, Roithner; ∼10 mW/mm²), both yielding similar results.

Behavioral Experiments

Fear Conditioning

Following recovery from guide cannulae implantation (1 week), female virgin rats of random hormonal cycle were exposed to a contextual fear-conditioning protocol. This consisted of three sessions on consecutive days (Figure 5B). On day 1, rats were individually introduced in the conditioning box (45 × 18 × 25 cm) and after 10 min received a first series of seven electric shocks (0.8 mA) at random intervals (15–120 s) over 7 min. After the last shock, the rats were left in the box for 3 more min. BL was applied in 10-ms pulses at 30 Hz via a glass fiber protruding 2 mm beyond the lower end of the cannulae and delivered light intensity of ∼10 mW. OTA injection was done via two injectors (cut to fit the 5.8 mm guide cannulae protruding 2 mm beyond the lower end of the cannulae) that were bilaterally lowered into the guide cannulae, connected via polyten tubing to two Hamilton syringes that were placed in an infusion pump, and 0.5 μl of liquid containing 21 ng OTA was injected in each hemisphere at 0.25 μl/min over a 2 min period.

Application of BL during Fear-Context Exposure. On day 2, the rats were habituated to the glass fibers by inserting them into the cannulae for the complete duration of the protocol, which was similar to the one of day 1 (Figure 5C). On day 3, the rats were tested in the context for 10 min before receiving bilateral BL stimulation for either 20 s or 120 s. The effect was video recorded for the complete 20 min of the test (see Figure 5B). Freezing time was analyzed per 10 s intervals.

Application of BL prior to Fear-Context Exposure. On day 2, rats received in addition a sham blue-light application during 6 min of very light isoflurane (5% induction, 1% for maintenance), during which time the glass fiber was inserted into the guide cannulae, as on day 3, without exposure to BL (Figure 5D). At the end of day 2, freezing levels were assessed to exclude differences possibly caused by the implantation of the cannulae before the rats were divided in four groups for testing on day 3 (see Figure 5D). On day 3, the rats received (1) sham BL (insertion of the glass fiber without exposure to BL), (2) BL, (3) OTA alone, or (4) OTA and BL. BL was applied bilaterally for 2 min, first on the right and then on the left hemisphere. Rats were allowed 2 min of recovery from anesthesia and introduced in the context, where their behavior was video recorded during a 20 min period without electric shocks. Freezing was assessed per periods of 1 min intervals.

Effects of BL on Mobility. Animal mobility was assessed using photobeam sensors placed at 1 cm distances. Each time of beam interruption by the rat was counted by the software as one passage (MED-PC, Med Associates).

Blue-Light Stimulation In Vivo and Verification of Optic Fiber Positions

For the in vivo experiments, we used two blue lasers (λ 473nm, output of 150 mW/mm², DreamLasers) coupled with optical fibers (BFL37-200-CUSTOM,

EndA = FC/PC, and EndB = FLAT CLEAVE; Thorlabs), which were directly inserted above the region of interest via guide cannulae (C313G-SPC 22 Gauge, 5.8 mm below pedestal, PlasticOne). Guide cannulae were chronically implanted under isoflurane anesthesia (5% induction, 2% maintenance) at stereotaxic positions of −2.5 mm anteroposterior and 3.9 mm lateral from Bregma and were stabilized with dental cement. On the days of the experiments, the optic fibers were inserted through the cannulae and fixed through a screw at a position 2 mm protruding beyond the lower end of the cannula. This should lead to a specific stimulation of the CeL, as prevalent measurements with BL stimulations in rodent brain have shown that the BL of the laser does not penetrate the tissue further than 500 μm (Yizhar et al., 2011).

After the behavioral experiments, 0.5 μl of green fluorescent latex microspheres (Lumafluor) was injected 2 mm below the lower end of the cannulae (i.e., the same position as the optical fibers). Rats were subsequently killed to assess the placement of the tip of the injector by sectioning the brain with a vibratome into 400 μm slices (see Figure 5A).

Drugs and Concentrations

Oxytocin-receptor antagonist d(CH2)5-Tyr(Me)-[Orn8]-vasotocin (1 μM, OTA, Bachem), glutamate-receptor (AMPA) antagonist 1,2,3,4-tetrahydro-6-nitro-2,3-dioxo-benzo[f]quinoxaline-7-sulfonamide (0.4 μM, NBQX, Sigma), (−) bicuculline methiodide (Sigma), or picrotoxin (50 μM, PTX, Sigma) were bath perfused for the in vitro experiments for 20 min before and several min beyond the expected response to BL application.

Data Acquisition and Analysis

Patch-clamp signals were acquired with pClamp 9.0 (Axon Instruments), filtered at 5 kHz, and digitized at 10 kHz with a Digidata 1200 A/D (Axon Instruments). Currents were detected and analyzed using Minianalysis Program 6.0 (Synaptosoft).

Statistical Analysis

Data in text are expressed as mean ± SEM.

For in vitro experiments, one-way ANOVA with factor treatment (i.e., respective drug used) was used for assessment of pharmacological effects; Student's t test was used for assessment of BL effect without drug.

For in vivo experiments, one-way ANOVA with factor time was used for assessment of the BL effect on both freezing and mobility; Student's t test was used for comparison of duration of BL effect. For the experiments in Figure 5D, two-way repeated ANOVA with factors treatment (Ctrl versus BL; Ctrl versus OTA + BL; BL versus OTA) and time were used for assessment of BL effect in presence of pharmacological effects on freezing response.

When the ANOVA test was significant, the Tukey test was used for post hoc multiple comparisons. Differences were considered significant for p < 0.05 (*, + and °; ANOVA) or p < 0.01 (++, t test). All statistical tests were performed with StatView 5 (StatView, SAS Institute).

SUPPLEMENTAL INFORMATION

Supplemental Information includes six figures, two tables, Supplemental Experimental Procedures, and one movie and can be found with this article online at doi:10.1016/j.neuron.2011.11.030.

REFERENCES

Ben-Barak, Y., Russell, J.T., Whitnall, M.H., Ozato, K., and Gainer, H. (1985). Neurophysin in the hypothalamo-neurohypophysial system. I. Production and characterization of monoclonal antibodies. J. Neurosci. 5, 81–97.

Bosch, O.J., Meddle, S.L., Beiderbeck, D.I., Douglas, A.J., and Neumann, I.D. (2005). Brain oxytocin correlates with maternal aggression: link to anxiety. J. Neurosci. 25, 6807–6815.

Boyden, E.S., Zhang, F., Bamberg, E., Nagel, G., and Deisseroth, K. (2005). Millisecond-timescale, genetically targeted optical control of neural activity. Nat. Neurosci. 8, 1263–1268.

Brownstein, M.J., Russell, J.T., and Gainer, H. (1980). Synthesis, transport, and release of posterior pituitary hormones. Science 207, 373–378.

Buijs, R.M. (1983). Vasopressin and oxytocin—their role in neurotransmission. Pharmacol. Ther. 22, 127–141.

Burbach, J.P.H., Luckman, S.M., Murphy, D., and Gainer, H. (2001). Gene regulation in the magnocellular hypothalamo-neurohypophysial system. Physiol. Rev. 81, 1197–1267.

Caldwell, J.D., Greer, E.R., Johnson, M.F., Prange, A.J., Jr., and Pedersen, C.A. (1987). Oxytocin and vasopressin immunoreactivity in hypothalamic and extrahypothalamic sites in late pregnant and postpartum rats. Neuroendocrinology 46, 39–47.

Cetin, A., Komai, S., Eliava, M., Seeburg, P.H., and Osten, P. (2006). Stereotaxic gene delivery in the rodent brain. Nat. Protoc. 1, 3166–3173.

Ciocchi, S., Herry, C., Grenier, F., Wolff, S.B., Letzkus, J.J., Vlachos, I., Ehrlich, I., Sprengel, R., Deisseroth, K., Stadler, M.B., et al. (2010). Encoding of conditioned fear in central amygdala inhibitory circuits. Nature 468, 277–282.

Davis, M. (2000). A functional analysis. In The Amygdala, J.P. Aggleton, ed. (New York: Oxford University Press), pp. 213–288.

De Dreu, C.K.W., Greer, L.L., Handgraaf, M.J.J., Shalvi, S., Van Kleef, G.A., Baas, M., Ten Velden, F.S., Van Dijk, E., and Feith, S.W.W. (2010). The neuropeptide oxytocin regulates parochial altruism in intergroup conflict among humans. Science 328, 1408–1411.

Dittgen, T., Nimmerjahn, A., Komai, S., Licznerski, P., Waters, J., Margrie, T.W., Helmchen, F., Denk, W., Brecht, M., and Osten, P. (2004). Lentivirus-based genetic manipulations of cortical neurons and their optical and electrophysiological monitoring in vivo. Proc. Natl. Acad. Sci. USA 101, 18206–18211.

Donaldson, Z.R., and Young, L.J. (2008). Oxytocin, vasopressin, and the neurogenetics of sociality. Science 322, 900–904.

Eliava, M., Yilmazer-Hanke, D., and Asan, E. (2003). Interrelations between monoaminergic afferents and corticotropin-releasing factor-immunoreactive neurons in the rat central amygdaloid nucleus: ultrastructural evidence for dopaminergic control of amygdaloid stress systems. Histochem. Cell Biol. 120, 183–197.

Ferris, C.F., Foote, K.B., Meltser, H.M., Plenby, M.G., Smith, K.L., and Insel, T.R. (1992). Oxytocin in the amygdala facilitates maternal aggression. Ann. N Y Acad. Sci. 652, 456–457.

Gimpl, G., and Fahrenholz, F. (2001). The oxytocin receptor system: structure, function, and regulation. Physiol. Rev. 81, 629–683.

Griffin, G.D., Ferri-Kolwicz, S.L., Reyes, B.A.S., Van Bockstaele, E.J., and Flanagan-Cato, L.M. (2010). Ovarian hormone-induced reorganization of oxytocin-labeled dendrites and synapses lateral to the hypothalamic ventromedial nucleus in female rats. J. Comp. Neurol. 518, 4531–4545.

Grinevich, V., Brecht, M., and Osten, P. (2005). Monosynaptic pathway from rat vibrissa motor cortex to facial motor neurons revealed by lentivirus-based axonal tracing. J. Neurosci. 25, 8250–8258.

Haubensak, W., Kunwar, P.S., Cai, H., Ciocchi, S., Wall, N.R., Ponnusamy, R., Biag, J., Dong, H.W., Deisseroth, K., Callaway, E.M., et al. (2010). Genetic dissection of an amygdala microcircuit that gates conditioned fear. Nature *468*, 270–276.

Hitchcock, J.M., and Davis, M. (1991). Efferent pathway of the amygdala involved in conditioned fear as measured with the fear-potentiated startle paradigm. Behav. Neurosci. *105*, 826–842.

Hökfelt, T. (1991). Neuropeptides in perspective: the last ten years. Neuron *7*, 867–879.

Huber, D., Veinante, P., and Stoop, R. (2005). Vasopressin and oxytocin excite distinct neuronal populations in the central amygdala. Science *308*, 245–248.

Kapp, B.S., Frysinger, R.C., Gallagher, M., and Haselton, J.R. (1979). Amygdala central nucleus lesions: effect on heart rate conditioning in the rabbit. Physiol. Behav. *23*, 1109–1117.

Kawasaki, A., Hoshi, K., Kawano, M., Nogami, H., Yoshikawa, H., and Hisano, S. (2005). Up-regulation of VGLUT2 expression in hypothalamic-neurohypophysial neurons of the rat following osmotic challenge. Eur. J. Neurosci. *22*, 672–680.

Krause, E.G., de Kloet, A.D., Flak, J.N., Smeltzer, M.D., Solomon, M.B., Evanson, N.K., Woods, S.C., Sakai, R.R., and Herman, J.P. (2011). Hydration state controls stress responsiveness and social behavior. J. Neurosci. *31*, 5470–5476.

Landgraf, R., and Neumann, I.D. (2004). Vasopressin and oxytocin release within the brain: a dynamic concept of multiple and variable modes of neuropeptide communication. Front. Neuroendocrinol. *25*, 150–176.

Lee, H.-J., Macbeth, A.H., Pagani, J.H., and Young, W.S., 3rd. (2009). Oxytocin: the great facilitator of life. Prog. Neurobiol. *88*, 127–151.

Liposits, Z., Sherman, D., Phelix, C., and Paull, W.K. (1986). A combined light and electron microscopic immunocytochemical method for the simultaneous localization of multiple tissue antigens. Tyrosine hydroxylase immunoreactive innervation of corticotropin releasing factor synthesizing neurons in the paraventricular nucleus of the rat. Histochemistry *85*, 95–106.

Lubin, D.A., Elliott, J.C., Black, M.C., and Johns, J.M. (2003). An oxytocin antagonist infused into the central nucleus of the amygdala increases maternal aggressive behavior. Behav. Neurosci. *117*, 195–201.

Ludwig, M., and Leng, G. (2006). Dendritic peptide release and peptide-dependent behaviours. Nat. Rev. Neurosci. *7*, 126–136.

McEwen, B.B. (2004). Brain-fluid barriers: relevance for theoretical controversies regarding vasopressin and oxytocin memory research. Adv. Pharmacol. *50*, 531–592, 655–708.

Meeker, R.B., Swanson, D.J., Greenwood, R.S., and Hayward, J.N. (1991). Ultrastructural distribution of glutamate immunoreactivity within neurosecretory endings and pituicytes of the rat neurohypophysis. Brain Res. *564*, 181–193.

Nagel, G., Szellas, T., Huhn, W., Kateriya, S., Adeishvili, N., Berthold, P., Ollig, D., Hegemann, P., and Bamberg, E. (2003). Channelrhodopsin-2, a directly light-gated cation-selective membrane channel. Proc. Natl. Acad. Sci. USA *100*, 13940–13945.

Navone, F., Di Gioia, G., Jahn, R., Browning, M., Greengard, P., and De Camilli, P. (1989). Microvesicles of the neurohypophysis are biochemically related to small synaptic vesicles of presynaptic nerve terminals. J. Cell Biol. *109*, 3425–3433.

Neumann, I.D. (2007). Stimuli and consequences of dendritic release of oxytocin within the brain. Biochem. Soc. Trans. *35*, 1252–1257.

Neumann, I.D. (2008). Brain oxytocin: a key regulator of emotional and social behaviours in both females and males. J. Neuroendocrinol. *20*, 858–865.

Paxinos, G., and Watson, C. (1998). The Rat Brain in Stereotaxic Coordinates, Fourth Edition (London: Academic Press).

Peters, J.H., McDougall, S.J., Kellett, D.O., Jordan, D., Llewellyn-Smith, I.J., and Andresen, M.C. (2008). Oxytocin enhances cranial visceral afferent synaptic transmission to the solitary tract nucleus. J. Neurosci. *28*, 11731–11740.

Pilpel, N., Landeck, N., Klugmann, M., Seeburg, P.H., and Schwarz, M.K. (2009). Rapid, reproducible transduction of select forebrain regions by targeted recombinant virus injection into the neonatal mouse brain. J. Neurosci. Methods *182*, 55–63.

Rancz, E.A., Franks, K.M., Schwarz, M.K., Pichler, B., Schaefer, A.T., and Margrie, T.W. (2011). Transfection via whole-cell recording in vivo: bridging single-cell physiology, genetics and connectomics. Nat. Neurosci. *14*, 527–532.

Roozendaal, B., Schoorlemmer, G.H., Wiersma, A., Sluyter, S., Driscoll, P., Koolhaas, J.M., and Bohus, B. (1992a). Opposite effects of central amygdaloid vasopressin and oxytocin on the regulation of conditioned stress responses in male rats. Ann. N Y Acad. Sci. *652*, 460–461.

Roozendaal, B., Wiersma, A., Driscoll, P., Koolhaas, J.M., and Bohus, B. (1992b). Vasopressinergic modulation of stress responses in the central amygdala of the Roman high-avoidance and low-avoidance rat. Brain Res. *596*, 35–40.

Roozendaal, B., Schoorlemmer, G.H., Koolhaas, J.M., and Bohus, B. (1993). Cardiac, neuroendocrine, and behavioral effects of central amygdaloid vasopressinergic and oxytocinergic mechanisms under stress-free conditions in rats. Brain Res. Bull. *32*, 573–579.

Ross, H.E., and Young, L.J. (2009). Oxytocin and the neural mechanisms regulating social cognition and affiliative behavior. Front. Neuroendocrinol. *30*, 534–547.

Ross, H.E., Cole, C.D., Smith, Y., Neumann, I.D., Landgraf, R., Murphy, A.Z., and Young, L.J. (2009). Characterization of the oxytocin system regulating affiliative behavior in female prairie voles. Neuroscience *162*, 892–903.

Sawchenko, P.E., and Swanson, L.W. (1983). The organization and biochemical specificity of afferent projections to the paraventricular and supraoptic nuclei. Prog. Brain Res. *60*, 19–29.

Simeon, D., Bartz, J., Hamilton, H., Crystal, S., Braun, A., Ketay, S., and Hollander, E. (2011). Oxytocin administration attenuates stress reactivity in borderline personality disorder: a pilot study. Psychoneuroendocrinology *36*, 1418–1421.

Skrundz, M., Bolten, M., Nast, I., Hellhammer, D.H., and Meinlschmidt, G. (2011). Plasma oxytocin concentration during pregnancy is associated with development of postpartum depression. Neuropsychopharmacology *36*, 1886–1893.

Sofroniew, M.V. (1983). Morphology of vasopressin and oxytocin neurones and their central and vascular projections. Prog. Brain Res. *60*, 101–114.

Swanson, L.W., and Petrovich, G.D. (1998). What is the amygdala? Trends Neurosci. *21*, 323–331.

Swanson, L.W., and Sawchenko, P.E. (1983). Hypothalamic integration: organization of the paraventricular and supraoptic nuclei. Annu. Rev. Neurosci. *6*, 269–324.

Theodosis, D.T. (1985). Oxytocin-immunoreactive terminals synapse on oxytocin neurones in the supraoptic nucleus. Nature *313*, 682–684.

Theodosis, D.T. (2002). Oxytocin-secreting neurons: A physiological model of morphological neuronal and glial plasticity in the adult hypothalamus. Front. Neuroendocrinol. *23*, 101–135.

Veenema, A.H., and Neumann, I.D. (2008). Central vasopressin and oxytocin release: regulation of complex social behaviours. Prog. Brain Res. *170*, 261–276.

Viviani, D., Charlet, A., van den Burg, E., Robinet, C., Hurni, N., Abatis, M., Magara, F., and Stoop, R. (2011). Oxytocin selectively gates fear responses through distinct outputs from the central amygdala. Science *333*, 104–107.

Wickersham, I.R., Lyon, D.C., Barnard, R.J., Mori, T., Finke, S., Conzelmann, K.K., Young, J.A., and Callaway, E.M. (2007). Monosynaptic restriction of transsynaptic tracing from single, genetically targeted neurons. Neuron *53*, 639–647.

Wickersham, I.R., Sullivan, H.A., and Seung, H.S. (2010). Production of glycoprotein-deleted rabies viruses for monosynaptic tracing and high-level gene expression in neurons. Nat. Protoc. *5*, 595–606.

Wilensky, A.E., Schafe, G.E., Kristensen, M.P., and LeDoux, J.E. (2006). Rethinking the fear circuit: the central nucleus of the amygdala is required for the acquisition, consolidation, and expression of Pavlovian fear conditioning. J. Neurosci. *26*, 12387–12396.

Wotjak, C.T., Ganster, J., Kohl, G., Holsboer, F., Landgraf, R., and Engelman, M. (1998). Dissociated central and peripheral release of vasopressin, but not oxytocin, in response to repeated swim stress: new insights into the secretory capacities of peptidergic neurons. Neuroscience *85*, 1209–1222.

Yizhar, O., Fenno, L.E., Davidson, T.J., Mogri, M., and Deisseroth, K. (2011). Optogenetics in neural systems. Neuron *71*, 9–34.

Zingg, H.H., and Lefebvre, D.L. (1988). Oxytocin and vasopressin gene expression during gestation and lactation. Brain Res. *464*, 1–6.

III - Mechanisms for Oxytocinergic Modulation of Emotional Processing

Since 2013, I'm a CNRS tenure researcher (CR2) at the INCI UPR3212. All along this period I was focused on establishing a small research lab with use of adequate electrophysiological, imaging and optogenetic approaches. The major part of the funding I acquired was dedicated to equip the lab with two *ex vivo* electrophysiology patch-clamp set-up, one *ex vivo* confocal calcium imaging setup and one *in vivo* electrophysiology extracellular recording setup. I also dedicated a significant part of the budget to hire students, with two PhD student salaries and a one year post-doctoral salary.

My scientific projects are now all centered on the oxytocinergic modulation of the very large "emotional processing", using an integrative techniques from cellular to behavioral levels and tacking advantage of the recently validated viral approaches. In order to ensure a minimum of security to the lab members, I have chosen to lead two parallel research lines, both scientifically very independent and technically similar:

1) Deciphering the oxytocinergic pathways and neuronal network underlying its main physiological functions. Oxytocin is responsible for the regulation of many physiological functions occurring all along the cycle of life, from the first social interaction to the perpetuation of life with pregnancy and birth (Lee et al., 2009). However, how this neuropeptide exert so many functions is unclear. Since a few years, we hence dedicate a project to unravel how oxytocin act – this led in our first publication illustrating the complex oxytocin function to control nociception by a dual mechanism (Eliava*, Melchior*, Knobloch*, Wahis* et al., *Neuron*, 2016).

2) Unraveling the cellular mechanisms underlying the oxytocin action with a particular emphasis in the neuron-glia interactions. A great interest raises from findings that astrocytes exhibit rapidly propagating "calcium waves", suggesting that they may form a parallel path of communication working with the neuronal one (Volterra and Meldolesi, 2005). On the other hand, there are few evidence for non-neuronal oxytocin binding sites in central nervous system (Di Scala-Guenot & Strosser, 1992). Given that glia is clearly involved in several disorders and diseases such as depression, anxiety and neuropathies (Johnson et al., 2010) we were interested in to characterize *in vitro* and *in vivo* involvement of astrocytes in the effects of endogenous oxytocin release (Wahis*, da Silva Gouveia* et al., *Science*, in revision).

1 - A New Population of Parvocellular Oxytocin Neurons Controlling Magnocellular Neuron Activity and Inflammatory Pain Processing

How are oxytocinergic neurons recruited? Central oxytocinergic system has the particularity to be located exclusively in the hypothalamus, and particularly in the namely the paraventricular (PVN), supraoptic (SON) and accessory nuclei (Sofroniew, 1983). In addition, OT neurons can be classified in magnocellular OT (magnOT) and parvocellular OT (parvOT) neurons, which are distinct in size, shape and electrical properties, subnuclear location, the amount of OT production, and involvement in distinct circuitries and functions (Armstrong et al., 1980; Swanson and Sawchenko, 1983; Lee et al., 2010). A long term dogma segregated the function of OT neurons to their nature: while magnOT provide systemic OT supply, parvOT project to distinct brainstem nuclei and spinal cord (Scharrer, 1928). However, we recently showed that MagnOT not only provide systemic OT supply but also send axonal projection to a number of brain nuclei (Knobloch et al., 2012). Then, while the oxytocinergic modulation of emotions such as pain and anxiety is now well described, it is still unclear how the underlying circuits are recruited and what are the places and roles of magnOT and parvOT. From the early 1980's, scientists have demonstrated the existence of OT modulation of OT neurons activity and hypothetized intra-hypothalamic connections between distinct oxytocinergic centers (Freund-Mercier and Richard, 1984; Moos et al., 1984) but unfortunately lacked the right tools to formally demonstrate their existence and characterize their roles.

We therefore hypothesized that **parvOT and magnOT neurons residing in spatially segregated nuclei could communicate together in order to coordinate their different actions**. We used a combination of viral tools with strong and established electrophysiological and behavioral recordings with three objectives: **a)** To determine if parvOT neurons do communicate with magnOT neurons; **b)** To understand how OT system is recruited upon pain; **c)** To decipher how the OT nuclei coordinate themselves for peripheral and central OT action.

As a result, we described a small population of 30 parvocellular oxytocinergic neurons of particular interest in the control of pain. Located in the PVN and activated upon a painful episode to coordinate the global analgesic effect of oxytocin. Indeed, they send simultaneous axonal projections to **i)** the SON, controlling magnocellular oxytocinergic neurons activity and hence the blood release of OT by magnOT. This leads to a diffuse analgesic effect by reducing the sensory perception of peripheral neurons that relay nociceptive information. **ii)** Via long-range axonal projection to the deep layers of the spinal cord, directly inhibiting wide dynamic range (WDR) sensory neurons to gate the nociceptive message. They thus secrete OT precisely at the level where the intensity of the nociceptive message is encoded in the central nervous system. Finally, the activity of those 30 oxytocinergic neurons is sufficient to elicit a strong analgesia during peripheral inflammatory sensitization.

This describes for the first time and in full detail the functional and anatomical characteristics of a specific population of hypothalamic oxytocinergic circuits that are selectively engaged during inflammatory pain. In addition, it provide evidence for anatomical and functional heterogeneity within the central oxytocin system and offer a new direction for research of mechanisms of coordinated oxytocin regulation of autonomic functions and behavior.

Neuron

A New Population of Parvocellular Oxytocin Neurons Controlling Magnocellular Neuron Activity and Inflammatory Pain Processing

Highlights

- Thirty parvocellular oxytocin neurons (ParvOT) alleviate acute pain

- ParvOT project to WDR sensory neurons in spinal cord (SC)

- ParvOT activate OT release from magnocellular OT neurons (magnOT)

- Dual pain suppression by peripheral magnOT and central SC OT

Authors

Marina Eliava, Meggane Melchior,
H. Sophie Knobloch-Bollmann, ...,
Ron Stoop, Alexandre Charlet,
Valery Grinevich

Correspondence

acharlet@unistra.fr (A.C.),
v.grinevich@dkfz-heidelberg.de (V.G.)

In Brief

Eliava, Melchior, Knobloch-Bollmann, Wahis et al. demonstrate that thirty specialized oxytocin neurons in the rat hypothalamus coordinate activity of oxytocin neurons and deep dorsal horn spinal processing, as revealed by the repression of nociceptive messages and the promotion of analgesia.

CellPress

Neuron

Article

A New Population of Parvocellular Oxytocin Neurons Controlling Magnocellular Neuron Activity and Inflammatory Pain Processing

Marina Eliava,[1,12] Meggane Melchior,[2,12] H. Sophie Knobloch-Bollmann,[1,3,12,14] Jérôme Wahis,[2,12]
Miriam da Silva Gouveia,[1] Yan Tang,[1,5] Alexandru Cristian Ciobanu,[4] Rodrigo Triana del Rio,[4] Lena C. Roth,[1,3]
Ferdinand Althammer,[1] Virginie Chavant,[2] Yannick Goumon,[2] Tim Gruber,[1,3] Nathalie Petit-Demoulière,[2] Marta Busnelli,[6]
Bice Chini,[6,7] Linette L. Tan,[8] Mariela Mitre,[9] Robert C. Froemke,[9] Moses V. Chao,[9] Günter Giese,[3] Rolf Sprengel,[3]
Rohini Kuner,[8] Pierrick Poisbeau,[2] Peter H. Seeburg,[3] Ron Stoop,[4,13] Alexandre Charlet,[2,10,13,*]
and Valery Grinevich[1,3,11,13,*]

[1]Schaller Research Group on Neuropeptides at German Cancer Research Center (DKFZ) and Cell Network Cluster of Excellence at the University of Heidelberg, Heidelberg 69120, Germany
[2]Institut of Cellular and Integrative Neurosciences (INCI) UPR3212, Centre National de la Recherche Scientifique (CNRS), University of Strasbourg, Strasbourg 67084, France
[3]Max Planck Institute for Medical Research, Heidelberg 69120, Germany
[4]Center for Psychiatric Neurosciences, Hôpital de Cery, Lausanne University Hospital (CHUV), Lausanne 1008, Switzerland
[5]Institute of Brain Functional Genomics, East China Normal University, Shanghai 200062, China
[6]National Research Council, Institute of Neuroscience, Milan 20129, Italy
[7]Humanitas Clinical and Research Center, Rozzano 20089, Italy
[8]Department for Molecular Pharmacology and Molecular Medicine Partnership Unit with European Molecular Biology Laboratories, Institute of Pharmacology, Heidelberg University, Heidelberg 69120, Germany
[9]Skirball Institute of Biomolecular Medicine, New York University School of Medicine, New York, NY 10016, USA
[10]University of Strasbourg Institute for Advanced Study (USIAS), Strasbourg 67000, France
[11]Central Institute of Mental Health (ZI), Mannheim 68159, Germany
[12]Co-first author
[13]Co-senior author
[14]Present address: Department of Molecular and Cellular Biology, Center for Brain Science, Harvard University, 52 Oxford Street, Cambridge, MA 02139, USA
*Correspondence: acharlet@unistra.fr (A.C.), v.grinevich@dkfz-heidelberg.de (V.G.)
http://dx.doi.org/10.1016/j.neuron.2016.01.041

SUMMARY

Oxytocin (OT) is a neuropeptide elaborated by the hypothalamic paraventricular (PVN) and supraoptic (SON) nuclei. Magnocellular OT neurons of these nuclei innervate numerous forebrain regions and release OT into the blood from the posterior pituitary. The PVN also harbors parvocellular OT cells that project to the brainstem and spinal cord, but their function has not been directly assessed. Here, we identified a subset of approximately 30 parvocellular OT neurons, with collateral projections onto magnocellular OT neurons and neurons of deep layers of the spinal cord. Evoked OT release from these OT neurons suppresses nociception and promotes analgesia in an animal model of inflammatory pain. Our findings identify a new population of OT neurons that modulates nociception in a two tier process: (1) directly by release of OT from axons onto sensory spinal cord neurons and inhibiting their activity and (2) indirectly by stimulating OT release from SON neurons into the periphery.

INTRODUCTION

Oxytocin (OT), a neuropeptide that plays an important role in sociability, is produced in the brain exclusively in the hypothalamic paraventricular (PVN), supraoptic (SON), and intermediate accessory nuclei (Swanson and Sawchenko, 1983). OT neurons can be classified in magnocellular OT (magnOT) and parvocellular OT (parvOT) neurons, which are distinct in size and shape, subnuclear location, the amount of OT production, and involvement in distinct circuitries and functions (Armstrong et al., 1980; Swanson and Kuypers, 1980; Sofroniew, 1983; Swanson and Sawchenko, 1983).

According to a long-held dogma, magnOT neurons provide systemic OT supply by release into the blood via the posterior pituitary (Scharrer, 1928; Scharrer and Scharrer, 1940, Bargmann and Scharrer, 1951). Simultaneously, magnOT neurons innervate the forebrain, including the nucleus accumbens (Ross et al., 2009; Knobloch et al., 2012; Dölen et al., 2013) and the central nucleus of the amygdala (Knobloch et al., 2012). The forebrain fibers, as exemplarily studied in the central amygdala, allow for focal release and discrete, modulatory action of OT (Knobloch et al., 2012). These characteristics might account for the distinct impact of OT on numerous types of brain-region specific behaviors (Lee et al., 2010).
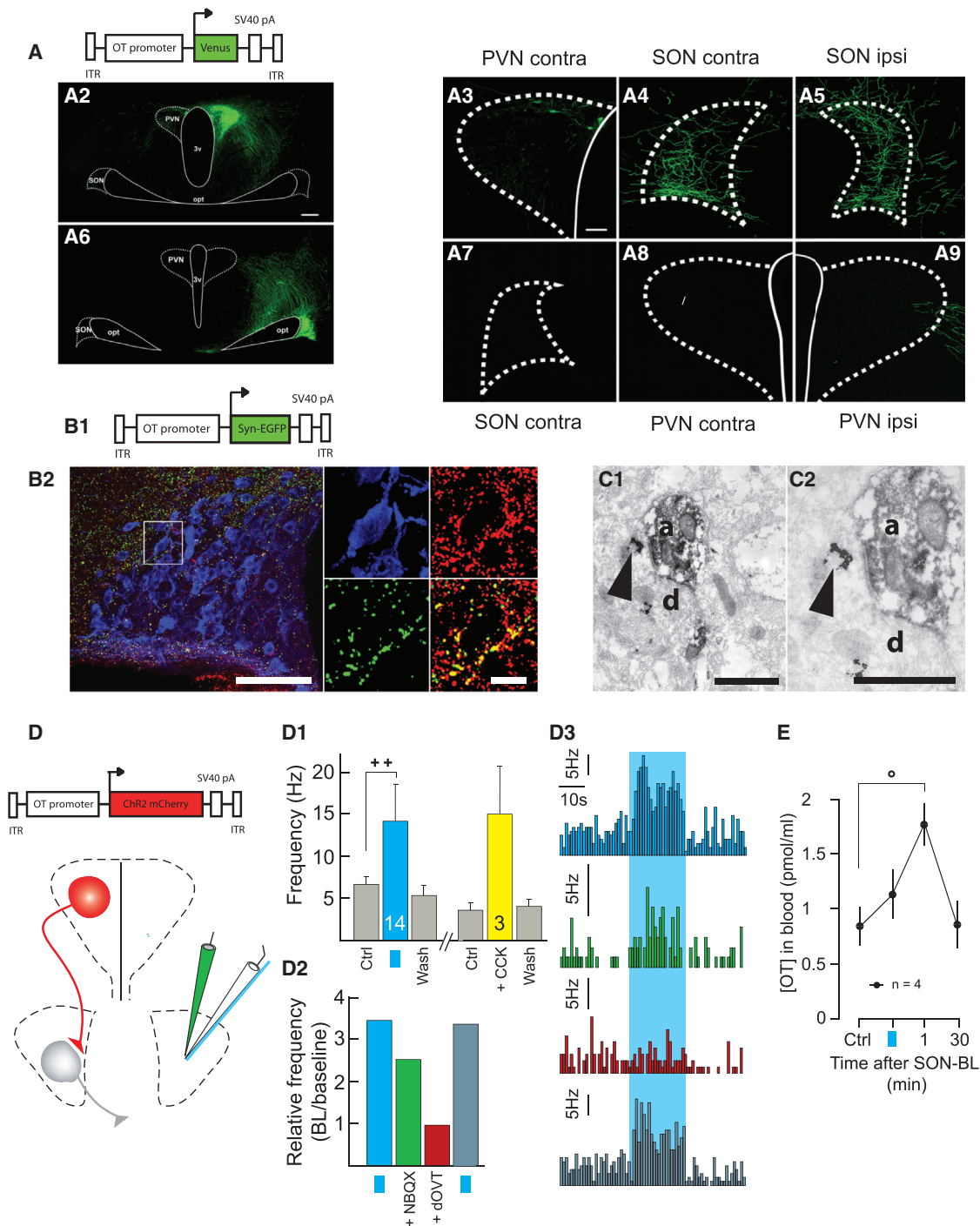
Figure 1. Anatomical and Functional Connectivity between OT Neurons of the PVN and SON

(A) OT projections from PVN to SON.

(A1) Scheme of the viral vector used to infect PVN neurons.

(A2–A9) PVN OT neurons infected with cell-type specific viral vector project Venus-positive axons to contralateral PVN (A3) and to contra- and ipsilateral SON (A4 and A5). OT neurons of the SON (A6) do not project Venus axons to contralateral SON (A7) or PVN (A8) and only marginally enter the external border of ipsilateral PVN (A9). The scale bars represent 200 μm (left) and 50 μm (right).

(B) OT axon terminals contain vGluT2.

(B1) Scheme of viral vector.

(B2) GFP-positive terminals in the area of the SON (left). In the magnified inset (right), the OT neuron (blue) is surrounded by GFP terminals, which also contain vGlut2 (red). Both of the immunosignals overlap (yellow) in virtually all of the terminals. The scale bars represent 100 μm (left) and 25 μm (right).

(legend continued on next page)

In contrast to magnOT neurons, parvOT neurons project to distinct brainstem nuclei and different regions of the spinal cord (SC) (Swanson and Sawchenko, 1983; Sawchenko and Swanson, 1982). Based on the location of parvOT axons and the effects of externally applied OT, it has been proposed that OT from parvOT axonal terminals contributes to modulation of cardiovascular functions, breathing, feeding behavior, and nociception (Mack et al., 2002; Petersson, 2002; Condés-Lara et al., 2003; Atasoy et al., 2012). However, no selective and specific genetic access to parvOT neurons has been available and, hence, there was no evidence for the capacity of parvOT axons to release endogenous OT and to selectively modulate the above-mentioned functions. Moreover, it has remained unknown how parvOT neurons are incorporated into the entire OT system and functionally interact with magnOT neurons.

Based on recent reports that OT-modulated nociception and pain response comprise a peripheral (Juif and Poisbeau, 2013) and a central component (Juif et al., 2013; González-Hernández et al., 2014), it is tempting to propose that these components are dependent on different OT cell types. The central component results from parvOT innervation of SC targets (Swanson and McKellar, 1979), whereas peripherally acting OT, in contrast, is provided to the blood stream by magnOT neurons and presumably targets C-type fibers in the dorsal root ganglion (DRG; Juif and Poisbeau, 2013). We therefore hypothesized that the complementary, analgesic OT action—at central and peripheral levels—depends on the communication between magnOT and parvOT neurons residing in spatially segregated OT nuclei. Our present results reveal that the modulation of pain signals by OT is triggered by only a handful of parvOT neurons that innervate simultaneously "sensory wide dynamic range" (WDR) neurons in the deep laminae of the SC, expressing neurokinin-1 (NK1R) and OT receptors (OTR), and SON neurons that secrete OT in the periphery. We show that these separate innervations underlie a two-tier modulation of pain by OT reaching the SC through fast, direct neuronal projections and a slower, indirect peripheral pathway.

RESULTS

Intrahypothalamic Axonal Trees of the OT System

To examine the intrahypothalamic OT system, we used recombinant adeno-associated virus (rAAV), allowing cell-type specific fluorescent labeling of OT neurons with 98%–100% cell-type specificity, as reported in Knobloch et al. (2012). To compare the OT system with the vasopressin (VP) system, we used AAV carrying different fluorescent markers driven by an evolutionarily conserved VP promoter (for specificity, see Table S1; Figure S1A).

After injection of rAAV expressing Venus, under the control of an OT promoter (Figure 1A), we observed that OT neurons of the PVN give rise to fibers connecting to the ipsi- and even contralateral SON and form a pronounced plexus (Figures 1A4 and 1A5). Interconnections within the intrahypothalamic VP system, in contrast, were absent (Figure S1C). The OT plexus might stem from PVN OT neurons projecting above the third ventricle to the contralateral PVN (Figure 1A3). OT connectivity from the PVN to SON was present in females and males (Figure S2A). The connection between the OT nuclei was one-way: the SON-arising OT fibers reached only marginally the ipsi- (Figure 1A9) and never the contralateral SON (Figure 1A7) or PVN (Figure 1A8).

The OT PVN-SON connection was reconstructed using light sheet microscopy. As presented in Figure S2B, descending fibers from the PVN mainly project rostro-ventrally, turn horizontally at the level of the SON, and enter the SON from the rostral position, to run caudally along the whole extent of the nucleus.

PVN OT Neurons Innervate the SON and Control MagnOT Neuron Activity to Induce OT Release into Blood Circulation

At the light microscopic level, Venus-labeled OT axons that arose from the PVN formed tight appositions to dendrites and somata of magnOT SON neurons resembling synaptic contacts. To assess if synapses were present, we injected the PVN with rAAV that expresses the synaptic marker synaptophysin fused to the green fluorescent marker EGFP in PVN OT neurons (Figure 1B1). GFP-positive puncta were found in the SON. The vast majority of terminals with GFP signal overlapped with VGluT2 signal (red, Figure 1B2). GFP/VGluT2 terminals engulfed OT cell bodies and dendrites (blue, Figure 1B2). We found that EGFP signals overlapped with VGluT2 in 92.6% ± 8.3% of all terminals (Figure 1B2). These light microscopic observations suggested the presence of synaptic contacts, which we further confirmed at the electron microscopic level: EGFP-positive OT axons from the PVN (EGFP: greyish filling) formed asymmetric (presumably glutamatergic) synapses on OT dendrites of the SON (OT: dark aggregate in pre- and postsynaptic elements; Figures 1C1 and 1C2).

Based on the anatomical evidence for OT connections between PVN and SON neurons, we aimed for a functional characterization of these connections. We expressed the blue-light

(C–C2) Electron microscopy OT axon terminals (Venus visualized as diaminobenzidine [DAB] endproduct, OT, as a silver-gold-intensified DAB) form asymmetric synapses on OT-ir dendrite within the SON. The OT-immunoreactivity (clusters of silver particles, arrows) are shown in the presynaptic axon (a) terminal and postsynaptic dendrite (d) at lower (C1) and higher magnifications (C2). The scale bar represents 0.5 μm.

(D) Scheme of the viral vector and setup of in vivo electrophysiological recordings (white pipette) in SON, together with SON-BL stimulation (blue fiber) and drug infusion (green pipette).

(D1–D3) Functional connection between PVN and SON OT neurons. (D1) Average spike frequencies of SON OT neurons before (Ctrl), after either SON-BL (n = 14, blue bar) or systemic injection of CCK (n = 3, yellow bar), and after washout effect (Wash). (D2) Relative frequency increase induced by SON-BL in control condition (blue bar), after infusion of NBQX (1 μM, 0.5 μl; green bar), after additional infusion of dOVT (1 μM, 0.5 μl; red bar), and after 30 min washout of the drugs (dark blue bar). (D3) Histograms of the frequency rates recorded under conditions described in (D2).

(E) Effect of unilateral SON-BL effect on OT blood concentration at the end of SON-BL, 1 min and 30 min after (n = 4). All results are expressed as average ± SEM. The statistical significances: ++ p < 0.01 and Wilcoxon's test. (°p < 0.05, Friedman's test followed by Dunn post hoc test) The blue squares represent 20 s BL stimulation at 30 Hz with 10 ms pulses of BL stimulation.

(BL)-sensitive ChR2 protein (Nagel et al., 2003) fused to mCherry in PVN OT neurons (for construct validation, see Knobloch et al., 2012). In vivo extracellular recordings in anaesthetized animals revealed the expression of functional ChR2 in the PVN, as evident from BL-induced (PVN-BL, 20 s at 30 Hz with 10 ms pulses), reversible, and reproducible increases of spike frequencies in these PVN neurons (on average the frequency increased from 4.1 ± 0.7 to 7.8 ± 0.7 Hz; data not shown).

We then further tested in vivo whether exposure to BL of PVN-OT axons in the SON (SON-BL, scheme in Figure 1D) could also activate, ipsilaterally, SON neurons. SON-BL exposure evoked a reversible increase in spike frequencies of SON neurons, from 6.7 ± 1.5 to 14.1 ± 2.7 Hz, confirming that BL stimulation of parvOT PVN axon terminals could excite SON neurons (Figure 1D1). To verify that OT was the main transmitter involved, we recorded the response of a single neuron to the SON-BL in the absence of any drug, or after sequential infusion of AMPA and OTR antagonists (respectively, NBQX and dOVT) into the SON, and after their washout (Figures 1D2 and 1D3). Interestingly, while NBQX decreased the baseline frequency of SON neurons, SON-BL paired to NBQX application still efficiently increased the relative frequency of discharge of the recorded neuron. Subsequent dOVT infusion totally blocked the SON-BL response, with full recovery 30 min after washout (Figures 1D2 and 1D3). These results are in accordance with our previous observations in the central amygdala (Knobloch et al., 2012).

We aimed at providing functional evidence for the OT nature of the SON neurons that were contacted by the PVN. To this purpose, we first of all injected into the blood circulation cholecystokinin (CCK) a hormone inducing the activation of OT neurons (Verbalis et al., 1986). CCK induced a prominent increase in spike frequencies of SON-BL responding neurons from 3.6 ± 0.8 to 15.0 ± 5.9 Hz (Figure 1D1), establishing an indirect argument of the OT identity of the in vivo recorded SON neuron. Second, as magnOT neurons are known to release OT in the blood, we performed a time-dependent measurement of OT concentrations in plasma by mass-spectrometry after SON-BL. This revealed a significant increase of OT plasma concentrations at 60 s after SON-BL (from 0.84 ± 0.17 to 1.76 ± 0.22 pmol/ml; Figure 1E). Taken together, these findings provide evidence for an OT identity of the SON neurons that are activated by axonal terminals originating from OT neurons in the PVN.

OT Neurons Projecting to SON MagnOT Neurons Are ParvOT Neurons Displaying Distinct Anatomical and Electrophysiological Characteristics

To identify PVN neurons projecting to the SON, we injected into the SON retrogradely transported and monosynaptically transmitted canine adenovirus 2 (CAV2). After counting of sections containing the entire PVN, we identified in total a very small population of GFP/OT-positive neurons residing bilaterally (Table S2; 31.5 ± 8.5 neurons). CAV spread occurs within 200 μm of the injection site (Schwarz et al., 2015), making unlikely the diffusion of the virus from the SON to PVN (the distance between these two nuclei is about 1.5 mm; see Paxinos and Watson, 1998).

To characterize the magno- versus parvocellular nature of back-labeled PVN cells, we combined CAV2 with systemic administration of Fluorogold (Figure S3A). Fluorogold, when injected intraperitoneal (i.p.), is taken up by neurons projecting beyond the blood brain barrier, for example, by magnOT neurons, thus allowing to distinguish them from the parvOT (Fluorogold-negative) neurons (Luther et al., 2002; Table S2). Notably, all magnOT neurons of the SON were Fluorogold-positive (data not shown). After neuron counting in sections containing the entire PVN, we established that the vast majority of the 31.5 ± 8.5 GFP/OT-positive neurons (90%) did not contain Fluorogold (Table S2). In addition to the detection of back-labeled GFP-positive neurons in the PVN, we observed GFP neurons in other structures typically known to innervate the SON, further confirming the specificity of our retrograde labeling (Miselis, 1981; Cunningham and Sawchenko, 1988; Figure S3B).

To characterize the parvOT neurons projecting to the SON, we next injected into the SON CAV2 expressing Cre recombinase and into the PVN rAAV carrying a double-floxed inverted open reading frame (ORF) (DIO) of GFP under the control of the OT promoter (Figure 2A1). By this combination, we limited GFP expression exclusively to SON-projecting parvOT neurons. In line with previous results, this revealed a unique position of back-labeled GFP neurons in the dorso-caudal PVN (Figures 2A2, 2A3, S2B, and S2C). Individual GFP neurons have bipolar spindle-like morphology (Figure 2A4) distinct from neighboring magnOT neurons (Figure 2A5). The number of back-labeled PVN GFP (exclusively OT) neurons was comparable (33.4 ± 9.1), with the estimation of non-selectively labeled PVN neurons identified by costaining with OT antibodies.

OT neurons similar in morphology and location were obtained in our initial study (data not shown) with the application of latex retrobeads (Katz and Iarovici, 1990) in the SON, which, however, labeled only few cells in the PVN (and other structures innervating the SON; Figure S3), precluding quantitative analysis.

We determined the electrophysiological characteristics of fluorescently labeled neurons in the PVN to assess their parvocellular nature. We conducted whole-cell patch clamp recordings in slices (Figure 2B) in current clamp applying a protocol of depolarizing current injections (Figure 2B1). This was aimed to determine the presence of a transient outward rectification, which is typically found in magnOT, but not in parvOT neurons (Luther et al., 2002). We recorded in a total of seven animals 11 fluorescent putative parvOT, and found that none, as expected, exhibited a hyperpolarizing notch. Conversely, all of the 13 non-fluorescent neurons from the same region (putative magnOT) showed the typical transient outward rectifying current, as known as (aka) "notch". Quantification of these differences was made by analyzing the time to spike (spike delay) and rise slope, which was the slope measured between beginning of the depolarization and the peak time of the first action potential. Both of these parameters showed highly significant differences between the two groups of neurons (Table S4; Figure S4). Differences in the spike frequency also showed a tendency, though with less significance than previously reported (Luther et al., 2000). The electrophysiological responses were in agreement with the morphology of the cells. Neurons classified electrophysiologically as parvOT had a small soma and a more elongated shape, while the ones classified as magnOT had a big soma and were more rounded (Figure 2B2).
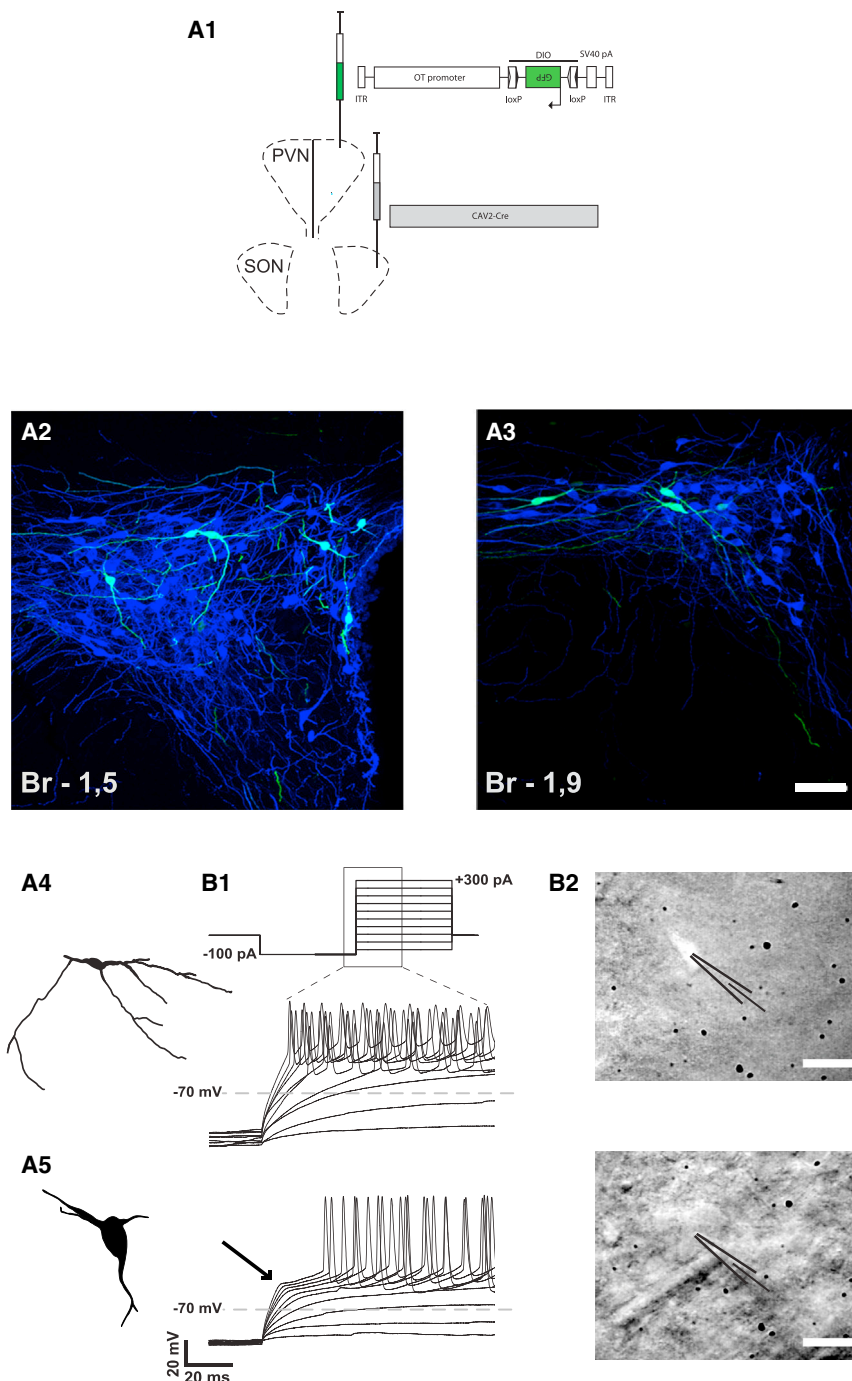
CellPress

Figure 2. Anatomical and Electrophysio-logical Characteristics of PVN OT Neurons Projecting to the SON

(A) Identification of a subset of OT neurons projecting from PVN to SON.

(A1) Scheme showing the injection of viruses in the SON and PVN.

(A2 and A3) Defined subset of back-labeled OT neurons (green) in dorso-caudal PVN displays consistent morphology: small oval somas (12 to 20 μm in diameter) with predominantly longer horizontal axes. The scale bar represents 50 μm in (A2) and 50 μm in (A3).

(A4 and A5) The morphology of these cells is clearly distinct from the typical magnocellular neurons with large cell bodies and less branching processes (A5).

(B) Functional differentiation of this subset of PVN OT neurons.

(B1) Current steps protocol starting from a hyper-polarizing current chosen to reach −100 mV (here 100 pA) followed by progressively more depolarizing current injections (upper trace). The representative changes in membrane potential for the parvOT and magnOT PVN neurons during the part of the current steps as indicated by the zoomed area are shown (lower traces). The ParvOT neurons (middle trace) do not display the transient outward rectification specific for the magnOT neurons (lower trace, arrow).

(B2) Photographs of a GFP-fluorescent parvOT neuron (upper) in the PVN (labeled by injection of CAV2-Cre into the SON and OT-DIO-GFP AAV in the PVN) and in the same area a typical magnOT neuron (lower) as indicated by the patch pipettes. The scale bars represent 20 μm.

SC layers (Figure S5A). In contrast, we found that synaptophysin-GFP-filled terminals from parvOT only were loosely and sparsely distributed in superficial laminae, but heavily innervate deep laminae, in close proximity to neurokinin 1 receptor (NK1R)-positive large cells (diameter 30–40 μm; Figure 3A2) identified as sensory WDR neurons (Ritz and Greenspan, 1985). Importantly, in an additional labeling (on separate slices because both OTR and NK1R antibodies had been raised in the same species), we found in this same region cells that expressed OTR (Figure 3A3). The specificity of the antibody was confirmed in transfected HEK cells (Figure S5B1) and brainstem sections of OTR knockout mice (Figure S5B2), in agreement with a previous study using these antibodies in mouse cortex (Marlin et al., 2015). To show the co-localization of NK1R and OTR in the same cells, we performed fluorescent in situ hybridization and found the presence of respective mRNAs in the same neurons of deep layers of the SC (Figures 3B1–3B4). As a next step, we wanted to demonstrate that NK1R-positive neurons of deep SC laminae could
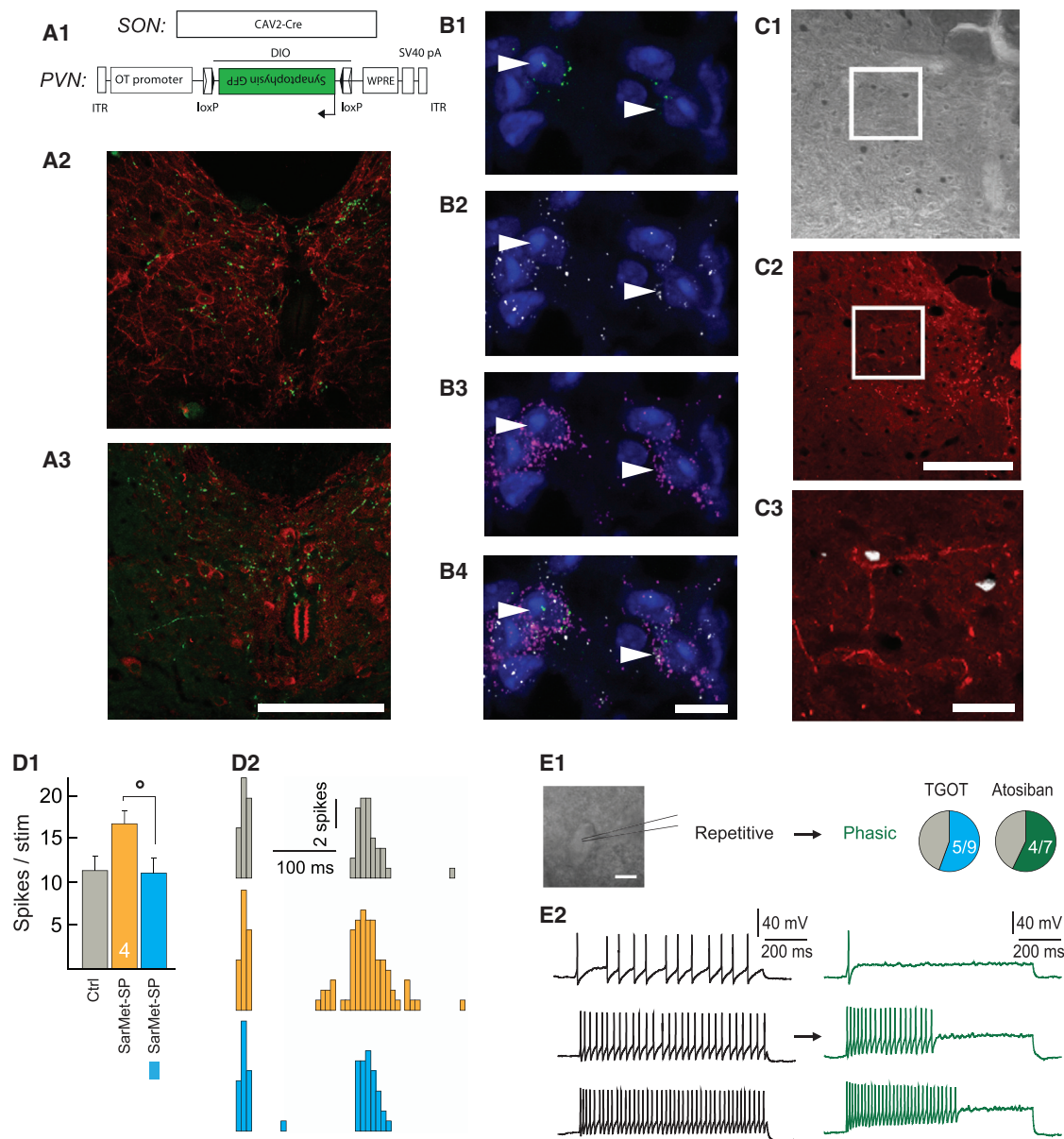
ParvOT Neurons Innervating MagnOT Neurons Also Project Specifically to NK1R/OTR Positive WDR Neurons in the Deep Layers of the SC

The above established exclusive labeling of parvOT neurons and all their processes using a combination of CAV2-Cre with OT cell typed-specific Cre-dependent rAAV (Figures 3A1–3A3) allowed us to follow projections of this OT cell population up to the distal (L5) segments of the SC. After labeling presumably all PVN OT neurons, axons can be visualized in both superficial and deep

Figure 3. ParvOT Neurons Project to SC and Innervate NK1R/OTR WDR Neurons in Deep Laminae

(A) ParvOT projections to the SC.

(A1) Scheme of the viruses injected into the SON and PVN.

(A2) Detection of synaptophysin-GFP containing terminals (green) in close proximity to NK1R-positive neurons (red) in SC deep laminae.

(A3) Synaptophysin-GFP terminals locate close to OTR-positive neurons of deep laminae. The scale bars represents 500 μm in (A2) and 500 μm in (A3).

(B–B4) Colocalization of NK1R and OTR mRNAs in the same neurons of SC deep laminae. Immunofluorescent in situ hybridization revealed the presence of OTR mRNA (green dots; B1 and B4) and NK1R mRNA (white dots; B2 and B4) in the same neurons, which were visualized by detection of vGlut1/2/3 mRNAs in their somas (pink/violet dots; B3 and B4). The nuclei of cells were stained by DAPI. The arrow heads point NK1R/OTR double positive neurons. The scale bars represent 10 μm.

(C–C3) NK1R-positive SC neurons start to express c-Fos after intraplantar injection of capsaicin in the hindpaw. The c-Fos signal (DAB) was detected in deep laminae of SC (C1), where the NK1R (red) were located (C2). The digital overlay of the two signals demonstrates localization of c-Fos in the NK1R-postive neuron (C3). The scale bars represent 500 μm in (C1) and (C2) and 50 μm in (C3).

(D) WDR C-fiber evoked spikes in response to a series of isolated hindpaw stimulations in control condition (Ctrl), during application of the specific agonist of NK1R SarMet-SP (orange), and during SarMet-SP paired with BL (blue).

(D1) Average of C-fiber evoked spikes (n = 5).

(D2) Representative traces.

(E) Discharge profile of putative WDR recorded in current clamp applying a protocol of depolarizing current injections before (black) and after bath application of 1 μM TGOT (blue, n = 9) or 1 μM Atosiban (green, n = 7).

CellPress
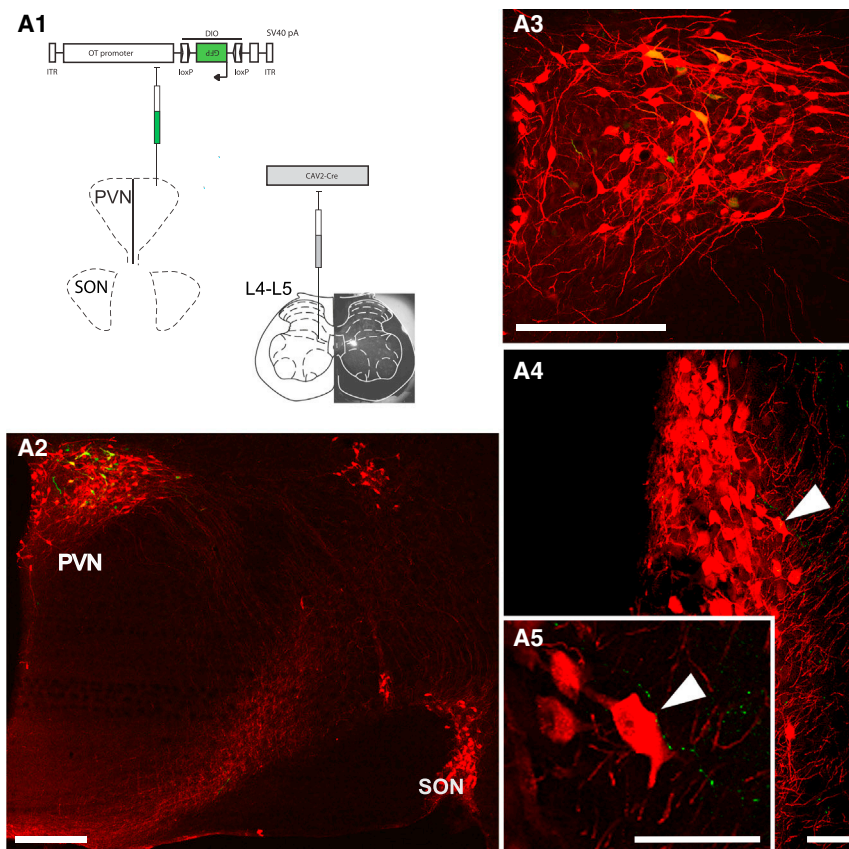
Figure 4. ParvOT-MagnOT-SC Anatomical Unit

(A) Scheme of viruses injected into the SC and PVN. The actual SC injection site (fluorescent latex bead accumulation) is shown as an insert underlying SC drawing.

(A2–A5) PVN parvocellular cells back-labeled from SC (green). The GFP-positive cell bodies were found in the caudal portion of the PVN and always colocalized OT (red) (A3, magnification from A2). Fibers, projecting from back-labeled PVN OT neurons to SON (arrow in A4, more caudal to A2) GFP-expressing varicouse axons in close proximity to cell bodies and dendrites of SON magnoOT neurons (high magnification in A5) are shown. The scale bars represent 500 μm in (A2) and (A3) and 75 μm in (A4) and (A5).

Putative WDR neurons, identified by their large cell body and repetitive firing related to stimulation intensities (Figure 3E; Ritz and Greenspan, 1985), were located around the central canal (cc) and in deep layers V–VI. As expected, [Thr4,Gly7]-OT (TGOT) was able to change the firing properties of these neurons, from repetitive to phasic in 5/9 of recorded cells (Figure 3E), similar to what was described in superficial layers (Breton et al., 2009). Importantly, the application of a specific biased agonist for OTR linked to G_i subunit, Atosiban (Busnelli et al., 2012), induced the exact same effects in 4/7 recorded cells (Figure 3E). This experiment demonstrates for the first time on living tissue that OTR can functionally bind a G_i protein, thus elucidating the inhibitory mechanism of OT on the firing properties of WDR neurons.

Finally, to demonstrate that the population of identified parvOT neurons is a single anatomical unit and that the same cells project collaterals to both the SON and SC, we injected a CAV2-Cre virus in deep laminae of L5 and Cre-responder AAV expressing GFP under the OT promoter in the PVN (Figure 4A1). We detected back-labeled cell bodies of GFP/OT neurons in the PVN and their axonal projections in close proximity to somas and dendrites of magnOT neurons of the SON (Figures 4A2–4A5).

ParvOT Neurons Projecting to MagnOT SON Neurons and NK1R/OTR Positive WDR Neurons in Deep Layers of the SC Control the Central Nociceptive Processing

To test whether the specific population of PVN-OT neurons projecting to both the SON and SC indeed acts on nociceptive input, we recorded SC neuronal responses in vivo during electrical stimulation of their hindpaw receptive field. The coding

be activated by sensory/pain stimulation. Bilateral injection of capsaicin in the hindpaws indeed induced c-Fos expression in large NK1R neurons (Figures 3C1–3C3). Furthermore, back-labeled parvOT neurons were also activated by capsaicin (data not shown).

To show that NK1R WDR neurons are functionally modulated by both NK1R specific agonist (SarMet-SP) and parvOT-deriving OT, we measured in vivo the WDR C-fiber evoked spikes in response to a series of isolated hindpaw stimulations. We found that the C-fiber evoked spikes were increased in the presence of SarMet-SP, as expected (Budai and Larson, 1996). Interestingly, BL-activation of ChR2 expressing parvOT fibers in the SC (SC-BL; schemes in Figures 5A and 5B) upon SarMet-SP significantly reduced the number of C-fiber evoked spikes from 16.8 ± 1.1 to 11.2 ± 1.5 (Figures 3D1 and 3D2). These findings show that release of OT from parvOT axons can effectively inhibit the activity of WDR neurons potentiated by NK1R activation.

Then, we analyzed the inhibitory effect of OT on WDR neuron firing properties. To do so, we performed in vitro whole-cell patch clamp recordings in current clamp applying a protocol of depolarizing current injections (Figure 3E; Breton et al., 2009).

(E1) Proportion of putative WDR neurons discharge pattern changed from repetitive to phasic after TGOT or Atosiban bath application.

(E2) Example response of putative WDR neuron to 20 pA (top), 40 pA (middle), and 60 pA (bottom) current injection before (black) and after (green) Atosiban bath application. The scale bar represents in (E1) 30 μm. All results are expressed as average ± SEM. The statistical significance: ° $p < 0.05$, Friedman's test followed by Dunn post hoc test.
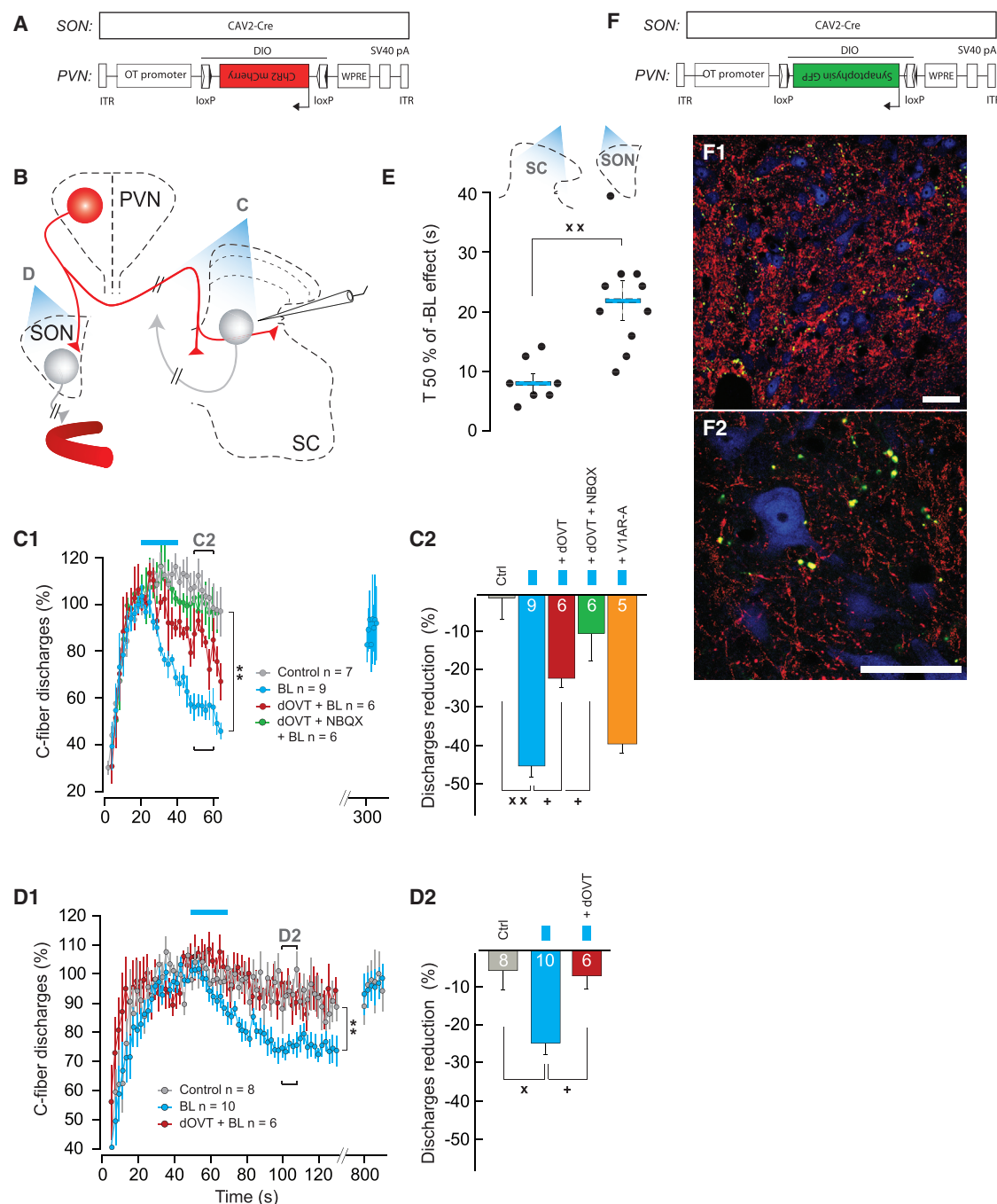
Figure 5. Stimulation of ParvOT PVN Axons in SON and SC Modulates Responses of WDR Neurons

(A) Viruses injected into the SON and PVN.

(B) Scheme of the experimental procedures.

(C) Effect of SC-BL on WDR-C discharges.

(C1) Time course of WDR-C in control condition (n = 7), when shining SC-BL alone (n = 9), after local dOVT application (n = 6), or local dOVT + NBQX application (n = 6).

(C2) Average discharge reduction of WDR-C on Ctrl (n = 7), when shining SC-BL alone (n = 9), after local dOVT application (n = 6), local dOVT + NBQX application (n = 6), or local V1AR-A application (n = 5). The statistical significance of drug modulation of the SON-BL effect was assessed by comparing the effect of SON-BL on the same neuron before and after drug injection.

(D) Effect of SON-BL on WDR-discharges.

(D1) Time course of WDR-C in control condition (n = 8), measured 30 s after shining SON-BL (as indicated in C1) alone (n = 10), or after systemic dOVT systemic injection (n = 6).

(legend continued on next page)

CellPress

properties and short-term potentiation (wind-up; WU) following repetitive receptive field stimulation were calculated from the response of WDR neurons in deep laminae. Recordings include the deep laminae, which integrate convergent peripheral sensory information from fast-conducting (A-type) and slow-conducting (C-type) primary afferent fibers (Figures 5 and S6).

We first tested the inhibitory action of OT released from parvOT-hypothalamo-spinal terminals by shining BL directly onto the dorsal surface of the SC (SC-BL). In this set of experiments, we used the same combination of viruses (CAV2-Cre and rAAV carrying OT promoter-DIO-ChR2-mCherry) to elicit OT release from parvocellular PVN fibers. SC-BL efficiently reduced the WDR discharges from C- ($-44.6\% \pm 3.7\%$; Figures 5C1 and 5C2) and Aδ- ($-36.3\% \pm 4.5\%$), but not from Aβ- fibers ($-0.3\% \pm 2.8\%$; Figure S6G2). The half-efficacy of SC-BL inhibition was 8.3 ± 1.3 s (Figure 5E). The WU returned to control values $\sim$300 s after SC-BL (Figure 5C1). SC-BL had no effect on superficial layer neuron activity in the same recording condition as for WDR neurons (Figure S6F). The OTR antagonist dOVT, directly applied to the surface of the SC, significantly, but not entirely, reduced Aδ- and C-fiber mediated discharges (Figures 5C1 and 5C2). In contrast, the VP receptor type 1A antagonist applied on SC failed to change the SC-BL inhibition of WU intensity (Figure 5C2), whereas it could efficiently block the effect of exogenously applied AVP (data not shown). Since VGluT2 was detected in synaptophysin-GFP-containing (Figures 5F1 and 5F2; overlap of GFP and vGluT2 signals was found in 89% $\pm$ 7.4% GFP terminals) axonal terminals of parvOT neurons near cell bodies of WDR-like neurons (Figure 5F2), we assessed the effect of NBQX in vivo. Coapplication of both dOVT and NBQX entirely blocked the SC-BL effects (Figures 5C1 and 5C2). Thus, stimulation of parvOT axons in SC deep layers leads to a fast, short-lasting decrease in nociceptive processing which is mediated by central OTR, and to a lesser extent by ionotropic Glut receptors.

We then assessed the efficiency of OT release from parvOT neurons onto magnOT SON neurons in modulating nociception (Figures 5B and S6A). Eliciting OT release from parvOT fibers in SON by BL (SON-BL) significantly reduced the WDR discharges evoked by slow-conducting C-type fibers ($-24.9\% \pm 3.1\%$; Figures 5D1 and 5D2) and fast-conducting fibers Aδ- ($-30.0\% \pm 6.8\%$), but not by non-nociceptive, fast-conducting Aβ- fibers ($-6.4\% \pm 3.5\%$; Figure S6G1). The half-efficacy of SON-BL induced inhibition of WU was 22.2 ± 3 s (T 50%; Figure 5E), a value which was significantly higher than the SON-BL effect (Figure 5E). The WU intensity returned to control values only 800 s after SON-BL (Figure 5D1). Moreover, to further confirm that the reduction in

WU intensity was related to the elevated level of blood OT (see Figure 1E), we injected the OTR antagonist dOVT intravenously before applying SON-BL. As expected, this abolished the SON-BL inhibition of WDR discharges that were evoked by both Aδ- and C-fibers (Figures 5D1, 5D2, and S6G1). Thus, the central release of OT from parvOT axons targeting magnOT SON neurons leads to a systemic release of OT, which reduces nociceptive processing by WDR neurons. This effect was slow to appear and long-lasting.

In summary, the subpopulation of PVN OT parvOT neurons projecting both to magnOT SON neurons and to NK1R/OTR WDR neurons from deep layers of SC exerts an inhibition of spinal nociceptive processing by fast action on SC neurons and a relatively slower effect on peripheral targets by stimulation of SON neurons and subsequent induction of OT release into blood.

Activation of ParvOT Neurons Results in Analgesia

In the last part of our work, we analyzed the functional importance of these parvOT neurons in the processing of inflammatory compared to nerve injury-induced neuropathic pain. To this purpose, we measured both the effects of stimulation or inhibition of parvOT neurons on the symptoms of either a peripheral painful inflammatory sensitization triggered by a single unilateral intraplantar injection of complete Freund adjuvant (CFA) or a nerve injury-induced neuropathy induced by the cuffing of the sciatic nerve (Cuff; Pitcher et al., 1999; Figure S7C1). To this purpose, we used rats that expressed either ChR2 or hM4Di (Zhu and Roth, 2014) restricted to parvOT PVN neurons synapsing on magnOT SON neurons (Figure 6A). The efficiency of ChR2-mediated activation and hM4Di-mediated inhibition of OT neurons was assessed respectively by targeting unilaterally the PVN by BL or by i.p. administration of CNO and was confirmed both in vitro (Figures S7A1 and S7A2) and in vivo (Figures S7B1–S7B4).

PVN-BL stimulation significantly, but not entirely, alleviated the CFA-mediated hyperalgesia by raising the threshold of response to both the mechanical (from 56.7 ± 7.6 g to 116.6 ± 16.4 g) and thermal hot stimulation (from 2.8 ± 0.2 to 4.8 ± 0.7 s; Figures 6C1 and 6C2). In contrast, PVN-BL failed to mitigate the mechanical hyperalgesia measured in condition of the Cuff peripheral neuropathy (Figures S7B2 and S7B3). Furthermore, return of the pain symptoms occurred after PVN-BL was fully blocked by i.p. injection of the blood brain barrier (BBB)-permeable OTR antagonist L-368,899 (Figures 6C1 and 6C2).

Conversely, CNO-induced inhibition of parvOT neurons significantly increased the CFA-mediated hyperalgesia by lowering

---

(D2) Average discharge reduction of WDR-C on Ctrl (n = 8), when shining SON-BL alone (n = 10), or after systemic dOVT injection (n = 6). The statistical significance of dOVT modulation of the SON-BL effect was assessed by comparing the effect of SON-BL on the same neuron before and after dOVT injection (n = 6).
(E) Comparison between individual (black dots) and average T 50% (blue bar) effect of SON-BL (n = 10) and SC-BL (n = 7) on recorded WDR.
(F) Viruses injected into the SON and PVN.
(F1 and F2) Axonal terminals containing synaptophysin-GFP fusion protein in proximity to SC L5 neurons.
(F1) Overview of fiber distribution within SC: VGluT2 (red), synaptophysin-GFP (green), and NeuN (blue).
(F2) A zoom-in shows the green signal (green) largely overlaps with the VGluT2 signal (red) in terminals surrounding cell bodies. The scale bars represent 50 μm in (F1) and (F2). All results are expressed as average $\pm$ SEM. The statistical significance: $^\circ$p < 0.05, Friedman with Dunn post hoc test; + p < 0.05, ++ p < 0.01, and Wilcoxon's test; xx p < 0.01 and Kruskal and Wallis test; and ** p < 0.01 BL versus Control, two-way ANOVA.
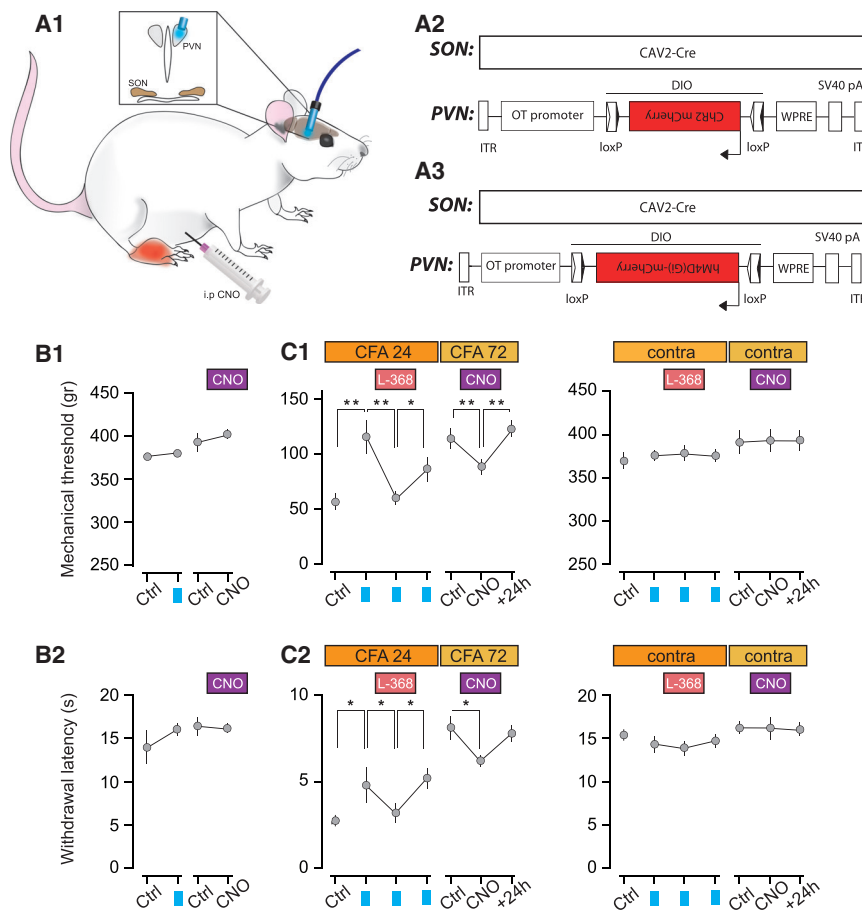
Figure 6. Activation/Inhibition of ParvOT PVN Neurons Modulates Mechanical Threshold and Thermal Hot Latency in Animals Subjected to Complete Adjuvant Injection

(A–A3) Scheme of the experimental procedure. The CAV2-Cre was injected in the SON and Cre-responding virus driving either (A2) ChR2 or (A3) hM4Di to achieve the expression of respective proteins in OT neurons of the PVN.

(B–B2) Mechanical thresholds and (B2) thermal hot latencies of naive animals before and after PVN-BL (ChR2, n = 6 and CNO, n = 10).

(C–C2) Mechanical thresholds and (C2) thermal hot latencies of the CFA-injected hindpaw (left graphs) and the contralateral hindpaw (right graphs). The effect of PVN-BL was assessed before, right after i.p. injection of OTR antagonist L-368,899 (1 mg/kg), and after its washout (n = 6). The effect of CNO (3 mg/kg) was measured 1 hr after i.p. injection and its 24 hr washout (n = 10). All results are expressed as average ± SEM. The statistical significance: * p < 0.05, ** p < 0.01, and one-way ANOVA followed by Tukey's multiple comparison post hoc test.

OTR-positive WDR neurons in the deep layers of the SC. Functionally, we demonstrated that this network can inhibit spinal pain processing in a dual manner with two distinct time courses. Thus, nociceptive transmission from Aδ- and C-type primary afferents to WDR neurons is efficiently repressed by OT release from parvOT in the deep layers of the SC and from SON magnOT in the blood. Release in the SC is directly triggered from parvOT-spinal projections and follows a fast mode of action; release in the blood is indirectly triggered from SON magnOT neurons that are activated by parvOT projections and follows a slower time course. The functional role of this subpopulation of parvOT neurons was further confirmed in two rat models of peripheral painful sensitization, indicating that activation of parvOT neurons can decrease mechanical and thermal sensitivities in inflammatory, but not nerve injury-induced neuropathic pain.

Synaptic Crosstalk between OT Neurons

The question of how OT neurons in different nuclei within the hypothalamus interact with each other is a recurrent theme in past literature, but has not been elucidated experimentally. Belin and colleagues recorded pairs of OT neurons from SON and PVN and proposed an internuclear connection serving as a basis for synchronous firing during lactation (Belin et al., 1984, Belin and Moos, 1986). The hypothesis of an OT-mediated communication was stated already in the early 80's (Silverman et al., 1981), following observations that application of OT (or dOVT) into the third ventricle or in the SON synchronized (respectively, de-synchronized) activity of OT neurons in PVN and SON (Freund-Mercier and Richard, 1984; Lambert et al., 1993). Furthermore,

the threshold of response to both the mechanical (from 115 ± 12.1 g to 88 ± 9.8 g) and thermal hot stimulation (from 8.1 ± 0.9 s to 6.3 ± 0.3 s; Figures 6C1 and 6C2). CNO had no effect in rats with the Cuff (Figures S7C2 and S7C3). These results from gain- and loss-of-function approaches highlight the role of parvOT control of peripheral painful sensitization, supported by our in vivo electrophysiological data.

In the course of our study, we observed that both PVN-BL and CNO failed to modify mechanical and thermal hot sensitivity in the absence of any peripheral sensitization, for example, in the contralateral paw or in naive animals (Figures 6B1, 6B2, 6C1, 6C2, S7C2, and S7C3).

Taken together, these findings provide evidence that 30 parvOT neurons are able to strongly promote analgesia in a pathological condition of inflammatory, but not nerve injury-induced neuropathic pain, presumably by both central (SC-mediated) and peripheral (SON-mediated) mechanisms.

DISCUSSION

Here, we identified, by a combination of latest state of the art viral-vector based (Grinevich et al., 2016a), anatomical, optogenetic, electrophysiological, and behavioral approaches, a small (n ~30) subpopulation of parvOT neurons in the PVN, which projects to magnOT neurons in the SON and to NK1R or

the presence of synapses containing OT-immunoreactivity was demonstrated in the SON (Theodosis, 1985). Although we did not examine internuclear connectivity that underlies synchronized burst firing, our anatomical and functional data demonstrate that PVN-SON interconnectivity plays an important role in inhibiting spinal nociceptive processing and alleviation of inflammatory pain.

In an early study, lesion of the SON did not cause any loss of magnOT neurons in the PVN (Olivecrona, 1957), providing a first indication that parvOT PVN neurons might be at the basis of internuclear connection to the SON. However, as of today, the parvOT neurons in the PVN have remained much less studied than the magnOT neurons, mostly because of technical difficulties, specifically in labeling and modulating the activity of parvOT neurons. To our knowledge, the possibility to study a direct parvOT innervation of the SON by retrograde tracing techniques has seldom been discussed (e.g., Lambert et al., 1993) and any potentially involved parvocellular neurons have never been identified.

At the SON level, Bruni and Perumal (1984) have described an extensive network of small-diameter, beaded, unmyelinated fibers with no particular organizational pattern and of unknown origin that establishes functional axo-somatic and axo-dendritic contacts with magnOT neurons. At 30 years later, we reveal here a monosynaptic connection between parvOT PVN and magnOT SON neurons as respective pre- and postsynaptic components. The detection of a postsynaptic SON component was further confirmed by their stimulation through application of CCK (Renaud et al., 1987) and an increase in peripheral OT levels.

In contrast to the OT system, direct connectivity between VP-ergic neurons in rats has not been convincingly demonstrated and, accordingly, we were unable to find VP/Venus positive fibers descending the PVN in the SON and vice versa.

ParvOT Neurons Modulate NK1R Positive WDR Neurons

In addition to the control of magnOT activity, this newly described subpopulation of parvOT neurons densely projects exclusively to the deep layers (V, VI, and X) of the SC. Axonal terminals from parvOT were found in close appositions with NK1R positive WDR neurons, some of which are likely OTR-positives. However, we are not excluding projections of these parvOT neurons to non-WDR deep neurons. Nevertheless, their functional and selective inhibition of C- and Aδ- mediated discharges in WDR suggest that nociceptive C-fiber project to deep layers, accordingly with models of dorsal horn circuits that include projections to the lamina V (Cervero and Connell, 1984; Ribeiro-da-Silva and De Koninck, 2008). Functionally, this fits with our results suggesting that OT modulates the excitability of WDR shown as an inhibition of discharges mediated by fibers containing substance P.

ParvOT Neurons Coordinate Neuroendocrine and Hardwired Inhibitory Pain Control

In accordance with our anatomical data, WDR action potential discharges in response to noxious peripheral stimulation are reduced by optogenetic manipulation of the subpopulation of OT neurons in the PVN and its subsequent stimulation at the level of the SON. This reduction was selective to sensory information transmitted by Aδ- and C-fibers, which are, in their majority, nociceptive-specific.

Regarding peripherally mediated OT effects, it has recently been shown that OTR could be expressed by non-peptidergic C-type sensory neurons in DRG (Moreno-López et al., 2013) and the in vitro application of OT suppresses their activity (Gong et al., 2015). Furthermore, intravenous administration of a selective OTR agonist induces an inhibition of discharges mediated by nociceptive-specific primary afferents (Juif et al., 2013). Our present work provides an additional support for this idea by selectively activating a circuit leading to release of OT to the blood (Figure 7). The effect was fully peripheral, since inhibition of nociceptive messages was completely abolished by the addition of the OTR selective antagonist dOVT in the blood flow.

Identification of a subpopulation of parvOT neurons projecting collaterals to both the SON and deep layers of the SC gave rise to the idea that these neurons may exert both a peripheral and central control by OT which we found to take place with a dual time course. This was confirmed by optogenetically stimulating parvOT PVN axons located either in the SON or in the SC. This stimulation led to a reduction of WDR discharges in response to a peripheral noxious stimulation, which was selective for Aδ- and C-type nociceptive fibers. The effects in deep layers of the SC seemed to be mediated by the OTR, as we did not find any effects of VP V1a receptor similar to what has been reported (Qiu et al., 2014). As OT terminals on WDR-like neurons contained VGluT2, we assessed glutamate (Glu) and OT contribution to the SC-BL effect on WU intensity. This revealed that both OT and Glu participated to the inhibition of WU. These results are in accordance with our in vitro patch-clamp experiment and can be interpreted by a network effect as OT axons are likely to form en passant synapses (Knobloch et al., 2012), allowing local (micro)volume-transmission from release sites (Knobloch and Grinevich, 2014; Grinevich et al., 2016b). The combination of two processes can then explain the observed effects: (1) OT acts on OTR in WDR neurons to inhibit them via G_i intracellular pathway (Figure 3E) and (2) coreleased Glu either activates local GABA-interneurons in layers V–VI and around the cc (Schneider and Lopez, 2002; Deuchars et al., 2005), which, in turn, inhibits WDR neurons, or binds a mGluR leading to the direct inhibition of WDR neurons by a $G_{i/o}$ pathway (Gerber et al., 2000; Niswender and Conn, 2010).

Surprisingly, evoked spinal OT release by this subpopulation of parvOT did not modify nociceptive processing by neurons in superficial layers. This suggested that the OT inhibition of WDR firing was not induced by OTR activation in superficial layers, but only in deep dorsal horn layers. This was in agreement with our anatomical data describing the vast majority of parvOT neurons projecting to the deep layers. We failed to reveal any functional contribution of this subpopulation of parvOT projecting to SON and SC in a nerve-induced neuropathic pain, which may be modulated by OT projections to superficial layers of the dorsal horn. In contrast, they exerted a tonic inhibitory control on WU and pain symptoms in the peripheral inflammation. We speculate that the inflammatory component in pain state
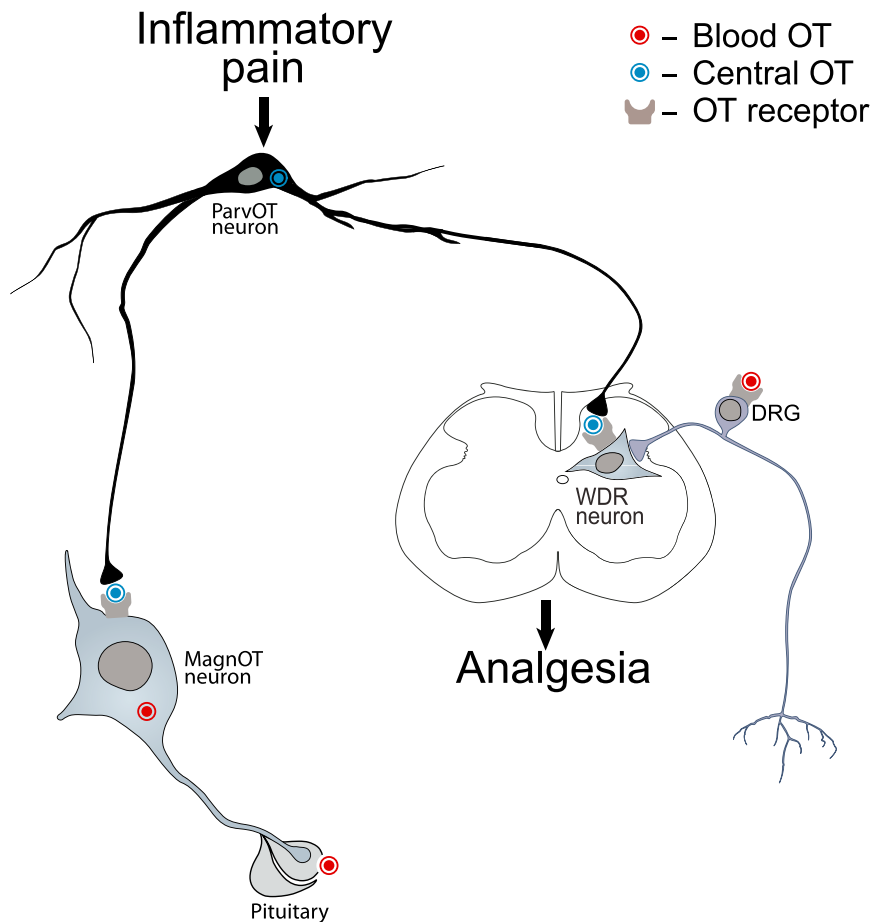
CellPress

Figure 7. The Role of the Novel Type of ParvOT Neurons in Coordinating Central and Peripheral OT Release to Promote Analgesia

We hypothesize that pain stimulates the identified subset of parvOT PVN neurons, which simultaneously release OT in the SON and SC, exerting respectively delayed and longer lasting and immediate and shorter lasting analgesia. The peripheral analgesic effect of OT is likely mediated by its action on BBB-free sensory neurons of the DRG.

of OT neurons, which coordinate central and peripheral inhibition of nociception and pain perception, and hence, play a role in promoting analgesia (Figure 7).

EXPERIMENTAL PROCEDURES

Animals

Anatomical, electrophysiological, optogenetic, and behavioral studies were performed with Wistar rats (for details of the experiment see the respective figure legend). If not mentioned, rats were housed under standard conditions with food and water available ad libitum. All experiments were conducted under licenses and in accordance with EU regulations.

Viruses

rAAVs (serotype 1/2) carrying conserved regions of OT and VP promoters and genes of interest in direct or "floxed" orientations were cloned and produced as reported previously (Knobloch et al., 2012). CAV2 equipped with GFP or Cre recombinase was purchased from the Institute of Molecular Genetics in Montpellier CNRS, France (Bru et al., 2010)

Neuroanatomy

To trace internuclear connections, rAAVs expressing Venus were injected into the PVN or SON to follow their axonal projections within the hypothalamus. Alternatively, CAV2-Cre was injected into the SON, while Cre-dependent floxed rAAV was injected into the PVN to identify OT PVN neurons synapsing onto SON neurons.

To trace hypothalamus-SC connections, a CAV2-Cre virus was injected into the SON and floxed rAAV, into the PVN or CAV2-Cre virus was injected in the SC, while Cre-dependent rAAV, into the PVN. This allowed us to visualize OT axon pattern in the SC and to identify projecting PVN OT neurons, respectively. After transcardial perfusion with 4% paraformaldehyde (PFA), brains and/or SC were sectioned and stained with antibodies against OT, VP, vGluT2, GFP, NeuN, NK1R, and OTR. Images for qualitative and quantitative analyses were taken on confocal microscopes Leica SP2 and SP5.

Electrophysiology Experiments

For in vitro patch-clamp recordings, 4 to 8 weeks after injection of virus in adult rats, brains were removed, the hypothalamus or lumbar SC was isolated, cut into 400 μm coronal slices, and kept in artificial cerebrospinal fluid (ACSF: 118 mM NaCl, 25 mM NaHCO3, 10 mM glucose, 2 mM KCl, 2 mM MgCl2*6H2O, 2 mM CaCl2*2H2O, and 1.2 mM NaH2PO4) saturated 95% dioxygen (O2), 5% carbon dioxide (CO2). Visualized neurons were patched with borosilicate glass pipette (4–9 MΩ) filled with 140 mM KMeSO4, 10 mM HEPES, 2 mM MgCl2, 0.1 mM CaCl2, 0.1 mM (1,2-bis(o-aminophenoxy)

regulates the excitability of this subset of parvOT neurons, as observed by c-Fos induction in parvOT neurons (data not shown). Our results indicate that the described subpopulation of parvOT neurons specifically targets NK1R and OTR positive neurons located in the deep layers of the SC to exert antinociceptive action on WDR to promote analgesia.

Described ParvOT Neurons as a New OT-Ergic Cell Type

Following pioneering works of Swanson and Kuypers (1980), Sawchenko and Swanson (1982), and Swanson and Sawchenko (1983), parvOT neurons have been considered as heterogeneous cell populations with descending projections to brainstem and/or SC regions. However, in the present study, we found a small group of parvOT neurons that forms a pathway distinct from the classical hypothalamo-neurohypophyseal axonal tract through the hypothalamus. Although we did not analyze in detail axonal collaterals of these parvOT cells in other forebrain regions, their existence in the hypothalamus adds a new feature to parvOT cells. In addition, these neurons simultaneously project collaterals to deep layers of the SC, representing a unique group of specifically located cells, which is likely distinct from the OT-immunoreactive neurons described by Jójárt et al. (2009) that massively project axons to the superficial layers of the SC. Based on the unique connectivity of the identified parvOT neurons, we speculate that they represent a new type

CellPress

ethane-N,N,N',N'-tetraacetic acid) (BAPTA), 2 mM ATP Na salt, and 0.3 mM guanosine triphosphate (GTP) Na salt (pH 7.3), adjusted to 300 mOsm, and voltage-clamped at −60 mV.

For in vivo extracellular recordings, 4 to 8 weeks after injection of virus, adult animals were anaesthetized with 4% isoflurane and placed in stereotaxic frame. Extracellular neuronal activity was recorded using a stainless electrode with 10 MΩ impedance (FHC; UE(FK1)).

Behavioral Experiments
Mechanical allodynia was measured using a calibrated forceps (Bioseb). Thermal allodynia/hyperalgesia was measured using the Plantar test using Hargeaves method (Ugo Basile). Peripheral painful inflammatory sensitization was obtained by a single unilateral intraplantar injection of CFA (Sigma-Aldrich, 100 µl in the right paw). Nerve injury-induced neuropathy was induced using the cuffing method.

SUPPLEMENTAL INFORMATION

Supplemental Information includes Supplemental Experimental Procedures, seven figures, and four tables and can be found with this article online at http://dx.doi.org/10.1016/j.neuron.2016.01.041.

REFERENCES

Armstrong, W.E., Warach, S., Hatton, G.I., and McNeill, T.H. (1980). Subnuclei in the rat hypothalamic paraventricular nucleus: a cytoarchitectural, horseradish peroxidase and immunocytochemical analysis. Neuroscience 5, 1931–1958.

Atasoy, D., Betley, J.N., Su, H.H., and Sternson, S.M. (2012). Deconstruction of a neural circuit for hunger. Nature 488, 172–177.

Bargmann, W., and Scharrer, E. (1951). The site of origin of the hormones of the posterior pituitary. Am. Sci. 39, 255–259.

Belin, V., and Moos, F. (1986). Paired recordings from supraoptic and paraventricular oxytocin cells in suckled rats: recruitment and synchronization. J. Physiol. 377, 369–390.

Belin, V., Moos, F., and Richard, P. (1984). Synchronization of oxytocin cells in the hypothalamic paraventricular and supraoptic nuclei in suckled rats: direct proof with paired extracellular recordings. Exp. Brain Res. 57, 201–203.

Breton, J.D., Poisbeau, P., and Darbon, P. (2009). Antinociceptive action of oxytocin involves inhibition of potassium channel currents in lamina II neurons of the rat spinal cord. Mol. Pain 5, 63.

Bru, T., Salinas, S., and Kremer, E.J. (2010). An update on canine adenovirus type 2 and its vectors. Viruses 2, 2134–2153.

Bruni, J.E., and Perumal, P.M. (1984). Cytoarchitecture of the rat's supraoptic nucleus. Anat. Embryol. (Berl.) 170, 129–138.

Budai, D., and Larson, A.A. (1996). Role of substance P in the modulation of C-fiber-evoked responses of spinal dorsal horn neurons. Brain Res. 710, 197–203.

Busnelli, M., Saulière, A., Manning, M., Bouvier, M., Galés, C., and Chini, B. (2012). Functional selective oxytocin-derived agonists discriminate between individual G protein family subtypes. J. Biol. Chem. 287, 3617–3629.

Cervero, F., and Connell, L.A. (1984). Distribution of somatic and visceral primary afferent fibres within the thoracic spinal cord of the cat. J. Comp. Neurol. 20, 88–98.

Condés-Lara, M., González, N.M., Martínez-Lorenzana, G., Delgado, O.L., and Freund-Mercier, M.J. (2003). Actions of oxytocin and interactions with glutamate on spontaneous and evoked dorsal spinal cord neuronal activities. Brain Res. 976, 75–81.

Cunningham, E.T., Jr., and Sawchenko, P.E. (1988). Anatomical specificity of noradrenergic inputs to the paraventricular and supraoptic nuclei of the rat hypothalamus. J. Comp. Neurol. 274, 60–76.

Deuchars, S.A., Milligan, C.J., Stornetta, R.L., and Deuchars, J. (2005). GABAergic neurons in the central region of the spinal cord: a novel substrate for sympathetic inhibition. J. Neurosci. 25, 1063–1070.

Dölen, G., Darvishzadeh, A., Huang, K.W., and Malenka, R.C. (2013). Social reward requires coordinated activity of nucleus accumbens oxytocin and serotonin. Nature 501, 179–184.

Freund-Mercier, M.J., and Richard, P. (1984). Electrophysiological evidence for facilitatory control of oxytocin neurones by oxytocin during suckling in the rat. J. Physiol. 352, 447–466.

Gerber, G., Zhong, J., Youn, D., and Randic, M. (2000). Group II and group III metabotropic glutamate receptor agonists depress synaptic transmission in the rat spinal cord dorsal horn. Neuroscience 100, 393–406.

Gong, L., Gao, F., Li, J., Li, J., Yu, X., Ma, X., Zheng, W., Cui, S., Liu, K., Zhang, M., et al. (2015). Oxytocin-induced membrane hyperpolarization in pain-sensitive dorsal root ganglia neurons mediated by Ca(2+)/nNOS/NO/KATP pathway. Neuroscience 289, 417–428.

González-Hernández, A., Rojas-Piloni, G., and Condés-Lara, M. (2014). Oxytocin and analgesia: future trends. Trends Pharmacol. Sci. 35, 549–551.

Grinevich, V., Knobloch, H.S., Roth, L.C., Althammer, F., Domansky, A., Vinnikov, I., Stanifer, M., and Boulant, S. (2016a). Somatic transgenesis (Viral vectors). In Molecular Neuroendocrinology: From Genome to Physiology, First Edition, D. Murphy and H. Gainer, eds. (John Wiley & Sons), pp. 243–274.

Grinevich, V., Knobloch-Bollmann, H.S., Eliava, M., Busnelli, M., and Chini, B. (2016b). Assembling the puzzle: Pathways of oxytocin signaling in the brain. Biol. Psychiatry 79, 155–164.

Jójárt, J., Jójárt, I., Boda, K., Gálfi, M., Mihály, A., B-Baldauf, Z., and Vecsernyés, M. (2009). Distribution of oxytocin-immunoreactive neuronal elements in the rat spinal cord. Acta Biol. Hung. 60, 333–346.

Juif, P.E., and Poisbeau, P. (2013). Neurohormonal effects of oxytocin and vasopressin receptor agonists on spinal pain processing in male rats. Pain 154, 1449–1456.

Juif, P.E., Breton, J.D., Rajalu, M., Charlet, A., Goumon, Y., and Poisbeau, P. (2013). Long-lasting spinal oxytocin analgesia is ensured by the stimulation of allopregnanolone-like neurosteroid synthesis which potentiates GABAA receptor-mediated synaptic inhibition. J. Neurosci. 33, 16617–16626.

Katz, L.C., and Iarovici, D.M. (1990). Green fluorescent latex microspheres: a new retrograde tracer. Neuroscience 34, 511–520.

Knobloch, S., and Grinevich, V. (2014). Evolution of central oxytocin pathways in vertebrates. Front. Behav. Neurosci. 8, 31.

Knobloch, H.S., Charlet, A., Hoffmann, L.C., Eliava, M., Khrulev, S., Cetin, A.H., Osten, P., Schwarz, M.K., Seeburg, P.H., Stoop, R., and Grinevich, V. (2012). Evoked axonal oxytocin release in the central amygdala attenuates fear response. Neuron 73, 553–566.

Lambert, R.C., Moos, F.C., and Richard, P. (1993). Action of endogenous oxytocin within the paraventricular or supraoptic nuclei: a powerful link in the regulation of the bursting pattern of oxytocin neurons during the milk-ejection reflex in rats. Neuroscience 57, 1027–1038.

Lee, H.-J., Pagani, J., and Young, W.S., 3rd (2010). Using transgenic mouse models to study oxytocin's role in the facilitation of species propagation. Brain Res. 1364, 216–224.

Luther, J.A., Halmos, K.C., and Tasker, J.G. (2000). A slow transient potassium current expressed in a subset of neurosecretory neurons of the hypothalamic paraventricular nucleus. J. Neurophysiol. 84, 1814–1825.

Luther, J.A., Daftary, S.S., Boudaba, C., Gould, G.C., Halmos, K.C., and Tasker, J.G. (2002). Neurosecretory and non-neurosecretory parvocellular neurones of the hypothalamic paraventricular nucleus express distinct electrophysiological properties. J. Neuroendocrinol. 14, 929–932.

Mack, S.O., Kc, P., Wu, M., Coleman, B.R., Tolentino-Silva, F.P., and Haxhiu, M.A. (2002). Paraventricular oxytocin neurons are involved in neural modulation of breathing. J. Appl. Physiol. 92, 826–834.

Marlin, B.J., Mitre, M., D'amour, J.A., Chao, M.V., and Froemke, R.C. (2015). Oxytocin enables maternal behaviour by balancing cortical inhibition. Nature 520, 499–504.

Miselis, R.R. (1981). The efferent projections of the subfornical organ of the rat: a circumventricular organ within a neural network subserving water balance. Brain Res. 230, 1–23.

Moreno-López, Y., Martínez-Lorenzana, G., Condés-Lara, M., and Rojas-Piloni, G. (2013). Identification of oxytocin receptor in the dorsal horn and nociceptive dorsal root ganglion neurons. Neuropeptides 47, 117–123.

Nagel, G., Szellas, T., Huhn, W., Kateriya, S., Adeishvili, N., Berthold, P., Ollig, D., Hegemann, P., and Bamberg, E. (2003). Channelrhodopsin-2, a directly light-gated cation-selective membrane channel. Proc. Natl. Acad. Sci. USA 100, 13940–13945.

Niswender, C.M., and Conn, P.J. (2010). Metabotropic glutamate receptors: physiology, pharmacology, and disease. Annu. Rev. Pharmacol. Toxicol. 50, 295–322.

Olivecrona, H. (1957). Paraventricular nucleus and pituitary gland. Acta Physiol. Scand. Suppl. 40, 1–178.

Paxinos, G., and Watson, C. (1998). The Rat Brain in Stereotaxic Coordinates, Fourth Edition (Academic Press).

Petersson, M. (2002). Cardiovascular effects of oxytocin. Prog. Brain Res. 139, 281–288.

Pitcher, G.M., Ritchie, J., and Henry, J.L. (1999). Nerve constriction in the rat: model of neuropathic, surgical and central pain. Pain 83, 37–46.

Qiu, F., Qiu, C.Y., Cai, H., Liu, T.T., Qu, Z.W., Yang, Z., Li, J.D., Zhou, Q.Y., and Hu, W.P. (2014). Oxytocin inhibits the activity of acid-sensing ion channels through the vasopressin, V1A receptor in primary sensory neurons. Br. J. Pharmacol. 171, 3065–3076.

Renaud, L.P., Tang, M., McCann, M.J., Stricker, E.M., and Verbalis, J.G. (1987). Cholecystokinin and gastric distension activate oxytocinergic cells in rat hypothalamus. Am. J. Physiol. 253, R661–R665.

Ribeiro-da-Silva, A., and De Koninck, Y. (2008). Morphological and neurochemical organization of the spinal dorsal horn. In Science of Pain, A.I. Basbaum and M.C. Bushnell, eds. (Elsevier), pp. 279–310.

Ritz, L.A., and Greenspan, J.D. (1985). Morphological features of lamina V neurons receiving nociceptive input in cat sacrocaudal spinal cord. J. Comp. Neurol. 238, 440–452.

Ross, H.E., Cole, C.D., Smith, Y., Neumann, I.D., Landgraf, R., Murphy, A.Z., and Young, L.J. (2009). Characterization of the oxytocin system regulating affiliative behavior in female prairie voles. Neuroscience 162, 892–903.

Sawchenko, P.E., and Swanson, L.W. (1982). Immunohistochemical identification of neurons in the paraventricular nucleus of the hypothalamus that project to the medulla or to the spinal cord in the rat. J. Comp. Neurol. 205, 260–272.

Scharrer, E. (1928). Die Lichtempfindlichkeit blinder Elritzen (Untersuchungen über das Zwischenhirn der Fische). Z. Vgl. Physiol. 7, 1–38.

Scharrer, E., and Scharrer, B. (1940). Secretory cells within the hypothalamus. Res. Publ. Assoc. Res. Nerv. Ment. Dis. 20, 170–194.

Schneider, S.P., and Lopez, M. (2002). Immunocytochemical localization of glutamic acid decarboxylase in physiologically identified interneurons of hamster spinal laminae III-V. Neuroscience 115, 627–636.

Schwarz, L.A., Miyamichi, K., Gao, X.J., Beier, K.T., Weissbourd, B., DeLoach, K.E., Ren, J., Ibanes, S., Malenka, R.C., Kremer, E.J., and Luo, L. (2015). Viral-genetic tracing of the input-output organization of a central noradrenaline circuit. Nature 524, 88–92.

Silverman, A.J., Hoffman, D.L., and Zimmerman, E.A. (1981). The descending afferent connections of the paraventricular nucleus of the hypothalamus (PVN). Brain Res. Bull. 6, 47–61.

Sofroniew, M.V. (1983). Morphology of vasopressin and oxytocin neurones and their central and vascular projections. Prog. Brain Res. 60, 101–114.

Swanson, L.W., and McKellar, S. (1979). The distribution of oxytocin- and neurophysin-stained fibers in the spinal cord of the rat and monkey. J. Comp. Neurol. 188, 87–106.

Swanson, L.W., and Kuypers, H.G. (1980). The paraventricular nucleus of the hypothalamus: cytoarchitectonic subdivisions and organization of projections to the pituitary, dorsal vagal complex, and spinal cord as demonstrated by retrograde fluorescence double-labeling methods. J. Comp. Neurol. 194, 555–570.

Swanson, L.W., and Sawchenko, P.E. (1983). Hypothalamic integration: organization of the paraventricular and supraoptic nuclei. Annu. Rev. Neurosci. 6, 269–324.

Theodosis, D.T. (1985). Oxytocin-immunoreactive terminals synapse on oxytocin neurones in the supraoptic nucleus. Nature 313, 682–684.

Verbalis, J.G., McCann, M.J., McHale, C.M., and Stricker, E.M. (1986). Oxytocin secretion in response to cholecystokinin and food: differentiation of nausea from satiety. Science 232, 1417–1419.

Zhu, H., and Roth, B.L. (2014). Silencing synapses with DREADDs. Neuron 82, 723–725.

2 - A key role for amygdala astrocytes in regulation of negative affective processing by oxytocin

After decades of research mostly linking brain functions to neuro-neuronal networks, a paradigm shift is occurring in neurobiology hypothesising that the complex integration of astrocyte-neuron networks in the temporal and spatial domains is required. Same may hold true for the crucial adaptive functions of neuropeptidergic systems. Oxytocin, "the molecule of the decade", presently is the most popular neuropeptide controlling pro-social behaviors as well as modulating numerous functions including anxiety control, pain perception, energy balance and cardiovascular system. In two recent studies (Knobloch et al., 2012; Eliava et al., 2016), we demonstrated new pathway of oxytocin action in the brain via axonal oxytocin release and characterized a unique, small but crucial, oxytocin population in the control of pain. These are highly shared and already classical references in the literature. However, all modern studies ignore the potential action of oxytocin on glia, leaving here a large gap to shed light on.

In the present study **we probed the hypothesis that oxytocin may act on astrocytes in the central amygdala to modulate local network activity transmitted into changes of amygdala-dependent behaviors**. Using *ex vivo* patch-clamp and calcium imaging combined with selective optogenetic manipulation of oxytocinergic neurons or local astrocytes, we demonstrated that endogenous oxytocin reliably and directly induces long-lasting calcium oscillations in astrocytes. Strikingly, the oxytocinergic recruitment of astrocytes appears to be both necessary and sufficient to mediate the strong action of oxytocin on the neuronal network. We confirmed the pivotal role of astrocytes *in vivo* using a behavioral model of neuropathy-induced-anxiety. To the best of our knowledge, it is the first time a neuropeptide is shown to control the astro-neuronal network, leading to a complete control of a brain function. Illustrated in the amygdala, a well-studied structure, and for pain and anxiety, this mechanism may be much more general and be of interest for the vast majority of neuroscientists.

In brief, our study revealed four major new insights:
1. The oxytocin receptor is expressed not only in neurons, but also in astrocytes, as demonstrated in the central amygdala.
2. Oxytocin-mediated receptor activation directly drives the astrocyte activity.
3. Astrocytes are both sufficient and necessary to the oxytocin modulatory action on the central amygdala microcircuits.
4. The astrocyte-mediated activity of local network is transmitted into brain-region specific behavior.

In conclusion, here we provide the first anatomical, electrophysiological and behavioral evidence for functionally relevant oxytocin signaling in astrocytes (exemplarily shown within the central amygdala). Our findings significantly alter the traditional view on oxytocin signaling exclusively via neurons, and open perspectives for studying interactions between glia and neurons upon oxytocin action to modulate a wide array of behaviors ranging from aggression to empathy.

Title: A key role for amygdala astrocytes in regulation of negative affective processing by oxytocin.

Short Title: Oxytocin-sensitive astrocytes in affect regulation.

Authors: J. Wahis[1*], M. da Silva Gouveia[2*], B. Bellanger[1], M. Eliava[2], M. Abatis[3], B. Boury-Jamot[3], H. S. Knobloch-Bollmann[4], M. Pertin[5], B. Boutrel[3], C. M. Lamy[6], I. Décosterd[5,7], J. Y. Chatton[5], R. Stoop[3], P. Poisbeau[1], V. Grinevich[2,8], A.Charlet[1,9]

Affiliations:

[1] Centre National de la Recherche Scientifique, Institut National de la Santé et de la Recherche Médicale and University of Strasbourg, Institute of Cellular and Integrative Neurosciences, 5 rue Blaise Pascal, 67084, Strasbourg, France;

[2] Schaller Research Group on Neuropeptides at German Cancer Research Center (DKFZ) and CellNetwork Cluster of Excellence at the University of Heidelberg, Heidelberg, Germany;

[3] Center for Psychiatric Neurosciences, Hôpital de Cery, Lausanne University Hospital (CHUV), Lausanne, Switzerland;

[4] Department of Molecular and Cellular Biology, Center for Brain Science, Harvard University, 52 Oxford Street, Cambridge, MA 02139, USA;

[5] Department of Fundamental Neurosciences, University of Lausanne, Lausanne, Switzerland;

[6] Department of Medicine, University of Fribourg, Chemin du musée 5, CH-1700 Fribourg, Switzerland;

[7] Pain Center, Department of Anesthesiology, Lausanne University Hospital (CHUV);

[8] Central Institute of Mental Health, Mannheim, Germany;

[9] University of Strasbourg Institute for Advanced Study (USIAS), Strasbourg, France.

* Equally contributing first author

Corresponding author:

Alexandre Charlet, PhD

CNRS

University of Strasbourg

INCI, UPR2112

USIAS Fellow, Group on Molecular Determinants of Pain

5, rue Blaise Pascal

67084 Strasbourg, France

Phone: + 33 (0) 607082506

E-mail: acharlet@unistra.fr

Abstract:

Complex integrations by astrocyte-neuron networks in both the temporal and spatial domains are crucially involved in brain circuits and functions. Oxytocin orchestrates social and emotional behaviors through modulation of brain circuits such as the central amygdala (CeA). We hypothesize that oxytocin effects in the CeA arise from modulation of such astro-neuronal networks. We found that a subpopulation of CeA astrocytes expresses the oxytocin receptor and responds to its activation by long-lasting increase in calcium transients. Those responses are necessary for oxytocin effects on neuronal activity in the CeA and astrocytic light-evoked calcium transients are sufficient to drive the neuronal network activity. Astrocyte-neuronal communication occurs through release of D-Serine and subsequent activation of NMDA receptors. Accordingly, impairing astrocytes in the CeA abolishes effects of oxytocin on both pain and anxiety. Thus, astrocytes play a critical role in the oxytocinergic modulation of CeA neuronal network and its beneficial modulation of emotional experiences.

One Sentence Summary:

Astrocytes of the CeA have complex responses to oxytocin receptor activation which modulate local neuronal network, leading to decreased pain and anxiety.

Main Text:

The neuropeptide oxytocin is involved in the regulation of many neurophysiological functions, among which anxiety and pain modulation, notably through its action on CeA microcircuits (*1– 4*). A possible role of astrocytes in conveying neuromodulatory effects of oxytocin in the central

nervous system has rarely been explored (*5*, *6*), despite numerous findings of their active involvement in the regulation of neural circuits (*7–10*) with yet many controversies about the mechanisms involved (*11*, *12*). Moreover, astrocytes seem to be key players in the etiology of chronic pain pathologies (*13*) as does the CeA (*14*). Here we tackle the role of astrocytes in the pain and anxiety relieving effects of oxytocin in the CeA of rats, through patch-clamp of output neurons of the CeA, found in its medial part (CeM), and calcium imaging or *in vivo* manipulation of astrocytes from the lateral and capsular part of the CeA (CeL), where oxytocin receptor (OT-R) are found (*1*).

As the cell types bearing the OT-R in CeL remain unknown, we performed *in situ* hybridization (ISH) to detect OT-R and glial fibrillary acidic protein (GFAP) mRNAs, and found cell transcripting both or only one (Fig. 1A). This indicates that OT-R is expressed in at least astrocytes of the CeL.

To test whether OT-R found in astrocytes could elicit astrocytic responses, we expressed C1V1(t/t) under the oxytocin promoter through rAAVs injected in the paraventricular and supraoptic nuclei, enabling activation of oxytocin neurons and their distant axons present in CeL (*3*, *4*) (Fig. 1B, C). Spinning disk calcium imaging of the calcium indicator Oregon Green® 488 BAPTA-1 loaded in astrocytes, identified by sulforhodamine 101 labelling (Fig. 1D, S1) showed that light-driven activation of C1V1 expressing axons evoked long-lasting calcium transients in astrocytes (Fig 1E). Presence of TTX excludes that responses of astrocytes are secondary to neuronal network activity.

Specificity of OT-R activation as the sole mechanism inducing increase in calcium transients in astrocytes was confirmed by the use of the exogenous agonist [Thr4Gly7]OT (TGOT) alone. TGOT responses were prevented by incubation of OT-R antagonist [d(CH2)5,Tyr(Me)2,Orn8]-

vasotocin (dOVT) but remained unchanged in the presence of TTX (Fig 2.A), which was used in all following calcium imaging experiments with OT-R agonists. This indicates a direct, OT-R specific, modulation of astrocytic calcium transients by oxytocin.

Hence we sought to elucidate the intracellular mechanisms underlying astrocytes responses upon OT-R activation. Calcium imaging experiments were conducted using calcium-free ACSF, which almost prevents any responses, in a partially reversible manner. Internal stores of calcium from the endoplasmic reticulum were also involved since thapsigargin, a SERCA pump blocker, diminished both the proportion of responding astrocytes and the magnitude of those responses (Fig. S2A). TGOT responses of astrocytes being dependent on extracellular calcium, we looked for functional calcium channels in CeL astrocytes. In a subpopulation of astrocytes, specific blockade of voltage gated calcium channels of the Ca_v3 family with TTA-P2 prevented the occurrence of calcium oscillations in response to TGOT, as illustrated by a decrease of area under the curve (AUC), but not of maximal amplitude (Fig. 2B). Immunohistochemistry confirmed the presence of $Ca_v3.3$ on CeL astrocytes (Fig. 2C), and further experiments using blockers of the Ca_v1 family excluded implication of those calcium channels in TGOT induced calcium transients increase (Fig. S2B). OT-R activation in astrocytes elicited complex intracellular signaling, raising the question of the identity of one of the primary effectors of G protein coupled receptors activation, the G_α subunit. We used recently described biased agonists for OT-R: atosiban, biased towards $G_{i/o}$ linked OT-R, and carbetocin, biased towards G_q ones (*15*, *16*). Both elicited calcium transients with similar value to TGOT. Furthermore, the use of N-ethylmaleimide (NEM) (*17*) proved that astrocytes responding to TGOT require a functioning set of $G_{i/o}$ (Fig 2D). Conversely, interfering with G_q linked pathways using the broad spectrum protein kinases inhibitor staurosporine diminished the proportion and amplitude of TGOT responses in astrocytes

(Fig S2C). Further experiments showed that protein kinase C is not involved, but phospholipase C is, to some extent (Fig S2C). These pharmacological experiments highlight the complex intermingle of both G_i and G_q signaling pathways in OT-R induced calcium transients in astrocytes (Fig. 2E)

To address the role of astrocytes in amygdala microcircuits, we conducted *ex vivo* patch-clamp of CeM projection neurons, the functional output neurons of the CeA (*1*, *2*). We first confirmed that repeated TGOT applications consistently induced an increase in inhibitory post synaptic currents (IPSCs) frequencies (Fig. S3A). We then asked whether astrocytes are necessary to support the oxytocinergic modulation of neuronal network. When astrocyte activity was abolished *ex vivo* using the specific gliotoxin fluorocitrate (FC), TGOT effects on CeM IPSCs frequencies were drastically reduced (Fig. 3A), a result confirmed with the use of another gliotoxin, L-α-aminoadipate (Fig. S3B). The inhibitory action of FC on astrocytic TGOT induced calcium transients was confirmed through calcium imaging experiments (Fig. S3C). This indicates the necessary presence of functional astrocytes to mediate oxytocin modulatory effects. Finally, we elicited calcium transients specifically in CeL astrocytes using rAAVs mediated expression of C1V1(t/t)-mCherry driven by the GFAP promoter (Fig. 3B). Light-driven calcium transients in CeL astrocytes led to an increase in CeM neurons IPSCs frequencies (Fig. 3C), proving that astrocytes alone are sufficient to modulate CeA neuronal networks.

We next tackled the question of how astrocytes do transmit information to the neuronal network and identified the activation of neuronal *N*-methyl-D-aspartate receptor (NMDAR) as the key component of astrocyte to neuron communication. Indeed, the blockade of NMDAR or its co-agonist site, through (2R)-amino-5-phosphonopentanoate (AP5) or 5,7-dichlorokynurenic acid (DCKA), respectively, decreased TGOT evoked increase of IPSCs frequencies (Fig. 3D-E). On

contrary, the blockade of α-amino-3-hydroxy-5-methyl-4-isoxazolepropionic acid receptor (AMPAR) had no effect (Fig. 3F), neither did ifenprodil, an antagonist specific to NR2B containing NMDAR (Fig. S3D). Moreover, AP5 did not impair astrocytic responses to TGOT (Fig. S3E), confirming that the TGOT message is conveyed directly from astrocytes to neurons through neuronal NMDAR activation. To identify the molecular actor released from astrocytes onto neuronal NMDAR, we used D-amino-acid oxidase (DAAO) to selectively degrade the NMDAR co-agonist D-Serine found in astrocytes (*18*). TGOT had no effect after DAAO incubation, but subsequent incubation of the same cells in D-Serine containing ACSF rescued the TGOT mediated increase in IPSCs frequency (Fig. 3G).

To ask whether those *ex vivo* conclusions were also relevant *in vivo*, we tested the effect of TGOT on the increased pain sensitivity and anxiety levels in rat model of neuropathy using the spared nerve injury model. Cannulae were implanted to infuse drugs micro volumes into the CeL (Fig. 4A, B). Infusion of TGOT alone did reduce the mechanical hyperalgesia in neuropathic animals, an effect that lasted for up to 4 hours. If prior to TGOT, FC was injected in the CeL, the pain relieving effect of TGOT was abolished (Fig. 4C). Later, using a similar injection procedure when anxiety levels were assessed, we found that TGOT did relieve anxiety in neuropathic animals, an effect diminished by prior injection of FC (Fig. 4D).

Oxytocinergic regulation of neural circuits and their physiological functions is under intense scrutiny (*19–21*). Here we show a new mechanism of oxytocin action, which induces complex modifications of astrocytic calcium transients, leading to changes of CeA neural network outputs and their behavioral correlates. The different characteristics of astro-neuronal networks dynamics provide new means for regulation of brain functions (*22–24*), on a different spatio-temporal scale than neuro-neuronal networks, with a complexity yet to unravel (*25*). Intracellular pathways

leading to the increase in somatic calcium concentrations in astrocytes after OT-R activation are complex and involve more than one classical pathway. This might explain some reports that sole activation or inactivation of G_q signaling in astrocytes was insufficient to evoke any effect on synaptic activity (*26*, *27*). In a larger perspective, with growing evidence showing that oxytocin dampens down inflammatory processes and modulates innate host defense mechanisms (*28*), our data revealing an astrocytic regulation of oxytocin-induced relief in anxiety and pain potentially offer a novel insight in the neurobiological mechanism underpinning the placebo response (*29*). Finally, given that oxytocin modulates emotions and behaviors through a variety of peripheral and central nervous systems actions (*4*, *19*, *30*), our study highlights a pivotal role of astrocytes in oxytocinergic neuromodulation and opens a general question about the role of astro-neuronal networks in the modulation of emotional experiences by neuropeptidergic systems.

References and Notes:

1. D. Huber, P. Veinante, R. Stoop, Vasopressin and oxytocin excite distinct neuronal populations in the central amygdala. *Science*. **308**, 245–8 (2005).

2. D. Viviani *et al.*, Oxytocin selectively gates fear responses through distinct outputs from the central amygdala. *Science*. **333**, 104–7 (2011).

3. H. S. Knobloch *et al.*, Evoked axonal oxytocin release in the central amygdala attenuates fear response. *Neuron*. **73**, 553–66 (2012).

4. M. Eliava *et al.*, A New Population of Parvocellular Oxytocin Neurons Controlling Magnocellular Neuron Activity and Inflammatory Pain Processing. *Neuron*. **89**, 1291–1304 (2016).

5. D. Di Scala-Guenot, D. Mouginot, M. T. Strosser, Increase of intracellular calcium induced by oxytocin in hypothalamic cultured astrocytes. *Glia*. **11**, 269–76 (1994).

6. J. Kuo, O. R. Hariri, P. Micevych, An interaction of oxytocin receptors with metabotropic glutamate receptors in hypothalamic astrocytes. *J. Neuroendocrinol.* **21**, 1001–6 (2009).

7. B. S. Khakh, M. V Sofroniew, Diversity of astrocyte functions and phenotypes in neural circuits. *Nat. Neurosci.* **18**, 942–52 (2015).

8. A. Volterra, J. Meldolesi, Astrocytes, from brain glue to communication elements: the revolution continues. *Nat. Rev. Neurosci.* **6**, 626–40 (2005).

9. A. Araque *et al.*, Gliotransmitters travel in time and space. *Neuron*. **81**, 728–39 (2014).

10. Z. Ma, T. Stork, D. E. Bergles, M. R. Freeman, Neuromodulators signal through astrocytes to alter neural circuit activity and behaviour. *Nature* (2016), doi:10.1038/nature20145.

11. N. B. Hamilton, D. Attwell, Do astrocytes really exocytose neurotransmitters? *Nat. Rev. Neurosci.* **11**, 227–238 (2010).

12. N. Bazargani, D. Attwell, Astrocyte calcium signaling: the third wave. *Nat. Neurosci.* **19**, 182–189 (2016).

13. R.-R. R. Ji, T. Berta, M. Nedergaard, Glia and pain: Is chronic pain a gliopathy? *Pain*. **154**, S10–S28 (2013).

14. V. Neugebauer, W. Li, G. C. Bird, J. S. Han, The amygdala and persistent pain. *Neuroscientist*. **10**, 221–234 (2004).

15. M. Busnelli *et al.*, Functional selective oxytocin-derived agonists discriminate between individual G protein family subtypes. *J. Biol. Chem.* **287**, 3617–3629 (2012).

16. I. Passoni, M. Leonzino, V. Gigliucci, B. Chini, M. Busnelli, Carbetocin is a Functional Selective Gq Agonist That Does Not Promote Oxytocin Receptor Recycling After Inducing β-Arrestin-Independent Internalisation. *J. Neuroendocrinol.* **28** (2016), doi:10.1111/jne.12363.

17. M. S. Shapiro, L. P. Wollmuth, B. Hille, Modulation of Ca2+ channels by PTX-sensitive G-proteins is blocked by N-ethylmaleimide in rat sympathetic neurons. *J. Neurosci.* **14**, 7109–7116 (1994).

18. M. J. Schell, M. E. Molliver, S. H. Snyder, D-serine, an endogenous synaptic modulator: localization to astrocytes and glutamate-stimulated release. *Proc. Natl. Acad. Sci. U. S. A.* **92**, 3948–52 (1995).

19. B. J. Marlin, M. Mitre, J. A. D'amour, M. V. Chao, R. C. Froemke, Oxytocin enables maternal behaviour by balancing cortical inhibition. *Nature*. **520**, 499–504 (2015).

20. L. L. Oettl *et al.*, Oxytocin Enhances Social Recognition by Modulating Cortical Control of Early Olfactory Processing. *Neuron*. **90**, 609–621 (2016).

21. K. Li, M. Nakajima, I. Ibañez-Tallon, N. Heintz, A Cortical Circuit for Sexually Dimorphic Oxytocin-Dependent Anxiety Behaviors. *Cell* (2016), doi:10.1016/j.cell.2016.08.067.

22. K. E. Poskanzer, R. Yuste, Astrocytes regulate cortical state switching in vivo. *Proc. Natl. Acad. Sci. U. S. A.* **2016**, 1–10 (2016).

23. S. Habbas *et al.*, Neuroinflammatory TNFα Impairs Memory via Astrocyte Signaling. *Cell*. **163**, 1730–1741 (2015).

24. R. Martín, R. Bajo-Grañeras, R. Moratalla, G. Perea, a Araque, GLIAL CELL SIGNALING. Circuit-specific signaling in astrocyte-neuron networks in basal ganglia pathways. *Science*. **349**, 730–4 (2015).

25. A. Volterra, N. Liaudet, I. Savtchouk, Astrocyte Ca(2+) signalling: an unexpected complexity. *Nat. Rev. Neurosci.* **15**, 327–35 (2014).

26. T. A. Fiacco *et al.*, Selective Stimulation of Astrocyte Calcium In Situ Does Not Affect Neuronal Excitatory Synaptic Activity. *Neuron*. **54**, 611–626 (2007).

27. C. Agulhon, T. A. Fiacco, K. D. McCarthy, Hippocampal short- and long-term plasticity are not modulated by astrocyte Ca2+ signaling. *Science*. **327**, 1250–4 (2010).

28. M. Clodi *et al.*, Oxytocin alleviates the neuroendocrine and cytokine response to bacterial endotoxin in healthy men. *Am. J. Physiol. Endocrinol. Metab.* **295**, E686-91 (2008).

29. P. Enck, F. Benedetti, M. Schedlowski, New Insights into the Placebo and Nocebo Responses. *Neuron*. **59**, 195–206 (2008).

30. M. Maroun, S. Wagner, Oxytocin and Memory of Emotional Stimuli: Some Dance to Remember, Some Dance to Forget. *Biol. Psychiatry*. **79**, 203–212 (2016).

31.   E. Shigetomi et al., Imaging calcium microdomains within entire astrocyte territories and endfeet with GCaMPs expressed using adeno-associated viruses. J. Gen. Physiol. 141, 633–647 (2013).

32.   J. T. Ting, T. L. Daigle, Q. Chen, G. Feng, Patch-Clamp Methods and Protocols (Springer New York, New York, NY, 2014; http://link.springer.com/10.1007/978-1-4939-1096-0), vol. 1183 of Methods in Molecular Biology.

33.   Y. Ikegaya, M. Le Bon-Jego, R. Yuste, Large-scale imaging of cortical network activity with calcium indicators. Neurosci. Res. 52, 132–138 (2005).

34.   O. Yizhar et al., Neocortical excitation/inhibition balance in information processing and social dysfunction. Nature. 477, 171–8 (2011).

35.   I. Decosterd, C. J. Woolf, Spared nerve injury: an animal model of persistent peripheral neuropathic pain. Pain. 87, 149–158 (2000).

36.   O. E. Luis-Delgado et al., Calibrated forceps: A sensitive and reliable tool for pain and analgesia studies. J. Pain. 7, 32–39 (2006).

37.   A. a Walf, C. a Frye, The use of the elevated plus maze as an assay of anxiety-related behavior in rodents. Nat. Protoc. 2, 322–8 (2007).

Author Contributions:

Conceptualization, AC; Methodology, AC, BBo, CLM, ID, JYC, PP, RS, VG; Analysis, AC, BBe, BBJ, CML, HSKB, JW; *In situ* hybridization, HSKB; Immunohistochemistry, JW, MdSG, ME; *Ex vivo* patch-clamp electrophysiology, AC, BBe, JW, MA; *Ex vivo* calcium imaging, CLM, JW; Behavior, AC, BBJ; viruses validation, MdSG, ME, VG; Spared nerve injuries, MP; Writing, AC, BBo, JYC, JW, PP, RS, VG; Supervision, AC; Project administration, AC; Funding acquisition, AC.

A

	OTR	GFAP	merge + DAPI
Probes			
Negative ctrl			

B

rAAV-pOT-C1V1(t/t)-mCherry
OGB1
SR101

PVN

ΔF/F

CeL/C
CeM

OT-R
Oxytocin

C

mCherry

PVN

rAAV-pOT-C1V1(t/t)-mCherry

500 pA
500 ms

20 mV
500 ms

D

SR101   OGB1

Merge
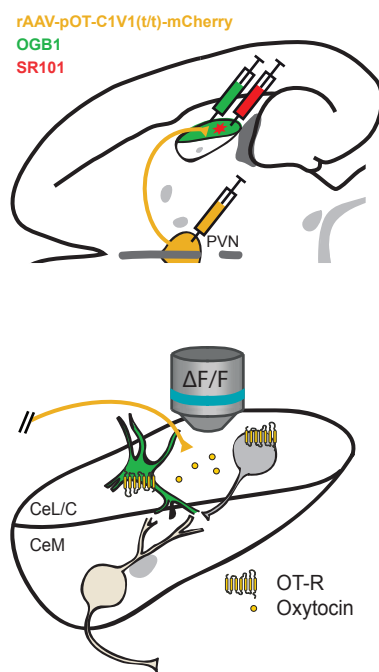
E
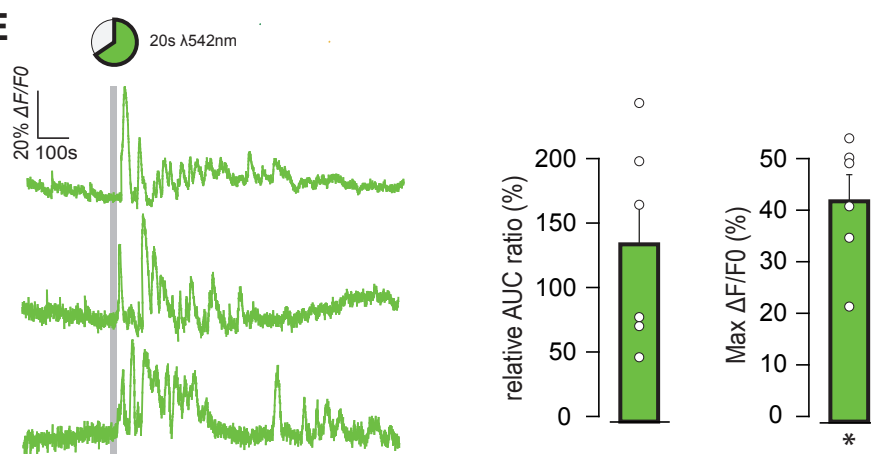
20% ΔF/F0
100s

20s λ542nm

relative AUC ratio (%)

Max ΔF/F0 (%)

*

Fig. 1. CeL astrocytes express OT-R mRNA and respond to light-driven activation of oxytocinergic axons of the CeL. (**A**) RNAscope in situ hybridization showing GFAP (red) and OTR (green) expressing cells in CeA. Merged images include DAPI stain (blue). (Bottom) Negative control probe targeting the bacterial gene DapB. Scale bar 10μm. (**B**) Experimental scheme showing PVN nucleus, in which rAAVs were injected to induce expression of C1V1(t/t)-mCherry in oxytocinergic neurons, some of which project to CeA. On CeA slices, co-incubation of SR101 and OGB1 allows calcium imaging of astrocytes. (**C**) (Top) C1V1-mCherry expressing oxytocin neurons of the PVN in which (bottom) λ542nm light exposure induced depolarizing currents, enabling precise spiking control. (**D**) Typical confocal image of CeL astrocytes co-labeled with SR101 and OGB1. Scale bar 20 μm. (**E**) Effect of activation of oxytocinergic axons in the CeL through a 20s λ542nm light pulse on calcium transients of CeL astrocytes. (Left) Pie charts of the proportion of responsive astrocytes and typical ΔF/F traces; (right) ratios of ΔF/F AUCs before and after light-driven activation of CeL oxytocinergic axons and maximal peak values (n slices (n_s)=6, n astrocytes (n_a)=37). Data are expressed as means across slices plus SEM. White circles indicate averages across responding astrocytes per slices. Values were statistically compared to TGOT+TTX ones found in figure 2. [*]$P<0.05$, independent samples Student's t-test.
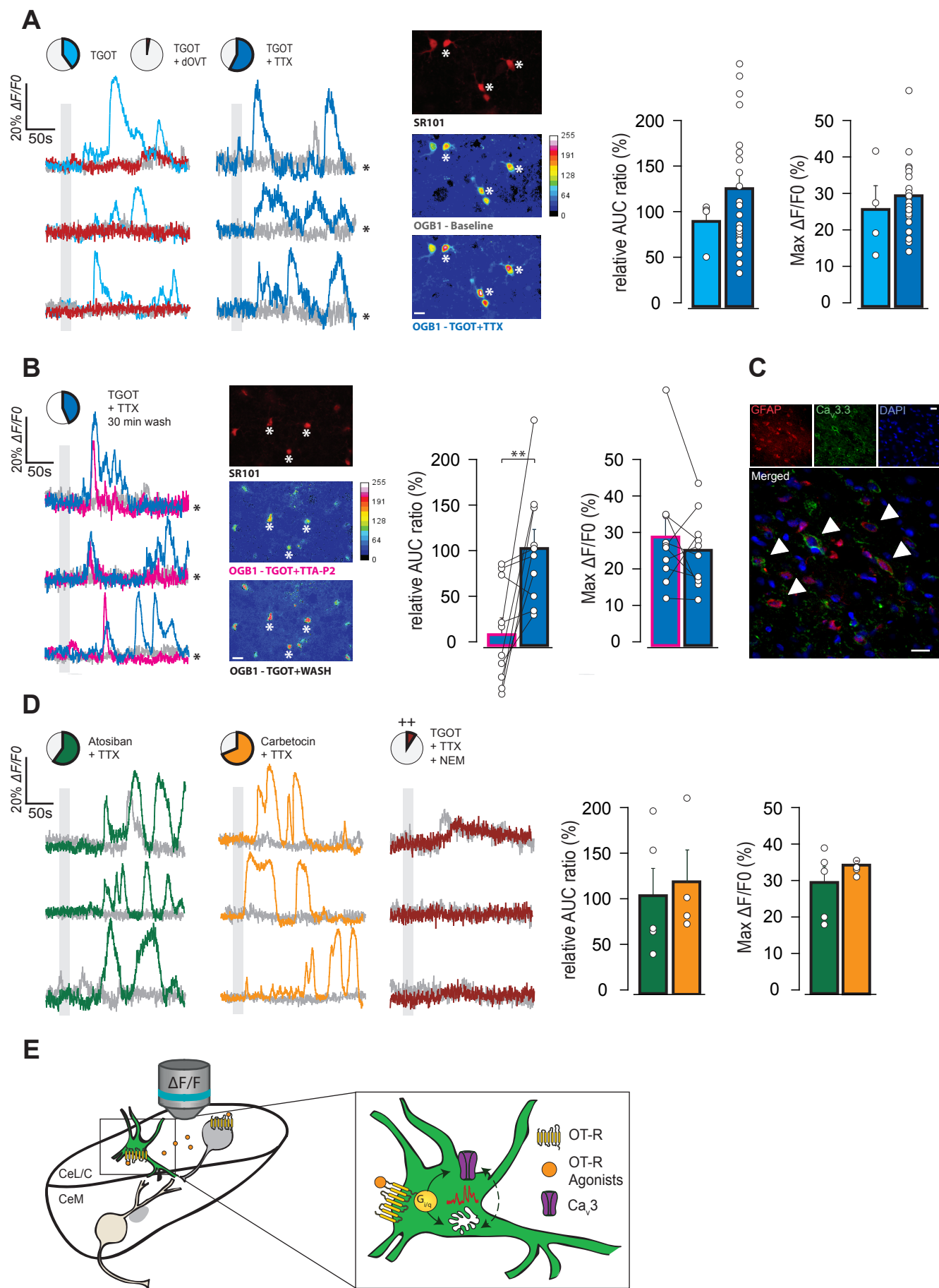
A

TGOT   TGOT + dOVT   TGOT + TTX

SR101

OGB1 - Baseline

OGB1 - TGOT+TTX

relative AUC ratio (%)

Max ΔF/F0 (%)

B

TGOT + TTX 30 min wash

SR101

OGB1 - TGOT+TTA-P2

OGB1 - TGOT+WASH

relative AUC ratio (%)

**

Max ΔF/F0 (%)

C

GFAP   Ca_v3.3   DAPI

Merged

D

Atosiban + TTX   Carbetocin + TTX   TGOT + TTX + NEM

++

relative AUC ratio (%)

Max ΔF/F0 (%)

E

ΔF/F

CeL/C

CeM

OT-R

OT-R Agonists

Ca_v3

$G_{i/q}$

Fig. 2. OT-R activation evokes astrocytic calcium transients, independent of neuronal network activity and partly dependent on CaV₃ channels. (A to B) (Left) Pie charts of the proportion of responsive astrocytes and typical $\Delta F/F$ traces; (middle) Astrocytes identified through SR101 (red) and corresponding pseudo-color images of OGB1 fluorescence during baseline and after drug application (stacks of 50 images/25s of recording). Asterisks indicate astrocytes from which the example $\Delta F/F$ traces are shown; (Right) ratios of $\Delta F/F$ AUCs before and after drug application and maximal peak values upon exposition to: (A) TGOT alone (400nM, $n_s=4$, $n_a=39$), with dOVT (1µM, $n_s=3$, $n_a=34$) or TTX (1µM, $n_s=22$, $n_a=182$); (**B**) TGOT+TTA-P2, followed by a 30 min wash (1µM, $n_s=3$, $n_a=23$). Only astrocytes that responded after wash are represented here. White circles here represent individual astrocytes values (**C**) Immunohistochemistry showed $Ca_v3.3$ expression in GFAP positive cells of the CeL (white arrows). (**D**) (left) Pie charts of the proportion of responsive astrocytes and typical $\Delta F/F$ traces; (right) ratio of $\Delta F/F$ AUCs before and after drug application and maximal peak value upon exposition to: atosiban (2µM, $n_s=5$, $n_a=47$), carbetocin (10µM, $n_s=4$, $n_a=50$) or NEM+TGOT (100µM, $n_s=7$, $n_a=52$). (**E**) Scheme summarizing conclusions of previous calcium imaging experiments. Data are expressed as means across slices plus SEM, White circles indicate averages across responding astrocytes per slices (except TTA-P2, see B). All values were statistically compared to those of TGOT+TTX, [++]$P<0.01$, independent samples Mann-Whitney U test except for TTA-P2 experiments: [**]$P<0.01$, paired samples Student's t-test. Scale bars 20µm

A
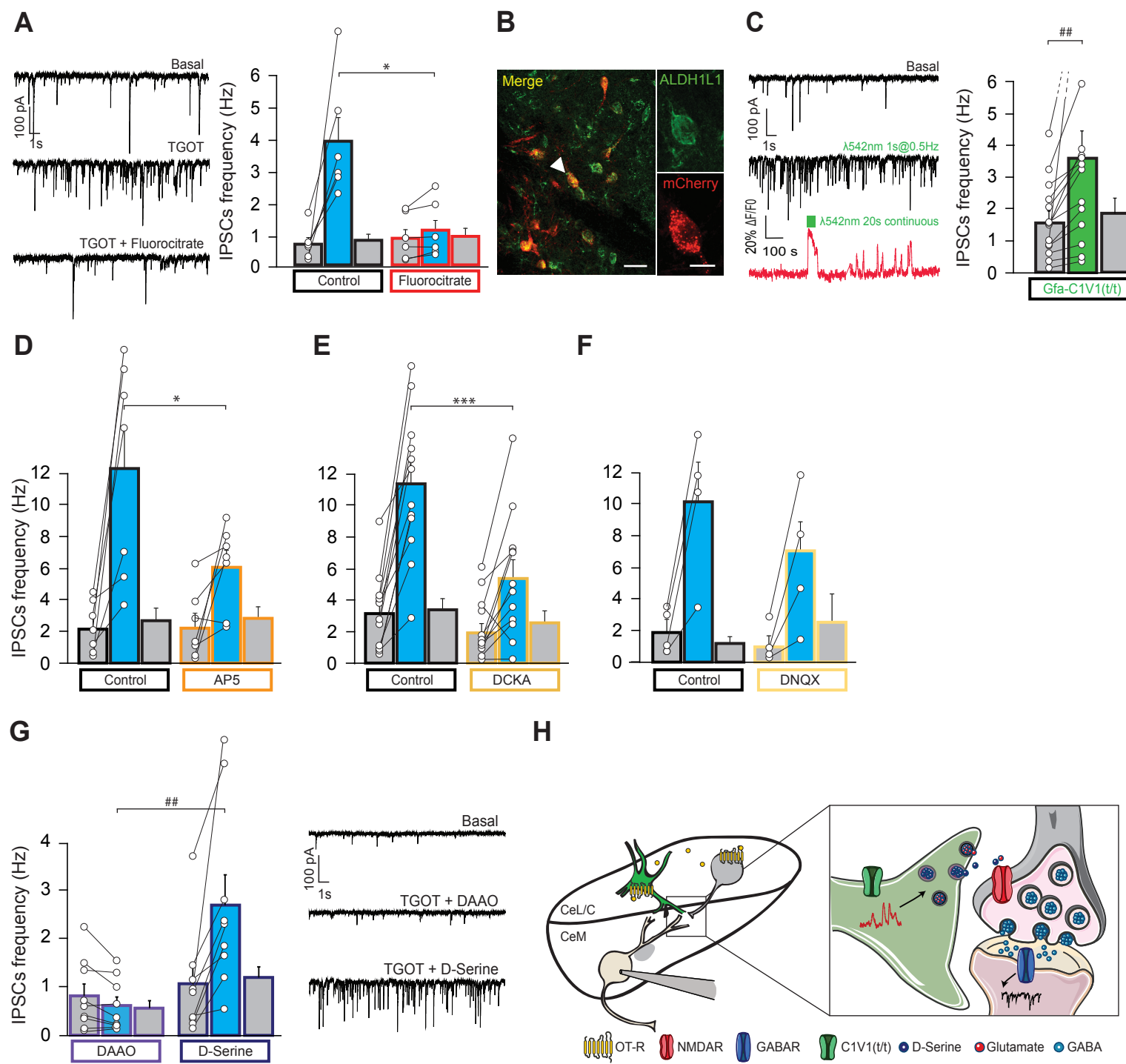
Basal

100 pA | 1s

TGOT

TGOT + Fluorocitrate

IPSCs frequency (Hz)

*

Control   Fluorocitrate

B

Merge

ALDH1L1

mCherry

C

Basal

100 pA | 1s

λ542nm 1s@0.5Hz

20% ΔF/F0 | 100 s   λ542nm 20s continuous

IPSCs frequency (Hz)

##

Gfa-C1V1(t/t)

D

IPSCs frequency (Hz)

*

Control   AP5

E

***

Control   DCKA

F

Control   DNQX

G

IPSCs frequency (Hz)

##

DAAO   D-Serine

Basal

100 pA | 1s

TGOT + DAAO

TGOT + D-Serine

H

CeL/C

CeM

OT-R   NMDAR   GABAR   C1V1(t/t)   D-Serine   Glutamate   GABA

Fig. 3. Astrocytes are sufficient and necessary to the OT-R mediated modulation of CeA neuronal network activity. (**A**) Effect of fluorocitrate on TGOT induced increase of IPSCs frequencies (TGOT 400nM, fluorocitrate 100µM, 1h, n=6). (**B**) Immunohistochemistry for CeL cells infected with AAV-Gfa-C1V1TSmCherry with co-labeling for ALDH1L1. White arrow shows one cell expanded in insets. Scale bars 25 and 10µm. (**C**) (Top) Effect of light induced activation of C1V1 expressing astrocytes on IPSCs frequencies (n=19). (Bottom) Effect of a 20s, continuous, λ542nm light exposure on the ΔF/F of a C1V1 expressing astrocyte. (**D-E**) Effect of AP5 (50µM, n=7) or DCKA (10µM, n=12) on TGOT induced increase in IPSCs frequencies. (**F**) DNQX (25µM, n=4) effect on TGOT induced increase in IPSCs frequencies. (**G**) Effect of DAAO (0.15U/ml, incubation time >1h30), followed by 20min incubation in D-Serine (100µM) on TGOT induced increase in IPSCs frequencies (n=9). (**H**) Scheme summarizing conclusions of previous patch-clamp and calcium imaging experiments. Data are expressed as averaged frequencies plus SEM before, during and after TGOT effect. Linked white circles represent individual cell values before and during TGOT effect. $^{*}P<0.05$, $^{***}P<0.001$, paired samples Student's t-test. $^{\#\#}P<0.01$ Wilcoxon signed rank test.
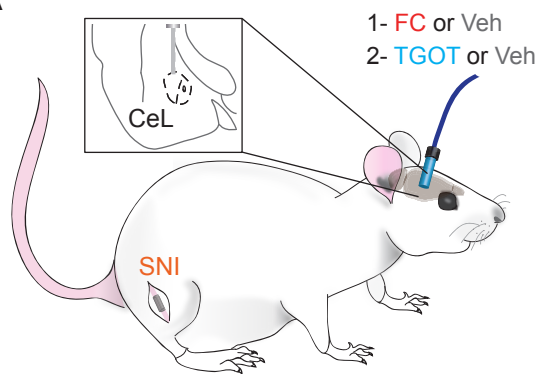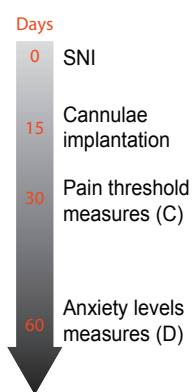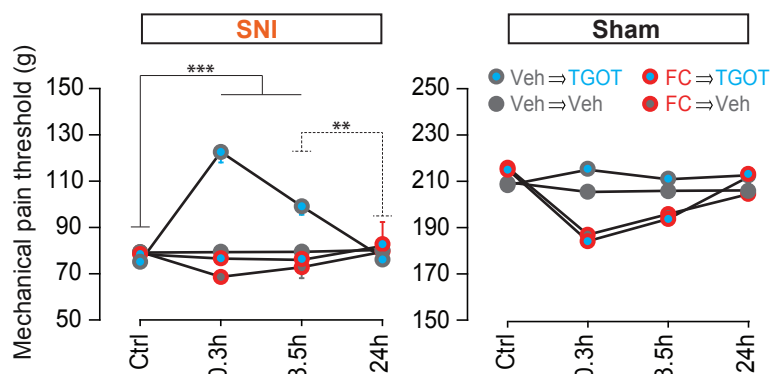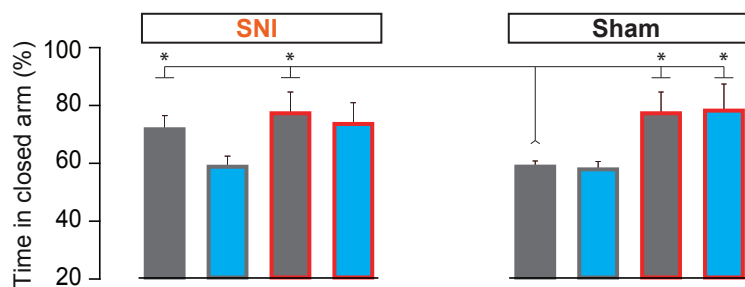
A

CeL

SNI

1- FC or Veh
2- TGOT or Veh

B

Days

0   SNI

15 Cannulae
    implantation

30 Pain threshold
    measures (C)

60 Anxiety levels
    measures (D)

C

Mechanical pain threshold (g)

SNI

***

**

Ctrl   0.3h   3.5h   24h

Sham

Veh⇒TGOT   FC⇒TGOT
Veh⇒Veh   FC⇒Veh

Ctrl   0.3h   3.5h   24h

D

Time in closed arm (%)

SNI   Sham

*   *   *   *

Fig. 4. CeL astrocytes are necessary for beneficial effect on pain and anxiety of OT-R activation. (**A**) Scheme of surgical procedures and drug injections in CeL. FC or vehicle were administered 1h before TGOT or vehicle, which were injected 20min before behavioral tests. (**B**) Timeline of the different procedures and behavioral tests. (**C**) On day 30 post SNI surgery, mechanical pain threshold was assessed on the neuropathic paw before (ctrl) and after drugs injections for sham and SNI animals. (**D**) On day 60 post-surgery, anxiety levels were assessed through measurements of the time spent in closed arms of the elevated plus maze after drugs injections for sham and SNI animals. n=4-12 per group. Data are expressed as averages across rats plus SEM. Pain threshold measures: [**]$P<0.01$, [***]$P<0.001$, mixed-design ANOVA followed by posthoc Bonferroni tests. Elevated plus maze: [*]$P<0.05$, ANOVA on log transformed data followed by posthoc Dunnett t-tests using Sham-Vehicle-Vehicle group as control.

Supplementary Materials for

A key role for amygdala astrocytes in regulation of negative affective processing by oxytocin.

J. Wahis[1*], M. da Silva Gouveia[2*], B. Bellanger[1], M. Eliava[2], M. Abatis[3], B. Boury-Jamot[3], H. S. Knobloch-Bollmann[4], M. Pertin[5], B. Boutrel[3], C. M. Lamy[6], I. Décosterd[5,7], J. Y. Chatton[5], R. Stoop[3], P. Poisbeau[1], V. Grinevich[2,8], A.Charlet[1,9]

correspondence to: acharlet@unistra.fr

This PDF file includes:

Materials and Methods
Figs. S1 to S4

Materials and Methods

Animals

Animals were housed under standard conditions with food and water available *ad libitum* and maintained on a 12-hour light/dark cycle and all experiments were conducted in accordance with EU rules and approbation from French Ministry of Research (01597.05). For *ex vivo* and *in vivo* experiments, male (if not stated otherwise) wistar rats were used. *Ex vivo* experiments used animals between 18 and 25 days old, except in experiments were rAAVs were injected, in which case animals were between 2 to 6 months old. In vivo experiments used animals of 2 months old at the moment of the first surgery.

Cloning and production of rAAV Vectors:

To construct the OTp-C1V1(t-t)-TS-mCherry AAV vector we used previously cloned OTp-DIO-GFP-WRE plasmid (*4*), equipped with characterized 2.6 kb OT promoter (*3*). In this plasmid the DIO-GFP sequence was replaced by C1V1 (t/t)-TS-mCherry from the pAAV CaMKIIa-C1V1(t/t)-TS-mCherry (Addgene, plasmid #35500). To generate GfaP-C1V1(t/t)-TS-mCherry AAV vector we replaced CamKIIa promoter from the pAAV CaMKIIa-C1V1(t/t)-TS-mCherry by the Gfa promoter from the pZac2.1 gfaABC1D-tdTomato (Addgene, plasmid: 44332). The cell type specificity of the rAAV carrying the Gfa promoter was recently confirmed (*31*).

Injections of rAAV viruses

Stereotaxic surgery was performed under deep ketamine-xylazine anesthesia, using KOPF (model 955) stereotaxic system. 3 female Wistar (180-200g. , age 8 weeks) were injected with ca. 200 nl of rAAV serotype 1/2 (AAV-Gfa-C1V1TSmCherry, GFAP promoter containing plasmid obtained from Addgene) unilaterally at the coordinates corresponding to CeA: rostro-caudal: -2,7mm, medio-lateral: 4,2mm, dorso-ventral: 8.mm (From Paxinos and Watson Atlas).

Horizontal and coronal slices preparation

In all cases, animals were anaesthetized using ketamine (Imalgene 90 mg/kg) xylazine (Rompun, 10 mg/kg) administered intra-peritoneally. Transcardial perfusion was then performed using one of the following artificial cerebro-spinal fluids (ACSFs) dissection solutions. For rats between 18 and 25 days old, an ice-cold sucrose based dissection ACSF was used containing (in mM): Sucrose (170), KCl (2.5), NaH_2PO_4 (1.25), $NaHCO_3$ (15), $MgSO_4$ (10), $CaCl_2$ (0.5), HEPES (20), D-Glucose (20), L-ascorbic acid (5), Thiourea (2), Sodium pyruvate (3), N-acetyl-L-cysteine (5), Kynurenic acid (2). For rats between 2 to 6 months old, an ice-cold NMDG based ACSF was used containing (in mM): NMDG (93), KCl (2.5), NaH_2PO_4 (1.25), $NaHCO_3$ (30), $MgSO_4$ (10), $CaCl_2$ (0.5), HEPES (20), D-Glucose (25), L-ascorbic acid (5), Thiourea (2), Sodium pyruvate (3), N-acetyl-L-cysteine (10), Kynurenic acid (2). In both cases, pH were adjusted to 7.4 using either NaOH or HCl, this after bubbling in 95% O_2-5% CO_2 gas, bubbling which was

maintained throughout the duration of use of the various ACSFs. Those ACSFs formulae were based on the work of (*32*). Following decapitation, brain was swiftly removed in the same ice-cold dissections ACSFs as for transcardial perfusion, and 350 µm thick horizontal slices containing the CeA obtained using a Leica VT1000s vibratome. For experiments in Fig. 1C, coronal slices of the same thickness containing the PVN were used. Upon slicing, brain slices were hemisected and placed, for 1 hour minimum before any experiments were conducted, in a room tempered holding chamber, containing normal ACSFs. For slices of 2 to 6 month old rats, slices were first let for 10 minutes in 35°C NMDG ACSF before placing them in the holding chamber at room temperature. Normal ACSF, also used during experiments, is composed of (in mM): NaCl (124), KCl (2.5), NaH_2PO_4 (1.25), $NaHCO_3$ (26), $MgSO_4$ (2), $CaCl_2$ (2), D-Glucose (15), adjusted for pH values of 7.4 with HCL or NaOH and continuously bubbled in 95% O_2-5% CO_2 gas. All ACSFs were checked for osmolarity and kept for values between 305-310 mOsm/L. In experiment using 0 Ca^{2+} ACSF, calcium was replaced by equimolar concentration of EGTA. In electrophysiology or calcium imaging experiments, slices were transferred from holding chamber to an immersion recording chamber and superfused at a rate 2 mL/min with normal ACSFs unless indicated otherwise.

Calcium imaging and astrocytes identification

To identify astrocytes, SR101 (1µM) was added to ACSF in a culture well and slices incubated for 30 minutes. The specificity of SR101 to astrocytes of the CeL was verified through patch-clamp experiments, which results can be found in Fig. S1. After SR101 loading, the synthetic calcium indicator OGB1 was bulk loaded following an adapted version of the method described previously (*33*) reaching final concentrations of 0.0025% (~20 µM) for OGB1, 0.002% Cremophor EL, 0.01% Pluronic F- 127 and 0.5% DMSO in ACSF, for 50 to 60 minutes at 35°C. Upon incubation time, slices were washed in ACSF for at least an hour before any recordings were performed. Astrocytes recorded for this study were then those co-labeled for SR101 and OGB1, as shown in the picture in Fig. 1D. Spinning disk confocal microscope used to perform astrocyte calcium imaging was composed of a Zeiss Axio examiner microscope with a 40x water immersion objective (numerical aperture of 1.0), mounted with a X-Light Confocal unit – CRESTOPT spinning disk. Images were acquired at 2Hz with either a Rolera em-c² emCCD or an optiMOS sCMOS camera (Qimaging, BC, Canada). Cells within a confocal plane were illuminated for 100 to 150 ms for each wavelength (SR101: 575 nm, OGB1: 475 nm) using a Spectra 7 LUMENCOR. The different hardware elements were synchronized through the MetaFluor software which was also used for online and offline quantitative fluorescence analysis. Astrocytic calcium levels were measured in hand drawn ROIs comprising the cell body plus, when visible, proximal processes, without distinctions. $[Ca^{2+}]_i$ variation were estimated as changes in fluorescence signals over the baseline (ΔF/F). Baseline was established for each ROI as the average fluorescence over all pictures. To take into account micro-movements of the specimen on long duration recordings, the ΔF/F values were also calculated for SR101 and subsequently subtracted to the ones of OGB1. Bleaching was corrected using a linear regression on the overall ΔF/F trace for each astrocyte, which values were then subtracted to the ΔF/F. Upon extraction of data, calculations and corrections of ΔF/F for each astrocyte, the area under

the curve before and after drug application (or light pulse for optogenetics experiments) was calculated and proportionally corrected relative to the different recording durations. An astrocyte was considered as being responsive if the relative ratio of AUCs after drug/light application over baseline was 20% greater than in baseline conditions. The relative AUCs ratios values were used for quantitative analysis and called "relative AUC ratio". Maximal peak reached after drug/light application was also measured in responsive cells and used in quantitative analysis. Data were averaged across astrocytes per slices, which were used as the statistical unit. Image J software was also used on SR101 / OGB1 pictures to produce illustrative pictures such as the one in fig. 2A-C. All calcium imaging experiments were conducted at room temperature.

Electrophysiology

Whole cell patch-clamp recordings of CeM neurons and CeL astrocytes were visually guided by infrared oblique light visualization of neurons, completed by SR101 fluorescence for astrocytes. Whole-cell voltage clamp recordings were obtained with an Axon MultiClamp 700B amplifier coupled to a Digidata 1440A Digitizer (Molecular Devices, CA, USA). Borosilicate glass electrodes (R = 3.5 - 7 MΩ) with inner filament (OD 1.5 mm, ID 0.86 mm; Sutter Instrument, CA USA) were pulled using a horizontal flaming/brown micropipette puller (P97; Sutter Instrument, CA, USA). Pipettes were filled with an intracellular solution containing (in mM): KCl (150), HEPES (10), $MgCl_2$ (4), $CaCl_2$ (0.1), BAPTA (0.1), ATP Na salt (2), GTP Na salt (0.3). For patch-clamp of astrocytes, the intracellular solution was composed of (in mM) $KMeSO_4$ (135), NaCl (5), $MgCl_2$ (2), HEPES (10), ATP Na salt (2), GTP Na salt (0.3). For both solutions, pH was adjusted to 7.3 with KOH and osmolarity checked to be between 290-295 mOsm/L, adjusted with sucrose if needed. All cells were hold at a membrane potential of -70 mV, astrocytes -80 mV. Series capacitances and resistances were compensated electronically throughout the experiments using the main amplifier. Recordings were filtered at 2 kHz, digitized at 40 kHz and stored with the pClamp 10 software suite (Molecular Devices; CA, USA). Analysis of patch-clamp data were performed using Clampfit 10.6 (Molecular Devices; CA, USA) and Mini analysis 6 software (Synaptosoft, NJ, USA) in a semi-automated fashion (automatic detection of events with chosen parameters followed by visual inspection). Average events frequencies per cells were calculated on 20s windows, chosen for TGOT or light stimulation at maximal effect, as determined by the visually identified maximal slope of the cumulative plot of the number of events. Baseline and recovery frequencies were measured at the beginning and end of each recording. All patch-clamp experiments were conducted at room temperature.

Optogenetics

We used C1V1(t/t) , a ChR1/VChR1 chimera with the combined mutations E122T/E162T (for more details, see (*4*)). Optogenetic green light stimulation of C1V1(t/t) was performed using either the Spectra 7 LUMENCOR (λ542 nm) or light source X-Cite® 110LED from Excelitas Technologies through a Cy3 filter, controlled via MetaFluor or Clampex driven TTL pulse, respectively.

Spared nerve injury procedure

Animals were randomly separated in two groups to undergo SNI or sham procedure. Animals were anaesthetized using isoflurane 1.5–2.5%. Incision was made at mid-thigh level using the femur as a landmark and a section was made through the biceps femoris. The three peripheral branches (sural, common peroneal and tibial nerves) of the sciatic nerve were exposed. Both tibial and common peroneal nerves were ligated using a 5.0 silk suture and transected. The sural nerve was carefully preserved by avoiding any nerve stretch or nerve contact (*34*). For animals undergoing sham surgery, same procedure was performed but the nerves remained untouched. Animals were routinely observed daily for 7 days after surgery and daily tested by the experimenter (Fig. S4). Besides observing weight, social and individual behavior, the operated hindpaw was examined for signs of injury or autotomy. In case of autotomy or suffering of the animal, the animal was euthanized in respect of the ethical recommendations of the EU. No analgesia is provided after the surgery in order to avoid interference with chronic pain mechanisms and this is in accordance with our veterinary authorization. Suffering is minimized by careful handling and increased bedding.

Cannulae implantation

Animals were bilaterally implanted with guide cannulae for direct intra-central amygdala infusions. As guide cannulae we used C313G/Spc guide metallic cannulae cut 5.8 mm below the pedestal. For this purpose, animals were deeply anesthetized with 5% isoflurane in pure oxygen and their heads were fixed in a stereotaxic fame. The skull was exposed and two holes were drilled according to coordinates that were adapted from a rat brain atlas (2.3 mm rostro-caudal; 4 mm lateral; 7.5 mm dorso-ventral relative to bregma) by comparing the typical bregma-lambda distance (9 mm) with the one measured in the experimental animal. Two screws were fixed to the caudal part of the skull in order to have an anchor point for the dental cement. The acrylic dental cement was finally used to fix the cannulae and the skin was sutured. In case of long lasting experiment (neuropathy-induced anxiety) with a cannulae implantation at distance of the behavioral assay (> 4 weeks) the cannulae were sometime lost and animals excluded from testing.

Drugs infusions through cannulae

Bilateral injections of 0.5 µl containing either vehicle (NaCl 0.9%), or oxytocin agonist TGOT (1 µM) or fluorocitrate (0.1 µM) dissolved in NaCl 0.9%. For this procedure two injectors (cut to fit 5.8 mm guide cannulae protruding 2 to 2.5 mm beyond the lower end of the cannulae in older animals and 1.8 mm in 3-4 week old rats) were bilaterally lowered into the guide cannulae, connected via polyten tubing to two Hamilton syringes that were placed in an infusion pump and 0.5 µl of liquid was injected in each hemisphere over a 2 minute period of time. After the injection procedure, the injectors were kept in place for an additional minute in order to allow a complete diffusion of liquid throughout the tissue. Rats were subsequently left in the home cage for 15 minutes to recover from the stress of the injection for and then handled for mechanical threshold or elevated plus maze assessment.

Mechanical sensitivity assessment

 In all experiments, we used a calibrated forceps (Bioseb, Chaville, France) previously developed in our laboratory to test the animal mechanical sensitivity (*35*). Briefly, the habituated rat was loosely restrained with a towel masking the eyes in order to limit stress by environmental stimulations. The tips of the forceps were placed at each side of the paw and a graduate force is applied. The pressure producing a withdrawal of the paw, or in some rare cases vocalization, corresponded to the nociceptive threshold value. This manipulation was performed three times for each hind paw and the values were averaged.

Elevated plus maze experiment

 Following protocol from (*36*), the arena is composed of four arms, two open (without walls) and two closed (with walls, 30 cm high). The arms are 10 cm wide, 50 cm long and elevated 50 cm off the ground. Two intensity adjustable up to 50 watts lamps positioned on the top of the maze uniformly illuminate it. Animals were video tracked using a video-tracking system (Ethovision Pro 3.16 Noldus, Wageningen, Netherlands). To avoid interaction and noise with the animal, the operator and the computer were physically separated from the maze by a black curtain and the test session occurred in a separated room from the housing room. After each trial, the maze was cleaned with 70% ethanol and dry with towel paper. Twenty minutes after intracerebral injections, animal was let to the center of the plus maze facing the open arm opposite to where the experimenter is and was able to freely explore the entire apparatus for six minutes. The total time and the time spend in closed and open arms were recorded in seconds and the percentage of time spent in closed arms was calculated as a measure of anxiety. Rats falling from the apparatus during the test, or freezing more than 50% of the total time were removed from the analysis.

Immunohistochemistry

Ca$_v$3.3: Immunohistochemistry for Ca$_v$3.3 was performed on cryostat-cut 20 μm in width horizontal sections prepared from fresh-frozen 20 days old rat brains, previously transcardially perfused with 4% paraformaldehyde PBS, after anesthesia. Slices were washed in PBS (6 times 5 min) then blocked 1 hour at room temperature using PBS containing 1% bovine serum albumin and a 10% mixture of normal serum from the species secondary antibodies were raised in. Primary antibodies were then added in the same medium and incubated overnight at 4°C. The following antibodies were used: Chicken raised antibody for GFAP (1:500) (ref: ab4674 from abcam), Rabbit raised antibody for Ca$_v$3.3 (1:200) (ref: ACC-009, Alomone).
The day after, upon washes of primary antibodies solutions, secondary antibodies were added for 1 hour at room temperature, using Alexa 555 against chicken (1:1000) and Alexa 488 against rabbit (1:500) (purchased from abcam), then washed (6 times 5 minutes). DAPI (1:2000) was added on the 5 out of 6 washes. Slices were then mounted using aqua-polymount (Polysciences, Inc) and pictures taken using the confocal spinning disk microscope (cf. Calcium imaging part).

AAV-Gfa-C1V1TSmCherry specificity: After 3 weeks of virus expression in the brain, the rats were transcardially perfused with 4% paraformaldehyde solution. Tissue blocks, containing CeA were dissected from the fixed brain and Vibratome-cut into 50 µm thick free-floating sections. After several rinse steps sampled sections were blocked with 5% NGS in PBS and incubated for 48 h at 4°C with polyclonal rabbit anti-ALDH1L1 antibody (1:500, Abcam) in 1% Triton-PBS buffer, containing 0,1 % NGS. Appropriate secondary antibody (AlexaFluor488 conjugated goat anti-rabbit (1:1000, LifeTechnologies) was used for further antigene detection. Intrinsic mCherry fluorescence of virus- expressing cells was strong enough to detect them in the tissue without any additional antibody enhancement. The immunolabeled sections were mounted onto Superfrost slides, cover-slipped with Moviol, analyzed and documented using LEICA SP5 confocal microscope.

In situ hybridization

In situ hybridization (ISH) in fig. 1A was performed on 25-µm cryostat-cut coronal sections prepared from fresh-frozen mouse brain (male C57BL/6J, P22). After extraction, brains were immediately frozen in Tissue-Tek O.C.T. compound and stored at -80 degrees Celsius. ISH was performed according to the manufacturer's instructions (Advanced Cell Diagnostics) for Fresh Frozen RNAscope Multiplex Fluorescent Assay. Treatment of amygdala containing sections were adjusted with the 3-plex negative control and then coexpression of OTR and GFAP examined using ACD designed target probes as well as the nuclear stain DAPI. Single plan images were collected with an upright laser scanning microscope (LSM-710, Carl Zeiss) using a 40x-objective with keeping acquisition parameters constant between control and probe treated sections.

Statistical analysis

All parametrical statistical tests presented in figures captions were performed following correct verification of the assumptions on the distribution of data, and if not either transformations of data or non-parametric tests were used. Tests were performed using either SPSS 23 (IBM) or statview 5 (SAS institute Inc.).
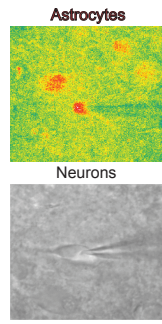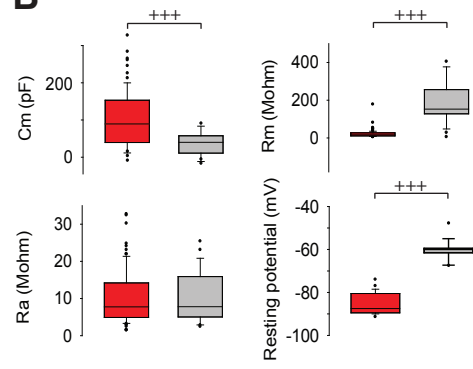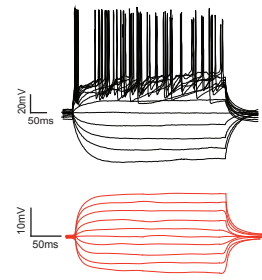
A

Astrocytes

Neurons

B

Cm (pF)
+++

Ra (Mohm)

Rm (Mohm)
+++

Resting potential (mV)
+++

C

20mV
50ms

10mV
50ms

Fig. S1. SR101 is specific to astrocytes (**A**) Pseudo-color pictures of an SR101 positive cell identified as an astrocyte compare to neurons identified under oblique infrared light. (**B**) Electrophysiological properties of patched SR101$^+$ (red, n=84) and SR101$^-$ cells (grey, n=21). (**C**) Responses to 20pA current steps of SR101$^+$ (red) and SR101$^-$ cells (black).

A

TGOT
+ TTX

\# TGOT
+ TTX
in ACSF 0 Ca^{2+}

TGOT
+ TTX
wash in normal ACSF

* TGOT
+ TTX
+ Thapsigargin

B

TGOT
+ TTX
+ Verapamine

TGOT
+ TTX
+ Nimodipine

C

TGOT
+ TTX
+ U73122

+ TGOT
+ TTX
+ Staurosporine

TGOT
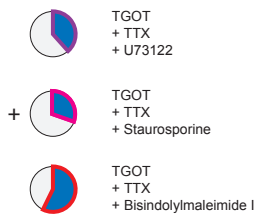+ TTX
+ Bisindolylmaleimide I
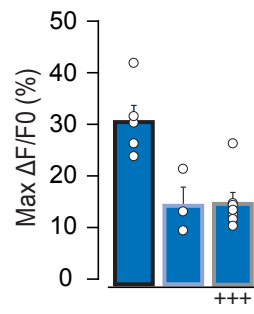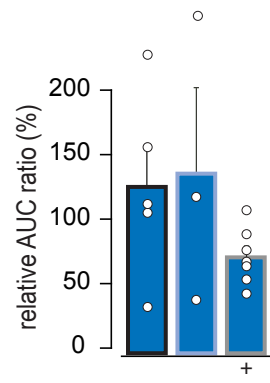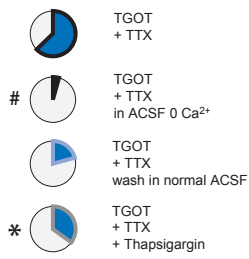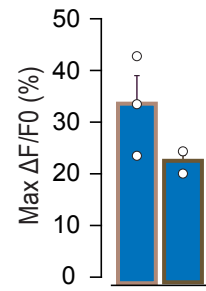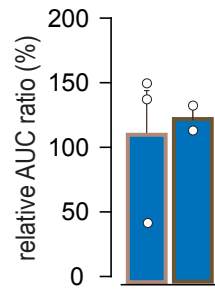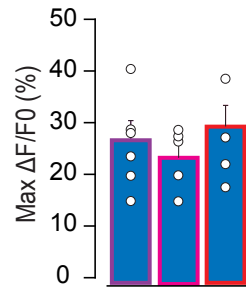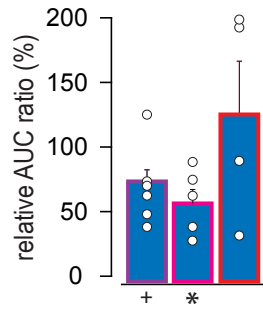
Fig. S2. Intracellular signaling involved in astrocytes responses to OT-R activation. (**A** to **B**) (Left) Pie charts of the proportion of TGOT+TTX responsive astrocytes and their (right) ratios of ΔF/F AUCs before and after drug application and maximal peak values upon exposition to: (A) removal of extracellular calcium (n_s=6, n_a=55. AUCs and Max values not shown, only 2/55 astrocytes still classified as responsive) followed by normal ACSF (n_s=3, n_a=29); thapsigargin (1µM, n_s=7, n_a=58); (B) verapamine (50µM, n_s=3, n_a=28) or nimodipine (10µM, n_s=2, n_a=20). (C) U73122 (10µM, n_s=6, n_a=45), staurosporine (1µM, n_s=5, n_a=43) or bisindolylmaleimide-I (1µM, n_s=4 slices, n_a=30 astrocytes); Data are expressed as mean across slices plus SEM. White circles indicate averages across responding astrocytes per slices. $^*P$<0.05, $^{**}P$<0.01 independent samples Students's t-test, ^+P<0.05, ^{+++}P<0.001 independent samples Mann-Whitney U test, $^\#P$<0.05 Wilcoxon signed rank test.
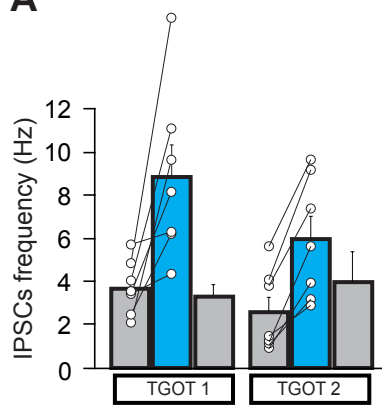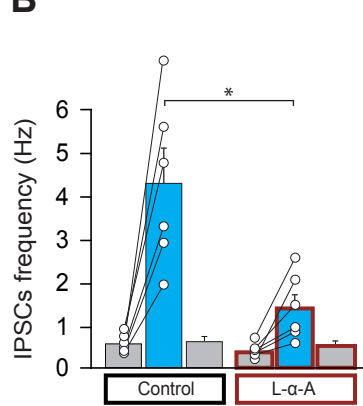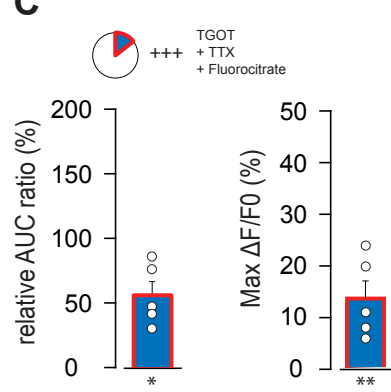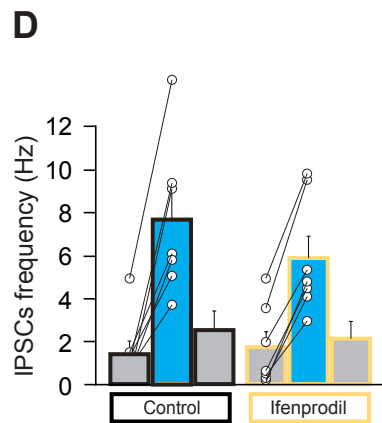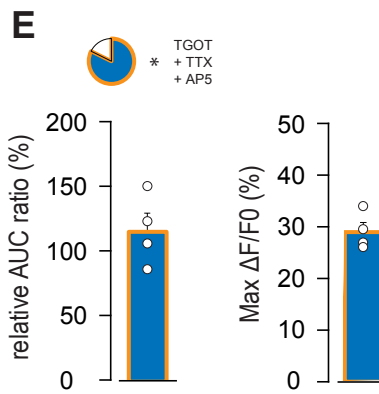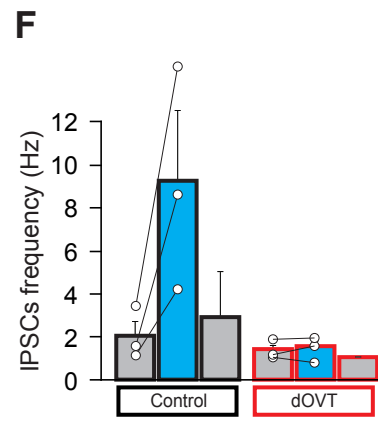
Fig. S3. TGOT effect on CeM neurons is repeatable, specific to OT-R and does need astrocytes as intermediary through non NR2B containing neuronal NMDA-R signaling. (**A**) Effect of double (20min apart) application of TGOT on IPSCs frequencies (n=7). (**B**) L-α-aminoadipate (100µM, 40min, n=6) effect on TGOT induced increase in IPSCs frequencies. (**C**) (Top) pie chart of the proportion of TGOT+TTX responsive astrocytes and (bottom) ratio of ΔF/F AUCs before and after drug application and maximal peak value upon exposition to fluorocitrate (200µM for 30min, n_s=8, n_a=81). (**D**) ifenprodil (3µM, n=7) effect on TGOT induced increase in IPSCs frequencies. (**E**) (Top) pie chart of the proportion of TGOT+TTX responsive astrocytes and (bottom) ratio of ΔF/F AUCs before and after drug application and maximal peak value upon exposition to AP5 (50µM, n_s=4, n_a=35). (**F**) dOVT (1µM, n=3) prevents the effect of TGOT on IPSCs frequencies. Patch-clamp experiments: data expressed as averaged frequencies plus SEM before, during and after TGOT effect. Linked white circles: individual cell values before and during TGOT effect. Calcium imaging experiments: data expressed as means across slices plus SEM. White circles: averages across responding astrocytes per slices. $^*P<0.05$, $^{**}P<0.01$ independent samples (calcium-imaging) or paired (patch-clamp) Students's t-test, $^{+++}P<0.001$ independent samples Mann-Whitney U test.
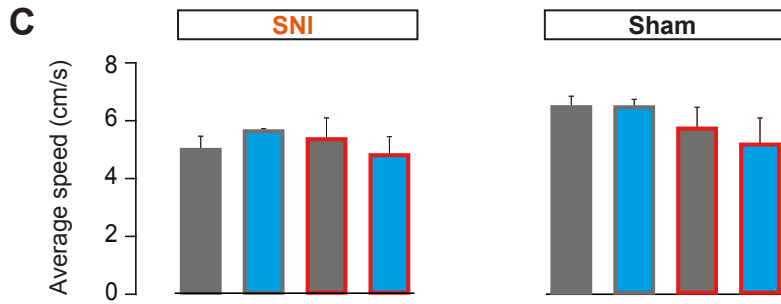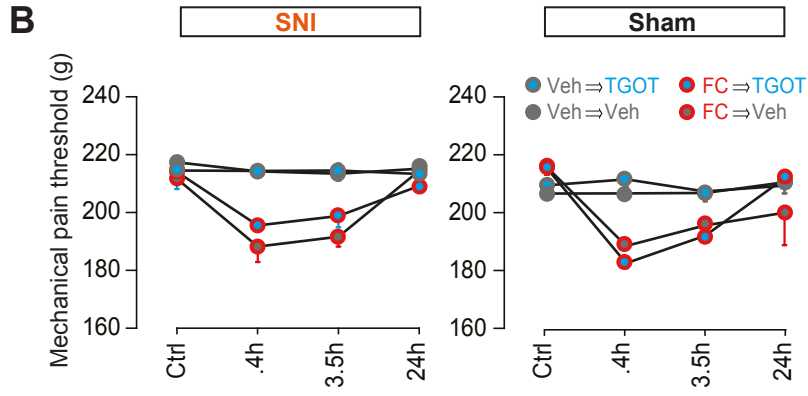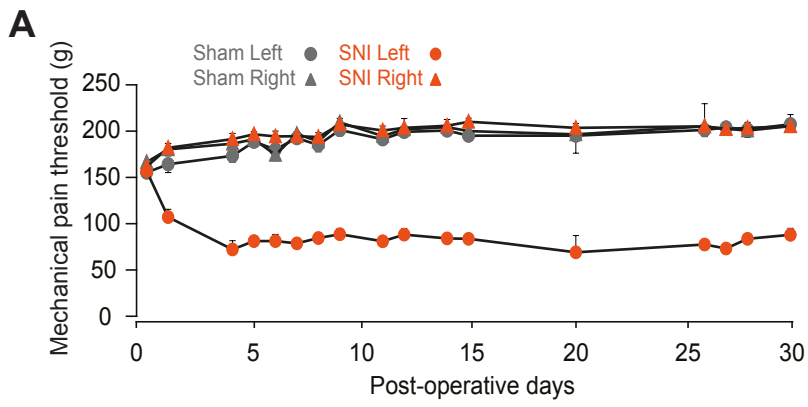
Fig. S4. SNI neuropathic pain model is specific to the injured paw and doesn't impair locomotion speed. (**A**) 30 days' time course of mechanical pain threshold evolution across the different groups (**B**) On day 30 post-surgery, mechanical pain threshold was also assessed on the non-injured paw. Different combination of FC or vehicle followed by TGOT or vehicle where administered in the CeL and mechanical pain threshold assessed again at different time points for sham and SNI animals. (**C**) On day 60 post-surgery, locomotion was assessed through measurements of the average speed during the time of the elevated plus maze experiment, after administration of different combination of FC or vehicle followed by TGOT or vehicle. n=4-12 per group. Data are expressed as averaged frequencies plus SEM. Pain threshold measures: Mixed-design ANOVA followed by posthoc Bonferroni tests. Elevated plus maze: Independent samples Kruskal-Wallis test.

Conclusion

From a scientific point of view, while those studies are certainly imperfect, I try to always place the obtained results in the perspective of the update knowledge, with great attention to the potentially deleterious over-interpretations. This is especially important when teaching how to interpret experimental results in the frame of a given hypothesis. Finally, considering the actual place of science in our modern society, with the drastically limited funding available, the increasing number of scientific publication in a worldwide context and the rising attention of the general public, I am particularly thoughtful to the potential impact of the work I perform and/or supervise. This is the reason for the publications as book chapters and/or for the less specialized public, but also why I chose to take an active part in the local ethical committee and the organization for scientific and private monthly seminars through the Strasbourg Neuropole.

From an organization and supervision point of view, I had a first occasion to supervise a master work in the course of my PhD thesis, while organizing the work of Maya Aouad. While in post-doc, this teaching / supervision activity took a great place and was, I believe, one of the reason for the success of my work. Since my appointment as CNRS researcher and regarding the actual organization of science in France, most of my activity consist to find funding for my scientific projects and to supervise the students responsible for testing these complex hypothesis. Up to now, this work repartition seems to be successful, with a first paper published in *Neuron* in 2016 and a second set of major results submitted in a high-profile journal and to be hopefully published in 2017.

Altogether, my past work should paves the way for a better understanding of emotions, with a particular emphasis on pain and anxiety and their modulation by endogenous neuropeptidergic systems. In the next years, I will continue these studies hopefully supported by motivated students and researchers.

Major Scientific Perspectives

I - Deciphering Oxytocin Circuitries Orchestrating Emotions

Oxytocin is a strong affects modulator. Over the last years, OT attracted attention regarding its regulatory functions of emotional behavior, among which positive behaviors, such as social recognition and socio-sexual arousal, and negative behaviors, such as pain integration and anxiety / fear (Donalson and Young, 2008). Previous studies revealed that OT can modulate intra-amygdala microcircuits (Viviani et al., 2011). Using optogenetic methods (Knobloch et al., 2012; Eliava et al., 2016), we demonstrated the efficiency of local axonal release of OT to modulate the intra-amygdala microcircuits leading to the anxiolytic, long-lasting, effect of this neuropeptide (Knobloch et al., 2012). Recently, we illustrated the crucial function of a very small subpopulation of OT neurons in the control of pain (Eliava et al., 2012). However, and in line with this last study, **we still don't know if specific OT neuronal populations are involved in the differential regulations of physiological functions, particularly considering their different "positive" or "negative" emotional valence**.

OT neurons are modulated by noradrenalin, serotonin and dopamine. Interestingly, we know that undefined OT neurons are activated by noradrenalin (NA), a neurotransmitter released during "negative" situations (Onaka, 2004). One of the main sources of NA to the PVN is the *loecus coeruleus* (LC) (Flak et al., 2014). On the other hand, dopamine (DA) is released during positive (*e.g.* socio-sexual behavior) events (Baskerville and Douglas, 2010). Among the various sources of DA, the *zona incerta* send particularly strong innervations to the PVN (Bujis et al., 1984) and, since part of the OT neurons express D2 receptors (Baskerville et al., 2009), it is tempting to hypothesize that they can be modulated by endogenous DA. In-between, serotoninergic (5HT) projections are found in the PVN and seem to be the efferences of the dorsal raphe magnus nucleus (dRM; Kubota et al., 2012).

Given the numerous functions of the oxytocinergic system and the specificity of NA/DA/5HT projections to the main nucleus of synthesis of oxytocin, we hypothesize that **there are several different subpopulations of OT neurons, some recruited during negative emotion *via* noradrenalin projections whereas others are recruited during positive emotion *via* dopaminergic projections.** If successful, this project will lead to major breakthrough in our current understanding of how emotions occur and are modulated.

Feasibility of the Project and Preliminary Results

To study OT neurons activated during anxious/fear situation (OTFear+), we will apply a new genetic technique named virus-based Genetic Activity-Induced Tagging of cell (vGAIT), recently developed by Dr. Hasan (Dogbevia et al., 2015). vGAIT allows the expression of a given protein in a specific neuronal population when activated in a determined time window. To tag activated OT neurons, a cocktail of three recombinant adeno-associated viruses (rAAV) will be injected in the hypothalamic OT PVN (Figure 4). This technique is especially suitable for OT neurons, which do not express c-fos in a basal, non-stimulated condition, so the background labeling of tagged OT neurons is minimal. Two different "virus 3" will be used, leading in the final expression of either mCherry, in order to be able to identify OTFear+ neurons during *ex vivo* electrophysiological and confocal calcium imaging recordings

experiments, or of ChR2 or hM4Di to activate/inhibit this specific population during complex behaviors (Eliava et al., 2016).
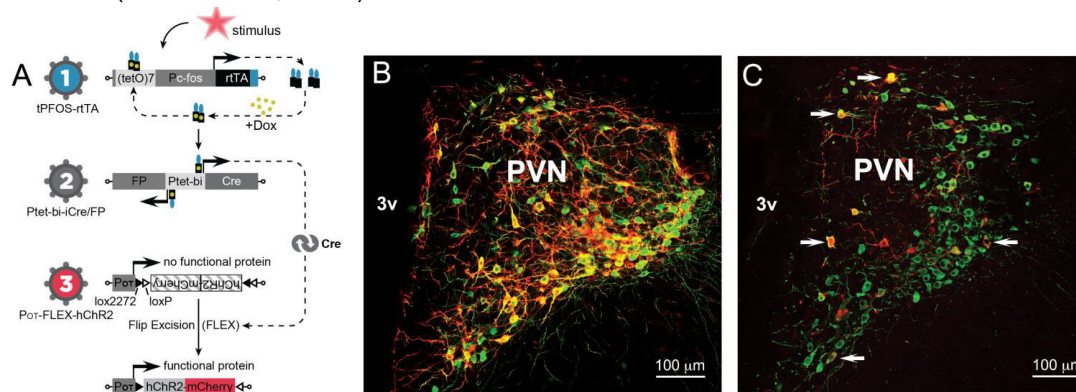

Figure 4**. **vGAIT approach to tag experience-activated OT neurons. (**A**) Schematic presentation of the viral-based Genetic Activity-Induced Tagging (*vGAIT*) method. The method is based on transcriptional activity of immediate early gene c-fos and requires three viruses to target activated OT neurons in antibiotic (Dox)-dependent manner. (**B**) Expression of ChR2-mCherry (virus 3) in virtually all OT neurons, which were activated upon osmotic challenge. (**C**) Tagging a small fraction of OT neurons (arrows) activated by associative fear learning. Yellow cells represent neurons co-expressing OT (green) and mCherry (red) in the hypothalamic paraventricular nucleus (PVN). 3v – third ventricle.

Using the vGAIT technique, we tagged a small population of OT neurons specifically activated during anxious situation (Figure 4). Preliminary data, obtain by expression of mCherry in OTFear+ and Venus in the entire OT population indicate that ~15% of OT neurons are OTFear+ (Figure 4C). We are currently investigating if similar or different neuronal populations may be involved in different behaviors, particularly socio-sexual behavior, taken as a "positive" event by comparison to the "negative" valence of fear.

In addition, we are now able to record OT neuronal activity through GCaMP6s confocal calcium imaging, hence demonstrating the validity of our approach for the present proposal. This new and promising strategy will be used in the course of the entire project. The Figure 5 illustrates our first preliminary results, indicating the existence of different populations of OT neurons depending on their sensitivities to NA, DA and 5HT. It is particularly interesting to note that all combinations of sensitivities are found, with OT neurons being activated by only DA, NA or 5HT but also some activated, in a similar manner, by two or even three of those. This may led to interesting hypothesis regarding the role of such interactions in the global regulation of brain functions. Next, the same *ex vivo* approach will be combined with classical optogenetic-driven deconstruction of brain circuits in order to decipher which pathways are involved in these differential modulations of specific populations of OT neurons.

Finally, we would like to go for *in vivo* freely moving calcium imaging and apply similar strategy in order to gain direct access to the activity of OT neurons in physiological conditions. This will allow us to identify how oxytocinergic neurons react in either a negatively (*e.g.* fear) or a positively (*e.g.* social interaction) valenced event and to unravel which brain circuits are involved in the complex regulation of such behaviors.
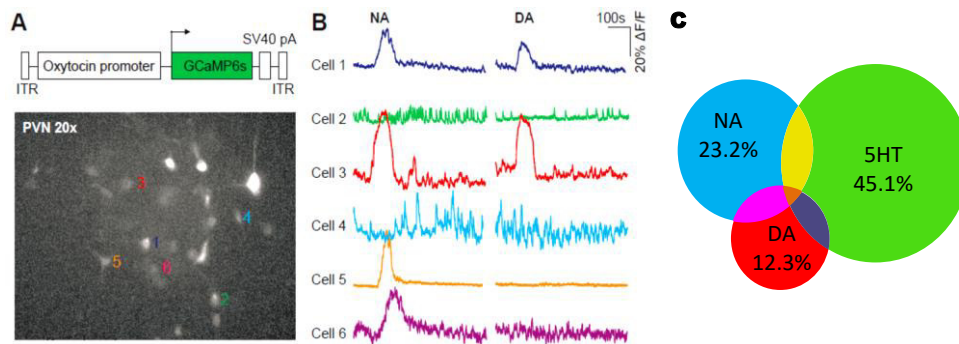
Figure 5. Calcium imaging monitoring of OT neurons. (**A**) rAAV viral construct and typical raw image of GCaMP6 fluorescence obtained using our setup. (**B**) 6 example traces of OT neurons responding either to DA, NA or both. (**C**) Proportion of activated OT neurons (n=244).

Impact of the proposal

Although importance of OT in the regulation of emotions was convincingly reported in mammalian species (Knobloch et al., 2012; Eliava et al., 2016), it is still unclear how segregated the oxytocinergic populations are. Here, using the advanced genetic approach (vGAIT), combined with state of the art tools to measure the cellular and behavioral output, we will be able to report if a given OT population underlies a specific behavior and, importantly, to decipher by which brain circuit this population is recruited. This is of particular importance when understanding how oxytocin is able to modulate such a broad spectrum of behaviors and emotions (Lee et al., 2009).

Funding sources

To date, this research project is granted by the NARSAD foundation (70.000 USD from 2017 to 2019) and the collaborative international grant ANR-DFG (410.000 € from 2017 to 2020 – 205.000 € per PI). Funds will mainly be used to cover the lab running cost and set up *in vivo* freely moving calcium imaging, probably taking advantage of Mightex clever development of a (not so expensive) system allowing calcium imaging and optical stimulations without having to implant a whole microscope in the head of the animal. A PhD student salary is included for the recruitment of Damien Kerpsern who will be, among others, in charge of implanting this technique. The project, including all the preliminary results, is currently developed by Stéphanie Goyon, PhD student for 2015-2018.

II - Subcortical Oxytocin Control of Cortical Glia-Neuron Networks during Associative Learning

Our daily life is a succession of cognitive actions influenced by our emotional status. In this context, the plasticity of the adult brain is a fundamental property enabling us to adapt our actions to our environment (LeDoux, 2014; Woodcock et al., 2015). But a tremendous question persists: **how does our brain support the enduring effects of emotions and how does it impact our cortical processing?**

Cortical processing is well illustrated with associative learning, a cognitive process which relies on changes in the spatial pattern and level of neuronal activity (Lee et al., 2010; Lai et al., 2012). However, after decades of research mostly linking cortical processing to neuro-neuronal networks, a paradigm shift is occurring in neurobiology hypothesizing that the complex integration of glia-neuron networks in the temporal and spatial domains is required for cortical processing (Volterra and Meldolesi, 2005; Araque et al., 2014; Chung et al., 2015). Indeed, astrocytes can modulate synaptic transmission and tune brain functions thanks to a dynamic interaction with neurons that is finely regulated in time and space (Araque et al., 2014). Interestingly, our recent findings indicate that astrocyte activity can be directly driven by oxytocin (III-2). Oxytocin, "the great facilitator of life" (Lee et al., 2009), orchestrates emotional behaviors and is present through rich innervations in the prefrontal cortex (PFC; Knobloch et al., 2012). Given that the PFC is critically involved in both the encoding and effective processing of associative memory (Salzman et al., 2010; Woodcock et al., 2015), we hypothesize that **oxytocin regulates the cortical glia-neuron network, a process at the basis of the emotional influence on cortical processing**. By developing new methods and sophisticated strategies both *ex vivo* and *in vivo* behaving mice, we aim to resolve several outstanding questions:

1. Considering the importance of astrocyte-mediated regulation (lee et al., 2010) of the balance of excitation and inhibition inputs to govern behavioral outputs, how are the complex glia-neuron microcircuits supporting the interactions between emotions and cortical processing organized? How do glia-neuron interactions drive the activity of the PFC networks?

2. Given that the PFC is part of the associative areas that process information from cortical and subcortical structures to generate appropriate behavioral outputs (Ray and Zald, 2012), what are the glia-neuron network dynamics underlying associative learning? Do subcortical structures drive this cortical processing?

3. In view of the emotional and cognitive impairments observed in many psychiatric disorders such as autism, anxiety, depression and chronic pain (Lee, 2013; Melzack et al., 1968) and the key role of PFC in the top-down control of the latter (Lorenz et al., 2003), is the PFC a hub for emotion-cognition interaction?

(WP1) Subcortical control of cortical microcircuit functions

Consciousness implies complex cortical processing to compute *i*) a stimulus as a perception, *ii*) the explicit memories associated with this stimulus and *iii*) the implicit consequences of the activation of subcortical structures in the brain and the entire organism (LeDoux, 2014). Cortical processing is well depicted by associative learning, a cognitive process which participates in the association of temporally disconnected events by actively maintaining

stimulus representation across a period of time (Perlstein et al., 2001). The rodent "frontal association cortex" (FrA) has been critically involved in associative learning (Sotres-Bayon and Quirk, 2010; Nakayama et al., 2015). Together with the "secondary motor area" (M2), it forms the "medial agranular cortex" (AGm), or "frontal area 2" (Fr2) (Paxinos and Franklin, 2012). As rodent Fr2 shares many structural and functional similarities with the human dorsolateral PFC (Van de Werd and Uylings, 2014), we thereafter indicate this structure as "dorsal PFC" (dPFC) for the sake of consistency (**Fig. 6a**).

While cortical microcircuits can perform pattern completion, placing neuronal ensembles at the focus of the study of cortical processing (Carrilo-Reid et al., 2016), neurons are not isolated units: complex integration of astrocyte-neuron networks in both the temporal and spatial domains seems to be a requisite to cortical functions (Araque et al., 2014; Fields et al., 2014). Notably, we recently found functional oxytocin receptors located in astrocytes (Mitre et al., 2016) resulting in a direct modulation of astrocyte activity by oxytocin.

WP1.1. Characterizing the influence of PVN-dPFC oxytocin projections on local microcircuits

Context/hypothesis: Oxytocin has firmly grasped our attention over the last several years and its central release has been shown to orchestrate the modulation of cognition and emotions, including enhanced salience of relevant stimuli (Lee et al., 2009; Knobloch et al., 2012; Mitre et al., 2016). Interesting new insights recently arose from clinical studies showing that oxytocin increases neuronal activity in the dPFC and induces a lower conditioned response in early extinction learning (Eckstein et al., 2015). Matching these observations, oxytocin receptors are richly present in the mouse dPFC (Eckstein et al., 2015; Mitre et al., 2016) (**Fig. 6b**), which concomitantly receives dense innervation from paraventricular nucleus (PVN) oxytocin neurons. Given the relevance of oxytocin functions in cognition and emotion, we hypothesize that the dPFC glia-neuron network is submitted to the bottom-up control of PVN-dPFC oxytocin projections.

Objective: **Despite few studies partially describing the oxytocin cortical innervation, the functional contribution of PVN-dPFC oxytocin to the dPFC glia-neuron network dynamics is entirely unknown. By using advanced optogenetic-assisted circuit deciphering applied to neuropeptides, we will address the causal relationship between subcortical oxytocin system and prefrontal processing.**

Methods/breakthrough: This will be achieved by a combination of optogenetics with *ex vivo* patch-clamp and spinning disk calcium imaging of astrocytes expressing genetically encoded Ca^{2+} indicator GCaMP6 (**Fig. 6d**). Whole-cell recording of dPFC layer 2/3 pyramidal neurons will be obtained through visual guidance. GCaMP6 fluorescence will be recorded for intracellular calcium dynamics of both surrounding astrocyte cell body and processes. The net effect of light-driven activation of local dPFC oxytocin axons will be monitored in detail including excitatory/inhibitory transmission. To benefit from the full advantages of *ex vivo* preparations, a battery of pharmacological experiments will be performed upon evoked oxytocin release in order to explore the cellular and molecular/transmitters cascade involved in the net effect recorded.
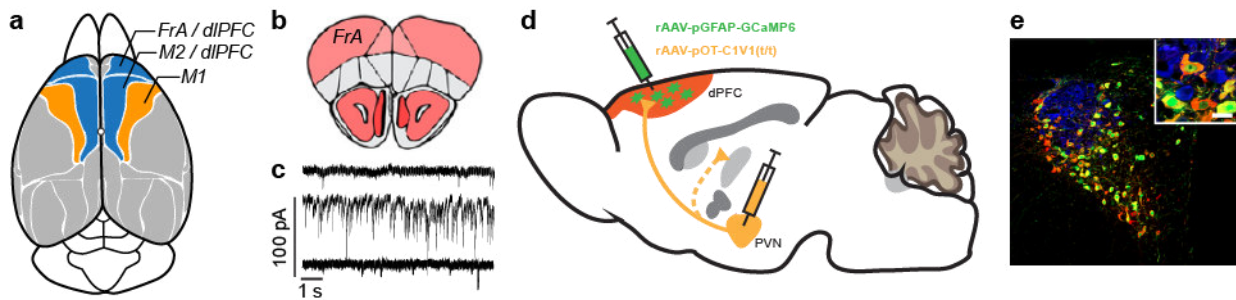
Figure 6. _Oxytocin drive of dPFC network_. _**a.** Dorsal prefrontal cortex in mice. **b.** Scheme of a mouse brain coronal section showing expression of OTR in the FrA (red); from [23]. **c.** Preliminary data indicates that local application of oxytocin receptor agonist (TGOT) induces a dramatic increase in the frequency and amplitudes of currents recorded in a layer 2/3 pyramidal cell of the FrA using high [Cl⁻] intrapipette solution. (top) baseline; (middle) TGOT; (bottom) after wash. **d.** Viral strategy used. **e.** Cell-type specificity of pOT virus. Green: Venus; Red: oxytocin; Blue: vasopressin. Picture from Knobloch*, Charlet*, et al., Neuron, 2012._

Feasibility: We do have extensive experience with all the techniques required (optogenetics for oxytocin system; virus injection; _ex vivo_ whole-cell recording and calcium imaging). All the rAAV tools are validated (**Fig. 6e**) and used in routine in our lab. In addition, we recently validated the _ex vivo_ monitoring calcium of dynamics in astrocytes in response to evoked release of oxytocin through C1V1(t/t) activation. We provide here preliminary data supporting our hypothesis (**Fig. 6c**).

WP1.2. Deciphering the contribution of dPFC glia-neuron interactions to oxytocin modulation

Context/hypothesis: At this point we should have a precise idea regarding both the functional organization and regulation of the dPFC glia-neuron network by the oxytocin system. However we will still be lacking direct, causal evidence of the spatio-temporal involvement of oxytocin influence on neuron or/and astrocyte populations. Given the recent evidences from Yuste's lab highlighting the active involvement of astrocytes in neural circuits underlying cortical-driven complex functions (Poskanzer and Yuste, 2016), we hypothesize that cortical astrocytes may be sufficient to drive the subcortical oxytocin influence on cortical processing.

Objective: **Taking full advantage of the recently validated OTR-Cre mouse line and specifically-designed rAAV tools, we will decipher the precise contribution of astrocytes and neurons to the subcortical modulation of prefrontal glia-neuron network activity.**

Methods/breakthrough: The causal role of astrocytes or neurons subsets has never been addressed in the context of cortical processing. The cellular specificity will be reached by using a combination of newly characterized OTR-Cre mouse line and modified rAAV to express light-sensitive channels (C1V1(t/t) for excitation; ArchT3 for inhibition). This will be achieved in a specific subset of astrocytes or neurons expressing the oxytocin receptor (**Fig. 7b**). We will combine _ex vivo_ patch-clamp recordings and calcium imaging with optogenetics to analyse with high temporal and spatial precision the effect of the activation/inhibition of either OTR positive astrocytes or neurons on the dPFC glia-neuron network. Our results will be of tremendous importance for the sake of understanding the complex astrocyte-neuron intermingle in the subcortical regulation of cortical processing.

Feasibility: We recently described that functional oxytocin receptor are found in astrocytes, confirming previous anatomical observations. In addition, while manipulating the astrocyte intracellular [Ca^{2+}] using rAAV-pGFAP-C1V1(t/t), we demonstrated that astrocyte recruitment is necessary and sufficient to strongly modulate the neuronal network activity). The use of the validated OTR-Cre line to gain specific access to oxytocin receptor positive cells represents a major step forward in the field and a great opportunity to decipher the specific contribution of the different cell types. Finally, the risk of failure is limited by analyzing two different subtypes of oxytocin receptor positive cells: astrocytes and neurons.

(WP2) The prefrontal glia-neuron functional dynamics in associative learning

WP2.1. Identifying the dPFC circuit dynamics occurring during associative learning

Context/hypothesis: Associative learning is a cognitive process which participates in the association of temporally disconnected events by actively maintaining stimulus representation across a period of time (Perlstein et al., 2001). Previous studies reported in mice that fear conditioning, extinction and reconditioning led to opposite synaptic modifications in the dPFC in a cue- and location- specific manner (Lai et al., 2012). In addition, inactivation of the dPFC alters both fear conditioning and extinction (Nakayama et al., 2015), leading to the idea that the dPFC computes subcortical inputs to process the stimulus integration during associative learning. In light of these recent evidences, we hypothesize that dPFC glia-neuron dynamics participate in the encoding of the associative memories.

Objective: **To decipher how associative memories are encoded within the cortical glia-neuron network, we will implement challenging and state-of-the-art 2PLSM to monitor, simultaneously and in a behaving animal, the calcium dynamics occurring in dPFC neurons and astrocytes over the whole process of associative learning and extinction.**

Methods/breakthrough: To address this issue with strong accuracy, we will implement 2-photon laser scanning microscopy (2PLSM)-based time lapse imaging to monitor in the behaving rodent the calcium activity of a large population of cells (**Fig. 7**). The spatial resolution will be achieved using modified AAV to express GCaMP6 and RCaMP2 in astrocytes and neurons, respectively (**Fig. 7**). The associative learning will be achieved by discriminative fear conditioning during which head-restrained mice will associate a conditioned neutral stimulus (CS+) to an unconditioned aversive stimulus (US). After a period of training occurring under the microscope, mice will associate the US to the CS+ and depict a freezing response measured by the nuchal muscles electromyogram (Karalis et al., 2016). Given that previous studies point the dPFC as being involved in both learning and extinction of the association, 2PLSM sessions will be performed over long-time frames during the associative task and the extinction phase at very high spatial and temporal resolution through the implantation of a non-invasive cranial window (Huber et al., 2012). This experimental strategy will allow us to track the temporal dynamics of the glia-neuron network both identified through different genetically encoded calcium indicators (**Fig. 7b**, **7c**). This will be the first time that dPFC glia-neuron processing will be identified in the course of associative learning.
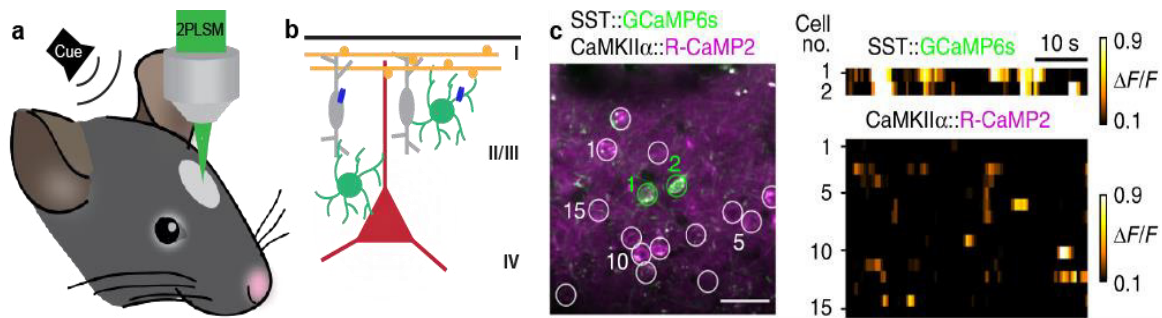
Figure 7. In vivo 2-photon laser scanning microscopy for associative learning mechanism deciphering.
a. Scheme of the setup. b. Scheme of the foreseen dPFC glia-neuron network. Astrocytes closely interact with interneurons/pyramidal cells to regulate the global network activity. Oxytocin (axon: yellow; receptor: blue) directly modulates a subtype of interneurons or astrocytes. Dual color imagery of GCaMP6 and RCaMP2 as described in Inoue et al., 2015. (left) Picture of two different cellular types labeled with either GCaMP6 or RCaMP2. (right) Raster plot depicting the calcium activity of the corresponding cells. From Inoue et al., 2015.
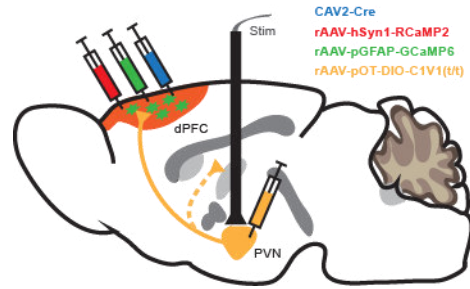
Feasibility: We have in-depth experience with most of the individual techniques required (extensive surgery, calcium imaging, fear conditioning). Importantly, dual colour based 2-photons imaging has been validated using a combination of GCaMP6 and RCaMP2 (Inoue et al., 2015) (**Fig. 7c**). Recently, Yuste's lab demonstrated the possibility to simultaneously image both cortical astrocytes and neurons using only GCaMP6 (poskanzer and Yuste., 2016), hence offering a potential alternative strategy. However, we expect the implementing of the forefront 2PLSM technology in behaving mice to be challenging in both terms of performing the experiments and analysing the results. Finally, this will provide invaluable data on the physiological cellular interactions within dPFC networks during a complex cortical processing. This is associate with very high-gain for the entire proposal and future research in our lab and region.

WP2.2. Characterizing the subcortico-cortical drive of associative learning

Context/hypothesis: Oxytocin has been strongly involved in associative learning and oxytocin receptors are highly present in the dPFC (**Fig. 6b**). Moreover, despite the fact that the dPFC has been involved in associative learning, the functional contribution of subcortical-cortical drive and the specific effect of endogenous oxytocin release on cortical processing is unknown. This leads us to propose the following logical hypothesis: The glia-neuron network dynamics occurring in the course of an associative learning in the dPFC are submitted to the bottom-up control of the hypothalamic oxytocinergic system (**Fig 7b**), hence demonstrating the influence of the emotion-related system on cortical-relevant function.

Objective: **Here, we will take full advantage of state-of-the-art *in vivo* approaches combining genetically-encoded calcium indicators and optogenetics to address the causal relationship between PVN-dPFC OT projections and the dPFC glia-neuron network dynamics occurring in the course of associative memory.**

Methods/breakthrough: In addition to the expression of RCaMP2 in neurons and GCaMP6 in astrocytes of the dPFC, the expression of the light-sensitive channels C1V1(t/t) will be specifically induced in PVN-dPFC oxytocin neurons (**Fig. enclosed**). We will thus combine optogenetic manipulation with long-term 2PLSM-based calcium imaging to provide a fast read-out of the effect of PVN-dPFC OT projecting neurons in behaving animals. This will be performed in a control situation, and upon associative learning and extinction. For the first time, we will address the causal relationship between specific subcortical population dynamics, prefrontal glia-neuron processing and associative learning.

Feasibility: We have extensive experience with the light-driven manipulation of the oxytocin system. If abundant in the dPFC when compared to other cortical regions, the number of OT axons remains relatively low. In addition, oxytocinergic axons need a strong photo-stimulation to release endogenous OT, in contrast with classical neurotransmitters (Hökfelt, 1991): 20s of 30Hz 10ms pulses at ~10mW.mm^{-2} at peak excitation wavelength of the opsin. In consequence, we expect such level of optical stimulation not to be reached during imaging GCaMP6 and RCaMP2, especially with the use of C1V1(t/t) due to its relatively low excitability when compared to ChR2. This results in the validity of our complex approach: to ensure stimulation/inhibition of PVN-dPFC OT neurons, we will directly stimulate the PVN-dPFC OT neurons in the PVN, where light pulses will be delivered through an optic fiber.

(WP3) The prefrontal glia-neuron network as a hub for emotion-cognition interaction

Context/hypothesis: Several psychiatric diseases display abnormal associative learning that may arise from a dysfunction of subcortico-cortical communication and/or local cellular networks. Pain is defined as "an unpleasant sensory and emotional experience associated with actual or potential tissue damage, or described in terms of such damage" (from the *International Association for the Study of Pain*). Pain is difficult to ignore and has a profound impact on concurrent cognitive activities (Lorenz et al., 2003). Furthermore, chronic pain is often associated with high anxio-depressive comorbidities (Yalcin and Barrot, 2014) and rearrangements in the glia-neuron network (Marcello et al., 2013). Given that the dPFC is interconnected with critical structures involved in pain processing, and that anxious individuals tend to have impaired associative learning, we hypothesize that chronic pain induces strong impairments of dPFC glia-neuron dynamics responsible for associative learning deficits.

Objective: **To understand the causative interactions between cortical processing and emotional status, we will decipher the impact of pain on associative learning and related dPFC glia-neuron network dynamics by combining *in vivo* 2PLSM with a reliable model of chronic pain.**

Methods/breakthrough: 2PLSM of GCaMP6 and RCaMP2 will be used as described before. Animals will be submitted to the cuffing of the sciatic nerve as a robust model of chronic pain. First, the dPFC glia-neuron network will be monitored during a discriminative fear conditioning protocol as described before. Second, given that chronic pain induces strong anxio-depressive symptoms 4 weeks after the surgery, the dPFC glia-neuron network will again be monitored at this stage during a second and independent discriminative fear conditioning protocol. This long-term strategy will shed light on two putative major sources of interference with cortical

processing and associative learning: first, from the sustained pain by itself; second, from the induced major anxio-depressive symptoms. In conclusion, this will bring important information regarding the intermingling of emotional status and cortical processing.

Feasibility: We have extensive experience with all the nociceptive threshold measurement and pain models used as well as with optogenetic manipulation in freely moving animals. Furthermore, our lab is implanted in a structure specialized in the study of pain with rich interactions between basic scientists and clinicians. This will be the first study deciphering the involvement of the dPFC in pain management and pain-induced associative learning deficiency. The expected outcome of these experiments will potentially participate in the design of new diagnoses or clinical strategies towards concrete daily life enhancement in the wide range of psychiatric disorders including chronic anxiety, major depression, and chronic pain.

Funding sources

This project is currently under evaluation for potential funding by the ERC Starting Grant and ANR JCJC 2017. It is the logical step following the previous work involving amygdala astrocytes in the oxytocinergic regulation of emotional processing (Jérôme Wahis 2013-2017). In addition to the ERC and ANR JCJC we foreseen the recruitment of Joana Duarte as PhD student if she succeed in the local doctoral school competition.

47

Bibliography

Araque A et al. (2014) Gliotransmitters travel in time and space. Neuron. 81(4):728-39.

Armstrong, W.E., Warach, S., Hatton, G.I., and McNeill, T.H. (1980). Subnuclei in the rat hypothalamic paraventricular nucleus: a cytoarchitectural, horseradish peroxidase and immunocytochemical analysis. Neuroscience 5, 1931–1958.

Baskerville TA. and Douglas AJ. (2010). Dopamine and oxytocin interactions underlying behaviors: potential contributions to behavioral disorders. CNS Neuroscience and Therapeutics, 16:e92-123.

Baskerville TA, Allard J, Wayman C, Douglas AJ. (2009). Dopamine-oxytocin interactions in penile erection. European journal of neuroscience, 30:2151-2164.

Bester H, Besson JM, Bernard JF (1997) Organization of efferent projections from the parabrachial area to the hypothalamus: a Phaseolus vulgaris-leucoagglutinin study in the rat. J Comp Neurol 383:245-281.

Breton JD, Poisbeau P, Darbon P (2009) Antinociceptive action of oxytocin involves inhibition of potassium channel currents in lamina II neurons of the rat spinal cord. Mol Pain 5:63.

Bujis RM, Geffard M, Pool CW, Hoorneman EMD. (1984). The dopaminergic innervation of the supraoptic and paraventricular nucleus—A light and electron microscopical study. Brain Research, 323:65–72.

Carrasquillo Y, Gereau RWt (2008) Hemispheric lateralization of a molecular signal for pain modulation in the amygdala. Mol Pain 4:24.

Carrillo-Reid L et al. Imprinting and recalling cortical ensembles. Science. 353(6300):691-4 (2016).

Charlet A, Lasbennes F, Darbon P, Poisbeau P (2008) Fast non-genomic effects of progesterone-derived neurosteroids on nociceptive thresholds and pain symptoms. Pain 139:603-609.

Charlet A, Muller AH, Laux A, Kemmel V, Schweitzer A, Deloulme JC, Stuber D, Delalande F, Bianchi E, Van Dorsselaer A, Aunis D, Andrieux A, Poisbeau P, Goumon Y (2010) Abnormal nociception and opiate sensitivity of STOP null mice exhibiting elevated levels of the endogenous alkaloid morphine. Mol Pain. 20;6:96.

Charlet A, Rodeau JL, Poisbeau P (2011a) Radiotelemetric and symptomatic evaluation of pain in the rat after laparotomy: long-term benefits of perioperative ropivacaine care. J Pain 12:246-256.

Charlet A, Rodeau JL, Poisbeau P (2011b) Poincare plot descriptors of heart rate variability as markers of persistent pain expression in freely moving rats. Physiol Behav 104:694-701.

Chung WS et al (2015). Do glia drive synaptic and cognitive impairment in disease? Nat Neurosci. 18(11):1539-45.

Condés-Lara M, González NM, Martínez-Lorenzana G, Delgado OL, Freund-Mercier MJ (2003) Actions of oxytocin and interactions with glutamate on spontaneous and evoked dorsal spinal cord neuronal activities. Brain Res 976(1):75-81.

Ciocchi S, Herry C, Grenier F, Wolff SB, Letzkus JJ, Vlachos I, Ehrlich I, Sprengel R, Deisseroth K, Stadler MB, Müller C, Lüthi A (2010) Encoding of conditioned fear in central amygdala inhibitory circuits. Nature 468(7321):277-82

Damasio A (2005) Human behaviour: brain trust. Nature 435:571-572

De Dreu CK, Greer LL, Handgraaf MJ, Shalvi S, Van Kleef GA, Baas M, Ten Velden FS, Van Dijk E, Feith SW (2010) The neuropeptide oxytocin regulates parochial altruism in intergroup conflict among humans. Science 328:1408-1411.

Di Scala-Guenot D, Strosser MT (1992) Oxytocin receptors on cultured astroglial cells. Kinetic and pharmacological characterization of oxytocin-binding sites on intact hypothalamic and hippocampic cells from foetal rat brain. Biochem J 284(2): 491-7

Di Scala-Guenot D, Mouginot D, Strosser MT (1994) Increase of intracellular calcium induced by oxytocin in hypothalamic cultured astrocytes. Glia. 11(3):269-76.

Dogbevia GK, Marticorena-Alvarez R, Bausen M, Sprengel R, Hasan MT. (2015). Inducible and combinatorial gene manipulation in mouse brain. Frontier of cellular neuroscience 9:142.

Donaldson ZR, Young LJ (2008) Oxytocin, vasopressin, and the neurogenetics of sociality. Science 322:900-904.

Eckstein M et al. Oxytocin facilitates the extinction of conditioned fear in humans. Biol Psychiatry 78:194–202 (2015).

Eliava M, Melchior M, Knobloch-Bollmann HS, Wahis J, da Silva Gouveia M, Tang Y, Ciobanu AC, Triana del Rio R, Roth LC, Althammer F, Chavant V, Goumon Y, Gruber T, Petit-Demoulière N, Busnelli M, Chini B, Tan LL, Mitre M, Froemke RC, Chao MV, Giese G, Sprengel R, Kuner R, Poisbeau P, Seeburg PH, Stoop R, Charlet A, Grinevich V. (2016) A New Population of Parvocellular Oxytocin Neurons Controlling Magnocellular Neuron Activity and Inflammatory Pain Processing. Neuron.89(6):1291-304.

Favrais G, Couvineau A, Laburthe M, Gressens P, Lelievre V (2007) Involvement of **VIP** and PACAP in neonatal brain lesions generated by a combined excitotoxic/inflammatory challenge. Peptides 28(9):1727-37.

Fields RD et al. Glial biology in learning and cognition. Neuroscientist. 20(5):426-31 (2014).

Flak JN, Myers B, Solomon MB, McKlveen JM, Krause EG, Herman JP. (2014). Role of paraventricular nucleus-projecting norepinephrine/epinephrine neurons in acute and chronic stress. European journal of neuroscience, 39:1903-11.

Fonnum F, Johnsen A, Hassel B (1997) Use of fluorocitrate and fluoroacetate in the study of brain metabolism. Glia 21:106-113.

Freund-Mercier MJ, Stoeckel ME, Klein MJ. (1994) Oxytocin receptors on oxytocin neurones: histoautoradiographic detection in the lactating rat. J Physiol. 480 (Pt 1):155-61.

Freund-Mercier, M.J., and Richard, P. (1984). Electrophysiological evidence for facilitatory control of oxytocin neurones by oxytocin during suckling in the rat. J. Physiol. 352, 447–466.

Gimpl G, Fahrenholz F. The oxytocin receptor system: structure, function, and regulation. Physiol Rev 81(2):629-83

Goncalves J, Grove KL, Deschepper CF (1995) Generation of cyclic guanosine monophosphate in brain slices incubated with atrial or C-type natriuretic peptides: comparison of the amplitudes and cellular distribution of the responses. Regul Pept 57:55-63.

González-Hernández A, Rojas-Piloni G, Condés-Lara M (2014) Oxytocin and analgesia: future trends. Trends Pharmacol Sci. 35(11):549-51.

Guthrie PB, Knappenberger J, Segal M, Bennett MV, Charles AC, Kater SB (1999) ATP released from astrocytes mediates glial calcium waves. *J. Neurosci.*, 19: 520–528.

Han Y, Yu LC (2009) Involvement of oxytocin and its receptor in nociceptive modulation in the central nucleus of amygdala of rats. Neuroscience Letters 454 (2009) 101–104

Haubensak W, Kunwar PS, Cai H, Ciocchi S, Wall NR, Ponnusamy R, Biag J, Dong HW, Deisseroth K, Callaway EM, Fanselow MS, Lüthi A, Anderson D (2010) Genetic dissection of an amygdala microcircuit that gates conditioned fear. Nature 11;468(7321):270-6.

Hermann GE, Van Meter MJ, Rood JC, Rogers RC (2009) Proteinase-activated receptors in the nucleus of the solitary tract: evidence for glial–neural interactions in autonomic control of the stomach. J Neuroscience 29(29): 9292-9300

Hökfelt T. Neuropeptides in perspective: the last ten years. Neuron 7, 867–879 (1991).

Hopkins DA & Holstege G (1978) Amygdaloid projections to the mesencephalon, pons and medulla oblongata in the cat. Exp Brain Res 32, 529-47

Huber D, Veinante P, Stoop R (2005) Vasopressin and oxytocin excite distinct neuronal populations in the central amygdala. Science 308:245-248.

Huber D et al. Multiple dynamic representations in the motor cortex during sensorimotor learning. Nature 484, 473–8 (2012).

Hummel P, van Dijk M (2006) Pain assessment: current status and challenges. SeminFetal Neonatal Med 2006;11:237–45.

Inoue M et al. Rational design of a high-affinity, fast, red calcium indicator R-CaMP2. Nat Methods. 12(1):64-70 (2015).

Janig W (1995) The sympathetic nervous system in pain. Eur J Anaesthesiol Suppl 10:53-60, 1995

Johnson RT, Breedlove SM, Jordan CL (2010) Chapter 2 - Astrocytes in the Amygdala; Vitamins & Hormones Volume 82, 2010, pages 23-45 Hormones of the Limbic System

Juif PE, Poisbeau P. (2013) Neurohormonal effects of oxytocin and vasopressin receptor agonists on spinal pain processing in male rats. Pain. 154(8):1449-56.

Karalis N et al. 4-Hz oscillations synchronize prefrontal-amygdala circuits during fear behavior. Nat Neurosci. 19(4):605-12 (2016).

Keller AF, Coull JA, Chery N, Poisbeau P, De Koninck Y (2001) Region-specific developmental specialization of GABA-glycine cosynapses in laminas I-II of the rat spinal dorsal horn. J Neurosci 21:7871-7880.

Kenshalo DR, editor. The skin senses. Spring®eld (IL): Charles C. Thomas; p. 423 ± 43. (1968).

Killcross S, Robbins T. W. & Everitt B. J. (1997) Different types of fear-conditioned behaviour mediated by separate nuclei within amygdala. Nature 388, 377-80

Kirsch P, Esslinger C, Chen Q, Mier D, Lis S, Siddhanti S, Gruppe H, Mattay VS, Gallhofer B, Meyer-Lindenberg A (2005) Oxytocin modulates neural circuitry for social cognition and fear in humans. J Neurosci 25:11489-11493.

Knobloch HS, Charlet A, Hoffmann LC, Eliava M, Khrulev S, Cetin AH, Osten P, Schwarz MK, Seeburg PH, Stoop R, Grinevich V (2012) Evoked axonal oxytocin release in the central amygdala attenuates fear response. Neuron 73:553-566.

Kramer K, Kinter LB (2003) Evaluation and applications of radiotelemetry in small laboratory animals. Physiol Genomics 13;13(3):197-205

Kubota N, Amemiya S, Motoki C, Otsuka T, Nishijima T, Kita I (2012).Corticotropin-releasing factor antagonist reduces activation of noradrenalin and serotonin neurons in the locus coeruleus and dorsal raphe in the arousal response accompanied by yawning behavior in rats. Neurosci Res. Apr;72(4):316-23.

Lai CS et al. Opposite effects of fear conditioning and extinction on dendritic spine remodeling. Nature 483, 87–91 (2012).

Le Bars D, Gozariu M, Cadden SW (2001) Animal models of nociception. Pharmacol Rev 53:597-652, 2001

LeDoux J. (2014) Low roads and higher order thoughts in emotion. Cortex. 59:214-5.

Lee HJ, Macbeth AH, Pagani JH, Young WS 3rd. Oxytocin: the great facilitator of life. Prog Neurobiol. 88(2):127-51 (2009).

Lee HJ, Pagani J, and Young WS, 3rd (2010). Using transgenic mouse models to study oxytocin's role in the facilitation of species propagation. Brain Res. 1364, 216–224.

Lee S et al (2010). Channel-mediated tonic GABA release from glia. Science. 330(6005):790-6.

Lee D. Decision making: from neuroscience to psychiatry. Neuron 78, 233–48 (2013

Lorenz J et al. Keeping pain out of mind: the role of the dorsolateral prefrontal cortex in pain modulation. Brain. 126(Pt 5):1079-91 (2003).

Ludwig M, Leng G (2006) Dendritic peptide release and peptide-dependent behaviours. Nat Rev Neurosci. 2006 Feb;7(2):126-36.

Maderspach K, Solomonia R (1988) Glial and neuronal opioid receptors: apparent positive cooperativity observed in intact cultured cells. Brain Res. 1988 441(1-2):41-7

Marcello L et al. Remodelling of supraspinal neuroglial network in neuropathic pain is featured by a reactive gliosis of the nociceptive amygdala. Eur J Pain. 17(6):799-810 (2013).

McDougal DH, Hermann GE, Rogers RC (2011) Vagal afferent stimulation activates astrocytes in the nucleus of the solitary tract via AMPA receptors: evidenceof an atypical neural–glial interaction in the brainstem. J Neuroscience 31(39): 14037-1405

Melzack R., Casey K. L. Sensory, motivational, and central control determinants of pain. In: Mitre M et al. A Distributed Network for Social Cognition Enriched for Oxytocin Receptors. J Neurosci. 36(8):2517-35 (2016).

Miller G Psychology (2010). The prickly side of oxytocin. Science 328:1343.

Miranda-Cardenas Y, Rojas-Piloni G, Martínez-Lorenzana G, Rodríguez-Jiménez J, López-Hidalgo M, Freund-Mercier MJ, Condés-Lara M (2006) Oxytocin and electrical stimulation of the paraventricular hypothalamic nucleus produce antinociceptive effects that are reversed by an oxytocin antagonist. Pain 122(1-2):182-9.

Miraucourt LS, Peirs C, Dallel R, Voisin DL. Glycine inhibitory dysfunction turns touch into pain through astrocyte-derived D-serine. Pain 152(6):1340-8

Moiniche S, Kehlet H, Dahl JB (2002) A qualitative and quantitative systematic review of preemptive analgesia for postoperative pain relief: The role of timing of analgesia. Anesthesiology 96:725-741

Mogil JS, Marek P, Flodman P, Spence MA, Sternberg WF, Kest B, Sadowski B, Liebeskind JC. (1995) One or two genetic loci mediate high opiate analgesia in selectively bred mice. Pain 60(2):125-35.

Moos F, Freund-Mercier MJ, Guerné Y, Guerné JM, Stoeckel ME, Richard P (1985) Release of oxytocin and vasopressin by magnocellular nuclei in vitro: specific facilitatory effect of oxytocin on its own release. J Endocrinol. 102(1):63-72.

Moos F, Richard P. (1989) Paraventricular and supraoptic bursting oxytocin cells in rat are locally regulated by oxytocin and functionally related. J Physiol. 408:1-18.

Nakayama D et al. Frontal association cortex is engaged in stimulus integration during associative learning. Curr Biol. 25(1):117-23 (2015).

Neugebauer V (2007) The amygdala: different pains, different mechanisms. Pain 127:1-2.

Neugebauer V, Galhardo V, Maione S, Mackey SC (2009) Forebrain pain mechanisms. Brain Res Rev 60:226-242.

Neumann ID (2008) Brain oxytocin: a key regulator of emotional and social behaviours in both females and males. J Neuroendocrinol 20:858-865.

Onaka T. (2004) Neural pathways controlling central and peripheral oxytocin release during stress. Journal of neuroendocrinology, 16:308-312.

Panigada T, Gosselin RD (2011) Behavioural alteration in chronic pain: are brain glia involved? Med Hypotheses 77(4):584-8.

Passemard S, El Ghouzzi V, Nasser H, Verney C, Vodjdani G, Lacaud A, Lebon S, Laburthe M, Robberecht P, Nardelli J, Mani S, Verloes A, Gressens P, Lelièvre V (2011) VIP blockade leads to microcephaly in mice via disruption of Mcph1-Chk1 signaling. J Clin Invest 121(8):3071-87.

Paxinos G, Franklin BJ. The mouse brain in stereotaxic coordinates, 4th Edition. Academic Press (2012).

Perlstein WM, Carter CS, Noll DC, Cohen JD. Relation of prefrontal cortex dysfunction to working memory and symptoms in schizophrenia. Am J Psychiatry. 158(7):1105-13 (2001).

Pertin M, Gosselin RD, Decosterd I (2012) The spared nerve injury model of neuropathic pain. Methods Mol Biol. 2012;851:205-12

Petrovich G. D. & Swanson L. W. (1997) Projections from the lateral part of the central amygdalar nucleus to the postulated fear conditioning circuit. Brain Res 763, 247-54.

Porro CA, Carli G (1988) Immobilization and restraint effects on pain reactions in animals. Pain 32(3):289-307.

Poskanzer KE, Yuste R. Astrocytes regulate cortical state switching in vivo. Proc Natl Acad Sci. 113(19):E2675-84 (2016).

Ray RD, Zald DH. Anatomical insights into the interaction of emotion and cognition in the prefrontal cortex. Neurosci Biobehav Rev. 36(1):479-501 (2012).

Salzman CD, Fusi S. Emotion, cognition, and mental state representation in amygdala and prefrontal cortex. Annu Rev Neurosci. 33:173-202 (2010).

Sarhan M, Freund-Mercier MJ, Veinante P (2005) Branching patterns of parabrachial neurons projecting to the central extended amgydala: single axonal reconstructions. J Comp Neurol 491:418-442.

Sawchenko PE, Plotsky PM, Pfeiffer SW, Cunningham ET, Jr., Vaughan J, Rivier J, Vale W (1988) Inhibin beta in central neural pathways involved in the control of oxytocin secretion. Nature 334:615-617.

Scharrer, E. (1928). Die Lichtempfindlichkeit blinder Elritzen (Untersuchungenu ber das Zwischenhirn der Fische). Z. Vgl. Physiol. 7, 1–38.

Scholz J, Woolf CJ (2002) Can we conquer pain? Nat Neurosci 2002;(5 Suppl):1062-1067

Singer T, Snozzi R, Bird G, Petrovic P, Silani G, Heinrichs M, Dolan RJ. (2008) Effects of oxytocin and prosocial behaviour on brain responses to direct and vicariously experienced pain. Emotion. Dec;8(6):781-91.

Sofroniew, M.V. (1983). Morphology of vasopressin and oxytocin neurons and their central and vascular projections. Prog. Brain Res. 60, 101–114.

Sontheimer H (1994) Voltage-dependent ion channels in glial cells. Glia 11:156-172.

Sotres-Bayon F and Quirk G. Prefrontal control of fear: more than just extinction. Curr Opin Neurobiol, 20(2): 231–235 (2010)

Swanson LW, Sawchenko PE (1983) Hypothalamic integration: organization of the paraventricular and supraoptic nuclei. Annu Rev Neurosci 6:269-324.

Tousignant-Laflamme Y, Rainville P, Marchand S (2005) Establishing a link between heart rate and pain in healthy subjects: a gender effect. J Pain 6:341–7.

Tracey I, Mantyh PW (2007) The cerebral signature for pain perception and its modulation. Neuron 55:377–91.

Tran L, Greenwood-Van Meerveld B (2012) Lateralized amygdala activation: importance in the regulation of anxiety and pain behavior. Physiol Behav 105:371-375

Tyzio R, Cossart R, Khalilov I, Minlebaev M, Hubner CA, Represa A, Ben-Ari Y, Khazipov R (2006) Maternal oxytocin triggers a transient inhibitory switch in GABA signaling in the fetal brain during delivery. Science 314:1788-1792.

Van de Werd HJ and Uylings HB. Comparison of (stereotactic) parcellations in mouse prefrontal cortex. Brain Struct Funct. 219(2): 433–459 (2014).

Viviani D, Charlet A, van den Burg E, Robinet C, Hurni N, Abatis M, Magara F, Stoop R (2011) Oxytocin selectively gates fear responses through distinct outputs from the central amygdala. Science 333:104-107.

Volterra A, Meldolesi J (2005) Astrocytes, from brain glue to communication elements: the revolution continues. Nat Rev Neurosci 6(8):626-40

Walz W (2002) Chloride/anion channels in glial cell membranes. Glia 40:1-10.

Wilder-Smith OH, Arendt-Nielsen L (2006) Postoperative hyperalgesia: Its clinical importance and relevance. Anesthesiology 104:601-607

Willis WD (1985) Nociceptive pathways: anatomy and physiology of nociceptive ascending pathways. Philos Trans R Soc Lond B Biol Sci 308:253-270.

Willis WD (1991) Role of the forebrain in nociception. Prog Brain Res 87:1–12.

Woodcock EA et al (2015). The dorsal prefrontal and dorsal anterior cingulate cortices exert complementary network signatures during encoding and retrieval in associative memory. Behav. Brain Res. 290, 152–160.

Young LJ (2009) Being human: love: neuroscience reveals all. Nature 457:148.

Yalcin I, Bohren Y, Waltisperger E, Sage-Ciocca D, Yin JC, Freund-Mercier MJ, Barrot M (2011) A time-dependent history of mood disorders in a murine model of neuropathic pain. Biol Psychiatry 15;70(10):946-53

Yalcin I, Charlet A, Cordero-Erausquin M, Tessier LH, Picciotto MR, Schlichter R, Poisbeau P, Freund-Mercier MJ, Barrot M. Nociceptive thresholds are controlled through spinal β2-subunit-containing nicotinic acetylcholine receptors. Pain 152(9):2131-7.

Yalcin I, Charlet A, Freund-Mercier MJ, Barrot M, Poisbeau P (2009) Differentiating thermal allodynia and hyperalgesia using dynamic hot and cold plate in rodents. J Pain 10:767-773.

Yalcin I, Barrot M. The anxiodepressive comorbidity in chronic pain. Curr Opin Anaesthesiol. 27(5):520-7 (2014).

Yu DH, Huang SC, Wank SA, Mantey S, Gardner JD, Jensen RT (1990) Pancreatic receptors for cholecystokinin: evidence for three receptor classes. Am J Physiol 258(1 Pt 1):G86-95